School of Pharmacy and Biomedical Sciences

Nanosystems in the Skin: from Undesirable Nanomaterial Exposure to Novel Nanoformulations

Christofori Maria Ratna Rini Nastiti

This thesis is presented for the Degree of
Doctor of Philosophy
of
Curtin University

August 2019

DECLARATION

To the best of my knowledge and belief this thesis contains no material previously published by any other person except where due acknowledgment has been made.

This thesis contains no material which has been accepted for the award of any other degree or diploma in any university.

Human Ethics The research presented and reported in this thesis was conducted in accordance with the National Health and Medical Research Council National Statement on Ethical Conduct in Human Research (2007) – updated March 2014. The work involving human skin preparation was carried out at the Translational Research Institute in Queensland and received human research ethics approval from the University of Queensland Medical Research Committee, Approval Number 2008001342.

Animal Ethics The research presented and reported in this thesis was conducted in compliance with the National Health and Medical Research Council Australian code for the care and use of animals for scientific purposes 8th edition (2013). The proposed research study received animal ethics approval from the University of Queensland Research and Innovation, Approval Number ANRFA/265/16

Signature: _____

Date: 02 / 08 / 2019

ABSTRACT

Nanomaterials are widely used in medical, pharmaceutical and industrial areas. People are exposed to nanomaterials by ingestion, respiration or skin contact. This body of work focused on skin contact. Nanomaterial exposure can be either accidental or intentional. Understanding how nanomaterials interact with the skin is essential to both avoiding potential toxicity in accidental exposure and to harnessing the potential of nanomaterials for targeted drug delivery. An extensive literature review focusing on current research of nanomaterial skin exposure and topical nanoformulations is provided in chapter 1.

This thesis is divided into two parts. The first part is an investigation of the effect of undesirable nanomaterial topical exposure on penetration into the skin. The first project of the first part provided satisfactory information of the visualisation of nanomaterial exposure on the compromised skin. Effects of acetone and tape stripping pre-treatments were investigated on porcine skin penetration of the nanomaterials. Hydrophilic CdTe/CdS quantum dots (QDs) were used as a model of the nanomaterials. Multiphoton tomography equipped with fluorescence lifetime imaging (MPT-FLIM) was used to capture the existence of QDs in the skin following the exposure. We revealed that the QDs were mostly deposited on the skin surface and furrows. There was no skin penetration of QDs detected on both types of compromised skin. However, some QDs were shown on the upper stratum granulosum (SG) as a consequence of stratum corneum (SC) removal by tape stripping.

The project progressed to investigate the influence of age and anatomical site on QDs penetration into porcine skin. Adult, weanling and newborn pigs were selected to represent age differences. Two anatomical sites on each donor (ear and abdomen) were examined by MPT imaging, with a focus on the keratinocytes and follicles. MPT images showed that the QDs were in the furrows and follicles, without further penetration. Inductively Coupled Plasma Mass Spectrometry (ICP-MS) analysis of cadmium provided quantitative confirmation that most QDs were deposited in the follicles (47-79%). The QDs follicular deposition at 24h was higher in ears than abdomen for adult and weanling pig ears, but similar for these anatomical sites in newborn piglets. This is associated with the high follicle density and small follicle diameter of the NBPS compared to the smaller density of much larger follicles on the adult pig skin (APS). Density and diameter of follicles in association with age of pigs and application site influenced the amount of QD deposited in follicles. In addition to

that, the structure of the SC, follicle density and diameter of newborn pig skin (NBPS) is similar to human skin suggesting that NBPS is an appropriate model for human skin in the evaluation of topical applications of a range of chemicals including nanosystems.

The first part of this thesis demonstrates the impact of different treatments on the skin, and different skin conditions, to nanomaterial skin penetration. It indicates that exposing the skin to nanomaterials would not lead to skin penetration unless the SC and other supporting skin barriers are significantly perturbed. The topically applied nanomaterials were localised in follicles and furrows without further penetration. In addition, differences of follicle density and diameter influence the degree of nanomaterial deposition.

The second part of the thesis focused on the development and evaluation of novel nanocarriers for skin delivery of resveratrol (RSV), a potent natural antioxidant. Nanoformulations of a lipid-based system, a micellar system and a microemulsion were developed and evaluated to initiate the nanoemulsion formulations. The role of terpenes (eugenol, D-limonene and eucalyptol) as the oil phase was also investigated. We successfully developed nanoemulsions for RSV skin delivery, meeting the quality criteria of clarity (aesthetic appearance), simplicity (in fabrication), stability and efficiency (skin penetration and permeation). The penetration of RSV into the skin was conducted in order to assess RSV deposition in SC and in area of epidermis, dermis, and follicles (E+D+F). The permeation of RSV through the skin was also carried out to evaluate the cumulative amount of RSV in the deeper area of dermis. Thermodynamic activity plays an important role on the degree of RSV penetrate into and permeate through the skin for non-terpene nanoformulations. The more soluble RSV in the non-terpene nanoformulations, the less RSV to penetrate into/permeate through the skin. Terpene addition was also examined. The formulation involving eugenol and triacetin (ETKTP) showed the highest skin deposition (2.342 ± 0.269 $\mu g/cm^2$). In addition to this, we also suggest that terpene addition enhanced the permeation by disrupting the SC intercellular lipids. The amount of RSV permeated through the skin was in correlation with the increased lipophilicity degree of the terpenes. The nanoemulsions containing D-limonene (Log P: 3.4) showed the highest cumulative amount at 8 hour (4.585 ± 0.936 µg) followed by formulations containing eucalyptol (Log P: 2.5) (4.036 ± 1.125 µg), and eugenol (Log P: 2) (0.918 ± 0.126 µg).

The study was extended to investigate the potential of the combination of chemical and physical enhancers on optimizing the RSV permeation through the skin. RSV saturated aqueous solution and two nanoformulations (TKTP and ETKTP) were examined.

Magnet application (magnetophoresis) and microneedles (MN) were the physical enhancers investigated alone and in combination. Magnet application enhanced the permeation of RSV in a saturated aqueous solution at 1.88-fold but did not affect permeation from the nanoformulations. MN significantly enhanced skin permeation of RSV in all formulations. TKTP with MN showed the highest cumulative amount of RSV (37.075 ± 7.150 μg). The combination of magnetophoresis and MN enhanced the deposition of RSV in the epidermis, dermis and follicles compared to MN alone for both nanoformulations, but it did not enhance RSV permeation through the skin. This suggests that magnet application in combination with MN results in enhanced lateral diffusion of RSV of nanoformulations in the skin.

This thesis makes a significant contribution to a better understanding of the behaviour of nanomaterials in the skin. We confirmed that solid nanoparticles accumulate on the skin furrows and follicles, with minimal potential for toxicity. We also developed a novel nanoemulsion delivery system for skin delivery of the natural antioxidant RSV. Nanoemulsions hold great promise for a range of cosmeceutical and dermatological purposes.

LIST OF PUBLICATIONS AND CONFERENCE ABSTRACTS

Publications:

- **Nastiti, C. M. R. R***., Ponto, T*., Abd, E., Grice, J. E., Benson, H. A. E., & Roberts, M. S. (2017). Topical Nano and Microemulsions for Skin Delivery. *Pharmaceutics*, 9(4), 37.

*equally contributed

- **Nastiti, C. M. R. R**., Mohammed, Y., Telaprolu, K. C., Liang, X., Grice, J. E., Roberts, M. S., & Benson, H. A. E. (2019). Evaluation of Quantum Dot Skin Penetration in Porcine Skin: Effect of Age and Anatomical Site of Topical Application. *Skin Pharmacology and Physiology*. doi:10.1159/000499435

Conference Abstracts:

- Mark Liveris Seminar, Curtin University, Western Australia, Australia September 2017

"Evaluation of Quantum Dots (QDs) skin penetration at different ages of pigs"

Award: Best Poster Presentation

- Mark Liveris Seminar, Curtin University, Western Australia, Australia September 2018

"Effect of Acetone and Tape Stripping on Skin: Application of Multiphoton Tomography-Fluorescence Lifetime Imaging (MPT-FLIM)"

- Controlled Release Asia (CRA) Meeting, Singapore, September 2018

"Evaluation of Quantum Dots Skin Penetration: Effect of Age and Anatomical Site of Topical Application"

ACKNOWLEDGMENTS

Praise be to God the Almighty, for great blessings and miracles throughout my life and many thanks to my grandparents, my parents, and my big family for always supporting me with amazing faith.

My highest appreciation goes to my sponsor, the Australia Awards Scholarship through the Department of Foreign Affairs and Trade, Australia. I am very thankful to Julie Craig and the International Sponsored Student Unit (ISSU) team for their wonderful care and continuing support during my study.

I would love to express my sincere gratitude to Associate Professor Dr Heather Benson, my main supervisor, for excellent supervision, invaluable insight, endless support, an amazing mutual relationship and her warmth of heart. I am extremely grateful to the School of Pharmacy and Biomedical Sciences, Curtin University, especially to Professor Kevin Batty, Professor Lynne Emmerton, Associate Professor Dr Cyril Mamotte, and to distinguished thesis examiners for their support and assistance during my thesis preparation and examination.

I sincerely thank my associate supervisors: Professor Michael S. Roberts and Dr Yousuf Hussain Mohammed, for amazing opportunities and guidance during my interstate laboratory work at the Translational Research Institute, Queensland. I would also like to extend my gratitude to Therapeutic Research Centre members, especially to Dr Jeff Grice, Dr Krishna C. Telaprolu, Dr Eman Abd, Dr Sarika Namjoshi, and Dr Xiaowen Liang.

My PhD thesis would not have been completed without invaluable assistance of Giuseppe Luna, Charmaine D Costa, Dr John Fielder, Diana Blackwood, Prof Paul Mills, Dr Sandrine Roy, Dr Ujang Tinggi, Dr Connie Jackaman, Dr Hendra Gunosewoyo, Dr Yu Yu, Jorge Martinez, Angela Samec, and other staff at Curtin University, the Translational Research Institute, Portec Veterinary Services Welshpool, and University of Queensland's piggery farm.

Many thanks also to my best friends in Australia, especially to Shahinda Alsayed, Thellie Ponto, Dr Yan Jing Yee, Maya Irjayanti, Lely Hiryanto, Tony, Yulisna Mutia Sari, Gressy Septarini, Pungky Hendrawijaya, Maharani Hendrawijaya, Vinci Mizranita, Mohammed Shohel, Chun Yuen Wong, Roselyne Bulonza, Dr Yeakuty M Jhanker, Fatima N Jahan, Louise Woodhams, Dilam Ardyansyah, Dr Isha Nanthini Haridass, Dr Imran Khan and Dr Behin Sundara Raj.

I really appreciate the invaluable support from colleagues at the Faculty of Pharmacy, Sanata Dharma University, Indonesia - especially Dr Enade P Istyastono, Dr Sri Hartati Yuliani, Dr Yustina Sri Hartini, Dr Dewi Setyaningsih, Dr Rita Suhadi (†), Dr Christine Patramurti, Dr Rini Dwiastuti, Yohanes Dwiatmaka, and Dr Agatha Budi Susiana Lestari.

Last, but the most importantly, my deep thanks goes to my beloved Stepanus Agus Susanto, Daniella Maria Hersanti Maharani (†), and Gabriel Cikal Hersanto, for their unconditional love and support throughout this journey.

TABLE OF CONTENT

ABBREVIATIONS

3D	:	three dimensions
5-ALA	:	5-aminolevulinic acid
APS	:	adult pig skin
CdS	:	cadmium sulphide
CdSe	:	cadmium/selenium
DLS	:	dynamic light scaterring
DMSO	:	dimethylsulfoxide
DOTAP	:	1,2-dioleyl-3-trimethylammonium propane chloride
DPPC	:	1,2-dipalmitoyl-sn-glycero-3-phosphocholine
DPPG	:	1,2-dipalmitoyl-sn-glycero-3-phosphoglycerol, sodium salt
EIM	:	ethanol injection method
ER	:	enhancement ratio
FLIM	:	fluorescence lifetime imaging
FTIR	:	Fourier-Transform Infrared Spectroscopy
H&E	:	hematoxylin and Eosin
HCl	:	hydrochloride
HEE	:	high–energy emulsification
HPLC	:	high performance liquid chromatography
HS	:	human skin
ICP-MS	:	Inductively Coupled Plasma-Mass Spectrometry
LEE	:	low-energy emulsification
LOD	:	limit of detection
LOQ	:	limit of quantification
LPP	:	lipid-protein-partitioning
ME	:	microemulsion
MN	:	microneedles
MPT	:	Multiphoton Tomography
MPT-FLIM	:	Multiphoton Tomography-Fluorescence Lifetime Imaging
MW	:	molecular weight
NaCl	:	natrium (sodium) chloride
NADH	:	nicotinamide adenine dinucleotide
NBPS	:	newborn pig skin
ND	:	2-(1-nonyl)-1,3-dioxolane
NE	:	nanoemulsion

NG	:	gel based nanoemulsion
NLC	:	nanostructured lipid carriers
NPs	:	nanoparticles
OCT	:	Optical Coherence Tomography
PADO	:	padimate O
PBS	:	phosphate buffer saline
PC	:	phosphatidylcholine
PCS	:	Photon Correlation Spectroscopy
PDI	:	polydispersity index
PE NE	:	penetration enhancer-containing nanoemulsion
PEMF	:	pulsed electromagnetic fields
PEVs	:	penetration enhancer-containing vesicles
QDs	:	quantum dots
RSD	:	relative standard deviation
RSV	:	resveratrol
SANS	:	small angle neutron scattering
SAXs	:	small angle X-ray scattering
SB	:	stratum basale
SC	:	stratum corneum
SG	:	stratum granulosum
SLN	:	solid lipid nanoparticles
SS	:	stratum spinosum
TEM	:	transmission electron microscopy
TEWL	:	trans-epidermal water loss
TFH-S	:	thin film hydration-sonication
TiO2	:	titanium dioxide
TJs	:	tight junctions
TS	:	tape stripping
UV	:	ultraviolet
VWD	:	variable wavelength detector
WPS	:	weanling pig skin
ZnO	:	zinc oxide
ZnS	:	zinc sulphide

LIST OF FIGURES

LIST OF TABLES

Chapter 1. Nanosystems in the Skin: A Literature Review

1.1 Skin

1.1.1 Terminology and functions

Human skin is the outermost and the third largest organ of the body after the gastrointestinal tract and the lung, with area of approximately 1.6 m^2 for adults and around 8% of the body weight.[1-3] Skin provides an effective physical protection against the entrance of foreign substances and microbes, as well as the excessive water loss from the body. As a flexible interface between the body and outer environment, skin also protects the body from mechanical contact friction. Having nerve fibres and endings, skin facilitates tactile senses, pain, itch and temperature-related feeling. Skin is also an ideal model to investigate immunological responses of the allergens and the pharmacodynamics of antibodies.[3] In addition, skin plays an important role to maintain body hydrodynamic balance and temperature by regulating sweat secretion. Advanced progress has been made in biometric technology for human identification involving not only fingerprints but also blood vessel patterns on the palm and fingers. Skin appearance is in relevance with aesthetic performance such as beautiful and healthy skin look. [2]

1.1.2 Skin structure

Skin is comprised of two anatomical layers, the dermis (the inner layer) and epidermis (the outer layer).[4]

Dermis (1-2mm thick) supports the skin mechanically.[3-5] It consists of dense and elastic connective tissues of elastin and collagenous fibre where blood capillaries, nerve fibres and endings, lymph vessels, secretory glands (sweat/eccrine, sebaceous, and apocrine glands), and hair follicles are located.[6] Sebaceous glands generate oils to lubricate the skin, whereas sweat glands regulate the hydrodynamic activity and produce sweat as a result of metabolic processes.

Epidermis (50-100 μm) consists of mostly keratinocytes.[5, 7] It is in a steady state between cell growth and cell desquamation, starting from proliferation at the stratum basale (SB) until terminal differentiation at the stratum corneum (SC). The squamous layers (strata) from upper dermis to the surface are the SB, stratum spinosum (SS), stratum granulosum (SG) and SC. The epidermis also contains melanocytes, that

produce melanin, the dark pigment which also acts as natural UV protection. Between the SB and dermis are two anatomical structures known as rete ridges and dermal papillae. Rete ridges are the extensions of epidermal layer to prevent the skin from shearing. Dermal papillae are uppermost of dermis layer containing blood vessels. Dermal papillae project from dermis to epidermis, while rete ridges project the opposite. Dermal papillae maintain adhesion between dermis and epidermis and provide nourishment to the epidermis and follicles. The SS is characterised by noticeable intercellular desmosomal connections. The SG consists of flattened keratinocytes and is rich in basophilic keratohyaline granules which contain fillagrin, an adhesive substance of keratin filaments. It also contains many lamellar bodies in which precursors of lipids (glucosylceramides, sphingomyelin, and phospholipids) are stored.[8] The SC is comprised of more than 20 layers of polyhedral corneocytes interconnected with lipid. Basket-weave pattern was initially observed as SC pattern[9], although this pattern was shown to be an artefact due to biopsy processing resulting in lipid loss.[10, 11] A concept of "brick and mortar" describes the SC further as a two-compartment system[12]. SC (10-20µm thick, 18-20 cell layers) consists of intracellular keratin filaments surrounded by protein-rich cell envelope which bond covalently to hydroceramide molecules of lipid envelopes, which are called corneocytes and act as bricks.[5, 13] These bricks are embedded in extracellular lipids as ceramides, cholesterol, free fatty acids, cholesterol esters and cholesterol sulfate in a well-arranged structure, which then called as mortar. The corneocytes are connected by protein structures called corneodesmosomes. Although proteins enrich the structure of SC, they do not affect the lipid organisation of SC.[5, 14, 15]

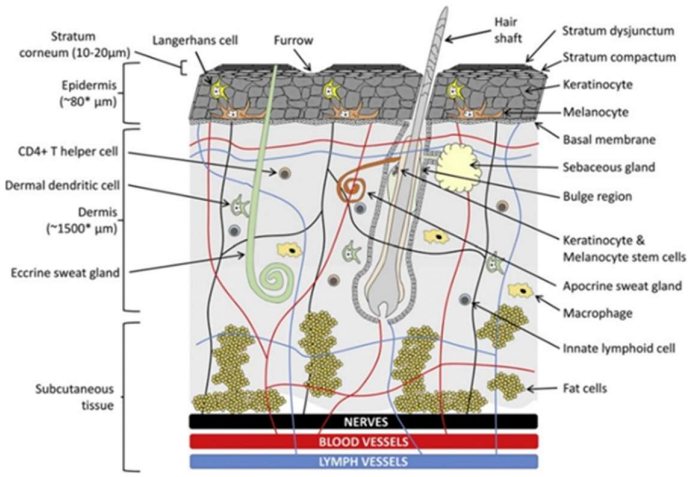

Figure 1.1 Human skin structure schematic representation. The thickness of skin layer was approximately measured, it may vary based on the sites and degree of hydration. The figure is reproduced from Roberts et al.[6] with permission.

1.1.3 SC and viable epidermis significance as skin barriers

The skin provides a physical, microbial, immunological and thermal barrier mutual through the roles of SC, tight junctions (TJs), antimicrobial peptides, microbiomes, and immunological biochemical.[16] With regard to skin drug delivery, the SC and TJs of the epidermis play the most important roles.

Despite the concept of a metabolically-dead, basket weave layer, and inert wrapping[9], the complex structure of the SC is believed as the foremost skin barrier against the penetration of molecules, microbes, and nanomaterials as well as excessive loss of water from the body.[17] The SC which is composed of dead cells embedded in metabolically active surroundings, facilitating enzymatic reactions, skin low pH, immune signaling, and natural moisturizing factors, in order to protect epidermis and maintain the skin integrity.[18]

The intercellular lipid lamellae of SC form hydrophobic skin barrier by preventing water permeation including hydrophilic substances.[19] Although water barely penetrates into the skin, the over hydration of SC is potential to disrupt the lipid structure in the SC thus allow substances to pass through SC.[5, 20]

The skin barrier function is also supported by tight junctional complexes which are transitional desmosomes in the interconnection between the SC and SG.[13, 21] TJ proteins are also located in between apical and basolateral cells, acting as a fence especially in the interfollicular epidermis.[16, 22] Among three layers of SG in human skin epidermis, SG2 layer was reported to have functional TJs.[23] TJs such as occluding, claudins, and zonal occluding proteins are essential in sealing the paracellular pathways to limit molecules movement within intercellular pores.[16, 21, 24, 25]

1.1.4 Pathways of penetration

1.1.4.1 Transepidermal pathway

The transepidermal pathway has been widely reported as the prominent pathway for penetration of xenobiotics into the skin[11, 26], with two potential routes. The *transcellular (intracellular) pathway* involves the passing of the substances directly through the SC and keratinocytes benefiting the water-rich corneocyte openings. It requires reasonable partition of the molecules into and through the corneocytes and intercellular lipids.[27] The tortuous *intercellular pathway* allows applied substances to penetrate within the lipid regions between the corneocytes in the SC.[11] The thickness of the SC is about 10-15 μm, however the tortuous pathway length is far longer (> 150 μm).[28] There has been a perspective that hydrophilic solutes were thought to diffuse intracellularly (within the

watery domain close to the outer surface of intracellular keratin filaments), whereas lipophilic substances diffuse intercellularly through the lipid matrix.[29] Whilst both pathways make important contributions, it is generally accepted that in general, the intercellular pathway contributes more in the skin penetration.[30-32]

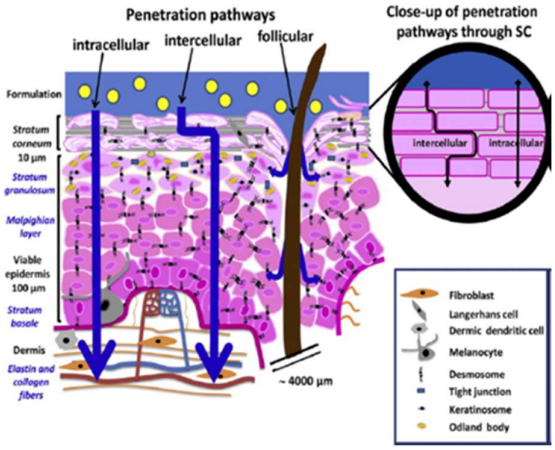

Figure 1.2 A schematic diagram of penetration pathways showing the major routes of intracellular, tortuous intercellular and follicular pathways. Adapted from Bolzinger et al.[33] with permission

1.1.4.2 Transappendageal pathway

The transappendageal (shunt) pathways through sweat glands, sebaceous glands and hair follicles has been debated for many years.[29] Initially, there was scepticism that these pathways contribute to the skin penetration of molecules due to their small surface area compared to skin surface. However, although hair follicles only occupy 0.1% area of skin surface[11, 26], several research groups have demonstrated the potential of the follicular pathway in skin penetration.[34-48] Follicles can act as a potential reservoir that may be valuable for the penetration of prolonged existence deliverables, although the distinctive barrier properties of the SC covering the follicles may be very challenging to manipulate.[35-37, 39, 49] Follicle density, follicle orifice diameter and follicle volume (related to the depth of follicles into the dermis) define the efficiency of follicle deposition of substances.[50]

1.2 Nanomaterial topical exposure

Nanotechnology has produced a range of nanomaterials which positively impact the scientific community, domestic and industrial environments in many ways.[51] The main ways in which people are exposed to nanomaterials is by ingestion, respiration or skin contact. Our focus is skin contact that can occur intentionally (while applying a topical formulation), or accidentally through the exposure of nanomaterials in workplaces or other environments involving nanoparticle handling.[52, 53]

Topical exposure of unintended foreign nanomaterials and surface-retained formulations (such as sunscreen and decorative cosmetics) need to be scrutinised in order to assess environmental and human health risks such as skin damage or systemic toxicity due to the potential of undesired penetration into deeper skin layers.[53-55]

1.2.1 Safety issues on nanomaterial exposure

Titanium dioxide (TiO_2) and zinc oxide (ZnO) have been widely used as inorganic physical UV reflectors in the form of nanoparticles (NPs) in sunscreen formulations and decorative cosmetics.[52, 53, 56, 57] Formulations containing TiO_2 and ZnO NPs have been developed to provide prolonged stay of the substances on the skin surface on repeated and daily basis application. Although the formulations are intended to remain on the skin surface, concerns have been raised whether these nanomaterials penetrate into the skin on application due to their nano-scale nature. The penetration of ZnO into human skin in the 5-day use of sunscreen on the beach condition was reported.[57] Stable isotope ^{68}Zn was used in the sunscreen to distinguish the Zn from the formulation and this element was detected in the blood and urine of the volunteers. The compromised skin condition adds more concerns regarding risk assessment of the formulations.[58, 59] Baroli[60] argued that the real beach conditions (UV exposure, high hydration as a result of sea water bath, accidental scratches, formulation type of sunscreen) might have an impact on the potential of ZnO and TiO_2 in the sunscreen to penetrate into the skin. This argument was supported by a theory that the function of the skin barrier may weaken while exposed to sunshine due to the biological UV ray-induced skin repair processes[61]. Several in vitro cell culture studies reported that the small size and larger surface area of NPs may result in higher risk of toxicity when in contact with viable cells.[62, 63] ZnO NPs were reported to be taken up by primary human epidermal keratinocytes and induced cytotoxic and genotoxic responses.[64] However the question remains, do these NPs penetrate the SC to reach viable cells?

Quantum dots (QDs) are strong fluorescent semiconductor nanocrystals which are used for a wide range of purposes, from electronic displays to diagnostic tools.[65, 66] QDs are generally composed of cadmium/selenium (CDSe) as the core, with cadmium sulphide (CdS) or zinc sulphide (ZnS) as the shells. The skin can be accidentally exposed in occupational environments. Accidental topical exposure of QDs may potentially lead to QDs penetration into the skin. Ryman-Rasmussenn et al.[67] suggested that cationic QDs penetrated into viable epidermis of weanling pig although no QDs were detected in the receptor chamber of flow-through cells. In this

ex vivo skin penetration study, they utilised different shape and surface charges of QDs in buffers pH 8.3 or pH 9.0. Jeong et al[68] further reported that QDs penetrated through the SC, although the QDs were not detected in the deeper layer.

1.2.2 Controversy of nanomaterial skin penetration

Whilst the potential for nanomaterial (nanosolid) skin penetration remains an area of some controversy, the balance of research evidence demonstrates that nanoparticles exposed to intact skin do not penetrate into the skin. *In vitro* and *in vivo* studies on human skin revealed the absence of TiO_2 penetration in the skin.[69-71] Those studies confirmed that TiO_2 micro-nanoparticles remained on the outer surface of SC and on the orifice of hair follicles after application. Roberts's group[72-76] has consistently shown that the ZnO NPs did not penetrate into human skin at any conditions of sunscreen application, such as flexing and massage[74], occlusion and skin barrier impairment[75], and a range of formulations applied[72, 73], and repetitive administration of the sunscreen.[76] Those studies applied multiphoton tomography-fluorescence lifetime imaging (MPT-FLIM), a state of the art of imaging technology allowing high resolution on imaging deeper skin layers. This technology allowed real-time imaging of the nanoparticles whilst also assessing metabolic changes on the treated skin that could identify penetration related toxicity.

Prow et al.[77] demonstrated that QDs applied topically in the pH 7 medium were located at SC and furrows with no evidence of penetration into the viable human epidermis. This contrasted with Ryman-Rasmussen et al.[67] who reported the penetration of QDs into the viable epidermis of weanling pig. Prow et al.[77] suggested that the penetration seen in the Ryman-Rasmussen study was likely due to the high pH medium used, which might perturb the SC allowing the penetration of QDs.

1.3 Topical/transdermal delivery

Topical/transdermal delivery offers opportunities to deliver drugs more effectively and conveniently compared to oral and parenteral administration.[6, 29, 78-80] In contrast to oral administration, topical/transdermal delivery avoids the risks of drug instability and initial termination due to gastric acidity, intestinal and hepatic first pass elimination. Topical delivery offers the potential to target the active pharmaceutical ingredients (API) to the skin, whilst transdermal delivery can allow controlled plasma levels. The main obstacle of topical/transdermal delivery is the barrier of SC. The ideal characteristics of deliverables suitable for skin penetration are low molecular weight

(<500kDa), reasonable value of aqueous solubility and lipophilicity (log P 2-3), low melting point and are highly potent.[6, 29, 81]

1.3.1 Factors affecting penetration

Many factors contribute to the extent of molecules penetrate to and permeate through the skin and they can be categorised into material factors and skin factors. Material factors include physicochemical properties of the solute (such as molecular size, particle size, partition coefficient and solubility of solutes in SC) and the nature of vehicle/formulation (such as viscosity, vesicle/droplet size, elasticity/deformability, and composition).[28, 29] The influence of vehicle is further discussed in the section 1.3.3. Skin condition such as hydration state, age, anatomical site, ethnicity and gender may also play important roles in the skin penetration as it may affect the integrity of SC as the skin barrier.

1.3.1.1 Molecular and particle size

Molecular size determines maximum flux of skin permeation.[82, 83] Maximum flux Is defined as the permeation rate of pure substance in a saturated solution where the vehicle or the substance does not affect permeation.[84] Pugh et al. [85] demonstrated the inverse correlation between molecular size and skin permeation. Particle size has also shown the same tendency. The smaller the particle size, the higher permeation would be.[6] In addition, shape, charge, surface properties (coating and ligand type), and aggregation state may also influence the penetration of particles into the skin.[86]

1.3.1.2 Lipophilicity and solubility of solutes in SC

Drug transport into the skin involves solute partitioning from the vehicle into the SC intercellular lipid, diffusion in the lipophilic environment of the SC and another partition to the more hydrophilic viable epidermis.[87] The process is governed by the solubility and diffusivity of solutes. Sloan et al.[88] argued that optimal skin penetration can be achieved by solutes that have enough oil and aqueous solubility. Roberts's group showed that maximum permeability is dependent on the SC solubility of solutes. [89-92] A parabolic dependence of maximum flux on lipophilicity has been established in solute log P 1-4 (moderately lipophilic solutes) range.[93]

1.3.1.3 Skin hydration

Skin hydration can increase the permeation of solutes by increasing SC solubility of the permeant, which then increases permeant partitioning from the vehicle to the skin.[80, 94] An increase of skin hydration is inversely correlated with decrease of trans-

epidermal water loss (TEWL) values. Low skin hydration is shown in perturbed skin with high TEWL value. SC swelling and lipid rearrangement was also predicted although it has not been experimentally proved.[80]

1.3.1.4 Age

Intrinsic aging affects the skin structure[95], resulting in dermo-epidermal interface flattening, reduced number of Langerhans cells and melanocytes, atrophic dermis, loosen keratinocytes, and the changes in collagen, elastin and glycosaminoglycans.[28, 96] Although there is a decrease in epidermal thickness, the SC thickness and the SC proteins remain the same.[95, 97] However, the major lipid components in the SC, particularly ceramides, are significantly reduced with age.[98] These changes in skin aging reduce the TEWL values.[99] Despite these anatomical changes, permeation studies on estradiol, aspirin, caffeine, water, and nicotinates[100, 101] suggested that skin aging did not alter the skin permeation of this range of solutes. In contrast, the paediatric skin barrier, especially in newborns is still developing, thus the skin tends to be more permeable than adults.[102-105] This needs to be taken into account in developing a topical formulation aimed for children, particularly neonates, due to the possible risks of toxicity.

1.3.1.5 Anatomical site

Regional variation of ^{14}C-labeled hydrocortisone skin permeation has been studied on human skin, with the scrotal area showing 42-fold permeation compared to the ventral forearm, while the heel showed the lowest permeation.[106] A similar experiment was also conducted to investigate the effect of regional variation of 14C-labeled benzoic acid penetration in male volunteers at 6 anatomical sites, using tape stripping at 30 minutes after permeant application.[107] The head and neck showed a three-fold permeability compared to back skin. Such variations may be due to the SC thickness, skin pH, follicle density and diameter, sebum production and skin hydration level.[28]

1.3.1.6 Ethnicity and gender

Extensive research has been done on the effects of ethnicity on skin penetration and the majority studies revealed no significant difference of skin penetration with different ethnic groups[108-110]. Moreover, inter-individual differences in a certain ethnic group are greater than the ethnic group difference.[111]

Few studies reported the effect of gender on skin barrier function and those available provide results that are contradictory.[112] Reed et al.[113] suggested that there was no difference in skin barrier function between genders. Whilst a couple of groups revealed that the barrier integrity of the human female skin reduced on pre-menstrual

period[114, 115], Jacobi et al.[112] further suggested that any differences of skin barrier structure in different genders were likely due to different hormonal states. This should be taken into consideration when selecting volunteers for skin penetration studies.

1.3.1.7 Skin disorders

Skin disorders such as eczema, psoriasis, ichtyosis, acne vulgaris, impetigo, herpes simplex and fungal infections reduce the skin barrier as they compromise the SC.[116, 117] However, the compromising effect can be resolved when the disorder is properly treated.

1.3.2 Penetration/permeation enhancement

Many smart strategies have been developed to overcome the barrier property of the SC thereby increasing the permeability of the skin to drug molecules. Penetration into the skin is essential for skin targeting delivery, whereas sufficient permeation through the skin is required to access the cutaneous circulation and achieve transdermal delivery.

Ideally, penetration/permeation enhancement techniques reduce the skin barrier temporarily, with the barrier then recovering to minimise the risk of foreign material penetration into the skin or the excessive water loss from skin and ultimately, to maintain skin function. Safety assessment must be considered due to the potential of skin irritation risk. Increasing the penetration or permeation can be done in two areas of development: alteration/modification of the intrinsic properties of the solute (by developing prodrugs, ion-pairs, supersaturated solution, eutectic systems, and complexes[29]); or influencing the solubility or diffusion of the solute in the skin.

1.3.2.1 Physical penetration/permeation enhancement

Penetration/permeation techniques involve physical enhancement techniques, chemical enhancement technique, or in combination of both techniques. The main objective of physical enhancement is to enlarge the skin pores to facilitate more penetration. Physical permeation enhancement techniques include the application of electric current, ultrasound magnetic field, and nano-microneedles. Iontophoresis (electric current) and sonophoresis (ultrasound) have been extensively investigated and are briefly described below. The focus here is on the physical enhancement techniques that have been investigated in this thesis: magnetophoresis and microneedles.

Iontophoresis

Iontophoresis is a non-invasive physical permeation enhancement technique for ionised solutes involving an electromotive power generating small electric currents (0.5-20 mA).[118, 119] The mechanism of enhancement involves electrorepulsion (electromigration), electroosmotic and permeabilisation under the influence of the electric field.[120, 121] Electrorepulsion is the ion movement across the membrane whereby negatively charged low molecular drugs are repelled under the cathode while positively charged drugs are repulsed under the anode. Electroosmotic is based on volume flow on the negatively charged skin under the current flow[121] In addition to enhancing low molecular drugs such as lidocaine, ketoprofen, ketorolac, idoruxidine, vidarabine monophosphate, iontophoresis also successfully increased the permeation of peptides and proteins.[122, 123] Iontophoretic delivery system has been commercially developed to deliver fentanyl (E-Trans™, Alza), lidocaine-epinefrine (LidoSite™, Vysteris-FDA approved) and iontocaine (Phoresor™, Iomed).[121, 124]

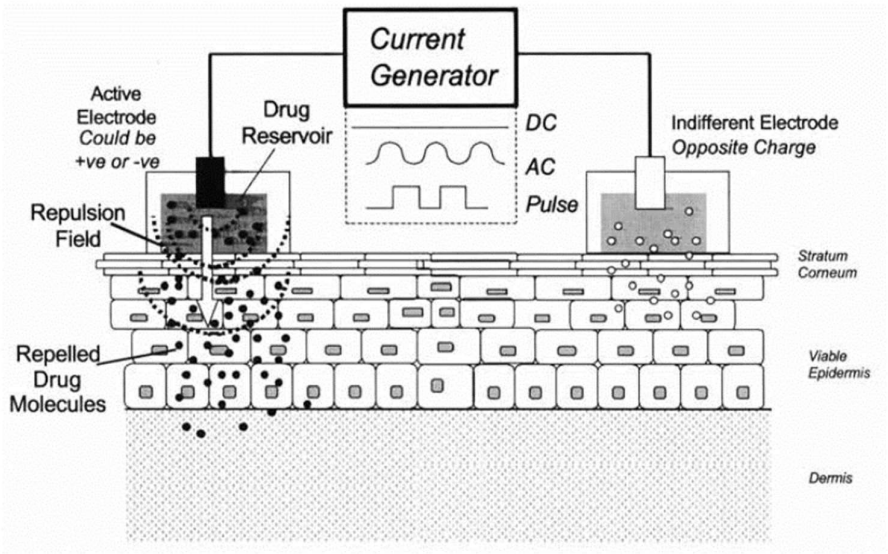

Figure 1.3 Iontophoretic delivery design. Reproduced from Cross et al.[119] with permission

Sonophoresis

Sonoporesis or phonophoresis is a physical enhancement technique using ultrasound in a range of 20kHz-16 MHz.[125] Sonoporesis was firstly introduced by Fellinger and Schmidt in polyarthritis treatment using hydrocortisone cream.[126] Low-frequency sonophoresis (frequency less than 100kHz) has shown transdermal enhancement of small molecules 1000-fold greater than therapeutic ultrasound (frequency of 1

Mhz).[127] Low-frequency sonophoresis enhances the permeation in two different ways: simultaneous sonophoresis and pre-treatment sonophoresis. Simultaneous sonophoresis involves concurrent application of ultrasound and the deliverables, whereas pre-treatment sonophoresis requires ultrasound treatment before deliveraboles application. Skin heating[128] and the formation and collapse of gaseous cavities, called acoustic cavitation[129], were reported as the mechanism by which low frequency sonophoresis enhances permeation.

Magnetophoresis

Magnetophoresis is defined as a physical enhancement technique using magnetic fields.[130] Magnetophoresis can be generated by static magnetic fields and pulsating magnetic fields. Pulsating magnetic fields generate an electrical current (electromagnetism), while static magnetic field do not[131], thus, the mechanism underlying any biological activities due to the application of static magnetic field does not relate to electrical matters. In 1845 Michael Faraday stated that organic materials are diamagnetic which respond to magnetic field.[131] This may produce diamagnetic repulsion whereby a topically applied solute is driven away from a magnet into the skin thereby enhancing the skin penetration of that applied material.

Static magnetic fields

Murthy's group investigated the effect of stationary magnetic fields in enhancing skin permeation of benzoic acid, salbutamol sulphate and terbutaline sulphate, lidocaine hydrochloride (HCl).[130, 132-134] They suggested that the enhancement of benzoic acid which is diamagnetically susceptible in nature, was due to the increase of diamagnetic flow, as benzoic acid was repelled away from the magnet and into the skin.[130] Murthy's group then continued to explore the mechanism underlying the magnetophoresis using static magnetic field with lidocaine as the model of permeant.[134] On the *in vitro* Franz diffusion cell study using porcine epidermis, they utilised two neodymium magnets located on either side of the donor with a distance of 2 mm from the epidermis to generate magnetic cells strengths (30, 150, and 300 mT). There was no significant difference of the amount of lidocaine permeate through the epidermis, with or without the magnetic fields in magnetic pretreatrment. In other words, there was no effect of magnetic fields in enhancing skin permeation of lidocaine if the magnet was not in contact. They also showed that the epidermal barrier was not altered by static magnets, based on no change in TEWL or in the Fourier-transform infrared spectrum (FTIR) in skin exposed to the magnetic field compared to control. In contrast, they reported a 2.7-fold increase of ^{3}H-water permeation through the porcine epidermis, suggesting

that magnetic field gradient resulted in the flow of water molecules. Based on their studies they concluded that the mechanism underlying skin permeation enhancement by a static magnetic field was magnetokinesis which is a combination of magnetohydrokinesis and diamagnetic repulsion.[134]

Electromagnetic fields

Dermaportation is a physical skin penetration/permeation enhancement technology involving pulsed electromagnetic fields (PEMF) which generate an electric current. This technology was developed by OBJ Pty Ltd, a biotechnology company in Perth, WA (www. obj.com.au) and is the underlying technology for the personalised cosmetic range under development with Procter & Gamble. Benson's group have demonstrated the enhancement of 5-aminolevulinic acid (5-ALA), lidocaine HCl, naltrexone HCl, diclofenac diethylammonium salt and the dipeptide Ala-Trp into and across human skin by PEMF technology.[135-139] The technology used a 3-voltage power to produce an asymmetrical pulse packet type electromagnetic field consisting of repeating quasi-rectangular electromagnetic energy of 400μs with a maximum peak of magnetic field strength of 5mT. The electromagnetic pulse was transmitted through the coils which were set on the exterior of the donor compartment of a Franz diffusion cell at 7mm above the skin surface. Thus, there was no contact between the magnetic coil and the skin or formulation. In the case of both 5-ALA[136] and Ala-Trp[137], there was a significant initial "push" of transdermal permeation over the first 20 minutes to 2 hours, which was then followed by a significant increase of permeation during PEMF application.

The permeation of Naltrexone HCl was enhanced 5.7-fold across human epidermis by Dermaportation[139], with an enhancement ratio (ER) of 6.5 over 4-hour-Dermaportation application and ER of 5.3 after Dermaportation was removed. This suggests that the PEMF has a residual effect in the skin which may be related to epidermal barrier disruption due to the PEMF application. In a parallel experiment, there was no significant difference of Naltrexone diffusion through a silicone membrane with the application of Dermaportation. Again, this suggests that the mechanism of permeation enhancement was skin structure related and that magnetokinesis was not the major mechanism underlying PEMF enhanced Naltrexone permeation. Further evidence was provided by the visualisation of PEMF induced permeation of 10 nm gold nanoparticles into human epidermis by multiphoton tomography, as the nanoparticles did not permeate when applied passively.[139]

Magnetic film array

Magnetic film array (OBJ Pty Ltd) consists of multiple magnetic elements which are arranged on a thin flexible polymer to generate complex 3D magnetic gradients with the maximum magnetic field strength of 40 mT, and 2T/m^2 total magnetic gradient. The potential of a magnetic field array (ETP 008) to enhance the penetration of urea (a moisturizing agent) in a hydrogel formulation was evaluated ex vivo and in vivo.[140] The *ex vivo* permeation increased approximately fourfold in comparison to passive diffusion of a non-magnetic occlusive film of 5% urea in gel and there was a fifty percent reduction of lag time. Epidermal thickness in a human volunteer, measured by Optical Coherence Tomography (OCT) to monitor hydration, increased by 16% and 11% at 30 and 60 minutes, respectively, compared to increases of 3% and 6% for non-magnetic film application.[140] This technology will be investigated in the current research.

Microneedles

Microneedles (MN) are arrays of micron-sized projections, with the length of no more than 1mm and the external diameter of less than 300 µm, applied/inserted into the skin with the specific aim to disrupt the SC.[141-143] MN are designed to insert the skin to a depth up to 200 µm, not to reach the dermis containing nerves, thereby minimizing pain feeling during application.[144] MN are ideal for overcoming the delivery problems of large molecules such as vaccines, protein and peptides.[142, 145-147] There is a substantial body of literature exploring the potential of MN and the factors affecting delivery in the skin.[143, 145, 148-150] MN have been shown to administer large molecules at significantly higher transdermal flux enhancement compared to conventional topical/transdermal systems.[151] In comparison to conventional injections they offer minimal invasion, less risk of microbial infection, and relatively painless administration.[143, 148]

The simplest form is solid MN, termed “poke and patch”, designed to be used as a pre-treatment to perforate the skin prior to applying a topical solute.[142, 152, 153] Other types are coated MN (“coat and poke”), MN designed to dissolve in the skin (“poke and release”), and hollow MN (“poke and flow”) as summarised in Figure 1.4.

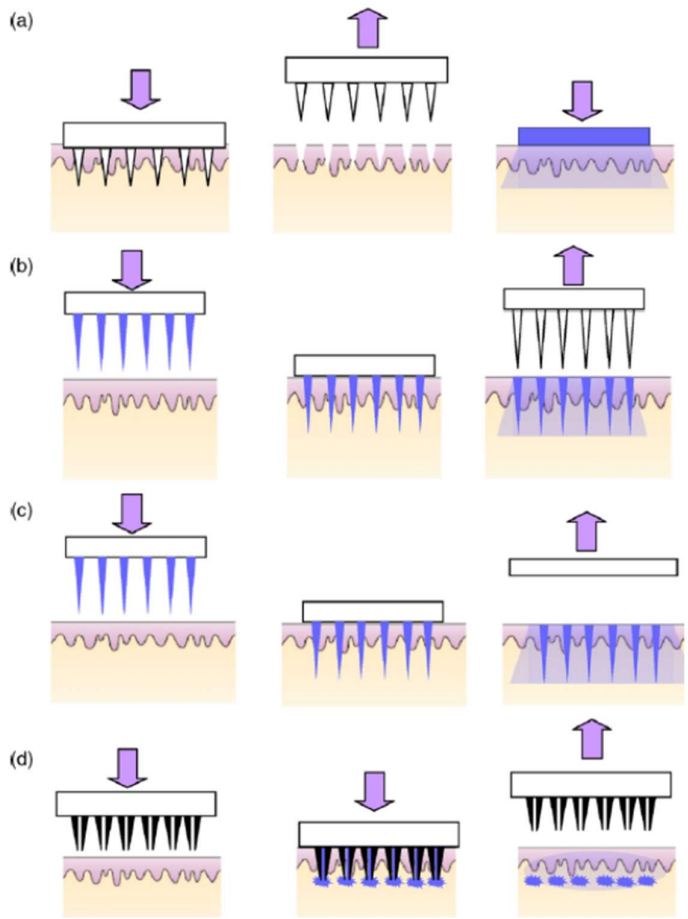

Figure 1.4 Schematic representative of solid MN administration. (a) "poke and patch", (b) "coat and poke", (c) "poke and release", (d) "poke and flow" Reproduced from Arora et al.[154] with permission

1.3.2.2 Chemical penetration/permeation enhancement technique

Chemical penetration enhancement can be carried out by SC manipulation or through drug and vehicle property optimisation.[29] Lipid-protein partitioning (LPP) theory can be used to get better understanding of the mechanism underlying the enhanced permeability by chemicals.[155, 156] In principle, chemical penetration enhancer can be utilised to manipulate the SC, such as disrupting the intercellular structure of lipid bilayers, interacting with the intracellular protein of SC, and improving the solubility and partitioning of the permeant into SC and deeper layers.[156-159] The enhancement can also be achieved by increasing the thermodynamic activity in the formulation (increasing the concentration of drug or lowering the solubility of the drug).[160]

A wide variety of chemicals can be used to manipulate the barrier function of the SC including water (a hydrating agent), fatty acids, alcohols, esters, essential oils and terpenes, surfactants, azone and its derivatives, dimethylsulfoxide (DMSO), glycols,

glycol ethers, pyrrolidones, sulphoxides, octyl salicylate, padimate O (PADO), and 2-(1-nonyl)-1,3-dioxolane (ND).[29, 156, 161-164]

1.3.3 Nanocarriers in topical/transdermal delivery

Extensive research has been carried to develop many types of cutaneous nanocarriers with the same objective to enhance the penetration/permeation of deliverables into the skin. Lipid-based nanocarriers were developed based on the role of lipid to aid the molecules partition-diffusion process into the skin and to occlude the skin, thereby increasing skin hydration and enhancing penetration. Vesicle-based nanocarriers were designed to produce nano-scale entrapment/encapsulation system, which could maintain the stability of the molecules encapsulated and deliver the substance into and through the skin in a reasonable amount. A number of nanocarriers will be further discussed on this review.

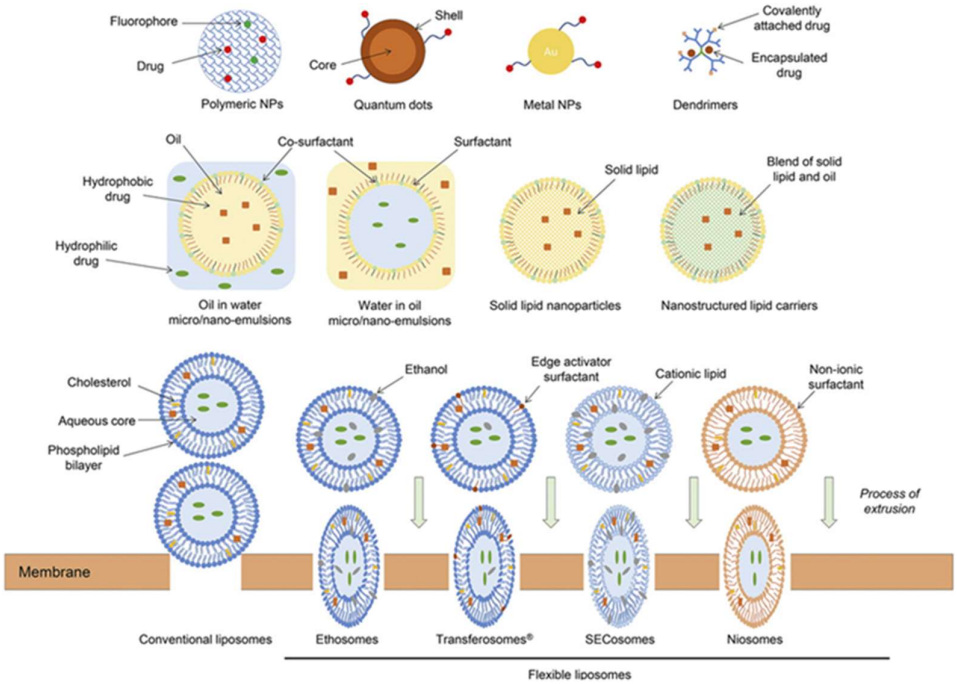

Figure 1.5 Schematic representation of topical-transdermal nanocarriers. Adapted from Roberts et al.[6] with permission

1.3.3.1 Lipid-based nanoparticles

Lipid-based nanoparticles as topical and transdermal nanocarriers are classified as solid lipid nanoparticles (SLN) and nanostructured lipid carriers (NLC).

SLN are spherical solid particles composed of mixtures of solid lipids or lipid-like materials dispersed in aqueous medium, which can further incorporate active ingredients for a range of drug delivery systems.[165, 166] SLN combine the properties of

lipid and polymeric nanoparticle systems. NLC are the second generation of SLN, involving blends of solid lipids and liquid lipids which stabilised by mixed surfactants.[165] Both SLN and NLC offer advantages including biocompatibility and biodegradability leading to excellent tolerability, prolonged and controlled release, excellent protection and stability enhancement, which support the marketing as cosmetic products.[166] Although SLN show excellent property of occlusion thus better skin hydration, NLC improve the SLN properties regarding drug loading and entrapment efficiency during storage[166, 167]. Das et al.[168], in their study of clotrimazole-loaded SLN and NLC, confirmed the superiority of NLC to SLN with respect of the physical stability at 25°C and release rate stability over 3-month storage. Zoubari et al.[169] when investigated the effect of drug solubility and the crystallinity of lipid on the release of diclofenac from lipid nanoparticles, reported that the release rate of diclofenac was dependent on the solubility in the lipid. They further indicated that a lipid with highly ordered crystalline structure released slower than the less ordered crystalline of mixtures of lipids.

A summary of the composition, method of fabrication, physical characteristics and skin penetration/permeation study of topical SLN and NLC is presented in Table 1.1.

Table 1.1 Representatives of SLN and NLC in topical/transdermal delivery

Formulation type - Compound delivered	Ingredients Drug load (DL)	Method of fabrication	Physical characteristic			*In vitro/in vivo* Penetration/permeation study	Ref.
			Size (nm)	Zeta Potential (mV)	PDI		
SLN							
Quercetin	Compritol ® 888 (glyceryl dibehenate) Precirol ®ATO 5 (glyceryl palmitostearate)	Ultrasonication	311.5 ± 5.5	-34.24 ± 1.29	0.232	*In vitro* Franz diffusion cell study Full thickness human skin Donor: 0.5mL of formulation Receptor fluid: 1% Tween 20 in PBS pH 7.4 **Result**: No quercetin in the receptor (no permeation) Skin uptake: ± 24 µg/g	[170]
Retinyl palmitate (RP) ***In favour of NE***	Compritol ® ATO 888 5% Span ® 80 5% DL: 1%	Ultrasonication	271.5 ± 2.4	-55.26 ± 1.27	0.475	*In vitro* Franz diffusion cell study Dermatomed human skin (400µm thick) Donor: ~ 200 µg RP Receptor fluid: Ethanol:transcutol P® (50:50) **Result:** Cumulative amount of RP permeated at 24h (µg): 3.64 ± 0.28 Flux (µg/h): 0.10 ± 0.05 Skin retention (µg/cm^2/mg): 0.06 ± 0.04	[171]

Vitamin E (α-tocopherol and α-tocopherolacetate)	*SLN ™, Lipopearls ™* Cetylpalmitate 15% Tego Care 450 1.8% DL: 5%	Hot homegenization	270-280	n. i	0.04-0.05	*In vivo* stratum corneum (SC) stripping Human volunteers (3 persons aged 20-30) Donor dose: 0.25 mg vitamin E /cm^2 (20µL) on 4cm^2 area for 30 min 5 tape stripping (under 1 kg pressure each) **Result:** The cumulative percentage of vitamin E in SLN was doubled than the control (vitamin E dissolved in isopropanol)	172
8-methoxypsoralen (8-MOP)	Precirol 12% Myverol 0.2% Pluronic F68 2.4% Water DL: n.i	Hot homogenisation	296.6 ± 49.5	-40.0 ± 5.9	n. i	*In vitro* Franz diffusion cell study Full thickness dorsal skin of nude mice Donor: 0.5 mL Receptor fluid: 30% ethanol in PBS pH 7.4 **Result:** Flux (nmol/cm^2/h): 67.17 ± 8.89	173
Benzophenone-3 (BP-3)	Suppocire AIML® 10% Montane 80 ® 6% Montanox 20 ® 4% Deionised water up to 100% DL: 5%	Hot emulsification and ultrasonic homogenisation	412 ± 15	-40.2 ± 3.6	0.242 ± 0.16	*In vitro* Franz diffusion cell study Dermatomed porcine ear skin (600 µm thick) Donor: 1mL of 5% BP-3 Receptor fluid: composition of albumin and PBS **Result:** Flux and skin distribution are similar to the control (BP-3 albumin aqueous solution)	174

Resveratrol (RSV)	**RS4** Compritol 888 ATO 300mg Poloxamer 188 150mg Tween 80 75mg Bidistilled water DL: 0.04%	High shear homogenisation	161.4 ± 2.7	-15.3 ± 0.4	0.263 ± 0.05	*In vitro* Franz diffusion cell study Rat abdominal skin Donor: 200µL Receptor fluid: 50% ethanol in water **Result:** No permeation of RSV observed Skin uptake at 24h (µg/cm^2): 1.55 ± 0.13	[175]
RSV	**F1.RES** Stearic acid 5% Poloxamer 407 3.5% Methylparaben 0.18% Propylparaben 0.02% Distilled water up to 10mL **F2.RES** Same composition above added with Soy phosphatidylcholine (SPC) 1.2% DL: 0.1%	Sonication	F1: 155.50 ± 0.26 F2: 166.23 ± 0.94	F1: -2.60 ± 1.27 F2: -2.66 ± 0.33	F1: 0.140 ± 0.02 F2: 0.196 ± 0.02	*In vitro* Franz diffusion cell study Pig ear skin Donor: 0.3mL Receptor fluid: 2% polysorbate 80 in water **Result:** Cumulative amount of RSV permeated at 24h F1: 45.26 ± 34.88 F2: 18.61 ± 16.99	[176]

Tretinoin (TRE)	**SLN based gel** Glyceryl monostearate (GMS) Epikuron 200 Benzyl alcohol Tween 80 Tween 20 Distilled water Carbopol ® DL: 0.05%	Emulsification solvent diffusion	400-500 (1-2% GMS)	n. i	0.65-0.8 (1-2% GMS)	*In vitro* modified Franz diffusion cell study Hairless abdominal Wistar rat skin Donor: 0.45g of gel Receptor fluid: PBS pH 7.4 containing albumin **Result:** Cumulative amount of TRE permeated at 12h (% of applied dose): 6.414 ± 1.031 Flux (ng/cm^2/h): 75.6 7.21, Not significantly different from the control (marketed cream Retino-A®)	[177]
RSV	**Formulation 2** Cetyl palmitate 10% Sesame oil 5% Tween 80 4% Water 80.8 DL: 0.2%	Microfluidisation (high pressure pneumatic homogenisation)	102-311	25-49	n. i	*In vitro* Franz diffusion cell study Stratum corneum (SC) of human cadaver skin Donor: 0.7 mL Receptor fluid: deionised water **Result:** Cumulative amount of RSV permeated through SC at 24h: 0.04 ± 0.01 µg/mL Control (0.2% RSV in ethanol-propylene glycol): 0.012 µg/mL Enhancement ratio (ER):3.33	[178]
Isotretinoin (IT)	Formula D PRECIROL ATO 5 3% Soybean lecithin (SL) 4% Tween 80 4.5% Water 88.44% DL: 0.06%	Hot homogenisation method	42.7 ± 5.50	-13.73 ± 1.51	0.258 ± 0.016	*In vitro* vertical diffusion cell study Full thickness abdominal rat skin Donor: 1g Receptor fluid: 30% ethanol in saline **Result:** No permeation of IT observed Skin uptake: 3.65 µg	[179]

Penciclovir	GMS 3% Egg-phosphatidylcholine 1% Poloxamer 188mg 2.5% Water 3.8mL DL: 0.15%	Double (W/O/W) emulsion	254. ± 9 8.2	-25 ± 0.05	n. i	*In vitro* Franz diffusion cell study Full thickness abdominal male Wistar rat skin Donor: 800µL containing 1.2mg penciclovir Receptor fluid: saline **Result:** Flux (µg/cm^2/h): 7.67 ± 0.19 Cumulative amount of penciclovir permeated at 12h (µg/cm^2): 88.44 ± 4.19 Control (commercial cream containing 1.2mg penciclovir) Flux (µg/cm^2/h): 3.31 ± 0.37 Cumulative amount of penciclovir permeated at 12h (µg/cm^2) : 41.07 ± 3.07 ER: 2.32	[180]
Triptolide (TP)	**Formulation B** Tristearin glyceride 5% SL 1.2% Polyethyleneglycol (400) monostearate 3.6% Water DL: 0.025%	Sonication	123 ± 0.9	-45	0.19	*In vitro* Franz diffusion cell study Full thickness abdominal rat skin Donor: 1mL Receptor fluid:10% ethanol in saline **Result:** Flux (µg/cm^2/h): 3.1±0.4 Control: TP solution (0.025%) Flux (µg/cm^2/h): 0.9±0.1 ER: 3.4	[181]
Aceclofenac (ACF)	**Hydrogel based SLN** GMS SL Tween 80	Ultrasonic emulsification	189±9.2	-32.51±0.12	0.162±0.02	*In vitro* Franz diffusion cell study Full thickness abdominal Sprague-Dawley rat skin Donor: n.i	[182]

	Water Carbopol ® 934 DL: n. i					Receptor fluid : Phosphate buffer pH 6.5 **Result:** 39.32±3.4% of dose permeated through the skin after 24h Skin stripping (μg/cm^2): 25.31±4.8 Skin uptake (μg/cm^2): 22.33±1.43 **Control (ACF gel)** 30.64±4.3% of dose permeated through the skin after 24h Skin stripping (μg/cm^2): 8.71±0.61 Skin uptake (μg/cm^2): 10.72±0.42 ER: 2.08 (skin uptake	
NLC							
Quercetin	Compritol ® 888 0.45g Oleic acid 0.05g Mixed surfactants in water 20mL (Tween 20 2.5% Dioctyl sodium sulfosuccinate 0.1%) DL: 0.025% & 0.05%	Ultrasonication	281.9 ± 2.9	-36.57 ± 2.67	0.306	*In vitro* Franz diffusion cell study Full thickness human skin Donor: 0.5mL of formulation Receptor fluid: 1% Tween 20 in PBS pH 7.4 **Result:** No quercetin in the receptor (no permeation) Skin uptake: ± 24 μg/g	[183]
RSV	RN1 Compritol 888 ATO 285mg Poloxamer 188 150mg Tween 80 75mg Miglyol 15mg Bidistilled water DL: 0.04%	High shear homogenisation	90.58 ± 1.7	-16.1 ± 0.1	0.280 ± 0.06	*In vitro* Franz diffusion cell study Rat abdominal skin Donor: 200μL Receptor fluid: 50% ethanol in water **Result:** No permeation of RSV observed Skin uptake at 24h (μg/cm^2): 1.99 ± 0.17	[175]

Tadalafil (TAD)	**F4** GMS : Oleic acid =1:1 Tween 80 3% Carbomer 940 0.5% Ethanol 30% in water Limonene 5% DL:	Hot ultrasonication	190.6 ± 5.1	-35.4 ± 4.5	0.241 ± 0.035	*In vitro* Franz diffusion cell study Spargue-Dawley rat dorsal skin Donor: 500µL Receptor fluid: 1% Tween 80 in phosphate buffer pH 7.4 **Results:** Flux: 1.463 µg/cm^2/h Enhancement ratio (ER): 4.8 Control: TAD solution (TAD in 30% ethanol) Flux: 0.307 µg/cm^2/h ER: 1	[184]
8-methoxypsoralen (8-MOP)	**NLC-PF** Precirol 6% squalene 6% Myverol 0.2% Pluronic F68 2.4% Water **NLC-Tw** Precirol 6% squalene 6% SPC 0.2% Tween 80 2.4% Water DL: n.i	Hot Homogenisation and sonication	210.2 ± 14.3 172.7 ± 1.2	-46.0 ± 2.2 -42.3 ± 2.0	n. i n. i	*In vitro* Franz diffusion cell study Full thickness dorsal skin of nude mice Donor: 0.5 mL of saturated solubility dose Receptor fluid: 30% ethanol in PBS pH 7.4 **Result**: NLC-PF Flux (nmol/cm^2/h): 96.71 ± 6.22 NLC-Tw Flux (nmol/cm^2/h): 107.51 ± 8.57 Control (lipid emulsion) Flux (nmol/cm^2/h): 38.31 ± 5.31 ER: 2.51 (NLC-PF) 2.8 (NLC-Tw)	[173]

Terbinafine HCl (TH)	**Gel based NLC** GMS Labrasol Pluronic F-127 Ratio solid:liquid lipid= 6:4 Manitol 5% Carbopol ® 940 1% DL: 1%	Hot emulsification	128 ± 4.5	n. i	0.211 ± 0.012	*In vitro* Franz diffusion cell study Full thickness Wistar albino rat abdominal skin Donor: 20mg drug Receptor fluid: 0.8% Tween 80 in PBS pH 7.4 **Result:** Cumulative amount of TH permeated at 12h (%): 23.16 ± 2.33 Skin uptake (%): 83.65 ± 2.51 Control (1% marketed cream) Cumulative amount of TH permeated at 12h (%): 16.72 ± 3.67 Skin uptake (%): 69.41 ± 1.85	185
Benzophenone-3 (BP-3)	Suppocire AIML ® 10% Oleic acid 5% Montane 80 ® 4% Montanox 20 ® 6 Deionised water up to 100% DL: 5%	Hot emulsification and ultrasonic homogenisation	315 ± 12	-43.2 ± 2.0	0.362 ± 0.06	*In vitro* Franz diffusion cell study Dermatomed porcine ear skin (600 µm thick) Donor: 1mL of 5% BP-3 Receptor fluid: composition of albumin and PBS **Result:** Flux and skin distribution are similar to the control (BP-3 albumin aqueous solution) but Nanostructured Polymeric Lipid Carrier with 0.5% poly-ε-caprolactone and nanocapsule (NPLC added with Plurol oleique and Poloxamer 188) were the best in terms of skin retainment	174

Coenzyme Q10 (Q10)	**Q10-loaded NLC 1** Cetyl palmitate 7.23% Miglyol® 812 0.38% Tego® Care 450 1.8% Water DL: 2.4%	High pressure homogenisation	225-250	n. i	0.1-0.2	*In vitro* Franz diffusion cell study Stratum corneum and epidermis (SCE) of human skin Donor: n.i Receptor fluid: 5% Labrasol in PBS pH 7.4 **Results** At 8h, the cumulative amount of Q10 permeated from NLC 3 was higher than from NLC 1. The opposite result occurred in skin penetration of Q10.	[186]
	Q10-loaded NLC 3 Cetyl palmitate 6.46% Miglyol® 812 1.14% Tego® Care 450 1.8% Water DL: 2.4%		225-250	n .i	0.1-0.2		
Q10	**CoQ10-loaded ultra-small NLC (usNLC)** Cetyl palmitate 1% Cetiol® OE 4% Span® 20 2.5 Tween® 80 2.5 Water 85% DL: 5%	Hot high-pressure homogenisation	81	-34.5	0.132	*In vitro* Franz diffusion cell study Dermatomed porcine abdominal skin (750µm thick) Donor: Receptor fluid: 5% Labrasol in PBS pH 7.4 **Results:** Trend of Q10 permeation: usNLC>NLC Trend of Q10 penetration: usNLC<NLC Data were not statistically significant	[187]
	CoQ10-loaded NLC (NLC) Cetyl palmitate 14.45% Miglyol® 812 0.75% Tego care® 450 1.8% Water 78% DL: 5%		226	-54.1	0.087		

1.3.3.2 Vesicle-based nanocarriers

Liposomes are colloidal particles of single or multiple layers of spherical phospholipid vesicles, with or without cholesterol, containing hydrophilic interior design which aims to encapsulate both hydrophilic and lipophilic molecules.[29] Hydrophilic molecules can be encapsulated in the vesicles, while the hydrophobic molecules can attach on outer bilayers of liposomes.[188] Topical liposomes were initially introduced by Mezei and Gulasekharan[189] for skin delivery of triamcinolone acetonide, achieving four times penetration compared to a conventional ointment at the same concentration. The main component of conventional liposomes is phosphatidylcholine (PC) derived from egg yolk or soybean which self-associated into multilamellar, small unilamellar, or large unilamellar vesicles. The natural source is in priority to avoid the toxicological issues of the synthetic ones.[188] The similarity of the structure of the lipid bilayer in liposomes with the corneocyte lipid bilayer in the SC facilitates more efficient penetration. Apart from that, low gel-liquid crystal transition temperature (Tm) is more preferred.[190] The molecules in a 'gel state' of liposomes, which are rigid, tend to accumulate on the skin and permeate less. The form of liquid crystalline of liposomes is desirable as it is more flowing and flexible. Natural lipids show low Tm. Cholesterol was added to increase the rigidity of liposomes thereby stabilising the structure, although in some cases it can reduce the permeation of the molecules to the skin.[190] Mechanism of liposomal drug delivery was reported due to the liposome accumulation and adhesion on the SC, possible interaction of associated molecules with SC and thermodynamic state of liposomal bilayers.[191] Although liposomes have been applied to deliver macromolecules such as vaccines, interferon and genes, the drawbacks of liposomes should be taken into consideration. Structural stability and deformability of liposomes are a couple of concerns in developing this delivery system. Liposomes are prone to leaking and less flexible to enter the SC.[192, 193] Due to these concerns, many efforts have been made to create smarter '-osomes' which facilitates flexibility. Transfersomes® (flexible liposomes), ethosomes, SECosomes, niosomes, invasomes, and PEVs are flexible vesicles, composed of materials which are self-associated to form stable vesicles, allowing sufficient shape deformability to squeeze through intact SC.

Transfersomes® are flexible liposomes originated by Cevc's group[193-196] composed of surfactants (mainly sodium cholate) which acts as the edge activators, cholesterol as rigidity improver and ethanol (3-10%). Edge activators facilitate the transfersomes® to flexibly squeeze individually in between corneocytes of SC to get through deeper layers of the skin. Transdermal gradient due to the water content disparity between

hydrated SC and aqueous viable epidermis appears to be the driving force of the penetration.[27, 193, 195-197] Whilst conventional liposomes get dehydrated and fuse to release the deliverables on the skin surface, Transfersomes® do not dehydrate as they squeeze and get into the deeper layers following the hydration gradient. Cevc et al.[198] suggested that at least 50% (of applied dose) of insulin was transported across NMRI mouse skin using transfersomes. El Maghraby et al.[27] demonstrated that oestradiol-loaded ultradeformable liposomes could enhance the permeation of oestradiol for about 17-fold under occlusion, while the conventional liposomes could only enhance 9-fold. Encapsulation of DNA plasmid for hepatitis B-antigen in cationic transfersomes has shown stronger immune response on Balb/c mice compared to control of naked plasmid DNA solutions in every 2-week time points from 2 to 8 weeks, with similar titration value of antibodies to the intramuscular injection of DNA plasmid after 6 weeks.[199]

Ethosomes are liposomes which mainly contain high concentration alcohol (up to 50%) thereby providing fluid state phospholipid bilayers with high permeability.[192] The alcohol acts as the edge activator to convey the deformability of ethosomes to be flexibly pass through the SC pores. Zhang et al.[200] demonstrated the superiority the psoralen-loaded ethosomes containing 0.2% psoralen, 5% Lipoid S 100 and 40% ethanol. The ethosomes transdermal flux and skin deposition were 3.50 and 2.15 times larger than conventional liposomes, respectively. A recent ethosomal formulation containing raloxifene HCl was developed by Mahmood et al.[201]. The transdermal flux was 21 times higher than the conventional liposomes. The mechanism of penetration enhancement was assumed by loosening the corneocyte layers tight conjugation due to high amount of the ethanol.[202] Although ethosomes have proved massive enhancement of permeation, the high content of ethanol may raise an issue of skin dryness and irritation.

SECosomes were nanosomes introduced by Geusens et al.[203] by combining the 'lipid fluidizing components' which were surfactant and ethanol, and 1,2-dioleyl-3-trimethylammonium propane chloride (DOTAP) as cationic lipid. This lipid replaced the conventional phospholipid in liposomal formulation. This invention, which later was called SECoplexes, was dedicated to deliver siRNA and anti-miRNAs cutaneously for psoriasis management.[203-205] SECosomes are basically a combination of Tranfersomes® and ethosomes features. The surfactant (sodium cholate) and ethanol were acting as the edge activator to facilitate the flexibility of the system and maintain the nano-size of the vesicles. [206-208] Cholesterol was added to stabilize the system. Zeta potential was in positive value due to the nature of DOTAP which

selected to enhance the interaction with negatively charge nucleic acids. This cationic lipid was also capable to protect siRNA from degradation and enhance the efficiency of transfection.[209]

Niosomes are vesicles composed of non-ionic amphiphiles in a hydrating medium which is structurally supported by cholesterol using energy input.[210] Niosomes have been demonstrated as excellent topical nanocarriers for drugs and cosmetics as they offer safety, biocompatibility, better stability, lower production cost, and higher yield compared to liposomes.[210-215] Amphiphiles with one or two hydrophobic alkyl, perfluoroalkyl or steroidal groups are usually employed in the formation of niosomes.[210] Cholesterol was used to obtain homogeneous dispersion of niosomes[216] as well as a vesicle stabilizer.[212] Balakrishnan et al.[214] demonstrated minoxidil-loaded niosomes composed of Brij™ or Span™ and cholesterol to treat Androgenetic alopecia. The niosomes potentially enhanced the permeation of minoxidil across hairless mouse skin due to the surfactant nature and the size of vesicles. Fang et al.[217] when developing enoxacin-loaded niosomes, suggested niosomes made from Span™ 40 or Span™ 60 were relatively more stable compared to liposomes. Pando et al.[218] indicated that ethanol injection modified method (EIM) was relatively superior to thin film hydration-sonication (TFH-S) method in providing resveratrol (RSV) niosomes with smaller size, smaller particle distribution index, and better stability compared to TFH-S. EIM also generated more effective RSV skin penetration (up to 21%) with both oleic and linoleic acid as enhancers than TFH-S.[218]

Invasomes consisted of unsaturated phospholipids (high % PC of soybean lecithin), ethanol, and terpene mixtures.[81, 219] The choice of unsaturated phospholipids was based on the low Tm, which resulted in the liquid crystalline form of liposomes. As liquid crystalline is superior to gel thermodynamic state (due to its flexibility)[220-222], it is important to select phospholipid with this liquid crystalline character.[81] Ethanol was added to fluidize the lipid bilayer to mimic the SC lipid fluidisation.[192] This composition was equipped with a mixture of terpenes to increase the elasticity of the liposomes. Terpenes are also known as potent chemical enhancers.[223-225] Dragicevic-Curic et al.[226], developed temoporfin-loaded invasomes for topical application, that were superior to liposomes in terms of physical stability and the penetration of temoporfin in human skin *in vitro*. The invasomes were fabricated using unsaturated soybean lecithin, ethanol, PBS pH 7.4 and a mixture of terpenes (cineole, citral and D-limonene) in concentration of 0.5% and 1%. Significant penetration enhancement of temoporfin was obtained with invasomes containing 1% terpenes. Trauer et al.[227], when investigated the depth of penetration of rigid liposomes and the invasomes in

full thickness human skin, revealed that the invasomes penetrated deeper than the liposomes in non-occluded system, although the size of invasomes were larger than that of the liposomes. The invasomes (flexible liposomes) composed of soybean lecithin, ethanol and mixed of terpenes (limonene:citral:cineol = 10:45:45 by volume) whereas the rigid liposomes were prepared from 1,2-dipalmitoyl-sn-glycero-3-phosphocholine (DPPC) and 1,2-dipalmitoyl-sn-glycero-3-phosphoglycerol, sodium salt (DPPG). Amnuaikit et al.[228] indicated that invasomes and transfersomes significantly enhanced the permeation of phenylethyl resorcinol across newborn pig skin, although the enhancement effect of invasomes was lower than transfersomes. Invasomes contain 1% D-limonene and 10% ethanol whereas transfersomes involved 15% sodium deoxycholate as the edge activator. The enhancement of invasomes and trasfersomes were reported 2.33-fold and 3.39-fold, respectively.

Penetration enhancer-containing vesicles (PEVs) involve the benefits of a combination of soy phosphatidylcholine or soybean lecithin and penetration enhancers (such as Transcutol®, Labrasol®, Oramix™ NS10, glycerol, propylene glycol and polyethyleneglycol 400) to enhance the penetration and permeation of molecules, into and through the skin.[229-231] Minoxidil was the first drug model for transdermal delivery of PEVs developed by Fadda's group[229, 232]. In comparison of PEV-1 (containing Labrasol), PEV-2 (containing Transcutol) and PEV-3 (containing cineol) they revealed that in terms of deformability and skin deposition of minoxidil, the order of magnitude was PEV 1 > PEV 3 > PEV 2. Fadda's group has further consistently developed the PEVs formulation of diclofenac[230, 233], tretinoin[234], quercetin.[235] Overall, PEVs were claimed to be potential as skin penetration enhancer due to the interaction of highly fluidised membrane with intercellular SC lipids. [231]

1.3.4 Topical and transdermal micro and nanoemulsion

1.3.4.1 Terminology

Microemulsion (ME) is a typical emulsion system involving dispersion of oil in water or *vice versa*, stabilised by surfactant with the addition of cosurfactant. ME is clear, isotropic, and thermodynamically stable.[236, 237] MEs exist in the form of equilibrated phases such as: oil-continuous, water-continuous, and bi-continuous phases. Although called as 'microemulsion', the clarity or transparency of ME indicates that the size of droplets is in the range of nanometer. This is due to high concentration of surfactant or mixed of surfactants, which spontaneously disperse the oil and aqueous components. Nanoemulsion (NE) also composed of oil, water, surfactants or mixed surfactants and cosurfactants. Although NE droplet size is also in nanoscale, most

NEs form a non-equilibrium state thermodynamically. NE will undergo phase separation by the time. As the kinetics of NE destabilisation is slow (due to minute size of the droplets), NE is considered as kinetically stable. Ostwald ripening is the dominant destabilizing mechanism observed in NE.[237, 238] NE generally needs high energy in preparation, although NE can also be fabricated by spontaneous emulsification.[237] Although both ME and NE are relatively homo-dispersed (poly dispersity index <10%), the prominent difference between both is the thermodynamic stability.[239]

Anton et al.[237], Mc Clements et al.[239], and Gupta et al.[240] have demonstrated a thorough review regarding the terminology, critical property differences and the formation of ME and NE, which can be summarised in table 1.2.

Table 1.2 Physical properties of raw emulsion, microemulsion and nanoemulsions in comparison. Adapted from Nastiti et al.[79]

	Emulsion	Microemulsion	Nanoemulsion
Physical description	Coarse dispersion	Colloidal dispersion	Colloidal dispersion
Particle size range	>500 nm	<100 nm	<100 nm
Polydispersity	High	Low	Low
Thermodynamic stability	Unstable	Stable	Unstable
Preparation	High energy	Low energy	Low/high energy
Composition: surfactant to oil ratio	Low	High	Moderate
Physical appearance	Creamy	Transparent	Transparent
Viscosity	Semi-solid	Liquid	Liquid

1.3.4.2 Formulation

ME and NE can be classified based on their dispersion natures as: water in oil (w/o), oil in water (o/w), water in oil in water (w/o/w), oil in water in oil (o/w/o) and bicontinuous system.[241-244] Bicontinuous system is an emulsion system consisting of a similar amount of oil and aqueous phases which are stabilised by sheet-like surfactant areas between the phases.[245] This system is dynamic, with greater interfacial fluctuation, lower interfacial tension and better solubilizing ability compared to w/o and o/w ME, due to higher surfactant capacity.[246, 247] Naoui et al.[247] suggested

that transdermal flux of o/w hydrophilic caffeine ME was highest, followed by bicontinuous ME and o/w ME, when composed of the same components. In addition, Bhatia et al.[246] demonstrated that lipophilic adapalene in a formulation of bicontinuous ME deposited into hair follicles three times greater than control, as the microstructure shifted from w/o to bicontinuous. The increased amount of adapalene deposition was in line with increasing amount of water in w/o ME.

A pseudo ternary diagram is generally constructed to indicate the boundaries as a function of oil, water, and mixture of surfactant-cosurfactants. It is also useful to predict the optimum area of ME composition showing by the clarity of the system. In principle, mixture of oils, surfactants and cosurfactants is diluted with water or aqueous solution under moderate agitation until it shows turbidity. The amount of water or aqueous solution is recorded just before it reaches turbidity.

1.3.4.3 Composition

Component selection and ratios of components play an important role to provide a stable and acceptable NE system. A variety of topical NE compositions is displayed in table 1.3.

A wide range of oil substances can be utilised individually or in combination as the oil phase in NE-ME[79], including fatty acids (oleic acid, myristic acid, lauric acid etc.), ester of fatty acids and alcohols (isopropyl myristate, isopropyl palmitate, ethyl oleate etc.), medium chain triglycerides, triacetin, terpenes (eugenol, eucalyptol, limonene, menthol, cineole etc.).Sodium chloride and buffer salts, water soluble preservatives and penetration enhancers can be added in the aqueous phase. NE-ME are liquids in nature. Gelling agents (Carbopol®, gelatine, Xanthan gum etc) are added to achieve appropriate consistency (gel formation) and to improve spread-ability on the skin.

Considering the issues between the effectiveness of the surfactant-cosurfactant combination (in lowering interfacial tension and generating stable nano-size emulsions) and the safety of their use, non-ionic surfactants are preferable. Non-ionic surfactants show minimum risk of skin irritation. Surfactants such as Tween® (polysorbates), Cremophor® (mixture of macrogol glycerol hydroxystearate, PEG-40 castor oil, polyoxyl 40 hydrogenated castor oil), Labrasol® (mixture of mono-, di-, and triglycerides of C8 and C10 fatty acids and mono- and di-esters of PEG) have been widely used in developing NE-ME. However, several NE formulation employ cationic surfactants with the rationale that the NE system will have a good contact with negatively charged SC thus improving the penetration/permeation of the

deliverables.[248-252] Cosurfactants, which are usually short and medium chain alcohols and derivatives of polyglyceryl, such as ethanol, isopropanol, propylene glycol, and Transcutol® (diethylene glycol monoethyl ester), are added to aid the functions of surfactants in stabilising the emulsion system.

Several commercial topical NE and ME finished products with lipophilic and hydrophilic active ingredients are available.[79] Estrasorb® (Novavax Inc., Malvern, PA, USA) is NE composed of soybean oil, water, polysorbate 80 and ethanol designed to deliver oestradiol hemihydrate, a hydrophobic compound (log P 3.3) indicated for vasomotor symptoms management related with menopause. Topicaine® (marketed by ESBA Laboratories Inc., USA) is a ME-based gel product containing lidocaine as local analgesic. This product is composed of jojoba oil, aloe vera, ethanol, benzyl alcohol, glycerine and water stabilised with glyceryl monostearate and gelled with Carbopol® 940. Ameluz® (Biofrontera Pharma GmBH, Leverkusen, Germany) is a topical NE-based gel formulation containing the hydrophilic compound aminolevulinic acid (log P 1.5) with the indication for actinic keratosis and basal cell carcinoma. The composition includes soybean phosphatidylcholine, water, polysorbate, propylene glycol and isopropyl alcohol.

1.3.4.4 Methods of fabrication

ME is generated spontaneously at optimal composition of oil, surfactant, co surfactant and water by the aid of low energy stirring and heat.[241-243, 253] In general, NE is initially prepared from ME which is further converted into NE. This process requires external energy application. Based on the power of the energy, the NE fabrication is categorised into high-energy emulsification (HEE) and low-energy emulsification (LEE).[238, 254] HEE methods generate high forces to allow the dispersion between oil and water droplets to form nano-sized droplets. These methods include high-pressure homogenizing, microfluidisation, and ultrasonication. LEE methods require less power such as moderate heating and stirring. NE can also be generated from diluted ME.[255-258]

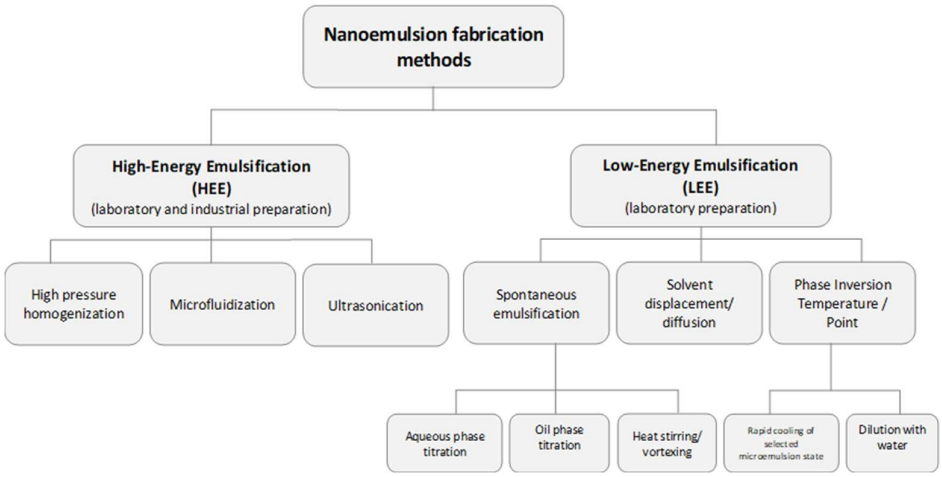

Figure 1.6 Schematic representation of methods of NE preparation. Adapted from Nastiti et al.[79]

1.3.4.5 Physical characterisation of NEs and MEs

Particle analysis and morphology

Rapid determination of particle/droplet size and polydispersity index can be carried out based on the principles of dynamic light scattering (DLS) or photon correlation spectroscopy (PCS). DLS captures the fluctuation frequency of light that is scattered ing when a laser beam passes through droplets or particles and converts the information into the average particle diameter size and the particle distribution index. In addition, particle distribution can also be analysed using small angle X-ray scattering (SAXs) and small angle neutron scattering (SANS).[259]

Nanostructures of NE/ME can be directly imaged using freeze fracture transmission electron microscopy (TEM) and cryo-TEM in high resolution.[260]

Viscosity and electrical conductivity

Viscosity is a function of oil, surfactant, water in their concentrations, which can be monitored to assess physical stability and the release of the drugs from NE and ME.[261] Lowering the concentration of surfactant and cosurfactant may result in increased viscosity due to the increasing interfacial tension between water and oil.

Electrical conductivity is a simple technique to determine the type of ME and NE by inserting the multimeter probes into ME/NE formulation. Conductivity defined values in aqueous phase. Phase inversion as a result of formulation or temperature change can be further shown by the simultaneous measurement of viscosity and electrical conductivity.[262,263] Bicontinuous structure can be further assessed by the presence of

the percolation effect due to water droplets attractive interactions which results in increasing the conductivity and lowering the viscosity.[263-265]

Podlogar et al[259] combined the data of physical characterisation including viscosity, conductivity, and SAXS techniques, to confirm the type of ME (Isopropyl myristate/Tween 40/ Imwitor 308®) and a percolation transition as a result of a bi-continuous structure. They further suggested that the techniques have potential to verify the structure and type of complex system and to predict the partitioning and drug release from the system.

1.3.4.6 Skin delivery of topical nanoemulsions

A wide variety of compounds have been delivered well into the skin using topical NEs and MEs for cosmetic, cosmeceutical, dermatological and transdermal purposes. Enhanced outcomes over conventional delivery systems due to the property and interaction of the components have been extensively reported.[79, 241, 243, 253, 266-269] As the current formulation study is focused on NE development, a key of literature on a range of topical NEs formulations is summarised, with particular emphasis on the composition, physical characteristics (size, zeta potential, polydispersity index-PDI, and viscosity) and skin permeation evaluation (Table 1.3). The compounds were classified into non-steroidal anti-inflammatory drugs (NSAID), antifungal agents, corticosteroids, vitamins and miscellaneous. Physical characteristics particularly permeant particle size and viscosity of NEs were evaluated as they might affect the skin permeability.[82, 93, 270] On the evaluation of *in vitro/in vivo* skin permeation, skin model selection was critical as it determined the accurate assessment of the amount of compound to potentially penetrate/permeate. Although human skin is the ideal skin model for skin penetration and permeation study, pig and newborn pig skin can be used as the surrogates owing to similar skin structures with human skin.[79, 271-274] It should be taken into consideration that overestimation may occur in using mouse skin, rat skin, and rabbit skin, as they are more permeable than human skin.[271, 275-277] The selection of receptor fluid is also essential for valid *in vitro* skin penetration-permeation study using Franz-type diffusion cells, especially for lipophilic compounds, to maintain the skin integrity, to facilitate sufficient solubility of permeant in order to obtain sink condition, and to minimise the presence of aqueous diffusion layers.[278]

Several features are also recognised in topical NE formulations summary (Table 1.3) including gel based NEs, lecithin based NEs, penetration enhancer (PE) containing NEs, and positively charged NEs. Gel-based NEs[279-286] were formulated by incorporating viscosity enhancing agents such as Carbopol™ at 0.75-1%

concentration or Viscolam AT100P at 5% concentration to improve the spread-ability property, to ease the application, and to prolong the retention of NE in the skin. Despite the benefits of gel formation of NE, we should consider that the permeation flux of gel based NEs is likely to be lower than that of the liquid NEs as the viscosity increased. Lecithin-based NEs take the benefits of lecithin as a natural surfactant to minimize the irritation risk of the formulation while showing comparable features as other surfactants.[250, 287-291] Terpenes, dimethylsulfoxide and N-methyl pirrolidone were employed in PE-containing NE in order to improve the skin permeation.[266, 292-294] Positively charged NEs involving cationic phytosphingosine were introduced as alternatives to enhance the skin permeation based on the assumption of the interaction of the formulation with negatively charged skin.[248-250]

Table 1.3 Examples of NE formulations evaluated for topical and transdermal delivery: hydrophilic (H) and lipophilic (L) nature of active compound, composition, preparation method and physical characterisation of emulsion formulation, and skin permeation experimental details and data. Adapted from Nastiti et al.[79]

Therapeutic class and active compound	H/L	Composition	Preparation method	Physical characterisation				Skin permeation evaluation	Ref
				Particle size (nm)	Surface charge (mV)	Polydispersity	Viscosity (mPa s)		
Non-steroidal anti-inflammatory drugs (NSAID)									
Aceclofenac	L	**Nanoemulsion NE31 (O/W)** O, A: Triacetin (13.6%), water (54.6%) S: Cremophore EL (23.9%), CoS: PEG 400 (7.9%), **Nanoemulsion gel NG31:** NE31 gelled with Carbopol 934 (1%) Drug load: 1.5 mg%	Spontaneous aqueous phase titration	39.48 (NE31)		0.230 (NE31)	339.51 ± 0.31 (NE31)	Full thickness rat abdominal skin Receptor fluid: Methanol-PBS pH 7.4 (3:7) **Flux J** ($\mu g.cm^{-2}.h^{-1}$) in 24 hours: NE31: 254.90 ± 1.25 NG31: 199.60 ± 6.93 **Control** (Hiffenac ™ Gel): 43.67 ± 2.11 **Enhancement ratio (ER):** NE31: 5.84 NG31: 4.57	279

Aceclofenac (ACF)	**L**	**Lecithin based Nanoemulsion** $L_{1.5}$ $S_{0.5}$ P_2A O, A: medium chain triglycerides (MCT): castor oil (1:1) (20%), water (76%) S/CoS: L: Lecithin 80 (1.5%), S: Sucrose stearate 970 (0.5%) P: Sucrose palmitate 1670 (2%) Drug load: 1% w/w	High pressure homogenisation	181.2±0.8	-39.2±1.5	0.110±0.006	3.60±0.23	Human skin (*in vivo* 12 times tape stripping) **Amount of drug in SC ($\mu g/cm^2$)** $L_{1.5}$ $S_{0.5}$ P_2A 39.85±1.29 **Control** L_2 $P80_2A$ 28.32 ± 4.39	291
Lornoxicam	L	**Nanoemulsion NE8:** O: Labrafac®, S: Tween 80, CoS: Pluronic F68®, S_{mix}= 3:1 Oil: S_{mix}=2:8 **Nanoemulsion gel NG8:** NE 8 gelled with Carbopol 934® (1%) Drug load: 1.5%	Spontaneous aqueous phase titration	139 ± 29		0.233	23.87 ± 1.86	Full thickness pig abdominal skin Receptor fluid: PBS pH 7.4 **Flux J ($\mu g.cm^{-2}.h^{-1}$) in 24 hours:** NE8: 254.90 ± 1.25 NG8: 199.60 ± 6.93 ***Control* (gel):** 43.67 ± 2.11	280
Indomethacin	L	**Nanoemulsion F6 (O/W)** O, A: Labrafil® (5%), water (50%) S: Tween 80 (33.75%)	Spontaneous aqueous phase titration	F6 25.53 ± 2.22		F6 0.087	F6 14.32 ± 1.12	Full thickness rat abdominal skin Receptor: methanol-PBS pH 7.4 (1:9)	281

		CoS: Transcutol-HP® (11.25%) S_{mix} ratio (3:1) S_{mix}/oil ratio 4.00 **Nanoemulsion gel NG6** F6 gelled with Carbopol 940® (1%) Triethanolamine (0.5%) Drug load: 0.5 %					**Flux J ($\mu g.cm^{-2}.h^{-1}$)** F6: 73.96 ± 2.89 NG6: 61.64 ± 2.38 **Control :** Indobene gel (Indo Gel™): 9.38 ± 0.41 **ER:** F6: 7.88 NG6: 6.57	
Naproxen and Caffeine	L, H	**Nanoemulsions with penetration enhancers in oil phase:** **E1** O, A: Eucalyptol (EU; 15.93%), water (30.97%) S: Volpo-N10® (26.55%) CoS: ethanol (26.55%) **E2** O, A: Eucalyptol (EU; 14.63%), water (36.59%) S: Volpo-N10® (24.39%)	Spontaneous aqueous phase titration and moderate agitation	Caffeine E1: 19.3±4.0 E2: 16.0±3.6 O1: 5.9±2.4 O2: 1.2±0.1 Naproxen E1: 37.8±5.9 E2: 25.0±3.0 O1: 11.6±3.8 O2: 13.5±4.5	Caffeine/Naproxen-EU 15.3 Caffeine/Naproxen-OA 15.3	Caffeine/ Naproxen-EU 13.7 ± 4.5 15.1 ± 4.0 Caffeine/ Naproxen-OA 23.7 ± 4.7 28.3 ± 4.5	Full thickness human skin Receptor fluid: PBS pH 7.4 <u>Caffeine:</u> **Flux J ($\mu g.cm^{-2}.h^{-1}$) in 24 hours** E1: 263.6 ± 1.2 E2: 267.7 ± 24.0 O1: 118.8 ± 57.3 O2: 136.4 ± 95.2 **Control (Caffeine)** C1: 2.2 ± 0.8 C2: 25.6±3.1	[266]

	CoS: ethanol (24.39%) **O1** O, A: Oleic acid (OA; 15.93%), water (30.97%) S: Volpo-N10® (26.55%) CoS: ethanol (26.55%) **O2** O, A: Oleic acid (OA; 14.63%), water (36.59%) S: Volpo-N10® (24.39%) CoS: ethanol (24.39%) Drug load : Caffeine (3%) Naproxen (2%) *Controls:* $C1^{C}$: water 100% $C2^{C,N}$: water 40%, ethanol 60% $C3^{C}$: water 75%, PEG-6000 25% $C4^{N}$: water 50%, ethanol 25%, Volpo-N10 25%		C3: 2.5± 0.7 C4: not identified <u>Naproxen</u> **Flux J** E1: 122.4± 27.1 E2: 86.6 ± 8.9 O1: 101.2 ± 41.7 O2: 74.0 ± 2.3 **Control** (Naproxen) C1: not identified C2: 23.4±4.8 C3: 6.2± 0.3 C4: 7.3± 2.7

Diclofenac diethylamine (DDEA)	L	**Nanoemulsion F1** O, A: Oleic acid (15%), water (30%) S: Polysorbate 20 (18.3%) CoS: ethanol (36.7%) S_{mix}: 1:2 (55%) **Nanoemulsion gel NE** F1 gelled with Carbopol 971P® (0.75%); and added: PG (10.0%) Methyl paraben (0.18%) Propyl paraben (0.02%) Drug load : 1.16% w/w DDEA (equivalent to 1% w/w diclofenac)	Spontaneous aqueous phase titration and vortex mixing	59.97±3.22		0.28 ± 0.07	1.002	Strat-M® membrane Receptor fluid: PBS pH 7.4 : methanol (70:30) **Flux J ($\mu g.cm^{-2}.h^{-1}$) in 12 hours:** F1: 11.5 NE gel: 12.0 **Controls:** DDEA solution: 1.71 Conventional gel: 11.7 Emulgel: 12.5 (coarse emulsion gel)	282
Indomethacin	L	**Nanoemulsion** O, A: Triacetin®:Capryol 90® (1:1) (10%), water (40%) S: Tween 80 (25%) CoS: Transcutol (25%) Drug load: 1%	Spontaneous aqueous phase titration and vortex mixing	101.1	n.a	n.a	60 ± 2.1	Full thickness hairless newborn albino rat Receptor fluid: PBS (pH 7.4) **Flux J ($\mu g.cm^{-2}.h^{-1}$) in 6 hours** 55.81±4.65	295

								No control	
Meloxicam (MLX)	L	**Nanoemulsion gel** O, A: Caprylic acid (0.95%), water (70%) S: Tween 80 (20%) CoS: Propylene glycol (PG) (10%) Carbopol 940 (0.05%)	Spontaneous aqueous phase titration	125 ± 1.9	-31.85 ± 0.61	0.193 ± 0.01		Abdominal rat skin Receptor fluid: Acetate buffer (pH 6.0) **Flux J ($\mu g.cm^{-2}.h^{-1}$)** 6.407±0.0911 Control (MLX solution): not identified Amount in skin layers at 24 h Tape strips: SC level *Control* > MLX-NE gel (1.02 folds) Epidermal level MLX-NE gel > *Control* (3.24 folds) Dermal level MLX-NE gel > *Control* (1.42 folds)	283
Flufenamic acid	L	**Nanoemulsion** *Aqueous phase*: Potassium sorbate (0.1%)	High pressure homogenisation	-	-	-	-	Dermatomed pig abdominal skin (1.2 mm) Receptor fluid:	289

	γ-Cyclodextrin (1.0%) water to 100% *Oil phase:* PCL liquid (cetearyl ethyl hexanoate, isopropyl myristate) (20%) S/CoS: sucrose stearate (2.5%) Drug load: 1%	PBS pH 7.4 **Flux J ($\mu g.cm^{-2}.h^{-1}$)** γ–SN Fluf 1.83±0.87 No control

Antifungal agents									
Amphotericin B	L	**Nanoemulsions** **F I** O, A: Sefsol 218®+DMSO (1:1) (18.7%), water (44%) S: Tween 80, CoS: PG, S_{mix} (ratio 2:1) (37.3%) **F III** O, A: Sefsol 218®+DMSO (1:1) (6%), water (64%) S: Tween 80, CoS: PG S_{mix} (ratio 1:2) (30%) **F VI** O, A: Sefsol 218®+DMSO (1:1) (16.8%), water (49.5%) S: Tween 80 CoS: PG S_{mix} (ratio 1:3) (33.6%) Drug load: 0.1%	Spontaneous aqueous phase titration	FI 67.33 ± 0.8 F III 252 ± 1.0 F VI 74.2 ± 1.2	FI -37.305 F III -28.202 F VI -18.148	FI 0.635 F III 0.468 F VI 0.453	FI 25.4 ± 1 F III 40.7 ± 1.3 F VI 43.1 ± 1.4	Albino Wistar rat abdominal skin Receptor fluid: 2% DMSO in PBS pH 7.4 **Flux J ($\mu g.cm^{-2}.h^{-1}$)** F I: 18.02 ± 4.34 F III: 8.808 ± 3.55 F VI: 17.581 ± 2.56 **Controls** Drug solution (0.1%): 5.895 ± 2.06 Fungisome® gel (0.1%): 9.704 ± 5.74	294
Amphotericin B	L	**Nanoemulsion NE (FV)** O, A: Sefsol-218® (10%), water (65%)	Spontaneous aqueous phase titration	FV 76.2 ± 1.4	FV -31.48	FV 0.303	FV 39.01 ± 1.4	Albino rat abdominal skin Receptor fluid:	284

		S: Tween 80, CoS: Transcutol® , S_{mix} (ratio 1:3) (25%) **AmpB-NE gel:** FV: Carbopol 980® (1%) =1:1 Drug load: 0.1%		AmpB-NE gel: 97.04 ± 7.4	AmpB-NE gel: -39.27 ± 0.25	AmpB-NE gel: 0.19 ± 0.01	AmpB-NE gel: 892 ± 9.64	2% DMSO in PBS pH 7.4 **Flux J ($\mu g.cm^{-2}.h^{-1}$)** FV: 15.74 ± 0.4 AmpB-NE gel: 18.09 ± 0.6 **Control** (AmpB solution): 4.59 ± 0.01 **ER:** FV: 8.97 AmpB-NE gel: 10.42	
Terbinafine (TER) **Citral (CIT)**	L L	**Nanoemulsion (NE)** O, A: CIT (4%), (water 71%) S : Cremophor ®EL-40 (18%) CoS: 1,2-propylene glycol (6%) S_{mix}: 3:1 **NG1** NE gelled with Carbopol® 934 (1%)=1:1	Spontaneous aqueous phase titration	NE 15.53±3.32 NG1 14.88±3.11	NE -7.4±1.8 NG1 -6.5±2.3	NE 0.074±0.009 NG1 0.084±0.025		Guinea pig abdominal skin Receptor fluid: PBS (pH 7.4) **TER** **Flux J ($\mu g.cm^{-2}.h^{-1}$)** NE: 11.30±0.56 NG1: 11.50±0.43 **Control:** 1.48±0.34 **CIT** **Flux J** NE: 54.71±1.34	285

	(NG 2 and NG 3 contains 2% and 3% Carbopol® 934, respectively, at the same ratio with NE) Drug load in NE: TER 1% and CIT 4% (oil phase) Controls: TER-CIT in conventional gels (1.5% Carbopol® 934)		NG1: 55.01±1.67 *Control:* 10.55±0.87 *Amount in stratum corneum (12 h) (µg.cm^{-2})* NE-TER: 1.65±0.29 NG1-TER: 6.27±1.03 *Control TER:* 5.63±0.76 NE-CIT: 0.95±0.52 NG1-CIT: 10.88±5.80 *Control CIT* 13.68±1.91 *Amount in epidermis-dermis (12h) (µg.cm^{-2})* NE-TER: 73.5±8.23 NG1-TER: 75.25±9.52 *Control TER* 17.42±5.63

							NE-CIT: 210.71±12.38 NG1-CIT: 214.64±.92 *Control CIT* 39.47±5.51	
Fluconazole	H	**Lecithin based NE** *Aqueous phase*: Potassium sorbate 0.1% (γ-Cyclodextrin 1.0%) water to 100% *Oil phase:* PCL liquid 20% S: Lecithin E-80 Drug load: 1%	High pressure homogenisation	LN Fluc 156.87±09.73 γ -LN Fluc 155.60±07.96	LN Fluc - 24.70±3.41 γ -LN Fluc - 22.50±2.20	LN Fluc 0.05±0.01 γ -LN Fluc 0.07±0.02	Dermatomed pig abdominal skin (1.2mm) Receptor fluid: PBS pH 7.4 **Flux J ($\mu g.cm^{-2}.h^{-1}$)** LN Fluc 109.55±11.30 γ -LN Fluc 93.63±3.80 No control	289
Corticosteroids								
Fludrocortisone acetate	L	**Lecithin based NE** *Oil phase:* PCL liquid 20% *Aqueous phase*: Potassium sorbate 0.1% γ-Cyclodextrin 0.5% or 1.0% water to 100%	High pressure homogenisation	γ-0.5% NE 171.03±0.32 γ-1% NE 169.73±2.35	γ-0.5% NE - 33.17±0.75 γ-1% NE - 31.73±1.52	γ-0.5% NE 0.098±0.042 γ-1% NE 0.033±0.049	Dermatomed pig abdominal skin (1.2mm thick) Receptor fluid: PBS pH 7.4 ***Flux J ($\mu g.cm^{-2}.h$) in 24 h***	288

		S: Lecithin E-80 (2.5%) Drug load: 1% Control: NE without cyclodextrin Applied as finite (5mg/cm^2) and infinite doses (500mg/cm^2) No significant different in drug flux between γ-1% NE and γ-0.5% NE					Finite dose γ-1% NE 0.067 ± 0.047 NE Control 0.008 ± 0.007 Infinite dose γ-1% NE 2.48 ± 0.68 NE Control 0.09 ± 0.07 **ER:** finite dose 8.38 infinite dose 27.55	
Fludrocortisone acetate (FA) **Flumethasone pivalate (FP)**	L	**Positively charged NEs :** *Oil phase:* PCL liquid (Ethylhexanoate) (20%), Lipoid S-75® (4%), α tocopherol (1%), Phytosphingosine (PS) (0, 0.4% *or* 0.6 %), *Aqueous phase:* water to 100%	High pressure homogenisation	FA NL 161 ± 0.7 FA NL-0.4PS 215 ± 2.8 FA NL-0.6 PS 254 ± 2.2 FA NT 170 ± 3.8 FA NT-0.4PS 216 ± 26.6 FA NT-0.6 PS	FA NL -6.2 ± 0.4 FA NL-0.4PS +46 ± 0.4 FA NL-0.6 PS +48 ± 0.7 FA NT -55 ± 0.7 FA NT-0.4PS	FA NL 0.12-0.22 FA NL-0.4PS 0.22-0.25 FA NL-0.6 PS 0.06-0.1 FA NT 0.15-0.18 FA NT-0.4PS 0.13-0.18 FA NT-0.6 PS	Dermatomed pig abdominal skin (1 mm) Receptor fluid: PBS pH 7.4 **Flux J (μg.cm^{-2}.h) in 48 hours:** FA NL 0.126 ± 0.027 FA NL-0.4PS 0.150 ± 0.010 FA NL-0.6 PS 0.189 ± 0.012	250

		S: Sucrose laurate L 1695 (1%) *or* Tween 80 (1%) Drug load: 1% **FA NL**: FA NE with sucrose laurate L 1695 **FA NT** : FA NE with Tween 80 **FP NL**: FP NE with sucrose laurate L 1695 **FP NT**: FP NE with Tween 80		170 ± 2.1	+45 ± 0.7 FA NT-0.6 PS +48 ± 1.1	0.10-0.14	FA NT 0.263 ± 0.043 FA NT-0.4PS 0.353 ± 0.018 FA NT-0.6 PS 0.377 ± 0.038 FP NT 2.290 ± 0.313 FP NT-0.4PS 2.698 ± 0.117 FP NT-0.6 PS 3.073 ± 0.104 No control Flux increased with PS concentration; Tween 80 > sucrose laurate	
Prednicarbate (PC)	L	**Positively charged NEs (PCNE)** Phytosphingosine (PS) (0.6%), S: Lecithin E 80® & Tween 80 (2%), CoS: Ethanol (20%), α tocopherol (0.03%),	High pressure homogenisation	PCNE: 157 NCNE: 136	PCNE: 50-60 NCNE : -(40-50)	0.05-0.1	Full thickness human skin Receptor fluid: Ethanol-PBS (1:1) No PC detected in receptor in 24 hours **Amount PC in skin at 24 hours**	[248, 249]

		Potassium sorbate (0.1%) **Negatively charged NE (NCNE)** Myristic acid (1%) was used to replace PS Drug load: 0.25%					PCNE: 18.4 ± 3.4 µg/mL NCNE: 11.7 ± 2.5 µg/mL No control Positive > negative charged NE	
Fludrocortisone acetate (FA)	L	**Lecithin based NE** *Aqueous phase*: Potassium sorbate 0.1% γ-Cyclodextrin 1.0% water to 100% *Lipid phase:* PCL liquid 20% S: Lecithin E-80 2.5% Drug load: 1%	High pressure homogenisation	γ -LN Flud 175.82±00.47	γ -LN Flud - 30.19±4.12	γ -LN Flud 0.09±0.04		Dermatomed pig abdominal skin (1.2mm thick) Receptor fluid: PBS pH 7.4 **FA Flux J ($\mu g.cm^{-2}.h^{-1}$)** γ -LN Flud 4.53±0.99 No control	[289]
Vitamins								
α tocopherol (vitamin E)	L	**Hyaluronic acid-based NE (L6)** O: methylene oxide,	Oil/water/surfactant emulsifying system	57.3 ± 0.2		0.260		Full thickness Wistar rat dorsal skin	[296]

		S/CoS: Tween 80-Span 20, A: HA-GMS solution, Mass ratio O:S:A = 2:3:95 Drug load: 0.1% HA-GMS is water soluble amphiphile from crosslinking esterification of hyaluronic acid and glycerol α-mono stearate (stearin) *Control*: 0.1% Vit E in ethanol solution	and solvent evaporation					Receptor fluid: PBS pH 7.4 **Flux J ($\mu g.cm^{-2}.h^{-1}$)** *in 24 hours:* L6: 14.68 ± 4.13 *Control*: not detected	
α tocopherol (vitamin E) and Vitamin K1 (VK1)	L	**Nanoemulsions** O, A: α- tocopherol (α-TOC) and VK1 10%, water 64% S: Tween 80 10% Cos : Ethanol 16% Drug load: 3% or 5%	Spontaneous aqueous phase titration and Ultrasonic nebulisation NE-neb-VK1 = ultrasonic nebulizer	NE-VK1 3% 254.8±10.7 NE-neb-VK1 3% 259.4±4.1 NE-VK1 5% 215.7±2.3 NE-neb-VK1 5% 233.2±0.2	NE-VK1 3% - 14.89±2.68 NEs-neb-VK1 3% - 16.60±1.01 NE-VK1 5% - 14.14±0.29	NE-VK1 3% 0.22±0.05 NEs-neb-VK1 3% 0.19±0.14 NE-VK1 5% 0.23±0.02 NE-neb-VK1 5% 0.26±0.02		Pig ear skin (thickness 1.7-2.3 mm) Receptor fluid: PBS: Ethanol (7:3 v/v) **Amount in epidermis at 24h (ng/mg)** NEs-VK1 3%: 46.7 NEs-neb-VK1 3%: 72.8 NEs-VK1 5%: 55.6	297

					NE-neb-VK1 5% -15.4±0.1			NEs-neb-VK1 5%: 51.4 **Amount in dermis at 24h (ng/mg)** NEs-neb-VK1 3%: 27.9 NEs-neb-VK1 5%: 24.8 No control	
Miscellaneous									
Thiocolchicoside (TCC) **anti inflammatory, analgesic, muscle relaxant**	H	**Nanoemulsion** **C1 (W/O type)** O, A: (linseed oil:Sefsol®=1:1) (35.44 %), water (10.81%) S: Span 80 (40.53%) CoS: Transcutol P® (13.51%) S_{mix} 3:1 **C3 (W/O type)** O, A: (linseed oil:Sefsol®=1:1) (35.19 %), water (9.26 %) S: Span 80 (41.67 %) CoS: Transcutol P® (13.89 %)	Spontaneous aqueous phase titration	C1 117.73 ± 13.71 C3 131.43 ± 15.15		C1 0.285 C3 0.311	C1 61.12 ± 5.28 C3 65.75 ± 6.08	Full thickness weanling pig abdominal skin Receptor: PBS pH 7.4 *TCC Flux J ($\mu g.cm^{-2}.h^{-1}$) in 24 h* C1: 30.63 ± 4.18 C3: 28.01 ± 3.41 *Control*: 5.99 ± 0.73 *ER:* C1: 5.114 C3: 4.676	298

		S_{mix} 3:1 Drug load: 0.2%						Type of NE did not influence *ER*	
Curcumin natural anti-inflammatory	L	**Nanoemulsion NE gel** O, A: Glyceryl monooleate (GMO) , water S : Cremophor RH40® CoS: PEG 400 O:S:CoS =1:8:1 Ratio water: oil phase= 5:1 NE gelled with Viscolam AT 100P® (5%) and added with: Methyl paraben (0.2%) Propyl paraben (0.05%) Glycerine (5%) Propylene glycol (15%) Drug load: 0.35%	Spontaneous aqueous phase titration with 1hour ultrasonic sonication	85.0±1.5	0.18±0.0	-5.9± 0.3	2000 - 2700	Shed snake skin Receptor fluid: PBS (pH 7.4) **Flux J ($\mu g.cm^{-2}.h^{-1}$)** NE gel: 1.699 ± 0.050 Control gel: 0.836 ± 0.004	286
Bovine albumin-fluorescein isothiocyanate	L	**Nanoemulsion**	Spontaneous aqueous phase titration with	85.2±15.5	-45.17±4.77	0.186±0.026	14.6±0.026	Mouse skin Receptor fluid: PBS (pH 7.4)	299

conjugate (FITC-BSA) **vaccine model**		O: Squalene (37.5%), water (52.5%) S: Span 80, Tween 80 (10%) S_{mix}: 1:1 Drug load: 0.25% *Controls:* CE: Emulsifiers solution (10% of S_{mix}) CA: Aqueous solution	high pressure homogenisation			**Flux J ($\mu g.cm^{-2}.h^{-1}$) in 48 hours:** NE: 23.44±17.230 *Controls:* CE: 6.10±0.977 CA: 3.15±0.897	
Granisetron HCl (GHCl) **anti emetic drug**	H	**Nanoemulsion with penetration enhancer NMP** O: Isopropyl myristate (IPM) (4%) S: Tween 85 (20%) CoS: Ethanol (20%) **PE: n-methyl pyrrolidone (NMP) (10%)** A: water up to 100% Drug load: 2.5% Control: NE without NMP	Spontaneous aqueous phase titration	48.3 ± 1.7	0.27 ± 0.02	Full thickness rat abdominal skin Receptor fluid: saline solution **Flux J ($\mu g.cm^{-2}.h^{-1}$)** NMP NE: 85.39 ± 2.90 *Control*: 71.17 ± 3.54 **Amount in skin at 12 h ($\mu g.cm^{-2}$)** NMP NE: 891.8 ± 2.86	[293]

							Control: 889.1 ± 2.24 NMP NE ≅ NE	
Minoxidil (Min) antihypertensive vasodilator (stimulate hair growth)	H	**Lecithin based NE** *Aqueous phase*: Potassium sorbate 0.1% γ-Cyclodextrin 1.0% water to 100% *Oil phase:* PCL liquid 20% S: **Lecithin E-80 2.5%** Drug load: 1%	High pressure homogenisation	-	-	-	Dermatomed pig abdominal skin (1.2mm thick) Receptor fluid: PBS pH 7.4 *Flux J* *($\mu g.cm^{-2}.h^{-1}$)* 102.56±9.41 No control	292

1.4 References

1. Godin B, Touitou E. Transdermal skin delivery: predictions for humans from *in vivo, ex vivo* and animal models. Advanced Drug Delivery Reviews. 2007;59(11):1152-1161.
2. Igarashi T, Nishino K, Nayar SK. The appearance of human skin: A survey. Foundations and Trends® in Computer Graphics and Vision. 2007;3(1):1-95.
3. Montagna W. The structure and function of skin. Elsevier Science; 2012.
4. Hadgraft JW, Somers GF. Percutaneous absorption. J Pharm Pharmacol. 1956;8(1):625-634.
5. Bouwstra JA, Honeywell-Nguyen PL, Gooris GS, Ponec M. Structure of the skin barrier and its modulation by vesicular formulations. Prog Lipid Res. 2003;42(1):1-36.
6. Roberts MS, Mohammed Y, Pastore MN, et al. Topical and cutaneous delivery using nanosystems. J Control Release. 2017;247:86-105.
7. Mauldin EA, Peters-Kennedy J. Chapter 6 - Integumentary system. In: Maxie MG, editor. Jubb, Kennedy & Palmer's pathology of domestic animals. 1. 6th-ed.: W.B. Saunders; 2016. p. 509-736.e1.
8. van Smeden J, Janssens M, Gooris GS, Bouwstra JA. The important role of stratum corneum lipids for the cutaneous barrier function. Biochimica et Biophysica Acta (BBA) - Molecular and Cell Biology of Lipids. 2014;1841(3):295-313.
9. Levine M. The growth of adult human skin *in vitro*. Br J Dermatol. 1972;86(5):481-490.
10. Kligman AM. A brief history of how the dead stratum corneum became alive. In: Elias PM, Feingold KR, editors. Skin barrier. Boca Raton: CRC Press; 2006. p. 18-24.
11. Scheuplein RJ, Blank IH. Permeability of the skin. Physiol Rev. 1971;51(4):702-747.
12. Michaels AS, Chandrasekaran SK, Shaw JE. Drug permeation through human skin: theory and *in vitro* experimental measurement. AIChE J. 1975;21(5):985-996.
13. Menon GK, Cleary GW, Lane ME. The structure and function of the stratum corneum. Int J Pharm. 2012;435(1):3-9.
14. Elias PM. Lipids and the epidermal permeability barrier. Archives of Dermatological Research. 1981;270(1):95-117.
15. Coderch L, López O, de la Maza A, Parra JL. Ceramides and skin function. Am J Clin Dermatol. 2003;4(2):107-129.
16. Bäsler K, Bergmann S, Heisig M, et al. The role of tight junctions in skin barrier function and dermal absorption. J Control Release. 2016;242:105-118.
17. Lademann J, Jacobi U, Surber C, Weigmann HJ, Fluhr JW. The tape stripping procedure - evaluation of some critical parameters. Eur J Pharm Biopharm. 2009;72(2):317-323.
18. Pouillot A, Dayan N, Polla AS, Polla LL, Polla BS. The stratum corneum: A double paradox. J Cosmet Dermatol. 2008;7(2):143-148.
19. Brown TN, Armitage JM, Egeghy P, Kircanski I, Arnot JA. Dermal permeation data and models for the prioritization and screening-level exposure assessment of organic chemicals. Environ Int. 2016;94:424-435.
20. Warner RR, Stone KJ, Boissy YL. Hydration disrupts human stratum corneum ultrastructure. J Invest Dermatol. 2003;120(2):275-284.
21. Kirschner N, Houdek P, Fromm M, Moll I, Brandner JM. Tight junctions form a barrier in human epidermis. Eur J Cell Biol. 2010;89(11):839-842.
22. Baroni A, Buommino E, De Gregorio V, et al. Structure and function of the epidermis related to barrier properties. Clin Dermatol. 2012;30(3):257-262.
23. Yoshida K, Yokouchi M, Nagao K, et al. Functional tight junction barrier localizes in the second layer of the stratum granulosum of human epidermis. J Dermatol Sci. 2013;71(2):89-99.

24. Svoboda M, Bílková Z, Muthný T. Could tight junctions regulate the barrier function of the aged skin? J Dermatol Sci. 2016;81(3):147-152.
25. Kirschner N, Rosenthal R, Furuse M, et al. Contribution of tight junction proteins to ion, macromolecule, and water barrier in keratinocytes. J Invest Dermatol. 2013;133(5):1161-1169.
26. Scheuplein RJ. Analysis of permeability data for the case of parallel diffusion pathways. Biophys J. 1966;6(1):1-17.
27. El Maghraby GM, Barry BW, Williams AC. Liposomes and skin: From drug delivery to model membranes. Eur J Pharm Sci. 2008;34(4–5):203-222.
28. Benson HAE. Chapter 1. Skin structure, function , and permeation. In: Benson HAE, Watkinson AC, editors. Topical and transdermal drug delivery: Principles and practice. John Wiley & Sons; 2012.
29. Benson HAE. Transdermal drug delivery: Penetration enhancement techniques. Current Drug Delivery. 2005;2(1):23-33.
30. Elias PM, Friend DS. The permeability barrier in mammalian epidermis. The Journal of Cell Biology. 1975;65(1):180-191.
31. Berenson GS, Burch GE. Studies of diffusion of water through dead human skin: The effect of different environmental states and of chemical alterations of the epidermis1. The American Journal of Tropical Medicine and Hygiene. 1951;s1-31(6):842-853.
32. Nemanic MK, Elias PM. *In situ* precipitation: a novel cytochemical technique for visualisation of permeability pathways in mammalian stratum corneum. J Histochem Cytochem. 1980;28(6):573-578.
33. Bolzinger M-A, Briançon S, Pelletier J, Chevalier Y. Penetration of drugs through skin, a complex rate-controlling membrane. Current Opinion in Colloid & Interface Science. 2012;17(3):156-165.
34. Knorr F, Patzelt A, Darvin ME, et al. Penetration of topically applied nanocarriers into the hair follicles of dog and rat dorsal skin and porcine ear skin. Vet Dermatol. 2016;27(4):256-e60.
35. Lademann J, Knorr F, Richter H, et al. Hair follicles - An efficient storage and penetration pathway for topically applied substances: Summary of recent results obtained at the Center of Experimental and Applied Cutaneous Physiology, Charité - Universitätsmedizin Berlin, Germany. Skin Pharmacol Physiol. 2008;21(3):150-155.
36. Lademann J, Knorr F, Richter H, et al. Hair follicles as a target structure for nanoparticles. Journal of Innovative Optical Health Sciences. 2015;8(4).
37. Lademann J, Otberg N, Richter H, et al. Investigation of follicular penetration of topically applied substances. Skin Pharmacol Appl Skin Physiol. 2001;14(SUPPL. 1):17-22.
38. Lademann J, Patzelt A, Richter H, et al. Comparison of two *in vitro* models for the analysis of follicular penetration and its prevention by barrier emulsions. Eur J Pharm Biopharm. 2009;72(3):600-604.
39. Lademann J, Richter H, Schaefer UF, et al. Hair follicles - A long-term reservoir for drug delivery. Skin Pharmacol Physiol. 2006;19(4):232-236.
40. Liu X, Grice JE, Lademann J, et al. Hair follicles contribute significantly to penetration through human skin only at times soon after application as a solvent deposited solid in man. Br J Clin Pharmacol. 2011;72(5):768-774.
41. Mak WC, Patzelt A, Richter H, et al. Triggering of drug release of particles in hair follicles. J Control Release. 2012;160(3):509-514.
42. Meinke MC, Patzelt A, Richter H, et al. Prevention of follicular penetration: Barrier-enhancing formulations against the penetration of pollen allergens into hair follicles. Skin Pharmacol Physiol. 2011;24(3):144-150.
43. Ossadnik M, Richter H, Teichmann A, et al. Investigation of differences in follicular penetration of particle-and nonparticle-containing emulsions by laser scanning microscopy. Laser Physics. 2006;16(5):747-750.

44. Otberg N, Patzelt A, Rasulev U, et al. The role of hair follicles in the percutaneous absorption of caffeine. Br J Clin Pharmacol. 2008;65(4):488-492.
45. Patzelt A, Knorr F, Blume-Peytavi U, Sterry W, Lademann J. Hair follicles, their disorders and their opportunities. Drug Discov Today Dis Mech. 2008;5(2):e173-e181.
46. Patzelt A, Lademann J. The increasing importance of the hair follicle route in dermal and transdermal drug delivery. In: Dragicevic N, Maibach HI, editors. Percutaneous penetration enhancers chemical methods in penetration enhancement: Drug manipulation strategies and vehicle Effects. Springer, Berlin, Heidelberg; 2015. p. 43-53.
47. Schaefer H, Lademann J. The role of follicular penetration. Skin Pharmacol Physiol. 2001;14(suppl 1)(Suppl. 1):23-27.
48. Teichmann A, Otberg N, Jacobi U, Sterry W, Lademann J. Follicular penetration: Development of a method to block the follicles selectively against the penetration of topically applied substances. Skin Pharmacol Physiol. 2006;19(4):216-223.
49. Lademann J, Richter H, Schanzer S, et al. Penetration and storage of particles in human skin: Perspectives and safety aspects. Eur J Pharm Biopharm. 2011;77(3):465-468.
50. Otberg N, Richter H, Schaefer H, et al. Variations of hair follicle size and distribution in different body sites. J Invest Dermatol. 2004;122(1):14-19.
51. Antonio JR, Antonio CR, Cardeal ILS, Ballavenuto JMA, Oliveira JR. Nanotechnology in dermatology. An Bras Dermatol. 2014;89:126-136.
52. Newman MD, Stotland M, Ellis JI. The safety of nanosized particles in titanium dioxide– and zinc oxide–based sunscreens. J Am Acad Dermatol. 2009;61(4):685-692.
53. Nohynek GJ, Dufour EK. Nano-sized cosmetic formulations or solid nanoparticles in sunscreens: A risk to human health? Arch Toxicol. 2012;86(7):1063-1075.
54. Nohynek GJ, Dufour EK, Roberts MS. Nanotechnology, cosmetics and the skin: Is there a health risk? Skin Pharmacol Physiol. 2008;21(3):136-149.
55. Nohynek GJ, Lademann J, Ribaud C, Roberts MS. Grey goo on the skin? Nanotechnology, cosmetic and sunscreen safety. Crit Rev Toxicol. 2007;37(3):251-277.
56. Pflücker F, Wendel V, Hohenberg H, et al. The human stratum corneum layer: An effective barrier against dermal uptake of different forms of topically applied micronised titanium dioxide. Skin Pharmacol Physiol. 2001;14(suppl 1)(Suppl. 1):92-97.
57. Gulson B, McCall M, Korsch M, et al. Small amounts of zinc from zinc oxide particles in sunscreens applied outdoors are absorbed through human skin. Toxicol Sci. 2010;118(1):140-149.
58. Burnett ME, Wang SQ. Current sunscreen controversies: a critical review. Photodermatol Photoimmunol Photomed. 2011;27(2):58-67.
59. Smijs TG, Pavel S. Titanium dioxide and zinc oxide nanoparticles in sunscreens: focus on their safety and effectiveness. Nanotechnology, science and applications. 2011;4:95-112.
60. Baroli B. Nanoparticles and skin penetration. Are there any potential toxicological risks? Journal für Verbraucherschutz und Lebensmittelsicherheit. 2008;3(3):330-331.
61. Jiang SJ, Chen JY, Lu ZF, et al. Biophysical and morphological changes in the stratum corneum lipids induced by UVB irradiation. J Dermatol Sci. 2006;44(1):29-36.
62. Zhang LW, Monteiro-Riviere NA. Mechanisms of quantum dot nanoparticle cellular uptake. Toxicol Sci. 2009;110(1):138-155.

63. Zhang LW, Yu WW, Colvin VL, Monteiro-Riviere NA. Biological interactions of quantum dot nanoparticles in skin and in human epidermal keratinocytes. Toxicol Appl Pharmacol. 2008;228(2):200-211.
64. Sharma V, Singh SK, Anderson D, Tobin DJ, Dhawan A. Zinc oxide nanoparticle induced genotoxicity in primary human epidermal keratinocytes. Journal of Nanoscience and Nanotechnology. 2011;11(5):3782-3788.
65. Hild WA, Breunig M, Goepferich A. Quantum dots – Nano-sized probes for the exploration of cellular and intracellular targeting. Eur J Pharm Biopharm. 2008;68(2):153-168.
66. Radenkovic D, Kobayashi H, Remsey-Semmelweis E, Seifalian AM. Quantum dot nanoparticle for optimisation of breast cancer diagnostics and therapy in a clinical setting. Nanomedicine: Nanotechnology, Biology and Medicine. 2016;12(6):1581-1592.
67. Ryman-Rasmussen JP, Riviere JE, Monteiro-Riviere NA. Penetration of intact skin by quantum dots with diverse physicochemical properties. Toxicol Sci. 2006;91(1):159-165.
68. Jeong SH, Kim JH, Yi SM, et al. Assessment of penetration of quantum dots through *in vitro* and *in vivo* human skin using the human skin equivalent model and the tape stripping method. Biochem Biophys Res Commun. 2010;394(3):612-615.
69. Tan M-H, Commens CA, Burnett L, Snitch PJ. A pilot study on the percutaneous absorption of microfine titanium dioxide from sunscreens. Australas J Dermatol. 1996;37(4):185-187.
70. Dussert AS, Gooris E, Hemmerle J. Characterization of the mineral content of a physical sunscreen emulsion and its distribution onto human stratum corneum. Int J Cosmet Sci. 1997;19(3):119-129.
71. Lademann J, Weigmann HJ, Rickmeyer C, et al. Penetration of titanium dioxide microparticles in a sunscreen formulation into the horny layer and the follicular orifice. Skin Pharmacol Physiol. 1999;12(5):247-256.
72. Cross SE, Innes B, Roberts MS, et al. Human skin penetration of sunscreen nanoparticles: *In-vitro* assessment of a novel micronized zinc oxide formulation. Skin Pharmacol Physiol. 2007;20(3):148-154.
73. Leite-Silva VR, Lamer ML, Sanchez WY, et al. The effect of formulation on the penetration of coated and uncoated zinc oxide nanoparticles into the viable epidermis of human skin *in vivo*. Eur J Pharm Biopharm. 2013;84(2):297-308.
74. Leite-Silva VR, Liu DC, Sanchez WY, et al. Effect of flexing and massage on *in vivo* human skin penetration and toxicity of zinc oxide nanoparticles. Nanomedicine. 2016;11(10):1193-1205.
75. Leite-Silva VR, Sanchez WY, Studier H, et al. Human skin penetration and local effects of topical nano zinc oxide after occlusion and barrier impairment. Eur J Pharm Biopharm. 2016;104:140-147.
76. Mohammed YH, Holmes A, Haridass IN, et al. Support for the safe use of zinc oxide nanoparticle sunscreens: Lack of skin penetration or cellular toxicity after repeated application in volunteers. J Invest Dermatol. 2019;139(2):308-315.
77. Prow TW, Monteiro-Riviere NA, Inman AO, et al. Quantum dot penetration into viable human skin. Nanotoxicology. 2012;6(2):173-185.
78. Benson HAE. Elastic liposomes for topical and transdermal drug delivery. In: D'Souza GGM, editor. Liposomes: Methods and protocols. New York, NY: Springer New York; 2017. p. 107-117.
79. Nastiti CMRR, Ponto T, Abd E, et al. Topical nano and microemulsions for skin delivery. Pharmaceutics. 2017;9(4):37.
80. Leite-Silva VR, De Almeida MM, Fradin A, Grice JE, Roberts MS. Delivery of drugs applied topically to the skin. Expert Review of Dermatology. 2012;7(4):383-397.
81. Dragicevic N, Verma DD, Fahr A. Invasomes: Vesicles for enhanced skin delivery of drugs. In: Dragicevic N, Maibach HI, editors. Percutaneous penetration

enhancers chemical methods in penetration enhancement: Nanocarriers. Berlin, Heidelberg: Springer Berlin Heidelberg; 2016. p. 77-92.
82. Magnusson BM, Anissimov YG, Cross SE, Roberts MS. Molecular size as the main determinant of solute maximum flux across the skin. J Investig Dermatol. 2004;122(4):993-999.
83. Potts RO, Guy RH. Predicting skin permeability. Pharm Res. 1992;9(5):663-669.
84. Grice J, Benson HAE. Analysing the skin barrier from down under. Skin Pharmacol Physiol. 2013;26(4-6):254-262.
85. Pugh WJ, Roberts MS, Hadgraft J. Epidermal permeability — Penetrant structure relationships: 3. The effect of hydrogen bonding interactions and molecular size on diffusion across the stratum corneum. Int J Pharm. 1996;138(2):149-165.
86. Larese Filon F, Mauro M, Adami G, Bovenzi M, Crosera M. Nanoparticles skin absorption: New aspects for a safety profile evaluation. Regul Toxicol Pharmacol. 2015;72(2):310-322.
87. Roberts MS, Cross SE, Pellett MA. Skin transport. In: Walters KA, editor. Dermatological and transdermal formulations. CRC Press; 2002.
88. Sloan KB, Koch SAM, Siver KG, Flowers FP. Use of solubility parameters of drug and vehicle to predict flux through skin. J Invest Dermatol. 1986;87(2):244-252.
89. Roberts MS, Pugh WJ, Hadgraft J, Watkinson AC. Epidermal permeability-penetrant structure relationships: 1. An analysis of methods of predicting penetration of monofunctional solutes from aqueous solutions. Int J Pharm. 1995;126(1–2):219-233.
90. Zhang Q, Grice JE, Li P, et al. Skin solubility determines maximum transepidermal flux for similar size molecules. Pharm Res. 2009;26(8):1974-1985.
91. Zhang Q, Li P, Liu D, Roberts MS. Effect of vehicles on the maximum transepidermal flux of similar size phenolic compounds. Pharm Res. 2012;30(1):32-40.
92. Zhang Q, Li P, Roberts MS. Maximum transepidermal flux for similar size phenolic compounds is enhanced by solvent uptake into the skin. J Control Release. 2011;154(1):50-57.
93. Roberts MS. Solute-vehicle-skin interactions in percutaneous absorption: The principles and the people. Skin Pharmacol Physiol. 2013;26(4-6):356-370.
94. Proksch E, Brandner JM, Jensen J-M. The skin: an indispensable barrier. Exp Dermatol. 2008;17(12):1063-1072.
95. Lober CW. Photoaging and the skin: differentiation and clinical response. Geriatrics. 1990;45:36-42.
96. Fenske NA, Lober CW. Structural and functional changes of normal aging skin. J Am Acad Dermatol. 1986;15(4, Part 1):571-585.
97. Batisse D, Bazin R, Baldeweck T. Influence of age on the wrinkling capacities of skin. Skin Res Technol. 2002;8(3):148-154.
98. Rogers J, Harding C, Mayo A, Banks J, Rawlings A. Stratum corneum lipids: the effect of ageing and the seasons. Archives of Dermatological Research. 1996;288(12):765-770.
99. Takahashi M. Physiological and morphological changes in facial skin with aging (II)-A study on racial differences. J Soc Cosmet Chem Jpn. 1989;23:22-30.
100. Roskos KV, Bircher AJ, Maibach HI, Guy RH. Pharmacodynamic measurements of methyl nicotinate percutaneous absorption: the effect of aging on microcirculation. Br J Dermatol. 1990;122(2):165-171.
101. Roskos KV, Maibach HI, Guy RH. The effect of aging on percutaneous absorption in man. J Pharmacokinet Biopharm. 1989;17(6):617-630.
102. Giusti F, Martella A, Bertoni L, Seidenari S. Skin barrier, hydration, and pH of the skin of infants under 2 years of age. Pediatr Dermatol. 2001;18(2):93-96.
103. King A, Balaji S, Keswani SG. Biology and function of fetal and pediatric skin. Facial Plastic Surgery Clinics. 2013;21(1):1-6.

104. Nikolovski J, Stamatas GN, Kollias N, Wiegand BC. Barrier function and water-holding and transport properties of infant stratum corneum are different from adult and continue to develop through the first year of life. J Invest Dermatol. 2008;128(7):1728-1736.
105. Visscher MO, Adam R, Brink S, Odio M. Newborn infant skin: Physiology, development, and care. Clin Dermatol. 2015;33(3):271-280.
106. Maibach HI, Feldmann RJ, Milby TH, Serat WF. Regional variation in percutaneous penetration in man. Archives of Environmental Health: An International Journal. 1971;23(3):208-211.
107. Rougier A, Dupuis D, Lotte C, et al. Regional variation in percutaneous absorption in man: measurement by the stripping method. Archives of Dermatological Research. 1986;278(6):465-469.
108. Berardesca E, Maibach H. Racial differences in skin pathophysiology. J Am Acad Dermatol. 1996;34(4):667-672.
109. Berardesca E, Maibach HI. Racial differences in sodium lauryl sulphate induced cutaneous irritation: black and white. Contact Dermatitis. 1988;18(2):65-70.
110. Kompaore F, Marty JP, Dupont C. *In vivo* evaluation of the stratum corneum barrier function in blacks, caucasians and asians with two noninvasive methods. Skin Pharmacol Physiol. 1993;6(3):200-207.
111. Warrier AG, Kligman AM, Harper RA, Bowman J, Wickett RR. A comparison of black and white skin using noninvasive methods. J Soc Cosmet Chem. 1996;47:229-240.
112. Jacobi U, Gautier J, Sterry W, Lademann J. Gender-related differences in the physiology of the stratum corneum. Dermatology. 2005;211(4):312-317.
113. Reed JT, Ghadially R, Elias PM. Skin type, but neither race nor gender, influence epidermal permeability barrier function. JAMA Dermatology. 1995;131(10):1134-1138.
114. Harvell J, Hussona-Saeed I, Maibach I. Changes in transepidermal water loss and cutaneous blood flow during the menstrual cycle. Contact Dermatitis. 1992;27(5):294-301.
115. Muizzuddin N, Marenus KD, Schnittger SF, Sullivan M, Maes DH. Effect of systemic hormonal cyclicity on skin. Int J Cosmet Sci. 2006;28(1):77-77.
116. Roberts MS. Common skin conditions and disorders. Drug Discov Today Dis Mech. 2008;5(2):125-126.
117. Roberts MS. Skin diseases. Drug Discov Today Dis Mech. 2008;5(1):e1-e2.
118. Kassan DG, Lynch AM, Stiller MJ. Physical enhancement of dermatologic drug delivery: Iontophoresis and phonophoresis. J Am Acad Dermatol. 1996;34(4):657-666.
119. Cross SE, Roberts MS. Physical enhancement of transdermal drug application: Is delivery technology keeping up with pharmaceutical development? Current Drug Delivery. 2004;1(1):81-92.
120. Grice J, Prow TW, Kendall MAF, Roberts MS. Electrical and physical methods of skin penetration enhancement. In: Benson HA, Watkinson AC, editors. Topical and transdermal drug delivery. New Jersey: John Wiley & Sons, Inc; 2012.
121. Roustit M, Blaise S, Cracowski J-L. Trials and tribulations of skin iontophoresis in therapeutics. Br J Clin Pharmacol. 2014;77(1):63-71.
122. Kalaria DR, Dubey S, Kalia YN. Clinical applications of transdermal iontophoresis. Transdermal and Topical Drug Delivery. 2012:67.
123. Gratieri T, Kalaria D, Kalia YN. Non-invasive iontophoretic delivery of peptides and proteins across the skin. Expert Opinion on Drug Delivery. 2011;8(5):645-663.
124. Dixit N, Bali V, Baboota S, Ahuja A, Ali J. Iontophoresis - an approach for controlled drug delivery: A review. Current Drug Delivery. 2007;4(1):1-10.
125. Mitragotri S. Sonophoresis: Ultrasound-mediated transdermal drug delivery. In: Dragicevic N, I. Maibach H, editors. Percutaneous penetration enhancers physical

methods in penetration enhancement. Berlin, Heidelberg: Springer Berlin Heidelberg; 2017. p. 3-14.
126. Fellinger K, Schmidt J. Klinik and therapies des chromischen gelenkreumatismus. Austria: Maudrich, Vienna; 1954. p. 549-552.
127. Mitragotri S, Blankschtein D, Langer R. Transdermal drug delivery using low-frequency sonophoresis. Pharm Res. 1996;13(3):411-420.
128. Brown L, Langer R. Transdermal delivery of drugs. Annu Rev Med. 1988;39(1):221-229.
129. Tezel A, Mitragotri S. Interactions of inertial cavitation bubbles with stratum corneum lipid bilayers during low-frequency sonophoresis. Biophys J. 2003;85(6):3502-3512.
130. Murthy SN. Magnetophoresis: an approach to enhance transdermal drug diffusion. Pharmazie. 1999;54(5):377-379.
131. Benson HAE, McIldowie M, Prow T. Magnetophoresis: Skin penetration enhancement by a magnetic field. In: Dragicevic N, I. Maibach H, editors. Percutaneous penetration enhancers physical methods in penetration enhancement. Berlin, Heidelberg: Springer Berlin Heidelberg; 2017. p. 195-206.
132. Murthy SN, Hiremath SRR. Physical and chemical permeation enhancers in transdermal delivery of terbutaline sulphate. AAPS PharmSciTech. 2001;2(1):1-5.
133. Murthy SN, Hiremath SRR. Effect of magnetic field on the permeation of salbutamol sulphate. Indian Drugs. 1999;36:663-664.
134. Murthy SN, Sammeta SM, Bowers C. Magnetophoresis for enhancing transdermal drug delivery: Mechanistic studies and patch design. J Control Release. 2010;148(2):197-203.
135. Benson HA, Cacetta R, Eijkenboom M, Edwards J, editors. Dermaportation treated skin is more permeable to Voltaren emulgel. 8th Worls Congress on Inflammation; 2007; Copenhagen.
136. Namjoshi S, Caccetta R, Edwards J, Benson HA. Liquid chromatography assay for 5-aminolevulinic acid: application to *in vitro* assessment of skin penetration via Dermaportation. J Chromatogr B Analyt Technol Biomed Life Sci. 2007;852(1-2):49-55.
137. Namjoshi S, Chen Y, Edwards J, Benson HA. Enhanced transdermal delivery of a dipeptide by dermaportation. Biopolymers. 2008;90(5):655-62.
138. Cacetta R, Eijkenboom M, Edwards J, Namjoshi S, Benson HA, editors. Increased transdermal delivery of local anaesthetics by the novel penetration enhancement technology Dermaportation: *in vitro* and *in vivo* assessment. . Pharmaceutical Sciences World Congress; 2007; Amsterdam.
139. Krishnan G, Edwards J, Chen Y, Benson HA. Enhanced skin permeation of naltrexone by pulsed electromagnetic fields in human skin *in vitro*. J Pharm Sci. 2010;99(6):2724-31.
140. Benson HA, Krishnan G, Edwards J, Liew YM, Wallace VP. Enhanced skin permeation and hydration by magnetic field array: preliminary *in-vitro* and *in-vivo* assessment. J Pharm Pharmacol. 2010;62(6):696-701.
141. Donnelly RF, Majithiya R, Singh TRR, et al. Design, optimisation and characterisation of polymeric microneedle arrays prepared by a novel laser-based micromoulding technique. Pharm Res. 2011;28(1):41-57.
142. Mohammed YH, Yamada M, Lin LL, et al. Microneedle enhanced delivery of cosmeceutically relevant peptides in human skin. PLoS One. 2014;9(7):e101956.
143. Bariya SH, Gohel MC, Mehta TA, Sharma OP. Microneedles: an emerging transdermal drug delivery system. J Pharm Pharmacol. 2012;64(1):11-29.
144. Xie Y, Xu B, Gao Y. Controlled transdermal delivery of model drug compounds by MEMS microneedle array. Nanomedicine: Nanotechnology, Biology and Medicine. 2005;1(2):184-190.
145. Kim Y-C, Park J-H, Prausnitz MR. Microneedles for drug and vaccine delivery. Advanced Drug Delivery Reviews. 2012;64(14):1547-1568.

146. Quinn HL, Kearney M-C, Courtenay AJ, McCrudden MTC, Donnelly RF. The role of microneedles for drug and vaccine delivery. Expert Opinion on Drug Delivery. 2014;11(11):1769-1780.
147. Xie S, Li Z, Yu Z. Microneedles for transdermal delivery of insulin. Journal of Drug Delivery Science and Technology. 2015;28:11-17.
148. Prausnitz MR. Microneedles for transdermal drug delivery. Advanced Drug Delivery Reviews. 2004;56(5):581-587.
149. Cheung K, Das DB. Microneedles for drug delivery: trends and progress. Drug Delivery. 2016;23(7):2338-2354.
150. Bhatnagar S, Dave K, Venuganti VVK. Microneedles in the clinic. J Control Release. 2017;260:164-182.
151. Ita K. Transdermal delivery of drugs with microneedles: Strategies and outcomes. Journal of Drug Delivery Science and Technology. 2015;29:16-23.
152. Escobar-Chávez JJ, Bonilla-Martínez D, Angélica M, et al. Microneedles: A valuable physical enhancer to increase transdermal drug delivery. The Journal of Clinical Pharmacology. 2011;51(7):964-977.
153. Larrañeta E, McCrudden MTC, Courtenay AJ, Donnelly RF. Microneedles: A new frontier in nanomedicine delivery. Pharm Res. 2016;33(5):1055-1073.
154. Arora A, Prausnitz MR, Mitragotri S. Micro-scale devices for transdermal drug delivery. Int J Pharm. 2008;364(2):227-236.
155. Barry BW. Lipid-protein-partitioning theory of skin penetration enhancement. J Control Release. 1991;15(3):237-248.
156. Barry BW. Vehicle effect: What Is an enhancer? In: Shah VP, Maibach HI, editors. Topical drug bioavailability, bioequivalence, and penetration. Boston, MA: Springer US; 1993. p. 261-276.
157. Barry BW. Mode of action of penetration enhancer in human skin. J Control Release. 1987;6(1):85-97.
158. Barry BW. Breaching the skin's barrier to drugs. Nat Biotechnol. 2004;22(2):165-167.
159. Hadgraft J. Passive enhancement strategies in topical and transdermal drug delivery. Int J Pharm. 1999;184(1):1-6.
160. Moser K, Kriwet K, Naik A, Kalia YN, Guy RH. Passive skin penetration enhancement and its quantification in vitro. Eur J Pharm Biopharm. 2001;52(2):103-112.
161. Pham QD, Björklund S, Engblom J, Topgaard D, Sparr E. Chemical penetration enhancers in stratum corneum — Relation between molecular effects and barrier function. J Control Release. 2016;232:175-187.
162. Lane ME. Skin penetration enhancers. Int J Pharm. 2013;447(1–2):12-21.
163. Maghraby GMME, Campbell M, Finnin BC. Mechanisms of action of novel skin penetration enhancers: Phospholipid versus skin lipid liposomes. Int J Pharm. 2005;305(1):90-104.
164. Williams AC, Barry BW. Penetration enhancers. Advanced Drug Delivery Reviews. 2012;64:128-137.
165. Sala M, Diab R, Elaissari A, Fessi H. Lipid nanocarriers as skin drug delivery systems: Properties, mechanisms of skin interactions and medical applications. Int J Pharm. 2018;535(1):1-17.
166. Pardeike J, Hommoss A, Müller RH. Lipid nanoparticles (SLN, NLC) in cosmetic and pharmaceutical dermal products. Int J Pharm. 2009;366(1):170-184.
167. Mehnert W, Mäder K. Solid lipid nanoparticles: Production, characterization and applications. Advanced Drug Delivery Reviews. 2012;64:83-101.
168. Das S, Ng WK, Tan RBH. Are nanostructured lipid carriers (NLCs) better than solid lipid nanoparticles (SLNs): Development, characterizations and comparative evaluations of clotrimazole-loaded SLNs and NLCs? Eur J Pharm Sci. 2012;47(1):139-151.

169. Zoubari G, Staufenbiel S, Volz P, Alexiev U, Bodmeier R. Effect of drug solubility and lipid carrier on drug release from lipid nanoparticles for dermal delivery. Eur J Pharm Biopharm. 2017;110:39-46.
170. Bose S, Du Y, Takhistov P, Michniak-Kohn B. Formulation optimisation and topical delivery of quercetin from solid lipid based nanosystems. Int J Pharm. 2013;441(1):56-66.
171. Clares B, Calpena AC, Parra A, et al. Nanoemulsions (NEs), liposomes (LPs) and solid lipid nanoparticles (SLNs) for retinyl palmitate: Effect on skin permeation. Int J Pharm. 2014;473(1–2):591-598.
172. Dingler A, Blum RP, Niehus H, R.H M, Gohla S. Solid lipid nanoparticles (SLNTM/LipopearlsTM) a pharmaceutical and cosmetic carrier for the application of vitamin E in dermal products. J Microencapsul. 1999;16(6):751-767.
173. Fang J-Y, Fang C-L, Liu C-H, Su Y-H. Lipid nanoparticles as vehicles for topical psoralen delivery: Solid lipid nanoparticles (SLN) versus nanostructured lipid carriers (NLC). Eur J Pharm Biopharm. 2008;70(2):633-640.
174. Gilbert E, Roussel L, Serre C, et al. Percutaneous absorption of benzophenone-3 loaded lipid nanoparticles and polymeric nanocapsules: A comparative study. Int J Pharm. 2016;504(1):48-58.
175. Gokce EH, Korkmaz E, Dellera E, et al. Resveratrol-loaded solid lipid nanoparticles versus nanostructured lipid carriers: Evaluation of antioxidant potential for dermal applications. International journal of nanomedicine. 2012;7:1841-1850.
176. Rigon R, Fachinetti N, Severino P, Santana M, Chorilli M. Skin Delivery and in Vitro Biological Evaluation of Trans-Resveratrol-Loaded Solid Lipid Nanoparticles for Skin Disorder Therapies. Molecules. 2016;21(1):116.
177. Shah KA, Date AA, Joshi MD, Patravale VB. Solid lipid nanoparticles (SLN) of tretinoin: Potential in topical delivery. Int J Pharm. 2007;345(1):163-171.
178. Chen J, Wei N, Lopez-Garcia M, et al. Development and evaluation of resveratrol, Vitamin E, and epigallocatechin gallate loaded lipid nanoparticles for skin care applications. Eur J Pharm Biopharm. 2017;117:286-291.
179. Liu J, Hu W, Chen H, et al. Isotretinoin-loaded solid lipid nanoparticles with skin targeting for topical delivery. Int J Pharm. 2007;328(2):191-195.
180. Lv Q, Yu A, Xi Y, et al. Development and evaluation of penciclovir-loaded solid lipid nanoparticles for topical delivery. Int J Pharm. 2009;372(1):191-198.
181. Mei Z, Chen H, Weng T, Yang Y, Yang X. Solid lipid nanoparticle and microemulsion for topical delivery of triptolide. Eur J Pharm Biopharm. 2003;56(2):189-196.
182. Raj R, Mongia P, Ram A, Jain NK. Enhanced skin delivery of aceclofenac *via* hydrogel-based solid lipid nanoparticles. Artificial Cells, Nanomedicine, and Biotechnology. 2016;44(6):1434-1439.
183. Bose S, Michniak-Kohn B. Preparation and characterization of lipid based nanosystems for topical delivery of quercetin. Eur J Pharm Sci. 2013;48(3):442-452.
184. Baek J-S, Pham CV, Myung C-S, Cho C-W. Tadalafil-loaded nanostructured lipid carriers using permeation enhancers. Int J Pharm. 2015;495(2):701-709.
185. Gaba B, Fazil M, Khan S, et al. Nanostructured lipid carrier system for topical delivery of terbinafine hydrochloride. Bulletin of Faculty of Pharmacy, Cairo University. 2015;53(2):147-159.
186. Junyaprasert VB, Teeranachaideekul V, Souto EB, Boonme P, Müller RH. Q10-loaded NLC versus nanoemulsions: Stability, rheology and in vitro skin permeation. Int J Pharm. 2009;377(1):207-214.
187. Schwarz JC, Baisaeng N, Hoppel M, et al. Ultra-small NLC for improved dermal delivery of coenyzme Q10. Int J Pharm. 2013;447(1):213-217.
188. Jain S, Patel N, Shah MK, Khatri P, Vora N. Recent Advances in Lipid-Based Vesicles and Particulate Carriers for Topical and Transdermal Application. J Pharm Sci. 2017;106(2):423-445.

189. Mezei M, Gulasekharam V. Liposomes—A selective drug delivery system for the topical route of administration: gel dosage form. J Pharm Pharmacol. 1982;34(7):473-474.
190. Jain S, Patel N, Madan P, Lin S. Quality by design approach for formulation, evaluation and statistical optimisation of diclofenac-loaded ethosomes via transdermal route. Pharm Dev Technol. 2015;20(4):473-489.
191. Ashtikar M, Nagarsekar K, Fahr A. Transdermal delivery from liposomal formulations – Evolution of the technology over the last three decades. J Control Release. 2016;242:126-140.
192. Touitou E, Dayan N, Bergelson L, Godin B, Eliaz M. Ethosomes — novel vesicular carriers for enhanced delivery: characterization and skin penetration properties. J Control Release. 2000;65(3):403-418.
193. Cevc G. Lipid vesicles and other colloids as drug carriers on the skin. Advanced Drug Delivery Reviews. 2004;56(5):675-711.
194. Cevc G, Blume G. Lipid vesicles penetrate into intact skin owing to the transdermal osmotic gradients and hydration force. Biochimica et Biophysica Acta (BBA) - Biomembranes. 1992;1104(1):226-232.
195. Cevc G, Blume G, Schätzlein A. Transfersomes-mediated transepidermal delivery improves the regio-specificity and biological activity of corticosteroids in vivo1. J Control Release. 1997;45(3):211-226.
196. Cevc G, Vierl U. Nanotechnology and the transdermal route: A state of the art review and critical appraisal. J Control Release. 2010;141(3):277-299.
197. Benson HA. Transfersomes for transdermal drug delivery. Expert Opin Drug Deliv. 2006;3(6):727-37.
198. Cevc G, Gebauer D, Stieber J, Schätzlein A, Blume G. Ultraflexible vesicles, Transfersomes, have an extremely low pore penetration resistance and transport therapeutic amounts of insulin across the intact mammalian skin. Biochimica et Biophysica Acta (BBA) - Biomembranes. 1998;1368(2):201-215.
199. Mahor S, Rawat A, Dubey PK, et al. Cationic transfersomes based topical genetic vaccine against hepatitis B. Int J Pharm. 2007;340(1):13-19.
200. Zhang Y-T, Shen L-N, Wu Z-H, Zhao J-H, Feng N-P. Comparison of ethosomes and liposomes for skin delivery of psoralen for psoriasis therapy. Int J Pharm. 2014;471(1):449-452.
201. Mahmood S, Mandal UK, Chatterjee B. Transdermal delivery of raloxifene HCl via ethosomal system: Formulation, advanced characterizations and pharmacokinetic evaluation. Int J Pharm. 2018;542(1):36-46.
202. Zhai Y, Xu R, Wang Y, et al. Ethosomes for skin delivery of ropivacaine: preparation, characterization and *ex vivo* penetration properties. Journal of Liposome Research. 2015;25(4):316-324.
203. Geusens B, Van Gele M, Braat S, et al. Flexible nanosomes (SECosomes) enable efficient siRNA delivery in cultured primary skin cells and in the viable epidermis of *ex vivo* human skin. Advanced Functional Materials. 2010;20(23):4077-4090.
204. Bracke S, Geusens B, Dynoodt P, et al. Synthesis and characterization of non-viral liposomal carriers for the local application of siRNA molecules and anti-miRNAs in the therapeutic treatment of psoriasis. J Transl Med. 2011;9(Suppl 2):P13-P13.
205. Bracke S, Carretero M, Guerrero-Aspizua S, et al. Targeted silencing of DEFB4 in a bioengineered skin-humanized mouse model for psoriasis: development of siRNA SECosome-based novel therapies. Exp Dermatol. 2014;23(3):199-201.
206. Chen Y, Lu Y, Chen J, et al. Enhanced bioavailability of the poorly water-soluble drug fenofibrate by using liposomes containing a bile salt. Int J Pharm. 2009;376(1):153-160.
207. Patra M, Salonen E, Terama E, et al. Under the influence of alcohol: The effect of ethanol and methanol on lipid bilayers. Biophys J. 2006;90(4):1121-1135.

208. Clerc SG, Thompson TE. A possible mechanism for vesicle formation by extrusion. Biophys J. 1994;67(1):475-476.
209. Kim A, Lee EH, Choi S-H, Kim C-K. *In vitro* and *in vivo* transfection efficiency of a novel ultradeformable cationic liposome. Biomaterials. 2004;25(2):305-313.
210. Uchegbu IF, Vyas SP. Non-ionic surfactant based vesicles (niosomes) in drug delivery. Int J Pharm. 1998;172(1):33-70.
211. Florence A. New Drug Delivery Systems. Chemistry and Industry. 24 ed; 1993. 5 p. p. 1000-1004.
212. Marianecci C, Di Marzio L, Rinaldi F, et al. Niosomes from 80s to present: The state of the art. Adv Colloid Interface Sci. 2014;205:187-206.
213. Baillie AJ, Florence AT, Hume LR, Muirhead GT, Rogerson A. The preparation and properties of niosomes—non-ionic surfactant vesicles. J Pharm Pharmacol. 1985;37(12):863-868.
214. Balakrishnan P, Shanmugam S, Lee WS, et al. Formulation and *in vitro* assessment of minoxidil niosomes for enhanced skin delivery. Int J Pharm. 2009;377(1):1-8.
215. van Hal DA. Nonionic surfactant vesicles for dermal and transdermal drug delivery: Rijksuniversiteit te Leiden; 1994.
216. Yoshioka T, Sternberg B, Florence AT. Preparation and properties of vesicles (niosomes) of sorbitan monoesters (Span 20, 40, 60 and 80) and a sorbitan triester (Span 85). Int J Pharm. 1994;105(1):1-6.
217. Fang J-Y, Hong C-T, Chiu W-T, Wang Y-Y. Effect of liposomes and niosomes on skin permeation of enoxacin. Int J Pharm. 2001;219(1–2):61-72.
218. Pando D, Matos M, Gutiérrez G, Pazos C. Formulation of resveratrol entrapped niosomes for topical use. Colloids and Surfaces B: Biointerfaces. 2015;128:398-404.
219. Verma D. Invasomes-novel topical carriers for enhanced topical delivery: characterization and skin penetration properties. Marburg/Lahn. 2002.
220. van Kuijk-Meuwissen MEMJ, Junginger HE, Bouwstra JA. Interactions between liposomes and human skin *in vitro*, a confocal laser scanning microscopy study. Biochimica et Biophysica Acta (BBA) - Biomembranes. 1998;1371(1):31-39.
221. El Maghraby GMM, Williams AC, Barry BW. Skin delivery of oestradiol from lipid vesicles: importance of liposome structure. Int J Pharm. 2000;204(1):159-169.
222. El Maghraby GMM, Williams AC, Barry BW. Oestradiol skin delivery from ultradeformable liposomes: refinement of surfactant concentration. Int J Pharm. 2000;196(1):63-74.
223. Aqil M, Ahad A, Sultana Y, Ali A. Status of terpenes as skin penetration enhancers. Drug Discovery Today. 2007;12(23):1061-1067.
224. Chen J, Jiang Q-D, Chai Y-P, et al. Natural terpenes as penetration enhancers for transdermal drug delivery. Molecules. 2016;21(12):1709.
225. Thakur RA, Wang Y, Michniak BB. Essential oils and terpenes. In: Smith EW, Maibach HI, editors. Percutaneous penetration enhancers. 2nd edition: CRC Press; 2005. p. 159-173.
226. Dragicevic-Curic N, Scheglmann D, Albrecht V, Fahr A. Temoporfin-loaded invasomes: Development, characterization and *in vitro* skin penetration studies. J Control Release. 2008;127(1):59-69.
227. Trauer S, Richter H, Kuntsche J, et al. Influence of massage and occlusion on the *ex vivo* skin penetration of rigid liposomes and invasomes. Eur J Pharm Biopharm. 2014;86(2):301-306.
228. Amnuaikit T, Limsuwan T, Khongkow P, Boonme P. Vesicular carriers containing phenylethyl resorcinol for topical delivery system; liposomes, transfersomes and invasomes. Asian Journal of Pharmaceutical Sciences. 2018;13(5):472-484.

229. Mura S, Manconi M, Sinico C, Valenti D, Fadda AM. Penetration enhancer-containing vesicles (PEVs) as carriers for cutaneous delivery of minoxidil. Int J Pharm. 2009;380(1):72-79.
230. Manconi M, Caddeo C, Sinico C, et al. Penetration enhancer-containing vesicles: Composition dependence of structural features and skin penetration ability. Eur J Pharm Biopharm. 2012;82(2):352-359.
231. Manconi M, Sinico C, Fadda AM. Penetration enhancer-containing vesicles for cutaneous drug delivery. In: Dragicevic N, Maibach HI, editors. Percutaneous penetration enhancers chemical methods in penetration enhancement: Nanocarriers. Berlin, Heidelberg: Springer Berlin Heidelberg; 2016. p. 93-110.
232. Mura S, Manconi M, Fadda AM, et al. Penetration enhancer-containing vesicles (PEVs) as carriers for cutaneous delivery of minoxidil: *in vitro* evaluation of drug permeation by infrared spectroscopy. Pharm Dev Technol. 2013;18(6):1339-1345.
233. Manconi M, Caddeo C, Sinico C, et al. *Ex vivo* skin delivery of diclofenac by transcutol containing liposomes and suggested mechanism of vesicle–skin interaction. Eur J Pharm Biopharm. 2011;78(1):27-35.
234. Manconi M, Sinico C, Caddeo C, et al. Penetration enhancer containing vesicles as carriers for dermal delivery of tretinoin. Int J Pharm. 2011;412(1):37-46.
235. Chessa M, Caddeo C, Valenti D, et al. Effect of penetration enhancer containing vesicles on the percutaneous delivery of quercetin through new born pig skin. Pharmaceutics. 2011;3(3):497.
236. Santos P, Watkinson AC, Hadgraft J, Lane ME. Application of microemulsions in dermal and transdermal drug delivery. Skin Pharmacol Physiol. 2008;21(5):246-259.
237. Anton N, Vandamme TF. Nano-emulsions and micro-emulsions: Clarifications of the critical differences. Pharm Res. 2011;28(5):978-985.
238. Anton N, Benoit J-P, Saulnier P. Design and production of nanoparticles formulated from nano-emulsion templates—A review. J Control Release. 2008;128(3):185-199.
239. McClements DJ. Nanoemulsions versus microemulsions: terminology, differences, and similarities. Soft Matter. 2012;8(6):1719-1729.
240. Gupta A, Eral HB, Hatton TA, Doyle PS. Nanoemulsions: formation, properties and applications. Soft Matter. 2016;12(11):2826-2841.
241. Vadlamudi HC, Narendran H, Nagaswaram T, et al. Microemulsions based transdermal drug delivery systems. Current Drug Discovery Technologies. 2014;11(3):169-180.
242. Danielsson I, Lindman B. The definition of microemulsion. Colloids and Surfaces. 1981;3(4):391-392.
243. Fanun M. Microemulsions as delivery systems. Current Opinion in Colloid & Interface Science. 2012;17(5):306-313.
244. Heuschkel S, Goebel A, Neubert RHH. Microemulsions—modern colloidal carrier for dermal and transdermal drug delivery. J Pharm Sci. 2008;97(2):603-631.
245. Scriven LE. Equilibrium bicontinuous structure. Nature. 1976;263(5573):123-125.
246. Bhatia G, Zhou Y, Banga AK. Adapalene Microemulsion for Transfollicular Drug Delivery. J Pharm Sci. 2013;102(8):2622-2631.
247. Naoui W, Bolzinger M-A, Fenet B, et al. Microemulsion microstructure influences the skin delivery of an hydrophilic drug. Pharm Res. 2011;28(7):1683-1695.
248. Baspinar Y, Borchert H-H. Penetration and release studies of positively and negatively charged nanoemulsions—Is there a benefit of the positive charge? Int J Pharm. 2012;430(1–2):247-252.
249. Baspinar Y, Keck CM, Borchert H-H. Development of a positively charged prednicarbate nanoemulsion. Int J Pharm. 2010;383(1):201-208.

250. Hoeller S, Sperger A, Valenta C. Lecithin based nanoemulsions: A comparative study of the influence of non-ionic surfactants and the cationic phytosphingosine on physicochemical behaviour and skin permeation. Int J Pharm. 2009;370(1):181-186.
251. Yilmaz E, Borchert H-H. Effect of lipid-containing, positively charged nanoemulsions on skin hydration, elasticity and erythema—An *in vivo* study. Int J Pharm. 2006;307(2):232-238.
252. Yilmaz E, Borchert H-H. Design of a phytosphingosine-containing, positively-charged nanoemulsion as a colloidal carrier system for dermal application of ceramides. Eur J Pharm Biopharm. 2005;60(1):91-98.
253. Date AA, Patravale VB. Microemulsions: Applications in transdermal and dermal delivery. Critical Reviews™ in Therapeutic Drug Carrier Systems. 2007;24(6):547-596.
254. Jasmina H, Džana O, Alisa E, Edina V, Ognjenka R, editors. Preparation of nanoemulsions by high-energy and low energy emulsification methods. CMBEBIH 2017: Proceedings of the International Conference on Medical and Biological Engineering; 2017; Singapore: Springer Singapore.
255. Solè I, Solans C, Maestro A, González C, Gutiérrez JM. Study of nano-emulsion formation by dilution of microemulsions. J Colloid Interface Sci. 2012;376(1):133-139.
256. Pons R, Carrera I, Caelles J, Rouch J, Panizza P. Formation and properties of miniemulsions formed by microemulsions dilution. Adv Colloid Interface Sci. 2003;106(1):129-146.
257. Vitale SA, Katz JL. Liquid droplet dispersions formed by homogeneous liquid−liquid nucleation: "The Ouzo Effect". Langmuir. 2003;19(10):4105-4110.
258. Lee HS, Morrison ED, Frethem CD, Zasadzinski JA, McCormick AV. Cryogenic electron microscopy study of nanoemulsion formation from microemulsions. Langmuir. 2014;30(36):10826-10833.
259. Podlogar F, Gašperlin M, Tomšič M, Jamnik A, Rogač MB. Structural characterisation of water–Tween 40®/Imwitor 308®–isopropyl myristate microemulsions using different experimental methods. Int J Pharm. 2004;276(1):115-128.
260. Danino D, Bernheim-Groswasser A, Talmon Y. Digital cryogenic transmission electron microscopy: an advanced tool for direct imaging of complex fluids. Colloids and Surfaces A: Physicochemical and Engineering Aspects. 2001;183-185:113-122.
261. Acharya DP, Hartley PG. Progress in microemulsion characterization. Current Opinion in Colloid & Interface Science. 2012;17(5):274-280.
262. Lutz R, Aserin A, Wachtel EJ, et al. A study of the emulsified microemulsion by SAXS, Cryo-TEM, SD-NMR, and electrical conductivity. Journal of Dispersion Science and Technology. 2007;28(8):1149-1157.
263. Allouche J, Tyrode E, Sadtler V, Choplin L, Salager J-L. Simultaneous Conductivity and Viscosity Measurements as a Technique To Track Emulsion Inversion by the Phase-Inversion-Temperature Method. Langmuir. 2004; 20(6):2134-2140.
264. Bhattacharya S, Stokes JP, Kim MW, Huang JS. Percolation in an Oil-Continuous Microemulsion. Phys Rev Lett. 1985;55(18):1884-1887.
265. Thevenin MA, Grossiord JL, Poelman MC. Sucrose esters/cosurfactant microemulsion systems for transdermal delivery: Assessment of bicontinuous structures. Int J Pharm. 1996;137(2):177-186.
266. Abd E, Namjoshi S, Mohammed YH, Roberts MS, Grice JE. Synergistic skin penetration enhancer and nanoemulsion formulations promote the human epidermal permeation of caffeine and naproxen. J Pharm Sci. 2016;105(1):212-220.
267. Azizi M, Esmaeili F, Partoazar A, Ejtemaei Mehr S, Amani A. Efficacy of nano- and microemulsion-based topical gels in delivery of ibuprofen: an *in vivo* study. J Microencapsul. 2017;34(2):195-202.

268. Kogan A, Garti N. Microemulsions as transdermal drug delivery vehicles. Adv Colloid Interface Sci. 2006;123-126:369-385.
269. Lawrence MJ, Rees GD. Microemulsion-based media as novel drug delivery systems. Adv Drug Deliv Rev. 2000;45.
270. Cross SE, Roberts MS, Jiang R, Benson HAE. Can increasing the viscosity of formulations be used to reduce the human skin penetration of the sunscreen oxybenzone? J Invest Dermatol. 2001;117(1):147-150.
271. Dick IP, Scott RC. Pig ear skin as an *in vitro* model for human skin permeability. J Pharm Pharmacol. 1992;44(8):640-645.
272. Jacobi U, Kaiser M, Toll R, et al. Porcine ear skin: An *in vitro* model for human skin. Skin Res Technol. 2007;13(1):19-24.
273. Songkro S, Purwo Y, Becket G, Rades T. Investigation of newborn pig skin as an *in vitro* animal model for transdermal drug delivery. S.T.P. Pharma Sciences. 2003;13(2):133-139.
274. Nastiti CMRR, Mohammed Y, Telaprolu KC, et al. Evaluation of quantum dot skin penetration in porcine skin: Effect of age and anatomical site of topical application. Skin Pharmacol Physiol. 2019.
275. Bronaugh RL, Stewart RF, Congdon ER. Methods for *in vitro* percutaneous absorption studies II. Animal models for human skin. Toxicol Appl Pharmacol. 1982;62(3):481-488.
276. Sato K, Sugibayashi K, Morimoto Y. Species differences in percutaneous absorption of nicorandil. J Pharm Sci. 1991;80(2):104-107.
277. Roberts ME, Mueller KR. Comparisons of *in vitro* nitroglycerin (TNG) flux across yucatan pig, hairless mouse, and human skin. Pharm Res. 1990;7(6):673-676.
278. Yousef S, Liu X, Mostafa A, et al. Estimating maximal *in vitro* skin permeation flux from studies using non-sink receptor phase conditions. Pharm Res. 2016;33(9):2180-2194.
279. Dasgupta S, Dey S, Choudhury S, Mazumder B. Topical delivery of aceclofenac as nanoemulsion comprising excipients having optimum emulsification capabilities: preparation, characterization and *in vivo* evaluation. Expert Opinion on Drug Delivery. 2013;10(4):411-420.
280. Dasgupta S, K. Ghosh S, Ray S, Singh Kaurav S, Mazumder B. *In vitro* & *in vivo* studies on lornoxicam loaded nanoemulsion gels for topical application. Current Drug Delivery. 2014;11(1):132-138.
281. Shakeel F, Ramadan W, Gargum HM, Singh R. Preparation and *in vivo* evaluation of indomethacin loaded true nanoemulsions. Sci Pharm. 2010;78(1):47.
282. Hamed R, Basil M, AlBaraghthi T, Sunoqrot S, Tarawneh O. Nanoemulsion-based gel formulation of diclofenac diethylamine: design, optimisation, rheological behaviour and *in vitro* diffusion studies. Pharm Dev Technol. 2016;21(8):980-989.
283. Khurana S, Jain NK, Bedi PMS. Nanoemulsion based gel for transdermal delivery of meloxicam: Physico-chemical, mechanistic investigation. Life Sci. 2013;92(6–7):383-392.
284. Hussain A, Samad A, Singh SK, et al. Nanoemulsion gel-based topical delivery of an antifungal drug: *in vitro* activity and *in vivo* evaluation. Drug Delivery. 2016;23(2):642-657.
285. Zheng Y, Ouyang W-Q, Wei Y-P, et al. Effects of Carbopol(®) 934 proportion on nanoemulsion gel for topical and transdermal drug delivery: a skin permeation study. International Journal of Nanomedicine. 2016;11:5971-5987.
286. Rachmawati H, Budiputra DK, Mauludin R. Curcumin nanoemulsion for transdermal application: formulation and evaluation. Drug Dev Ind Pharm. 2014;41(4):560-566.
287. Guo J, Ping Q, Sun G, Jiao C. Lecithin vesicular carriers for transdermal delivery of cyclosporin A. Int J Pharm. 2000;194(2):201-207.

288. Klang V, Haberfeld S, Hartl A, Valenta C. Effect of γ-cyclodextrin on the *in vitro* skin permeation of a steroidal drug from nanoemulsions: Impact of experimental setup. Int J Pharm. 2012;423(2):535-542.
289. Klang V, Matsko N, Raupach K, El-Hagin N, Valenta C. Development of sucrose stearate-based nanoemulsions and optimisation through γ-cyclodextrin. Eur J Pharm Biopharm. 2011;79(1):58-67.
290. Klang V, Valenta C. Lecithin-based nanoemulsions. Journal of Drug Delivery Science and Technology. 2011;21(1):55-76.
291. Isailović T, Đorđević S, Marković B, et al. Biocompatible nanoemulsions for improved aceclofenac skin delivery: Formulation approach using combined mixture-process experimental design. J Pharm Sci. 2016;105(1):308-323.
292. Abd E, Benson H, Roberts M, Grice J. Minoxidil skin delivery from nanoemulsion formulations containing eucalyptol or oleic acid: Enhanced diffusivity and follicular targeting. Pharmaceutics. 2018;10(1):19.
293. Zheng W-w, Zhao L, Wei Y-m, Ye Y, Xiao S-h. Preparation and the *in vitro* evaluation of nanoemulsion system for the transdermal delivery of granisetron hydrochloride. Chem Pharm Bull (Tokyo). 2010;58(8):1015-1019.
294. Hussain A, Samad A, Singh SK, et al. Enhanced stability and permeation potential of nanoemulsion containing sefsol-218 oil for topical delivery of amphotericin B. Drug Dev Ind Pharm. 2014;41(5):780-790.
295. El-Leithy ES, Ibrahim HK, Sorour RM. *In vitro* and *in vivo* evaluation of indomethacin nanoemulsion as a transdermal delivery system. Drug Delivery. 2015;22(8):1010-1017.
296. Kong M, Chen XG, Kweon DK, Park HJ. Investigations on skin permeation of hyaluronic acid based nanoemulsion as transdermal carrier. Carbohydrate Polymers. 2011;86(2):837-843.
297. Campani V, Biondi M, Mayol L, et al. Development of nanoemulsions for topical delivery of vitamin K1. Int J Pharm. 2016;511(1):170-177.
298. Kumar D, Ali J, Baboota S. Omega 3 fatty acid-enriched nanoemulsion of thiocolchicoside for transdermal delivery: Formulation, characterization and absorption studies. Drug Delivery. 2016;23(2):591-600.
299. Ledet G, Pamujula S, Walker V, et al. Development and *in vitro* evaluation of a nanoemulsion for transcutaneous delivery. Drug Dev Ind Pharm. 2014;40(3):370-379.

Chapter 2. Effect of Acetone and Tape Stripping on Porcine Skin: Application of Multiphoton Tomography-Fluorescence Lifetime Imaging (MPT-FLIM)

2.1 Introduction

Despite the concept of a metabolically-dead, basket weave layer, and inert wrapping[1], SC is acknowledged to be skin barrier against the penetration of molecules, microbes, and nanomaterials.[2] However, any physical or chemical disruption on this barrier may result in increased permeability of foreign materials into the skin.

Dermal exposure of organic solvents may increase the risk of skin dryness, oxidative damage and induce irritant contact dermatitis.[3, 4] Acetone is a highly flammable, volatile and colourless liquid which is used as an organic solvent for a range of industrial, medical and cosmetic purposes. Acetone disrupts the skin barrier by SC lipid extraction.[5-9] In human skin, extraction of skin surface lipid by acetone resulted in dry and scaly skin but it did not increase the TEWL and did not disrupt the deeper skin layers.[10] Under *in vitro* conditions of skin exposure, acetone poorly extracts human SC lipids up to 12 minutes, hence it showed less ability to disrupt the skin barrier.[11]

Tape stripping involves the repeated mechanical movement of applying and then peeling adhesive tapes off the skin surface to remove layers of the SC.[12] Tape stripping is applied to partially remove the SC to provide a compromised skin model[13-16] that can be useful for some experimental protocols including skin penetration study of substances. Tape stripping can also be utilised in both *in vitro* and *in vivo* protocols to determine the deposition of topically applied chemicals within the SC, furrows and follicle orifices.[17-21] Determination of SC protein[22, 23] and lipid[24] within the tape strip samples allows the amount of SC in each strip to be determined and thereby quantifies the amount of applied chemical per amount of SC.

Hence, solvent exposure and tape stripping have the potential to compromise the SC barrier and may lead to the skin permeation of nanomaterials. To explore this, it is useful to identify a technique that will permit real time monitoring of the penetration of nanoparticles into the skin. Multiphoton tomography (MPT) is a powerful, non-invasive fluorescence-based microscopic technology that has become a well-established tool

for optical skin imaging. It is used to investigate a wide range of *in vitro* and *in vivo* skin conditions[25-33], including cancerous skin cells such as: melanoma[34, 35], basal cell carcinoma[36], melanocytic nevi[37] and non-melanoma cancer.[38] MPT has also been reported as a promising method for imaging thick tissues/organs of living animals (intravital microscopy), such as liver [39-49], kidney [50-54], and brain [55-58]. In principle, MPT involves simultaneous energy absorption of two photons (or more) of a fluorophore which are excited at a longer infra-red wavelength (less energy) using highly spatial and temporal intensity of excitation light.[26, 59] This excitation is then followed by emission of fluorescence which is detected at certain wavelengths on high submicron resolution. The emission wavelengths of two-photon excitation are shorter than the excitation wavelengths, resulting in higher energy, MPT thereby offers advantages over confocal laser microscopy including higher resolution, deeper observation through the tissues and less risk of photo-damage as it involves less energy to excite the photons.[26, 28, 29, 60-62] Fluorescence lifetime is the average time of photons being at an excited state. This lifetime is unique for each fluorophore therefore it allows the researchers to distinguish fluorophores more accurately. MPT equipped with fluorescence lifetime imaging (FLIM) is a powerful tool to visualize the skin structure and the deposition of chemicals or particles within the skin layers with better resolution and accuracy.[60, 63]

This study aimed to investigate the effect of acetone and tape stripping on the permeability of nanomaterials in porcine skin using MPT-FLIM. Changes in skin morphology after the acetone and tape stripping treatments and the deposition/ distribution of nanomaterials within skin layers after treatments were examined. We hypothesized that nanomaterials did not penetrate into deeper layers of viable epidermis.

2.2 Experimental section

2.2.1 Materials

Acetone was purchased from Thermo Fisher Scientific Pty Ltd (Australia). Sterile normal saline (0.9% sodium chloride) was purchased from Baxter Healthcare Pty Ltd (Australia). Hydrophilic CdTe/CdS QDs (size ~ 2.1 nm) were synthesised and characterised in house, as previously described [43, 64]. The QDs were stabilised by mercaptosuccinic acid and coated with carboxyl groups to provide a negatively charged surface. These QDs show excitation wavelength range of 200-450nm and emission wavelength range 490-520 nm. The QDs were vortexed prior to dilution with normal saline immediately before application. Initial concentration of QDs solution

was 14.55 μM which was further diluted into 2.5 μM as a working concentration. A dose of 62.5 pmoles/cm^2 was applied, adapted from the previously reported exposure scenario of 40μL of 1 μM QDs onto 0.64 cm^2 skin.[30, 65]

2.2.2 Skin preparation and Franz cell experimental protocol

Porcine skin was obtained from the abdomen of adult female Yorkshire pigs that underwent scheduled execution due to aging issues, under approval of The University of Queensland Research and Innovation (ANRFA/265/16). The subcutaneous tissue was removed using blunt dissection. Freshly excised skin at the abdominal site was cut to 2x2 cm^2 pieces and placed onto saline wetted-non-woven swab in a 6-well plate, SC side up. The donor chamber of a Franz-type diffusion cell with average surface area of 1.16 cm^2 was then attached to the surface of the skin using a double-sided "O"-ring sticker. The skin was incubated at 35ºC (to reach the skin temperature of 32°C) for 24 hours.

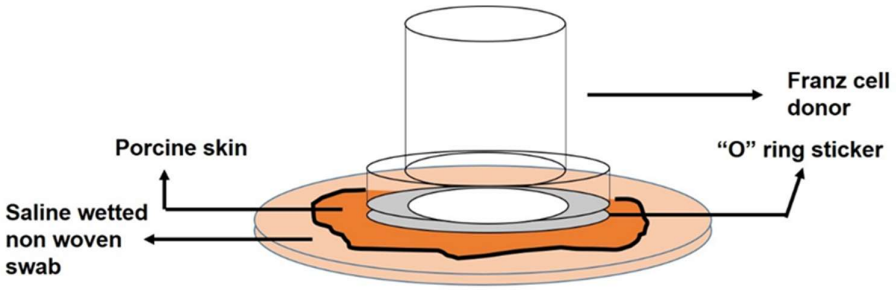

Figure 2.1 Set up of Franz cell experimental equipment

2.2.2.1 Saline application

One mL of normal saline (0.9% NaCl) was applied onto the skin with intact SC followed by skin incubation at 35°C for 2, 4, 6, 8, and 24 hours. Skin with 24h-saline application was used as a control for the next treatments.

2.2.2.2 Acetone application

One mL of 10% or 100% acetone was applied to the skin surface and the donor chamber was covered with a microscope coverslip to minimize the evaporation of acetone. After 24 hours of incubation (at 35°C), the acetone was wiped off and the skin prepared for histology examination or MPT-FLIM imaging.

2.2.2.3 Tape stripping treatment

Adhesive D Squame® stripping tapes (22mm diameter: CuDerm, Dallas, Texas) were applied and peeled off thirty times (30x) on the surface of each skin prior to 24h incubation at 35°C. Each tape stripping was applied with a pressure of 225g/cm^2 using

a D-Squame® disc applicator (CuDerm, Dallas, Texas) for 5 seconds prior to removal. The protocol was carried out based on the study of Jacobi et al.[19] with some modification.

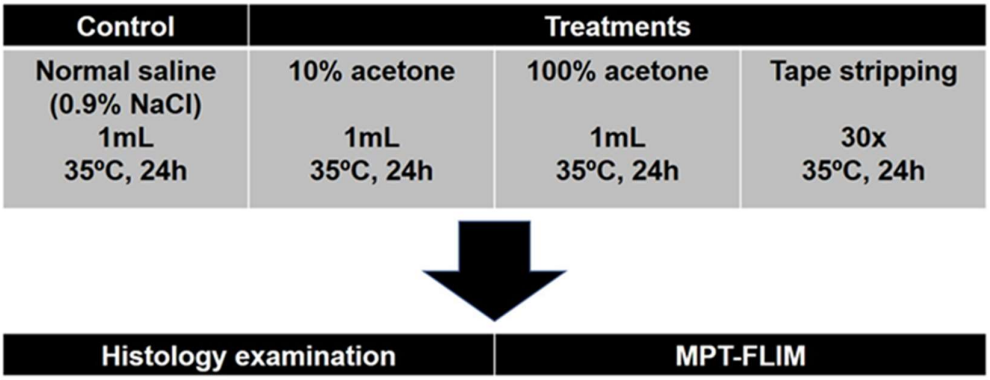

Figure 2.2 Experimental protocol of acetone topical exposure and tape stripping on porcine skin

Application of hydrophilic QDs

QDs were dispersed in saline (for control and tape stripped skin) or in 10% acetone (for acetone treatment) and applied on skin with a dose of 62.5 pmole/cm^2 prior to 24h incubation at 35°C.

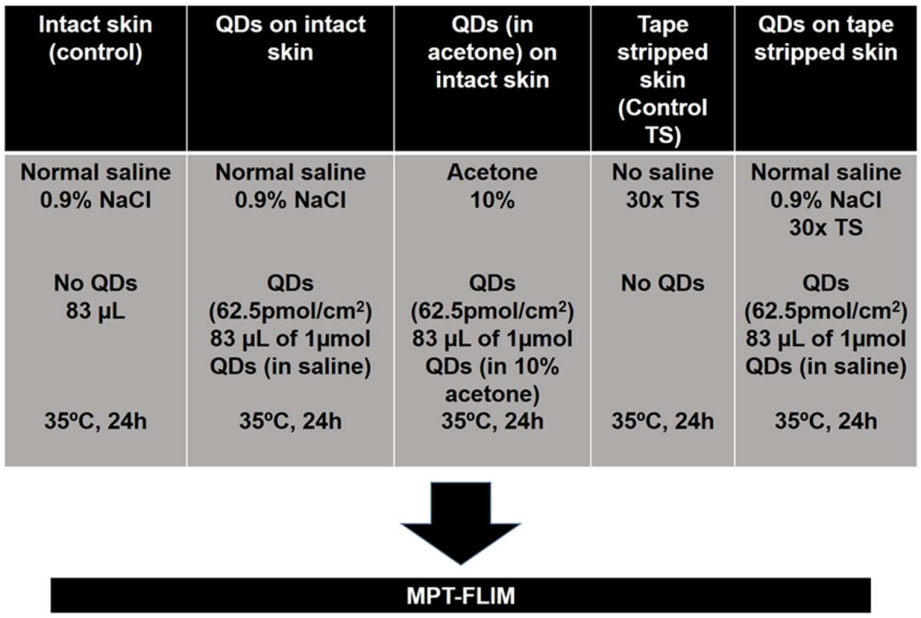

Figure 2.3 Experimental protocol of QDs application on porcine skin

2.2.3 Histology examination

Skin fixation was carried out using 10% formaldehyde solution for 24 hours followed by 70% ethanol immersion for another 24 hours. The fixed skin was then embedded in paraffin and sectioned. Hematoxylin and Eosin (H&E) counter-staining was applied on the skin sections prior to examination under a light microscope (Zeiss GmBH, Oberkochen, Germany) with a 40x objective magnification.

2.2.4 Skin imaging using MPT-FLIM

Images of the skin layers (SC, SG, SS and SB) were acquired using a Multiphoton tomography (LaVision™ GmBH, Göttingen, Germany) equipped with a time-corrrelated single photon-counting module SPC-830 (Becker and Hickl, Berlin, Germany). Photons were excited at 760nm using a tunable titanium-sapphire femtosecond laser (MaiTai, Spectra Physics, Mountain View, CA, USA) with 100mW laser power. Emission wavelengths were set at 387-507nm for channel 1 and 485-585nm for channel 2. Channel 1 facilitated the emission of nicotinamide adenine dinucleotide (NADH) as the skin auto-fluorescence, whereas Channel 2 filtered mostly the emission of QDs. The layer of the skin was determined based on its keratinocyte morphology. Images were collected at 502 x 502 pixels. SPCImage 5.2 software (Becker and Hickl, Germany) was used to analyse the MPT-FLIM images.

2.3 Results

2.3.1 Epidermal morphology of intact porcine skin

Histology examination was conducted prior to MPT-FLIM in order to assist the investigation of the effect of acetone exposure and tape tripping on porcine skin. The skin tissue was examined under a light microscope with the aid of H&E staining. The principle of this staining was based on the combination of deep blue-purple colour of hematoxylin which stains nucleic acids and nuclei in tissues and pink colour of eosin which stain nucleoli, protein (non-specifically), and cytoplasm and extracellular matrix on various pink colour gradation.[66]

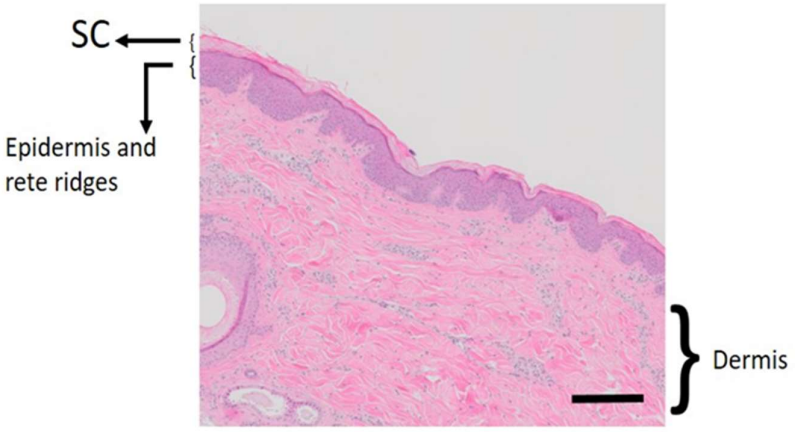

Figure 2.4 H&E image of abdominal porcine skin hydrated with normal saline. Scale bar indicates 200μm

The porcine skin structure is described as it is: the intact SC layers at the outermost site, followed by layers of epidermis (purple colour), with the large area of dermis site (pink colour) where the follicles and sebaceous glands are located (Figure 2.4). Epithelial extensions, known as rete ridges or rete pegs, were the inward projection of epidermis site to dermis.

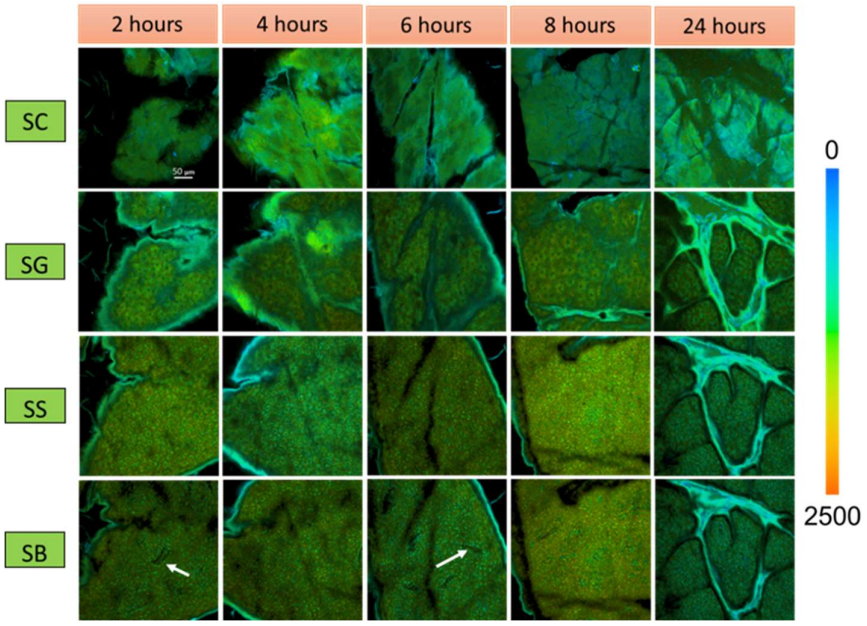

Figure 2.5 MPT FLIM images of skin layers after saline application on the surface of porcine skin (scale bar indicates 50μm). The white arrows denote dermal papillae. The pseudo-colour is based on the average fluorescence lifetime τm (0-2500ps); blue-green-red

Figure 2.5 shows the skin condition acquired by MPT-FLIM after saline application during incubation time of 2,4,6,8, and 24 hours. Those images are displayed in pseudo-colour based on the average fluorescent lifetime of the fluorophores. The fluorescence lifetime is in a range of 0-2500ps with the colour order of blue-green-red. The prominent green colour of the images is generated by the skin auto-fluorescence. Several fluorophores of the skin such as NADH, keratin, and melanin form a configuration of auto-fluorescence with different lifetimes.[33, 60] Skin layers are further designated based on the morphology of keratinocytes. SC is identified by a tissue-paper-like appearance with polygonal patterns of corneocytes surrounded by furrows. Deeper down, the SG layer is represented by large keratinocytes with the nuclei in the centre. Double nuclei in some cells can be seen in this layer. The furrows are located on the outer side of keratinocyte sacks. The keratinocytes in SS appear to be smaller than the ones in SG. SB shows more rigid and even smaller keratinocytes than the SS. Some dermal papilla is located on the deeper site of SB in a form of irregular shape dark holes. Normal condition of keratinocytes is indicated by the small ratio of nucleus diameter to the cell. Saline-hydrated keratinocytes were in normal condition and there was no change in morphology of the keratinocytes during 24h incubation at 35°C.

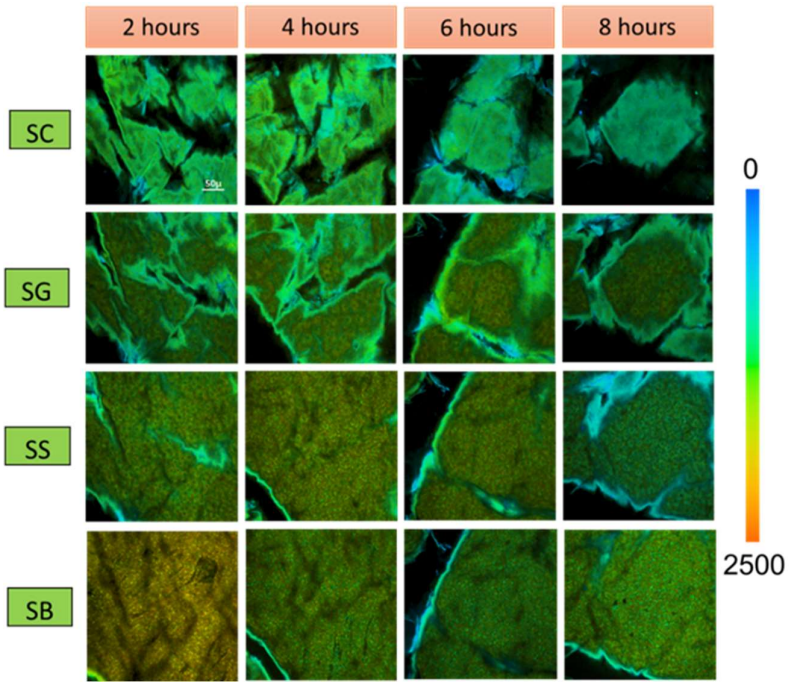

Figure 2.6 MPT FLIM images of skin layers in 8 hour incubation without saline application on top (scale bar indicates 50μm). The pseudo-colour is based on the average fluorescence lifetime τm (0-2500ps); blue-green-red

Figure 2.6 illustrates the MPT FLIM of non-saline-hydrated skin condition in 8 hours. The morphology of the skin layers are similar to the ones in Figure 2.5. The higher tendency of ratio of nucleus diameter to the cell in a longer time of incubation, suggesting that skin was undergoing dehydration during incubation at 35°C.

2.3.2 Epidermal morphology of porcine skin after acetone topical application

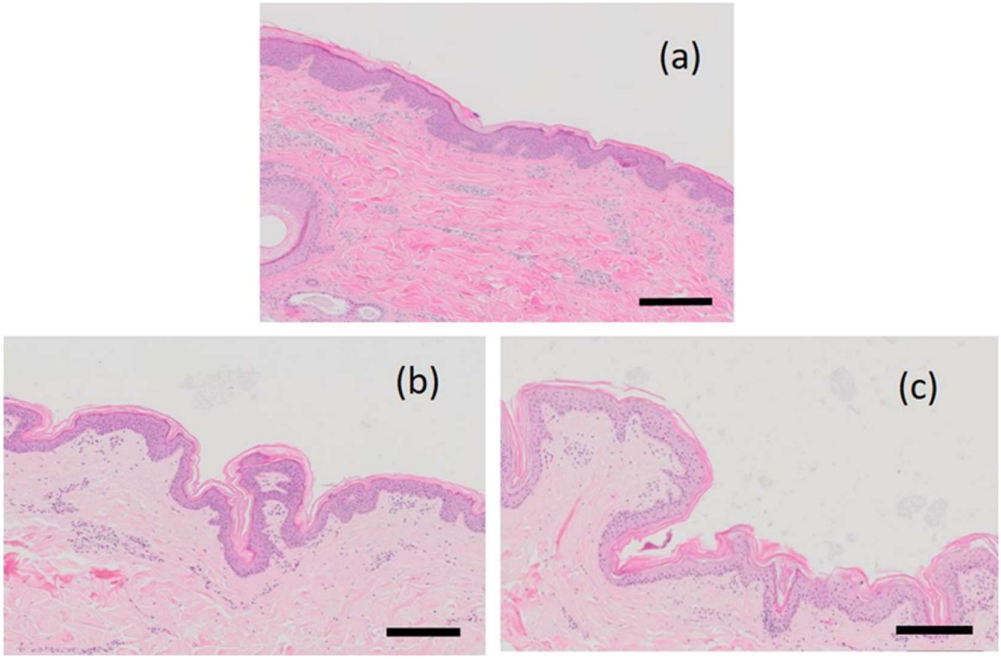

Figure 2.7 H&E images of abdominal porcine skin before and after acetone application for 24h: (a) control: saline application; (b) 10% acetone application; (c) 100% acetone application (scale bars indicate 200μm)

Figure 2.7 shows the effect on porcine skin morphology of exposure to 10% and 100% acetone application for 24h. In comparison to untreated skin (a), the outer SC surface has contracted due to skin shrinkage after 10% (b) and 100% (c) acetone application, respectively. The pink colour intensity of the dermis is decreased in the acetone-treated skin, with a marked difference from untreated to 10% acetone treated and a further loss of colour intensity in the 100% acetone treated skin. In addition, the purple colour intensity of the epidermis has decreased slightly when exposed to 10% acetone, and markedly with the higher concentration of 100% acetone.

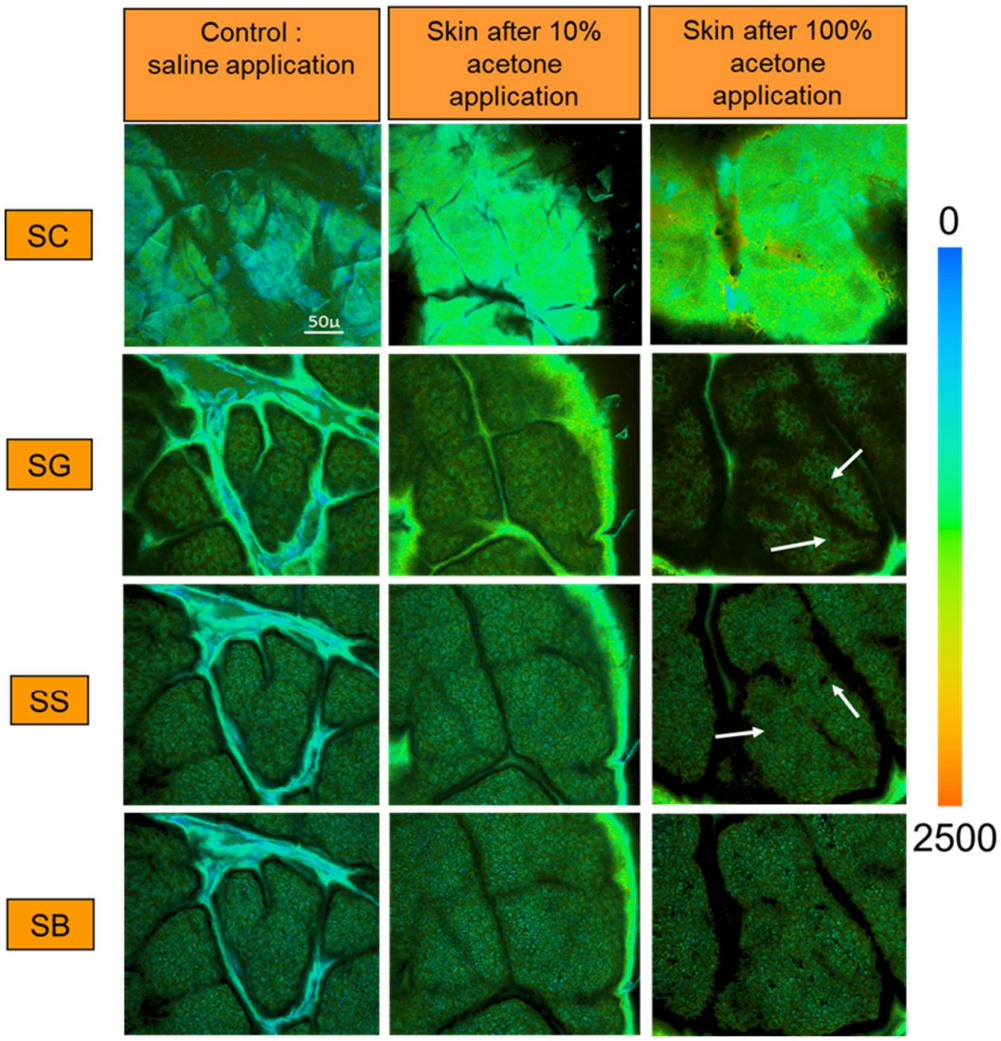

Figure 2.8 MPT-FLIM images of skin strata before and after acetone application (scale bar represents 50µm). The white arrows denote the keratinocytes disappearance. The pseudo-colour is based on the average fluorescence lifetime τm (0-2500ps); blue-green-red

The SC on the acetone-treated skin shows more intense fluorescence compared to the control (Figure 2.8). There is no observable difference of SG, SS, and SB morphologically between control and 10% acetone-treated skin. However, the skin treated with 100% acetone shows holes indicating disappearance of keratinocytes in the SG and SS layers. Larger ratios between the nucleus and cytoplasm in the cells are also observed following exposure to 100% acetone.

2.3.3 Epidermal morphology of porcine skin after tape stripping

Thirty times tape stripping resulted in skin shrinkage and less intense pink colour of dermis (as seen with acetone exposure: Figure 2.7), although the skin was less constricted than the acetone-treated skin (Figure 2.9). We observed a greater than 80% of SC removed on porcine skin that had been incubated with saline for 24h (Figure 2.9. (b)).

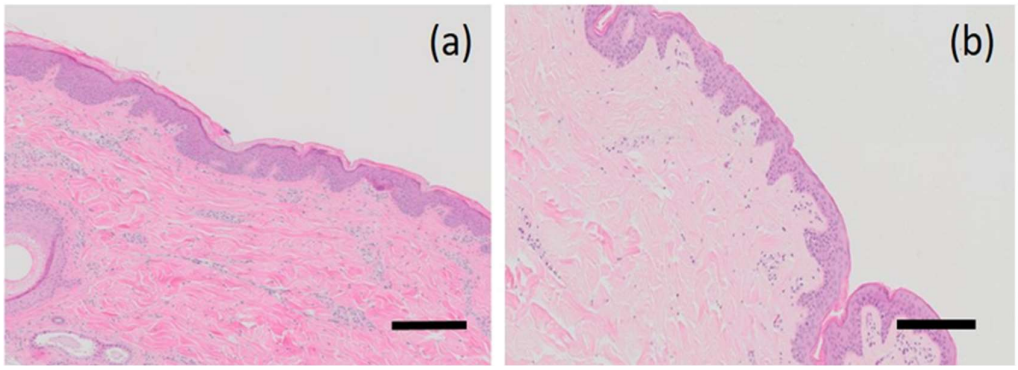

Figure 2.9 H&E images of abdominal porcine skin before and after tape stripping: (a) control: saline application; (b) 30x tape stripping (scale bars indicate 200µm)

Both saline-hydrated intact skin and tape stripped skin show intense green auto-fluorescence (Figure 2.10).

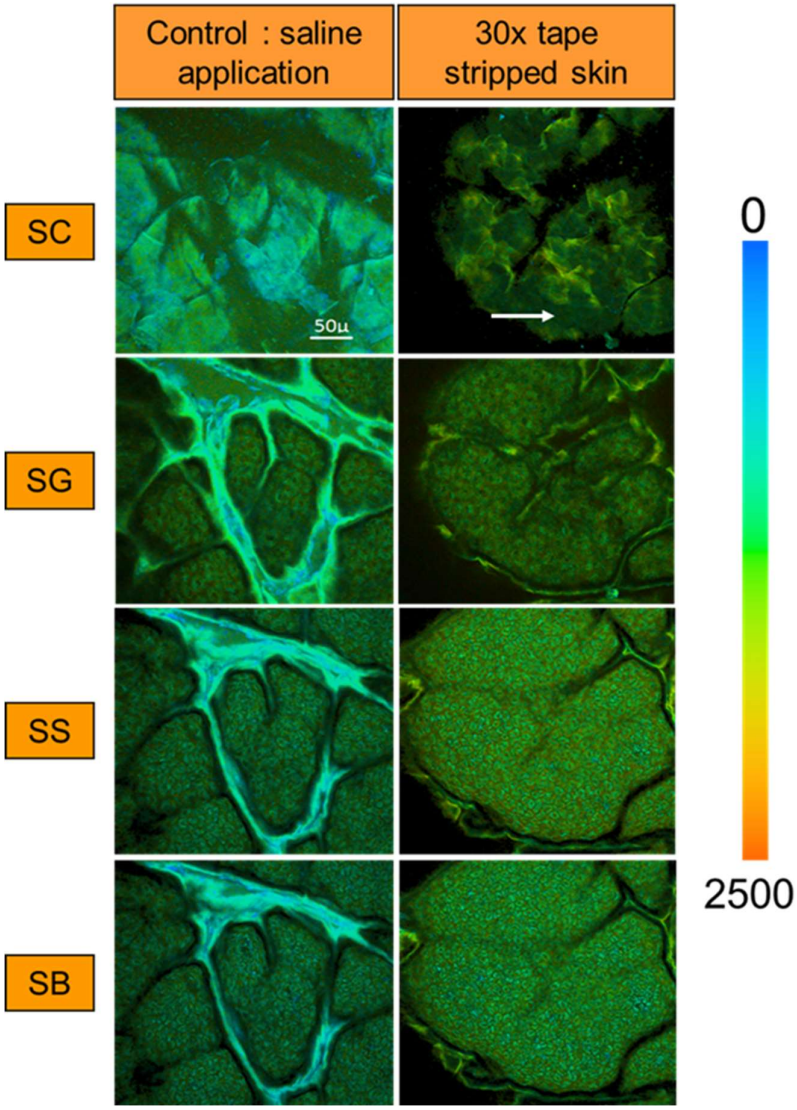

Figure 2.10 MPT-FLIM images of skin strata before and after tape stripping (scale bar represents 50µm). The white arrow denotes the keratinocytes shown on the skin surface. The pseudo-colour is based on the average fluorescence lifetime τm (0-2500ps); blue-green-red

The SC of saline hydrated skin was fully intact; however, parts of the SG was observed on the SC of tape-stripped skin. In the deeper layers, the keratinocytes of both saline-hydrated skin and tape-stripped skin were arranged well. There was no evidence of keratinocytes loss.

2.3.4 Effect of acetone application on the penetration of QDs into porcine skin

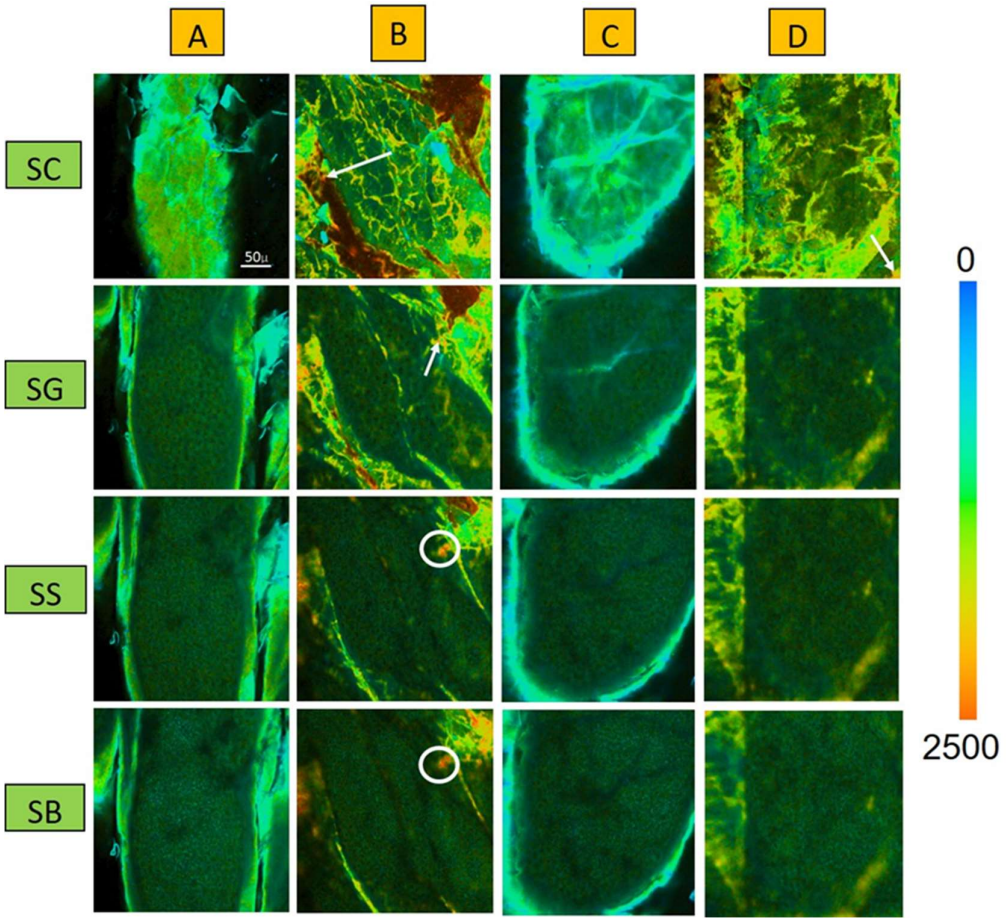

Figure 2.11 Visualisation of QDs on the acetone-treated porcine skin, after 24h QDs incubation (scale bar indicates 50µm). MPT-FLIM images represent: A. Auto-fluorescence of skin controls; B. QDs application on intact skin; C. Auto-fluorescence of acetone-treated skin; D. QDs (in 10% acetone) application on intact skin. White arrows denote the existence of QDs. White circles denote "out of focus" imaging. The pseudo-colour is based on the average fluorescence lifetime τm (0-2500ps); blue-green-red

Figure 2.11 shows the visualisation of QDs deposition on saline-hydrated intact skin and 10% acetone-treated skin. Saline-hydrated intact skin shows green auto-fluorescence with small ratio of nuclei diameter to cells (Figure 2.11.A). The QDs (orange spots-Figure 2.11 B) were located in the furrows of keratinocytes after 24h QDs in saline incubation. On the SS and SB of Figure 2.11. B, the blurred orange spots next to the edge (in white circles) appeared to be out-of-focus emission signals of QDs imaging. A similar issue of out of focus emission signals was also observed on the QDs (in 10% acetone-Figure 2.11.D) application with some SC part overlapped on the deeper layers.

2.3.5 Effect of tape stripping on the penetration of QDs into porcine skin

Figure 2.12 illustrates the MPT-FLIM visualisation of tape-stripped porcine skin after 24h QDs incubation. Saline-hydrated intact skin and tape-stripped porcine skin show intense green colour of auto-fluorescence and well-arranged keratinocytes.

QDs (orange colour) applied on non-tape stripped skin were in the furrows with no evidence of penetration into the keratinocytes (Figure 2.12 B). In contrast, removal of the SC by 30x tape stripping resulted in QDs in the SG (Figure 2.7).

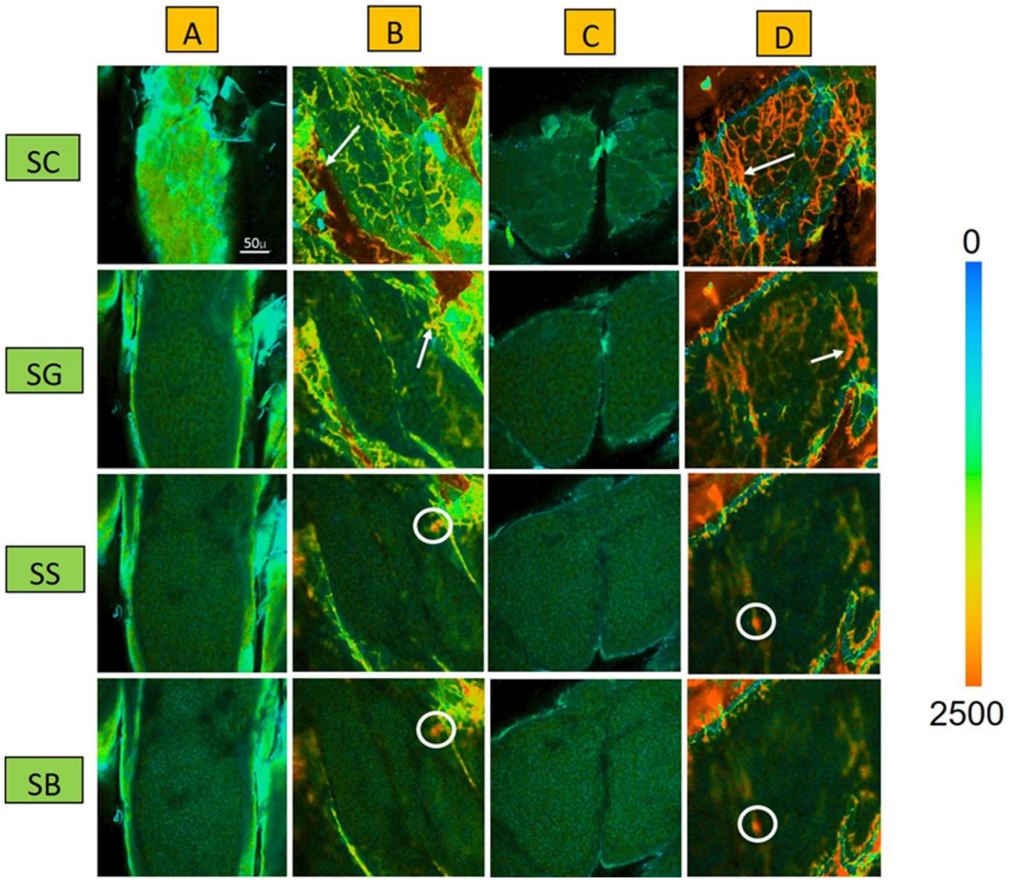

Figure 2.12 Visualisation of QDs on 30xtape stripped porcine skin, after 24h QDs incubation (scale bar indicates 50µm). MPT-FLIM images represent: A. Auto-fluorescence of skin controls; B. QDs application on intact skin; C. Auto-fluorescence of 30x tape stripped skin; D. QDs (in saline) application on tape-stripped skin. White arrows denote the existence of QDs. White circles denote "out of focus" imaging. The pseudo-colour is based on the average fluorescence lifetime τm (0-2500ps); blue-green-red

The blurred orange spots (in white circles) on SS and SB appeared to be out-of-focus emission signals, as described on section 2.3.4.

2.4 Discussion

In this study, we demonstrate the application of MPT-FLIM in visualizing the skin layers on saline-hydrated intact skin, acetone-treated skin and tape-stripped skin. We also investigated the penetration of QDs in those skin conditions to gain an understanding of the deposition of nanomaterials penetrated into normal and compromised skin. We used porcine skin as it mimics human skin and is more readily available.[67-69] As a powerful tool to visualize *in vitro* and *in vivo* skin pharmacokinetics of nanomaterials, MPT is believed to give much information, thanks to its excellent resolution, deeper imaging reach and less risk of photo-bleaching.[26, 28, 59, 60, 70] We hypothesized that long duration application of acetone on the skin, and tape stripping pre-treatment, will induce skin barrier disruption that could allow the penetration of foreign nanomaterials into the skin.

Initial study was conducted by examining saline hydrated intact skin during 24h incubation time to gain an understanding of the saline hydrated-skin morphology (Figure 2.4 and Figure 2.5). The condition of saline-hydrated skin remained the same in 24h incubation. There were no obvious differences between saline-hydrated and non-hydrated skin in terms of morphology up to 8h, except that the non-hydrated skin (Figure 2.6) tended to be less hydrated along the incubation, as shown by a small increase in the ratio of nucleus to the cell.

Skin histology images show that skin surface alteration, such as shrinkage and untied SC, was observed on the acetone-treated skin after 24h incubation in both concentrations of acetone applied (10% and 100%) (Figure 2.7). MPT-FLIM images also suggest that the SC was damaged by 10% and 100% acetone application. The severity increased with increasing concentration of acetone applied. Disappearance of some keratinocytes was observable in the SG and SS on 100% acetone-treated skin, whereas 10% acetone application did not affect the deeper layers (Figure 2.8). This finding supported a previous study reported by Rissmann et al.[71] They showed that applying ten times of 100% acetone using a wiping procedure disrupted the skin barrier in hairless mouse skin. Although the condition of keratinocytes was not clearly mentioned, they suggested that there was substantial nonpolar lipid extraction by acetone treatment and that the skin barrier was disturbed due to corneocytes removal.

Our H&E images (Figure 2.9) confirmed that 30xTS on pressure at around 225g/cm^2 using a D-Squame® disc applicator (CuDerm, Dallas, Texas) for 5 seconds, removed greater than 80% of SC and caused skin shrinkage (Figure 2.9). The MPT-FLIM

images indicate that the SG was exposed as a consequence of SC removal (Figure 2.10), although no keratinocytes loss was observable.

To investigate the effect of acetone exposure and tape stripping pre-treatment on porcine skin permeability, we applied hydrophilic QDs as a model of nanomaterials on intact porcine skin. MPT-FLIM images were acquired after 24h incubation at 37°C. The hydrophilic QDs have a long fluorescence lifetime (≥ 10ns)[72], therefore it can be easily distinguished as a bright orange colour from the green-coloured auto-fluorescence. We applied hydrophilic QDs in 10% acetone to maintain the dispersion of QDs in the solvent and minimize the potential of QDs aggregation due to the non-polar side of acetone characteristics.

No QDs penetration was evident in acetone-treated porcine skin (Figure 2.11). QDs were only localised in the furrows. Although acetone may alter the skin (shrinkage and untied SC), the alteration did not facilitate nanomaterial penetration into the skin. This result may be associated with the low capacity of acetone solution in disrupting the skin barrier although it was applied in long duration. Furthermore, it is possible that there was some aggregation of QDs at the application site, which could influence the skin penetration. Although initially the size of QDs were very small (~ 2.1 nm), the aggregation tendency of nanomaterials might lead to larger particles which then deposited in the furrows.[73] Labouta et al.[74] when investigated the human skin penetration of gold nanoparticles, reported the deposit of large aggregates of gold nanoparticles dispersed in water occurred in the furrows.

Whilst the bulk of the applied QDs deposited on the furrows of the SC, on tape stripped skin, QDs were also observable in the SG, as a consequence of SC removal in tape stripping. There are conflicting reports in the literature. For example, Prow et al.[30] reported that QDs can reach the viable epidermis when applied on tape stripped human skin, whilst Gratieri et al.[75] argued that QDs only deposited in the SC of tape-stripped human skin. This present study demonstrated that although there is evidence in SG, the QDs penetration did not go further to the deeper layers. This finding is in agreement with the result of Leite-Silva et al.[76] when applying zinc oxide nanoparticles (ZnO NPs) on tape-stripped human skin *ex vivo* and *in vivo*. They suggested that the ZnO was localised on the upper area of the SG. The localization is likely due to the role of skin tight junctions located in the SG and acting to support the skin barrier mechanism.[77-79]

The degree of barrier disturbance in tape stripping pre-treatment depends on various factors. Intrinsically, age and anatomical sites of the subjects and skin (SC)

disorders/diseases may affect the outcome.[80] Furthermore, the types of adhesive tapes, frequency of tape stripping, the pressure of tape application and the rate of tape removal, could affect the results.[2]

Blurred orange spots (pointed in white circles) present in MPT images were not believed to show the real presence of QDs (Figure 2.11 and Figure 2.12). These blurred spots were believed to be “out-of-focus” emission signals, which might come from QD agglomerates that unintentionally floated around the upper laser excitation cone, resulting in randomly aberrant signals. This out-of-focus phenomenon was discussed by Leite-Silva et al.[76] when they investigated the effects of occlusion and barrier impairment on human skin penetration of topical nano zinc oxide using MPT-FLIM. They managed to minimize the out-of-focus effects by applying soft-continuous pressure to flatten the skin in between a glass slide and the coverslip.

To the best of our knowledge, the present study is the first to demonstrate the visual skin condition due to acetone topical application and tape-stripping pre-treatment using MPT-FLIM. Although acetone exposure to the skin may lead to skin shrinkage and flakiness, the barrier disturbance effect does not facilitate nanomaterials skin penetration. However, the concentration and the duration of application may determine the chance of skin penetration of foreign materials. Tape stripping, which physically removes the SC, may disrupt the skin barrier thus allowing the penetration of unexpected chemicals and nanomaterials to some extent, but the depth of penetration is limited to the outer regions of the epidermis.

2.5 References

1. Levine M. The growth of adult human skin *in vitro*. Br J Dermatol. 1972;86(5):481-490.
2. Lademann J, Jacobi U, Surber C, Weigmann HJ, Fluhr JW. The tape stripping procedure - evaluation of some critical parameters. Eur J Pharm Biopharm. 2009;72(2):317-323.
3. Wahlberg JE, Boman A. Prevention of Contact Dermatitis from Solvents. 1996.
4. Costa C, Pasquale RD, Silvari V, Barbaro M, Catania S. *In vitro* evaluation of oxidative damage from organic solvent vapours on human skin. Toxicol *In Vitro*. 2006;20(3):324-331.
5. Grubauer G, Elias PM, Feingold KR. Transepidermal water loss: the signal for recovery of barrier structure and function. J Lipid Res. 1989;30(3):323-33.
6. Grubauer G, Feingold KR, Elias PM. Relationship of epidermal lipogenesis to cutaneous barrier function. J Lipid Res. 1987;28(6):746-52.
7. Grubauer G, Feingold KR, Harris RM, Elias PM. Lipid content and lipid type as determinants of the epidermal permeability barrier. J Lipid Res. 1989;30(1):89-96.
8. Scheuplein R, Ross L, editors. Effects of surfactants and solvents on the permeability of epidermis. J. Soc. Cosmet. Chem; 1970: Citeseer.
9. Menon GK, Feingold KR, Moser AH, Brown BE, Elias PM. *De novo* sterologenesis in the skin. II. Regulation by cutaneous barrier requirements. J Lipid Res. 1985;26(4):418-27.
10. De Paepe K, Roseeuw D, Rogiers V. Repair of acetone- and sodium lauryl sulphate-damaged human skin barrier function using topically applied emulsions containing barrier lipids. J Eur Acad Dermatol Venereol. 2002;16(6):587-594.
11. Abrams K, Harvell JD, Shriner D, et al. Effect of organic solvents on *in vitro* human skin water barrier function. J Invest Dermatol. 1993;101(4):609-613.
12. Trebilcock KL, Heylings JR, Wilks MF. *In vitro* tape stripping as a model for *in vivo* skin stripping. Toxicol In Vitro. 1994;8(4):665-667.
13. Bashir SJ, Chew A-L, Anigbogu A, Dreher F, Maibach HI. Physical and physiological effects of stratum corneum tape stripping. Skin Res Technol. 2001;7(1):40-48.
14. Davies DJ, Heylings JR, Gayes H, McCarthy TJ, Mack MC. Further development of an *in vitro* model for studying the penetration of chemicals through compromised skin. Toxicol In Vitro. 2017;38:101-107.
15. Davies DJ, Heylings JR, McCarthy TJ, Correa CM. Development of an *in vitro* model for studying the penetration of chemicals through compromised skin. Toxicol *In Vitro*. 2015;29(1):176-181.
16. Dabboue H, Builles N, Frouin É, et al. Assessing the Impact of Mechanical Damage on Full-Thickness Porcine and Human Skin Using an *In Vitro* Approach. BioMed Research International. 2015;2015:434623.
17. Wolf M, Halper M, Pribyl R, Baurecht D, Valenta C. Distribution of phospholipid based formulations in the skin investigated by combined ATR-FTIR and tape stripping experiments. Int J Pharm. 2017;519(1):198-205.
18. Jacobi U, Meykadeh N, Sterry W, Lademann J. Effect of the vehicle on the amount of stratum corneum removed by tape stripping. JDDG - Journal of the German Society of Dermatology. 2003;1(11):884-889.
19. Jacobi U, Weigmann HJ, Ulrich J, Sterry W, Lademann J. Estimation of the relative stratum corneum amount removed by tape stripping. Skin Res Technol. 2005;11(2):91-96.
20. Hoppel M, Baurecht D, Holper E, Mahrhauser D, Valenta C. Validation of the combined ATR-FTIR/tape stripping technique for monitoring the distribution of surfactants in the stratum corneum. Int J Pharm. 2014;472(1):88-93.

21. Pellett MA, Roberts MS, Hadgraft J. Supersaturated solutions evaluated with an in vitro stratum corneum tape stripping technique. Int J Pharm. 1997;151(1):91-98.
22. Clausen M-L, Slotved HC, Krogfelt KA, Agner T. Tape stripping technique for stratum corneum protein analysis. Sci Rep. 2016;6:19918.
23. Klang V, Schwarz JC, Hartl A, Valenta C. Facilitating *in vitro* tape stripping: Application of infrared densitometry for quantification of porcine stratum corneum proteins. Skin Pharmacol Physiol. 2011;24(5):256-268.
24. Weerheim A, Ponec M. Determination of stratum corneum lipid profile by tape stripping in combination with high-performance thin-layer chromatography. Archives of Dermatological Research. 2001;293(4):191-199.
25. Balu M, Mazhar A, Hayakawa Carole K, et al. *In vivo* multiphoton NADH fluorescence reveals depth-dependent keratinocyte metabolism in human skin. Biophys J. 2013;104(1):258-267.
26. Köenig K, Riemann I. High-resolution multiphoton tomography of human skin with subcellular spatial resolution and picosecond time resolution. Journal of Biomedical Optics. 2003;8(3):432-439.
27. König K, Ehlers A, Stracke F, Riemann I. *In vivo* drug screening in human skin using femtosecond laser multiphoton tomography. Skin Pharmacol Physiol. 2006;19(2):78-88.
28. König K, Baldeweck T, Balu M, et al. Multiphoton microscopy and fluorescence lifetime imaging: Applications in biology and medicine. De Gruyter; 2018.
29. Seidenari S, Arginelli F, Bassoli S, et al. Multiphoton laser microscopy and fluorescence lifetime imaging for the evaluation of the skin. Dermatology Research and Practice. 2012;2012:8.
30. Prow TW, Monteiro-Riviere NA, Inman AO, et al. Quantum dot penetration into viable human skin. Nanotoxicology. 2012;6(2):173-185.
31. Sanchez WY, Obispo C, Ryan E, Grice JE, Roberts MS. Changes in the redox state and endogenous fluorescence of *in vivo* human skin due to intrinsic and photo-aging, measured by multiphoton tomography with fluorescence lifetime imaging. Journal of Biomedical Optics. 2012;18(6):061217-061217.
32. Sanchez WY, Prow TW, Sanchez WH, Grice JE, Roberts MS. Analysis of the metabolic deterioration of *ex vivo* skin from ischemic necrosis through the imaging of intracellular NAD(P)H by multiphoton tomography and fluorescence lifetime imaging microscopy. Journal of Biomedical Optics. 2010;15(4):046008-046008-11.
33. Dancik Y, Favre A, Loy CJ, Zvyagin AV, Roberts MS. Use of multiphoton tomography and fluorescence lifetime imaging to investigate skin pigmentation *in vivo*. Journal of Biomedical Optics. 2013;18(2):026022-026022.
34. Dimitrow E, Riemann I, Ehlers A, et al. Spectral fluorescence lifetime detection and selective melanin imaging by multiphoton laser tomography for melanoma diagnosis. Exp Dermatol. 2009;18(6):509-515.
35. Dimitrow E, Ziemer M, Koehler MJ, et al. Sensitivity and specificity of multiphoton laser tomography for *in vivo* and *ex vivo* diagnosis of malignant melanoma. J Invest Dermatol. 2009;129(7):1752-1758.
36. Seidenari S, Arginelli F, Dunsby C, et al. Multiphoton laser tomography and fluorescence lifetime imaging of basal cell carcinoma: morphologic features for non-invasive diagnostics. Exp Dermatol. 2012;21(11):831-836.
37. Balu M, Kelly KM, Zachary CB, et al. Distinguishing between benign and malignant melanocytic nevi by *in vivo* multiphoton microscopy. Cancer Res. 2014;74(10):2688-2697.
38. Paoli J, Smedh M, Wennberg A-M, Ericson MB. Multiphoton laser scanning microscopy on non-melanoma skin cancer: Morphologic features for future non-invasive diagnostics. J Invest Dermatol. 2008;128(5):1248-1255.
39. Thorling CA, Jin L, Weiss M, et al. Assessing steatotic liver function after ischemia-reperfusion injury by *in vivo* multiphoton imaging of fluorescein disposition. Drug Metabolism and Disposition. 2015;43(1):154-162.

40. Wang H, Liang X, Gravot G, et al. Visualizing liver anatomy, physiology and pharmacology using multiphoton microscopy. Journal of Biophotonics. 2017;10(1):46-60.
41. Wang H, Liang X, Mohammed YH, et al. Real-time histology in liver disease using multiphoton microscopy with fluorescence lifetime imaging. Biomedical Optics Express. 2015;6(3):780-792.
42. Wang H, Thorling CA, Liang X, et al. Diagnostic imaging and therapeutic application of nanoparticles targeting the liver. Journal of Materials Chemistry B. 2015;3(6):939-958.
43. Liang X, Grice JE, Zhu Y, et al. Intravital multiphoton imaging of the selective uptake of water-dispersible quantum dots into sinusoidal liver cells. Small. 2015;11(14):1711-1720.
44. Thorling CA, Crawford D, Burczynski FJ, et al. Multiphoton microscopy in defining liver function. SPIE; 2014. 11 p.
45. Thorling CA, Dancik Y, Medley G, et al. Multiphoton microscopy and fluorescence lifetime imaging provide a novel method in studying drug distribution and metabolism in the rat liver *in vivo*. SPIE; 2011. 8 p.
46. Thorling CA, Jin L, Roberts MS. Intravital multiphoton imaging of rhodamine 123 in the rat liver after intravenous dosing AU - Liu, Xin. IntraVital. 2012;1(1):54-59.
47. Thorling CA, Liu X, Burczynski FJ, et al. Intravital multiphoton microscopy can model uptake and excretion of fluorescein in hepatic ischemia-reperfusion injury. SPIE; 2013. 12 p.
48. Thorling CA, Liu X, Fletcher LM, et al. Multiphoton microscopy can visualize zonal damage and decreased cellular metabolic activity in hepatic ischemia-reperfusion injury in rats. SPIE; 2011. 9 p.
49. Weiss M, Liu X, Thorling CA, Roberts MS. Functional characterization of hepatic transporters using intravital microscopy. Eur J Pharm Sci. 2013;49(5):845-849.
50. Liang X, Wang H, Zhu Y, et al. Short- and Long-Term Tracking of Anionic Ultrasmall Nanoparticles in Kidney. ACS Nano. 2016;10(1):387-395.
51. Small DM, Sanchez W, Roy S, Hickey MJ, Gobe G. Multiphoton fluorescence microscopy of the live kidney in health and disease. SPIE; 2014. 14 p.
52. Small DM, Sanchez WY, Gobe GC. Intravital multiphoton imaging of the kidney: Tubular structure and metabolism. In: Hewitson TD, Smith ER, Holt SG, editors. Kidney research: Experimental protocols. New York, NY: Springer New York; 2016. p. 155-172.
53. Small DM, Sanchez WY, Roy S, Hickey MJ, Gobe G. Multiphoton fluorescence microscopy of the live kidney in health and disease. SPIE; 2014. 14 p.
54. Peti-Peterdi J, Burford JL, Hackl MJ. The first decade of using multiphoton microscopy for high-power kidney imaging. American Journal of Physiology-Renal Physiology. 2012;302(2):F227-F233.
55. Kantelhardt SR, Kalasauskas D, König K, et al. *In vivo* multiphoton tomography and fluorescence lifetime imaging of human brain tumor tissue. J Neurooncol. 2016;127(3):473-482.
56. Kantelhardt SR, Leppert J, Kantelhardt JW, et al. Multi-photon excitation fluorescence microscopy of brain-tumour tissue and analysis of cell density. Acta Neurochir (Wien). 2009;151(3):253.
57. Levene MJ, Dombeck DA, Kasischke KA, Molloy RP, Webb WW. *In Vivo* multiphoton microscopy of deep brain tissue. J Neurophysiol. 2004;91(4):1908-1912.
58. Bacskai BJ, Hickey GA, Skoch J, et al. Four-dimensional multiphoton imaging of brain entry, amyloid binding, and clearance of an amyloid-β ligand in transgenic mice. Proceedings of the National Academy of Sciences. 2003;100(21):12462-12467.

59. König K, Raphael AP, Lin L, et al. Applications of multiphoton tomographs and femtosecond laser nanoprocessing microscopes in drug delivery research. Advanced Drug Delivery Reviews. 2011;63(4–5):388-404.
60. Roberts MS, Dancik Y, Prow TW, et al. Non-invasive imaging of skin physiology and percutaneous penetration using fluorescence spectral and lifetime imaging with multiphoton and confocal microscopy. Eur J Pharm Biopharm. 2011;77(3):469-488.
61. Helmchen F, Denk W. Deep tissue two-photon microscopy. Nature Methods. 2005;2:932.
62. Wang BG, König K, Halbhuber KJ. Two-photon microscopy of deep intravital tissues and its merits in clinical research. J Microsc. 2010;238(1):1-20.
63. Sanchez WY, Song Z, Becker W, Köenig K, Roberts MS. Fluorescence lifetime imaging for diagnostic and therapeutic intravital microscopy. In: Weigert R, editor. Advances in intravital microscopy: from basic to clinical research. Dordrecht: Springer Netherlands; 2014. p. 371-418.
64. Zhu Y, Li Z, Chen M, et al. One-pot preparation of highly fluorescent cadmium telluride/cadmium sulfide quantum dots under neutral-pH condition for biological applications. J Colloid Interface Sci. 2013;390(1):3-10.
65. Ryman-Rasmussen JP, Riviere JE, Monteiro-Riviere NA. Penetration of intact skin by quantum dots with diverse physicochemical properties. Toxicol Sci. 2006;91(1):159-165.
66. Fischer AH, Jacobson KA, Rose J, Zeller R. Hematoxylin and eosin staining of tissue and cell sections. Cold Spring Harbor Protocols. 2008;2008(5):pdb.prot4986.
67. Barbero AM, Frasch HF. Pig and guinea pig skin as surrogates for human *in vitro* penetration studies: A quantitative review. Toxicol In Vitro. 2009;23(1):1-13.
68. Bronaugh RL, Stewart RF, Congdon ER. Methods for *in vitro* percutaneous absorption studies II. Animal models for human skin. Toxicol Appl Pharmacol. 1982;62(3):481-488.
69. Simon GA, Maibach HI. The pig as an experimental animal model of percutaneous permeation in man: Qualitative and quantitative observations – An overview. Skin Pharmacol Physiol. 2000;13(5):229-234.
70. Kirejev V, Guldbrand S, Borglin J, Simonsson C, Ericson MB. Multiphoton microscopy. a powerful tool in skin research and topical drug delivery science. Journal of Drug Delivery Science and Technology. 2012;22(3):250-259.
71. Rissmann R, Oudshoorn MHM, Hennink WE, Ponec M, Bouwstra JA. Skin barrier disruption by acetone: observations in a hairless mouse skin model. Archives of Dermatological Research. 2009;301(8):609-613.
72. Fisher BR, Eisler H-J, Stott NE, Bawendi MG. Emission intensity dependence and single-exponential behaviour in single colloidal quantum dot fluorescence lifetimes. The Journal of Physical Chemistry B. 2004;108(1):143-148.
73. Liang XW, Xu ZP, Grice J, et al. Penetration of nanoparticles into human skin. Curr Pharm Des. 2013;19(35):6353-6366.
74. Labouta HI, Liu DC, Lin LL, et al. Gold nanoparticle penetration and reduced metabolism in human skin by toluene. Pharm Res. 2011;28(11):2931.
75. Gratieri T, Schaefer UF, Jing L, et al. Penetration of quantum dot particles through human skin. J Biomed Nanotechnol. 2010;6(5):586-95.
76. Leite-Silva VR, Sanchez WY, Studier H, et al. Human skin penetration and local effects of topical nano zinc oxide after occlusion and barrier impairment. Eur J Pharm Biopharm. 2016;104:140-147.
77. Bäsler K, Bergmann S, Heisig M, et al. The role of tight junctions in skin barrier function and dermal absorption. J Control Release. 2016;242:105-118.
78. Kirschner N, Houdek P, Fromm M, Moll I, Brandner JM. Tight junctions form a barrier in human epidermis. Eur J Cell Biol. 2010;89(11):839-842.

79. Yoshida K, Yokouchi M, Nagao K, et al. Functional tight junction barrier localizes in the second layer of the stratum granulosum of human epidermis. J Dermatol Sci. 2013;71(2):89-99.
80. Zheng Y, Choi M. Stratum corneum tape-stripping method. In: Dermatotoxicology, Eighth Edition. CRC Press; 2012. p. 348-359.

Chapter 3. Evaluation of Quantum Dots (QDs) Skin Penetration in Porcine Skin: Effect of Age and Anatomical Site of Topical Application

Nastiti CM, Mohammed Y, Telaprolu KC, Liang X, Grice JE, Roberts MS, Benson HA. Evaluation of Quantum Dot Skin Penetration in Porcine Skin: Effect of Age and Anatomical Site of Topical Application. *Skin Pharmacology and Physiology*. 2019 May 14;32(3):1-0.

"Publication has been removed due to copyright restrictions".

Abstract

Background: Pig skin is a widely acknowledged surrogate for human skin for in vitro/ex vivo skin penetration studies with application for small molecules and nanosystems. We have investigated the influence of biological factors such as age and anatomical site on the penetration and distribution of nanoparticles (2.1nm Hydrophilic CdTe/CdS quantum dots: QDs) in adult pig skin (APS), weanling pig skin (WPS) and newborn pig skin (NBPS) at two different anatomical sites (ear and abdomen). ***Methods:*** QDs in saline were applied to 1x1 cm^2 skin (62.5 pmole/cm2) with 2-minute finger rubbing using a standardised protocol. After 6 or 24h incubation on Franz diffusion cells, tape stripping (x10) followed by manual follicular casting was conducted. Cadmium in QDs was quantified using Inductively Coupled Plasma-Mass Spectrometry (ICP-MS) for all samples. The presence of QDs in similarly treated skin samples was also captured using Multiphoton Tomography. ***Results:*** QDs were mainly localized in hair follicles after 6h and 24h exposure with no cadmium detected in the Franz cell receptor compartment regardless of pig age or anatomical site. The amount of QDs deposited in the follicles was similar at 6h but higher on APS and WPS ears compared to NBPS ears at 24h. This is associated with the high follicle density and small follicle diameter of the NBPS compared to the smaller density of much larger follicles on the APS. NBPS showed consistent QDs distribution for ear and abdomen up to 24h. ***Conclusions:*** There is minimal penetration of QDs through pig skin. Density and diameter of follicles in association with age of pigs and application site influenced the amount of QD deposited in follicles. The structures of the SC, follicle density and diameter of NBPS are similar to human skin suggesting that NBPS is an appropriate model for human skin in the evaluation of topical applications of a range of chemicals including nanosystems

Chapter 4. Development and Evaluation of Novel Nanocarriers for Skin Delivery of Resveratrol (RSV)

4.1 Background

Resveratrol (E-5-(4-hydroxystyryl) benzene-1,3-diol; RSV) is a potent natural polyphenolic antioxidant [1, 2] that can be extracted abundantly from grape skin and seeds, berries, peanuts, and red wine.[3-6] In its natural role as a phytoalexin compound, RSV acts in response to fungal and bacterial attacks, UV light exposure and general injuries to the plants.[3, 7] RSV has gained much interest due to its potential to generate a range of therapeutic effects. It has been suggested that RSV may be a contributing factor in the so-called "French paradox": the observed reduced risk of coronary artery disease in French people attributed at least in part to the regular consumption of red wine.[8] Extensive reviews of a large number of *in vitro* and *in vivo* studies have been dedicated to the evidence for RSV therapeutic effects. There is good evidence for RSV supporting heart function and providing heart protection against cardiovascular diseases [8, 9], protecting against neuro-disorders and cancer chemoprevention, due to its anti-oxidant and anti-inflammatory effects.[2, 10-13] RSV also shows anti-diabetic activities by improving glucose homeostasis and insulin secretion, lowering insulin resistance, and protecting pancreatic βcells, again attributed to the antioxidant and anti-inflammatory effect of RSV.[14] Of particular relevance to this thesis, RSV has demonstrated potential for antiaging effects and protecting against UV damage in the skin due to its antioxidant activity.[7, 15, 16]

RSV (MW: 228.25 g/mL) is a lipophilic compound (log $P_{o/w}$ 3.1), that is poorly soluble in water (50 – 60 µg/mL) [17, 18], with little change in solubility over the pH 1.2 - 7.4 range.[18] RSV is highly soluble in DMSO and organic solvents including ethanol.[19] RSV has three different pKa: 8.8, 9.8, and 11.4 corresponding to deprotonation of the three hydroxyl groups: 4-OH, (3-OH or 5-OH), and (5-OH or 3-OH), respectively.[19]

RSV exists as two isomers, trans-resveratrol and cis-resveratrol (Figure 4.1). The trans isomer is more common and is more stable and bioactive than the cis-isomer. [20] However, trans- resveratrol converts to cis-resveratrol in the presence of UV light[18, 20-25] with the UV irradiation time, RSV physical forms (in solid or solution), pH and temperature affecting isomerization.[25]

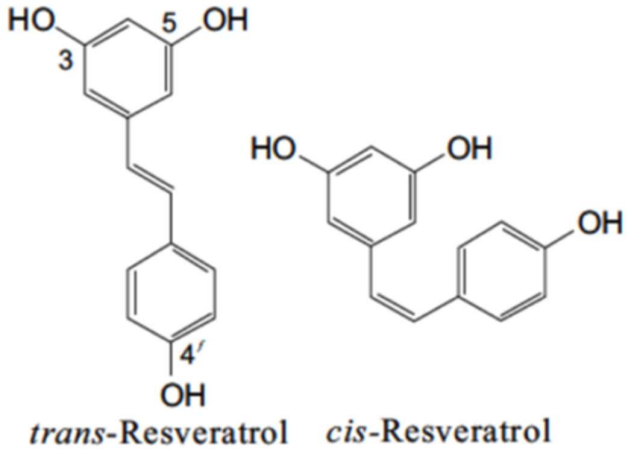

Figure 4.1 Structure of RSV. Adapted from Rege et al[13]

A considerable impediment to the therapeutic potential of RSV is that whilst RSV is relatively well absorbed (approximately 70%)[26], it is subject to extensive first pass hepatic elimination.[27, 28] Two studies conducted in human volunteers revealed that less than 10ng/mL of RSV was found in human following oral administration with the dose of 25mg RSV.[26, 29, 30]

Direct application to the skin is an attractive alternative administration route to avoid first pass hepatic elimination and is particularly appropriate where RSV is being administered for antiaging of skin or other dermatological or cosmeceutical purposes. It remains important to consider metabolism by enzymes in the skin, however RSV metabolism in skin is significantly less than in the liver.[31]

As a small molecule (MW: 228.25), RSV is actually a good candidate for topical-transdermal. However, poor aqueous solubility of RSV[17, 18] may limit the loading capacity of a topical formulation. RSV is also less stable in the presence of UV light and in basic solution, which must be considered in formulation development. Hung et al [32] reported that the flux of RSV from a saturated solution in PBS pH 6 through female nude mouse skin was very low (1.59 ± 0.08 nmol/cm^2/h), thus it is imperative to formulate RSV topical formulation with an enhancement strategy. Based on its physicochemical properties, the formulation must be able to increase the solubility of RSV, protect the RSV from degradation thereby enhancing stability, and enhance diffusion of RSV through the stratum corneum and deeper epidermal layers.

A good quality skin-targeted formulation must deliver sufficient amounts of the intended substance safely across the SC with minimal side effects. This can be achieved by manipulating the barrier property of SC using chemical or physical approaches. Whilst physical approaches are mainly related to physical enhancement

tools such as: electrophoresis, magnetophoresis, microneedles, etc., chemical approaches can be conducted by complexing the active ingredient with other chemicals (conjugation, complexation, or pro-drug design) to negate an unfavourable physicochemical characteristic or by incorporating the active ingredient into a delivery system which can enhance its penetration into the skin.[33-39]

A range of approaches have been investigated for the topical delivery of RSV.[40-50] For example, RSV in combination with 5-fluorouracil was incorporated into ultradeformable liposomes which were evaluated with carcinoma-related skin abnormalities.[42] Phospholipon 90G® was used for vesicle formation, cholesterol improved the vesicle stability and sodium cholate provided the flexibility required to allow the vesicles to squeeze into the SC. Those ingredients were able to enhance the flux through human skin epidermis of approximately 8-fold compared to RSV solution. Although this study provided a promising headline, it was difficult to interpret the data due to a lack of information on the actual amount of RSV penetrated to the skin and the stability of the carrier formulations. This study also demonstrated a relatively complicated procedure of fabrication. There is a clear need for a simple but scalable formulation that can effectively deliver RSV to the skin in a formulation thus can be commercially available.

Micro-nanoemulsion formulations have properties that suggest they have potential for successful skin delivery of RSV.[51-55] Micro-nanoemulsions consist of an oil phase, surfactant, cosurfactant and aqueous phase, which create an isotropic, transparent/translucent, single-phase system of nano-sized droplets.[51, 56-59] They have excellent solubilizing capacity for lipophilic compounds and provide protection for relatively unstable molecules. These formulations also offer simplicity in fabrication and good stability.[51] In addition, micro-nanoemulsion preparation is relatively production scalable and therefore practical for industrial development. Several nanoemulsion formulations have been in the market including the Oxalgin NanoGel™ (Zydus Cadilla, India) containing diclofenac sodium[55], Estrasorb® (Novavax Inc., Malvern, PA, USA) containing oestradiol hemihydrate, and Topicaine (ESBA laboratories Inc., Jupiter, FL, USA) containing lidocaine.[51]

Juškaitė et al.[60] developed an RSV microemulsion containing ethyl oleate (oil phase), PEG-8-caprylic/capric glycerides (surfactant), polyglyceryl-6-isostearate (co-surfactant) and water. The highest penetration in the human skin was achieved using a formula with S_{mix} ratio of 5:1 (1.96 ± 0.41μg/cm^2). The concentration of both surfactant and cosurfactant in the formula was higher than 45% which might increase

the irritation potential as a topical formulation[61], and the pH of the optimized formulations was 7.01-7.15 which may further contribute as it is above the ideal skin pH range. In addition, RSV is only stable in an acidic environment[18] therefore the stability of RSV in this developed formulation may be problematic.

In this current study we develop self-assembly and stable nanoemulsions for RSV skin delivery which can solubilize RSV with a relatively low composition of oil, surfactant-cosurfactant, and provide good skin penetration and permeation of RSV. The nanoemulsions also protect RSV for long duration of storage.

4.1.1 Objectives of the study

The objectives of the study are:

1. To develop an HPLC validated assay for RSV determination
2. To develop simple, stable, emulsion-based nanocarriers for skin delivery of RSV
3. To characterise the physical properties of the RSV nanocarriers
4. To assess the skin penetration and skin permeation of RSV released from the nanocarriers, into and through the skin
5. To assess the stability of RSV in the nanoformulations

4.2 Experimental section

4.2.1 Materials

RSV was purchased from PCCA (99% purity, PCCA, USA). Triacetin, eugenol, D limonene, eucalyptol were purchased from Sigma-Aldrich (USA). Kolliphor® RH 40 was purchased from BASF (USA). Labrasol® and Transcutol® were gifts from Gattefossé (France). Orthophosphoric acid, hematoxylin, eosin and ethanol were purchased from Thermo Fisher Scientific (Australia). Sodium hydroxide and sodium chloride were purchased from Chem-Supply (Australia). Acetonitrile (HPLC grade, Fisher Chemical, USA), deionised water-passed through a Milli Q apparatus (Millipore Corporation, Bedford, MASS, USA).

4.2.2 Assay method validation

Agilent™ (Agilent Technologies, Germany) high performance liquid chromatography (HPLC) analytical system consists of:

1. degasser (Agilent™ G1379B, Serial No: JP82012305, Germany)
2. binary pump system (Agilent™ G1312A, Serial No: DE63062063, Germany),
3. automated injection system/autosampler system (Agilent™ G1329A, Serial No. DE64775011, Germany)
4. variable wavelength (VWD) detector (Agilent™ G1314B, Serial No. DE 1365734, Germany)
5. Chemstation Rev.B.03.01 (Agilent Technologies Inc., Germany)

The HPLC system conditions are described on Table 4.1.

Table 4.1 HPLC system set-up

System set up	Description
Stationary phase	HPLC C18 5µ column, 150mm x 4.6mm (Apollo, India)
Mobile phase	Acetonitrile: water: phosphoric acid = 50:50:0.05
Flow rate	1 mL/min
Detection	VWD, λ_{max} = 307 nm
Retention time	2.4 ± 0.1 minutes
Total analysis time	7.2 minutes
Running system	isocratic

4.2.2.1 Linearity

To assess the linearity, a series of RSV concentrations was made with serial dilution. A stock solution of 100 µg/mL was made by dissolving 1mg of RSV into 10.0 mL solvent. Two types of solvent system were set up with different series of concentration. The mobile phase-solvent system (A) was used for general purposes of RSV determination, whereas a mixture of mobile phase and 20% ethanol in phosphate buffer saline (PBS) pH 6 = 1:1 (B) was used to determine the RSV in the receptor fluid samples of Franz diffusion cell studies. RSV concentration series of 0.3125, 0.625, 2.5, 5, 10, and 25 µg/mL was made with system A. Solvent system B

was used with a lower series of RSV concentrations typical of skin experiment samples: 0.0078, 0.0156, 0.0625, 0.625, 2.5 and 5 µg/mL.

4.2.2.2 System suitability

Precision

RSV solutions with the concentration of 0.078 µg/mL (A), 0.3125 µg/mL (B), 5 µg/mL (A and B) and 10µg/mL (B) were used to assess the precision. The injections were carried out in six replicates for each concentration. The relative standard deviation (RSD), which is the percentage of the ratio of standard deviation to the mean, was used to investigate the data point dispersion (degree of variation).

Sensitivity

The sensitivity of the assay was assessed by determining the limit of detection and limit of quantification. Six injections of solvents (blanks) were conducted with the analysis time of 10 minutes for each injection. The noise to peak ratio was calculated by dividing the standard deviation of the blanks with the slope of peak height of the calibration curve. Limit of detection (LOD) was three times the noise to peak ratio, whereas limit of quantification (LOQ) was ten times the noise to peak ratio.

Accuracy

A mass balance study of RSV extraction from the skin was conducted to assess the accuracy of the assay. The end point of this study was the recovery of RSV skin extraction. Briefly, a section of pre-weighted skin was soaked in 5 mL of 100 µg/mL RSV ethanolic solution at 35ºC. After 24h immersion, the skin was blotted dry, then sectioned and the RSV in the skin was extracted using a solvent extractor. The mobile phase in HPLC analysis was used as the solvent extractor. The extraction was carried out for 3 hours at room temperature. The RSV in the remaining donor, in the wash water, and in the extractor were then determined using HPLC assay described above.

4.2.3 Formulation

Spontaneous emulsification method was used to generate the nanocarriers with the aid of mild agitation at room temperature based on the study of Pund et al.[62] with some modification. The formulation study was initiated by developing three types of formula (Table 4.2). The mnemonic system was applied in order to name the formulations. Triacetin was selected as the oil phase, Kolliphor® RH 40 and Labrasol® as surfactants, and Transcutol® was selected as the cosurfactant. PBS pH 6 was utilised

as the aqueous phase. PBS pH 6 was applied as the aqueous system to maintain the stability of RSV. RSV is stable in acidic environment with pH 5-6.[18]

Surfactant and cosurfactant were initially mixed prior to the process. Oil phase was added in the mixture of surfactant and cosurfactant with mild agitation to produce the lipid based nanoformulation (TKLT2). TKLT2 applied S_{mix} (surfactant-cosurfactant ratio) of 2:1 and ratio of oil to S_{mix} 1:2, without the existence of aqueous phase. The micellar system was designed as PKLT2 with PBS pH 6 as the aqueous phase and the same S_{mix} but without the existence of triacetin (oil phase). The TKLT2P was the microemulsion system involving triacetin, Kolliphor® RH 40, Labrasol®, Transcutol® and PBS pH 6. It was made by mixing the oil phase with the mixture of surfactant and cosurfactant prior to aqueous phase addition. The aqueous phase addition was carried out until the system started to show translucency. All processes were conducted at room temperature. The RSV was further incorporated into each system at 8% (w/w) concentration.

Table 4.2 Initial RSV nanoformulations (all as % w/w)

Ingredients	Formula		
	TKLT2	TKLT2P	PKLT2
Triacetin	33	25.7	-
Kolliphor® RH 40	33.5	25.7	33.5
Labrasol®	16.75	12.8	16.75
Transcutol®	16.75	12.8	16.75
PBS pH 6	-	23	33

The initial nanocarriers were then characterised in terms of physical appearance, viscosity, RSV solubility, refractive index and their RSV skin penetration and permeation profiles.

Based on the results of characterisation and evaluation of the initial formulations, the nanoformulations were taken forward for further development and evaluated to obtain the optimal nanoformulation for skin delivery of RSV (Table 4.3). RSV was loaded in the formulations at a concentration of 2% (w/w). The RSV solution and RSV loaded nanocarriers were kept out of light throughout the process, including the analysis. Three different terpenes (eugenol, d-limonene, and eucalyptol) were incorporated into the formulations to evaluate the potential of adding these chemical penetration enhancers.

Table 4.3 RSV nanoemulsions (all as % w/w)

Ingredients	Formula							
	TKLT2P	TKTP	ETKTP	E5K30TP	E5K20TP	E1K20TP	LKTP	EuKTP
Triacetin	25.7	5	5	-	-	-	-	-
Kolliphor® RH 40	25.7	20	30	30	20	20	20	20
Labrasol®	12.8	-	-	-	-	-	-	-
Transcutol®	12.8	10	10	10	10	10	10	10
Eugenol	-	-	5	5	5	1	-	-
D-limonene	-	-	-	-	-	-	1	-
Eucalyptol	-	-	-	-	-	-	-	1
PBS pH 6	23	65	50	55	65	69	69	69

4.2.4 Physical characterisation and stability evaluation

The RSV nanocarriers were physically characterised in terms of physical appearance, RSV solubility, viscosity and refractive index. The stability of RSV nanocarriers was evaluated based on physical appearance and RSV quantity over the length of storage.

4.2.4.1 Globule size and dispersion index

Globule size and polydispersity index (PDI) of the nanocarriers was analysed using Zetasizer Nano™ ZSP (Malvern instruments, UK) based on photon correlation spectroscopy. The formulations were diluted with water four times prior to the measurement.

4.2.4.2 pH measurement

The pH of formulations was determined qualitatively by immersing the universal pH indicator strips MColourpHast™ (Merck, Germany) in the RSV nanoformulations for a minute and matching the colour after immersion with the colour reference on the package.

4.2.4.3 Solubility testing

Excess amount of RSV was dispersed in the blank nanoformulations and stirred for 24 hours at room temperature. The dispersion was then centrifuged (Eppendorf, USA) at 6000 rcf for 5 minutes. The supernatant was carefully taken and centrifuged at 15,000 rcf for 10 minutes. The RSV in the supernatant was assayed using HPLC after adequate dilution of the supernatant.

4.2.4.4 Viscosity measurement

A cup and bob viscometer (Bohlin Visco 88, Malvern, USA) was used to measure the viscosity of the nanoformulations. In brief, 15 mL of the formulation was placed into the cup. After cup installation, the viscometer was started at room temperature with the approximate speed of 572 rpm (speed number 7). The viscosity value is displayed in dPa.s.

4.2.4.5 Refractive index measurement

The refractive index of the blank nanoformulations was measured using a pocket refractometer (Atago, USA) with the range of refractive index measurement 1.3-1.5. Briefly, not less than 300 µL of the nanoformulation was added on top of the prism prior to measurement. The measurement was conducted in four replications at room temperature.

4.2.5 *In vitro* penetration/permeation study

In vitro penetration/permeation study in this project was performed using Franz-type diffusion cells.

4.2.5.1 Skin preparation

The skin was obtained from newborn Yorkshire pigs which died due to natural causes. The skin was removed from the body and the subcutaneous tissue was carefully removed using a scalpel. The hairs were reduced using Veet™ cream applied for 10 minutes prior to removal. The skin was further rinsed thoroughly to remove dirt and cream and blotted dry prior to storage in the -20ºC freezer.

4.2.5.2 Skin experimental design

Experimental set up

Three different subjects were used for each experiment to provide 4-6 replications. Full thickness excised skin was thawed at room temperature. The thickness of the skin was measured using a digital Vernier calliper (Kincrome, Australia) before experiment. In brief, the skin was sandwiched between two glass slides prior to thickness measurement. Skin of 400-600 µm thickness was used. The skin was then mounted in between the donor and receptor compartments of a Franz-type diffusion cell (SC side up) and clamped (Figure 4.2). Skin integrity testing was conducted by measuring the resistance using a digital multimeter (UNI-T®, Opava-Předměstí, Česko). Briefly, both donor and receptor compartments were then filled with PBS pH 7.4 and the cells were incubated in the water bath at 35ºC for 20 minutes. One probe of multimeter was applied in the donor and the other was in the receptor fluid, and the resistance was read in a maximum level of 1 MΩ. The baseline reading was considered and the skin with resistance less than 50 kΩ was excluded. The PBS pH 7.4 in the donor compartment was then discarded, while the PBS pH 7.4 in the receptor compartment was replaced by a solution of 20% ethanol in PBS pH 6. A magnetic stirrer was added into the receptor compartment prior to donor addition. One gram of the RSV nanocarriers or the RSV saturated aqueous solution was then added into the donor compartment (infinite dose). Parafilm was used to cover the donor cell to minimize evaporation and to facilitate the process of total replacement sampling. The cells were incubated in the water bath at 35ºC (to reach the skin temperature of 32°C[63]) and the receptor fluid was stirred at 350 rpm. Samples were taken from the receptor compartment at time points by taking all the receptor fluid and replacing it

with the fresh fluid pre-warmed to 35°C (total replacement). The details of the experimental set up are displayed on Table 4.4.

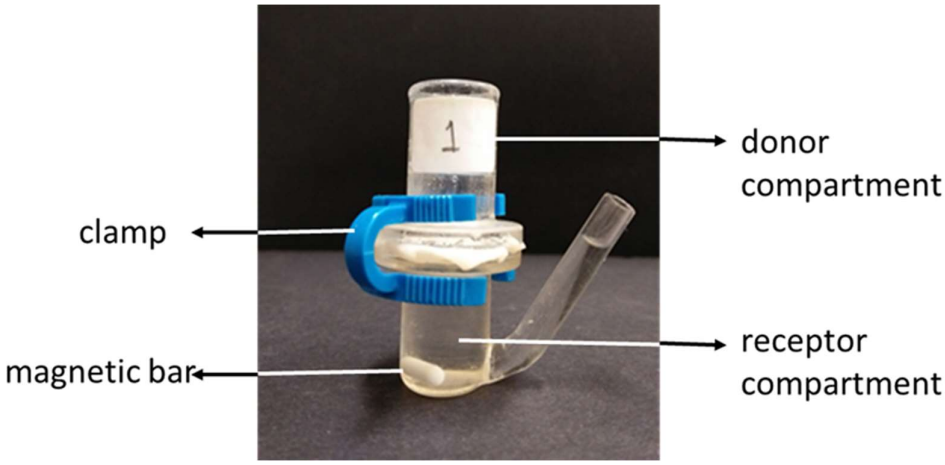

Figure 4.2 Franz cell set up

The RSV in liquid samples was determined by HPLC assay, following suitable dilution with mobile phase and centrifugation at 15,000 rcf. for 10 minutes.

Skin distribution study

After completing the sampling at 8 hours, the donor was transferred into a volumetric flask and made up to 10.0 mL with acetonitrile. The RSV of the remaining donor was determined by HPLC.

A tape stripping process was conducted to assess the amount of RSV on the SC. The procedure of tape stripping is similar to that described in Chapter 3 section 3.2.2.

The first two tapes were kept aside for mass balance study and the remaining tapes were used to determine the RSV penetrated into the SC. The skin was then sectioned prior to RSV extraction. RSV in the tapes and sectioned skin were extracted using mobile phase with the aid of magnetic stirring at room temperature for 3 hours, prior to determination of RSV content by HPLC.

Table 4.4 Experimental set up of *in vitro* penetration/permeation study

System set up	Description
Membrane type	Full thickness of newborn pig skin
Area of cell orifice	1.2-1.3 cm^2
Volume of receptor compartment	3-3.5 mL
Receptor fluid	20% ethanol in 10mM Phosphate Buffer Saline (PBS) pH 6
Donor application	1 g (infinite dose) of either RSV saturated solution or 2% RSV in formulation
Incubation temperature	35ºC (to reach the skin temperature of 32ºC)
Magnetic stirring rate	350 rpm
Duration of incubation	8 hours
Receptor sampling time	1, 2, 4, 6, 8 hours
Sampling type	Total replacement

Stability of RSV in fluid samples

Stability study was carried out in order to ensure that RSV was stable during the experiment and analysis procedures. Briefly, pre-weighted skin was soaked in the experimental solvents for 24 hours: 20% ethanol in PBS pH 6 was used to mimic the receptor fluid, and mobile phase was used to represent the solvent extractor in the skin distribution study. These skin solutions then were used to provide 1 µg/mL RSV solutions. The solutions underwent a similar process as conducted on the real experiment. The first scenario was similar to the process of receptor fluid sampling, where the RSV skin-solution (in ethanol: PBS pH 6 = 20:80) underwent three conditions:

1. RSV solution + mobile phase → centrifuged (10 minutes, 15,000 rcf) → analysed as initial concentration
2. RSV solution → incubated at 35ºC for 2 hours → added with mobile phase → centrifuged (10 minutes, 15,000 rcf) → analysed
3. RSV solution → incubated at 35ºC for 2 hours → kept at 4ºC for 24h → centrifuged (10 minutes, 15,000 rcf) → analysed

The second scenario was based on the RSV extraction process involving two conditions:

1. RSV solution → centrifuged (10 minutes, 15,000 rcf) → analysed as initial concentration
2. RSV solution → incubated at 35ºC for 3 hours → centrifuged (10 minutes, 15,000 rcf) → analysed

4.2.6 Stability of RSV nanoformulations

To assess the stability in short term of storage, RSV in the nanocarriers was initially analysed after preparation (day 0) and considered as 100% potency. The RSV nanocarriers were further kept protected from light at ambient temperature (22-25°C) for one month. To assess the stability of RSV nanocarriers without light protection, the formulations in sealed clear vials were placed on the bench at 22-25°C.

Long term storage stability of RSV nanoformulations was assessed after 5-8-month storage. The formulations were kept at 2-5°C, in sealed amber glass vials, and protected from light after underwent initial determination of RSV.

4.2.7 Data analysis

For assay validation, LOD was calculated as:

$$LOD = 3x \frac{average\ SD\ of\ noises}{slope\ of\ peak\ heigh \quad vs\ standard\ concentration} \ldots\ldots\ldots \quad (1)$$

LOQ was calculated as:

$$LOQ = 10x \frac{average\ SD\ of\ noises}{slope\ of\ peak\ heights\ vs\ standard\ concentration} \ldots\ldots\ldots \quad (2)$$

To perform the results of the *in vitro* skin permeation study, curves of cumulative amount per area (μg/cm^2) versus time of sampling (h) were established. Parameters on the *in vitro* skin permeation study include steady state flux (J_{ss}), maximum flux (J_{max}), lag time, and enhancement ratio (ER). J_{ss} is defined as the rate of RSV permeated in a steady state in a certain area. J_{max} is the RSV flux of RSV saturated solution/vehicle. J_{ss} is determined from the slope of linear portion of a graph of RSV cumulative amount/area vs time, whereas:

$$Jmax = Jss\ x \frac{Sv}{Cv} \ldots\ldots\ldots\ldots\ldots\ldots\ldots \quad (3)$$

S_v is saturated solubility of RSV in the vehicles (formulations) and C_v is donor concentration.

Lag time is the initial time of RSV permeated to the skin. Lag time is calculated based on the linear portion of graph of the cumulative amount/area vs time (y=0) as:

$$lag\ time = \frac{-(intercept\ of\ the\ graph)}{slope} \quad \ldots\ldots\ldots\ldots\ldots\ldots (4)$$

4.2.8 Statistical analysis

All data were presented as mean ± SD (physical characteristics-related measurements) and mean ± SEM (biological system-related experiments). Normally distributed data were analysed using parametric statistical analysis while non-parametric analysis was conducted if the data were not normally distributed. In parametric analysis, ANOVA was used for more than two datasets whereas unpaired t test was used to analyse two data sets. In non-parametric analysis, two datasets were analysed using Wilcoxon test, whereas more than two data were analysed based on Kruskal Wallis. Significant differences were considered if $P < 0.05$ (two tails). All data were analysed using GraphPad Prism™ 8 software (GraphPad Software, San Diego, CA).

4.3 Results

4.3.1 HPLC assay method validation

The isocratic HPLC assay method for RSV determination was well developed using Agilent system (Table 4.1). RSV was detected at $\lambda_{max:}$ 307nm. The RSV peak retention time was 2.4 ± 0.05 minutes in total analysis time of 7.2 minutes (Figure 4.3), at a mobile phase flow rate of 1 mL/min. The internal pressure was at 80-90 bar.

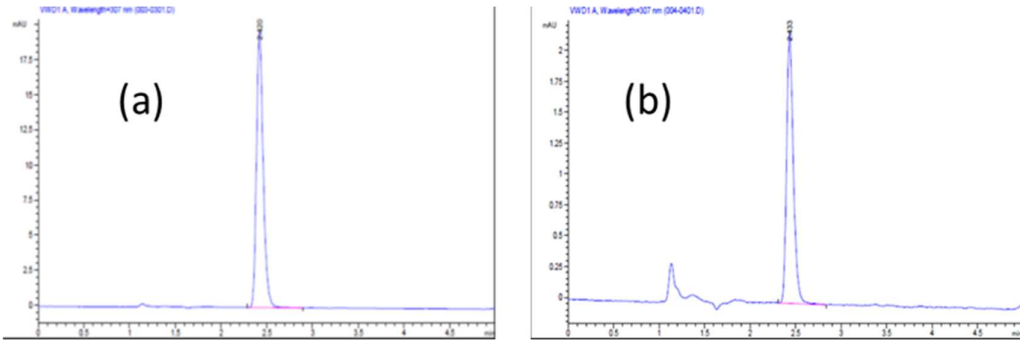

Figure 4.3 HPLC chromatogram of RSV in (a) solvent system A and (b) solvent system B. (a) and (b) were in different concentrations of RSV

This assay method was further validated in terms of linearity and range, and system suitability (precision, sensitivity and accuracy). The A solvent system containing mobile phase (see section 4.2.2.1) was applied for general purposes, such as RSV

solubility determination, assessment of amount of RSV in the donor compartment, and RSV skin uptake in the *in vitro* penetration/permeation study. The B solvent system (20% ethanol:mobile phase=1:1) was prepared to determine the RSV amount in the receptor compartment in the *in vitro* penetration/permeation study. In terms of linearity, there was good linearity between concentrations and responses (peak area; AUC) with r 0.9999-1 in two different solvent systems, thus in two different ranges of concentration (Figure 4.4).

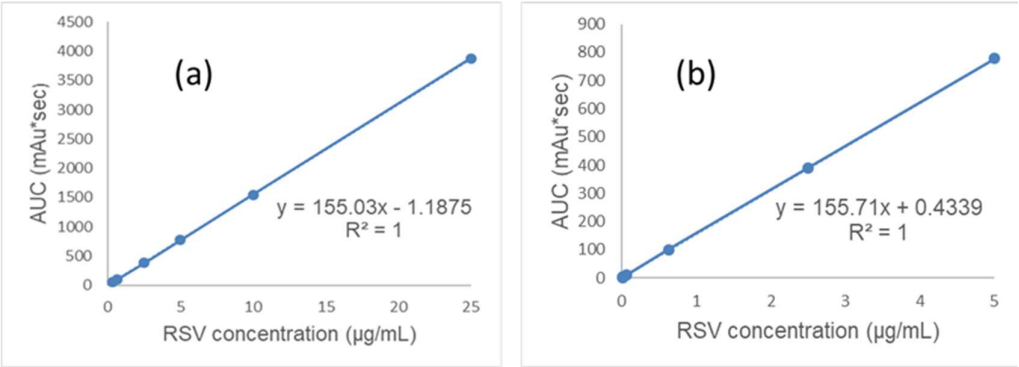

Figure 4.4 Representatives of calibration curves of (a) solvent system A and (b) solvent system B

The assay was sensitive, shown by the LOD/LOQ of solvent system A which was 4.37/14.47 ng/mL and solvent system B which was 4.01/13.37 ng/mL.

Table 4.5 Precision of RSV assay ($\bar{x}$ ± SD; 6 replications)

	Solvent system A			Solvent system B		
Concentration (µg/mL)	0.3125	5	10	0.0078	0.625	5
RSD (%)	0.29	0.19	0.08	9.51	0.23	0.17

Table 4.6 Mass balance study of RSV skin extraction ($\bar{x}$ ± SD; 3 replications)

RSV Donor (µg)	Distribution of RSV (µg)			Total distribution (µg)	Recovery (%)
	Remaining donor	Wash	Skin extraction		
423.15 ± 6.93	361.34 ± 2.59	3.57 ± 0.10	23.16 ± 0.91	388.07 ± 2.38	91.77 ± 1.79

Table 4.5 shows precision of RSV assay in two types of solvent systems. The medium and high concentrations showed good precision with RSD < 0.5%, but the low concentration (0.0078 µg/mL) of solvent system B was less than LOQ and close to

LOD. The low concentration was useful to anticipate the analytical limits for receptor fluid sampling.

The accuracy of the assay was determined from the recovery of RSV extraction from the skin (Table 4.6). Mass balance for each of the solvent extraction systems was determined based on the amount of RSV added in the initial donor, by adding the amount of RSV recovered in the remaining donor, wash liquid and skin extraction liquids. Mass balance recovery of RSV was 91.77 ± 1.79 % (as percentage of initial RSV applied).

4.3.2 Optimisation of *in vitro* penetration/permeation study

4.3.2.1 Skin preparation

In vitro Franz-type diffusion cell study was conducted to assess the penetration and permeation of RSV from the nanoformulations, into and through newborn pig skin (NBPS). Ideally, human skin is used for *ex vivo* or *in vitro* penetration/permeation studies. However, human skin was not available, so a suitable alternative was used. NBPS is a good surrogate for human skin as it provides similar skin properties to human skin[64] and can be sourced by utilising stillborn piglets, collected from local piggeries by our collaborating veterinary surgeons (Portec Veterinary Services, Welshpool).

NBPS is pink-white skin with fine hairs that were easily removed by Veet™ cream. Microscopic examination confirmed that the cream only worked on the surface by breaking the hair shafts without damaging the SC and follicles (Figure 4.5 and Figure 4.6).

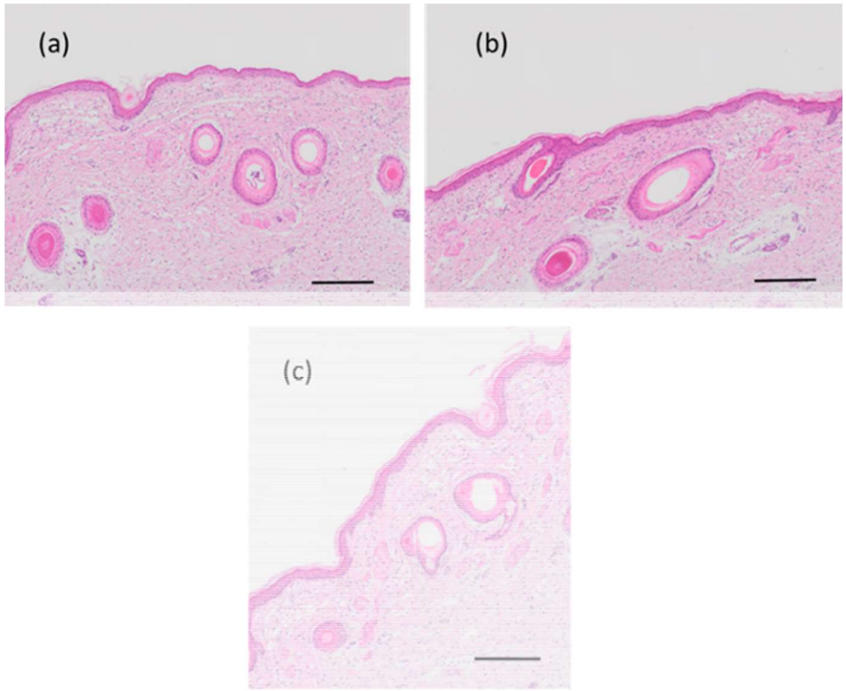

Figure 4.5 Hematoxyllin and eosin stained images of NBPS: (a) after being shaved using a razor; (b) after Veet™ cream application: (c) untreated skin (scale bars indicate 200 µm)

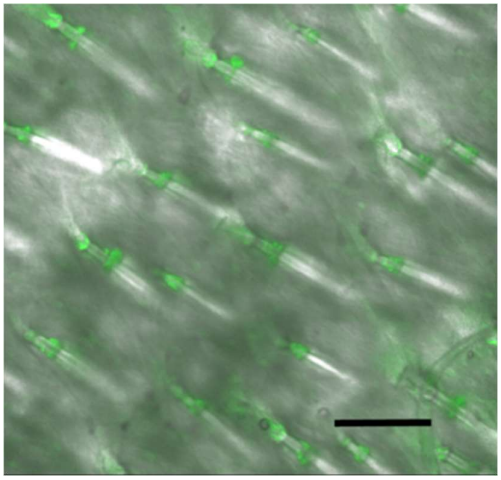

Figure 4.6 Confocal image of NBPS after Veet™ cream application (scale bar indicates 500 µm)

4.3.2.2 Selection of receptor fluid

The choice of suitable receptor phase was primarily based on ensuring sink conditions for the poorly aqueous soluble RSV. RSV solubility was approximately 5 times greater in 2% polyethylene glycol oleyl ether (Volpo 20™) than in 20% ethanol solution (2.766 ± 0.021 mg/mL and 0.701 ± 0.045 mg/mL respectively). However, during diffusion cell

stirring and manipulation, the Volpo™ created air bubbles due to its surfactant nature that resulted in high variability of RSV in samples taken from the receptor compartment (Figure 4.7). In comparison, RSV results using 20% ethanol in PBS pH 6 were more consistent and adequate solubility was achieved.

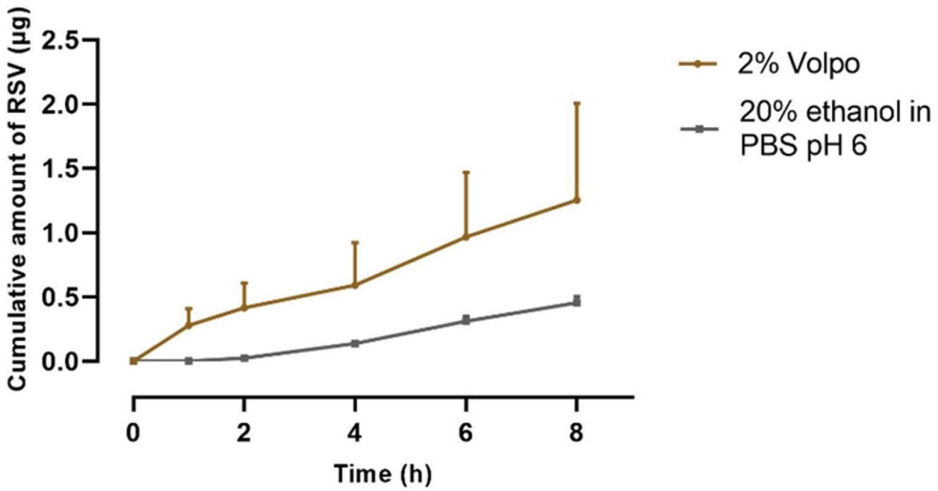

Figure 4.7 The permeation profile of RSV through NBPS using 2% Volpo™ and 20% ethanol in PBS pH 6 as the receptor fluids ($\bar{x}$ ± SEM; 4 replications)

4.3.2.3 Permeation profile of RSV saturated solution in PBS pH 6

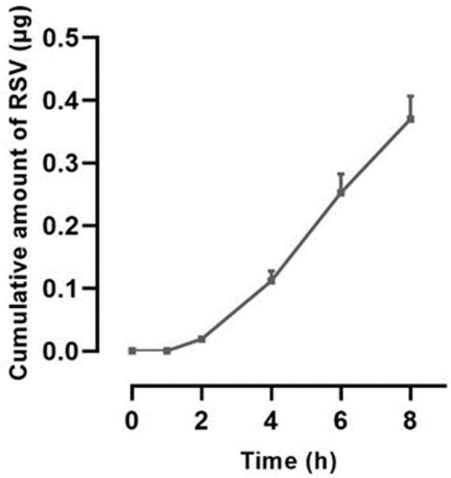

Figure 4.8 The permeation profile of RSV from saturated aqueous solution (in PBS pH 6) through NBPS over 8 hours ($\bar{x}$ ± SEM; 4 replications)

Figure 4.8 presents the permeation profile of RSV of its saturated solution in PBS pH 6. The saturated solubility of the RSV in PBS pH 6 was 34.13 ± 0.20 µg/mL and the maximum transdermal flux of RSV in PBS pH 6 through NBPS was 0.051 ± 0.009 µg/cm^2/h.

4.3.2.4 Stability of RSV in sample fluids

RSV was stable in the receptor solution (20% ethanol in PBS pH 6) for 2 hours at 35°C (100.30 ± 0.190 % remaining), and in the skin extraction fluid (mobile phase) for 3 hours at 35°C (99.730 ± 0.101 % remaining). It was also stable on storage at -20°C (100.52 ± 0.411 % remaining).

4.3.3 Formulation, characterisation and *in vitro* penetration-permeation study

4.3.3.1 Initial formulation

Initial formulation study of RSV nanocarriers was performed to investigate the effect of lipid-based formulation, micellar formulation and microemulsion on the RSV penetration into- and permeation through the skin (table 4.3), with loading dose of 8% RSV.

The appearance of most formulations was clear-transparent, except the blank TKLT2P which was translucent (Figure 4.9). pH of all formulations was 6. Physical characteristics of TKLT2, PKLT2 and TKLT2P are displayed in the table 4.7.

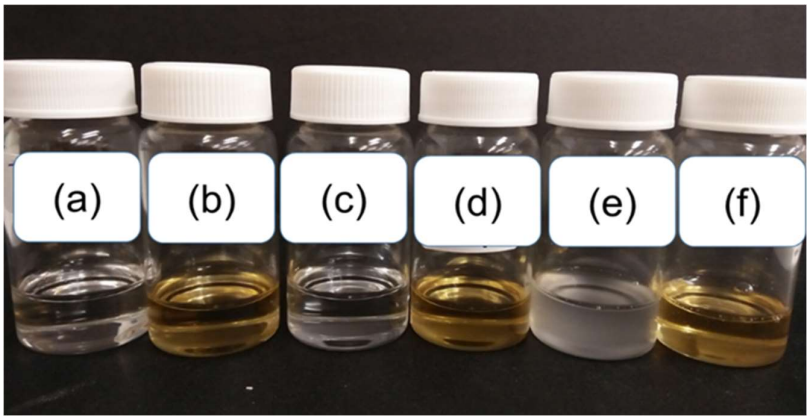

Figure 4.9 Physical appearance of initial nanoformulations: (a) blank TKLT2; (b) RSV-TKLT2; (c) blank PKLT2; (d) RSV-PKLT2; (e) blank TKLT2P; (f) RSV-TKLT2P

The solubility of RSV in the nanoformulations significantly increased compared to the RSV saturated aqueous solution.

The globule size was less than 20 nm with PDI less than 0.25 for PKLT2 and TKLT2P. The globule size of TKLT2P was slightly larger than that of PKLT2 and the PDI was also higher. The globule size and PDI of TKLT2 could not be measured as it is totally lipid-based formulation which could not be diluted with water to meet similar procedure with the others.

Table 4.7 Physical characteristics of initial RSV nanoformulations ($\bar{x}$ ± SD; 4 replications)

Formula	Appearance			Globule size (nm)*	PDI*	RSV solubility (mg/mL)	Viscosity (dPas)*	Refractive index*
	Clarity	Single phase	Colour					
TKLT2	transparent	✓	Light brown	n. a	n. a	149.64 ± 0.83	0.730 ± 0.010	1.4473 ± 0.0001
PKLT2	transparent	✓	Light brown	12.85 ± 0.28	0.136 ± 0.010	165.98 ± 3.18	2.467 ± 0.025	1.4232 ± 0.0001
TKLT2P	translucent	✓	Light brown	14.30 ± 0.05	0.229 ± 0.010	177.16 ± 25.95	0.790 ± 0.070	1.4253 ± 0.0007

Notes:
n. a not available
* measurements were carried out on blank nanoformulations

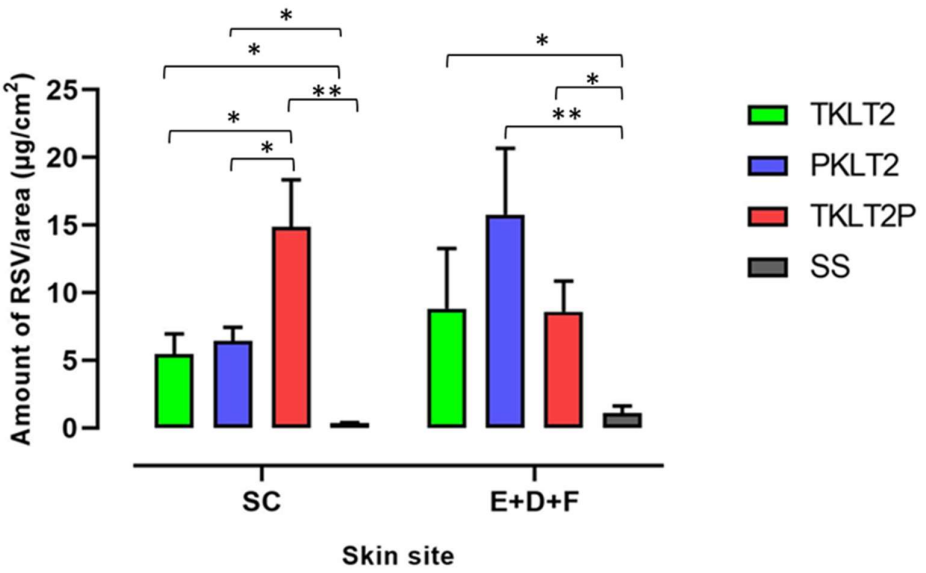

Figure 4.10 The skin distribution of RSV in the stratum corneum (SC) and in the area of epidermis, dermis and follicles (E+D+F) of TKLT2, PKLT2, and TKLT2P ($\bar{x}$ ± SEM; 4 replications; * P < 0.05, ** P < 0.01)

Figure 4.10 and table 4.8 present the amount per area of RSV of TKLT2, PKLT2, and TKLT2P penetrated into NBPS skin in 8 hours. In the SC, TKLT2P showed the highest penetration of RSV. In the area of epidermis, dermis and follicles, the RSV distribution of TKLT2, TKLT2P and PKLT2 were comparable.

Table 4.8 Experimental data of RSV skin penetration in initial nanoformulations ($\bar{x}$ ± SEM; 5-6 replications)

Formula	RSV distribution in the skin		Enhancement Ratio (ER)
	SC	E+D+F	
TKLT2	5.471 ± 1.495	8.827 ± 4.450	9.52
PKLT2	6.417 ± 1.028	15.768 ± 4.918	14.73
TKLT2P	14.864 ± 3.471	8.593 ± 2.267	15.62
RSV saturated solution	0.378 ± 0.025	1.124 ± 0.519	1.00

Notes: SC: stratum corneum; E+D+F: epidermis, dermis, and follicles; ER: enhancement ratio, was calculated based on the ratio of average values of the RSV amount deposited in the skin from the nanoformulations to RSV saturated aqueous solution.

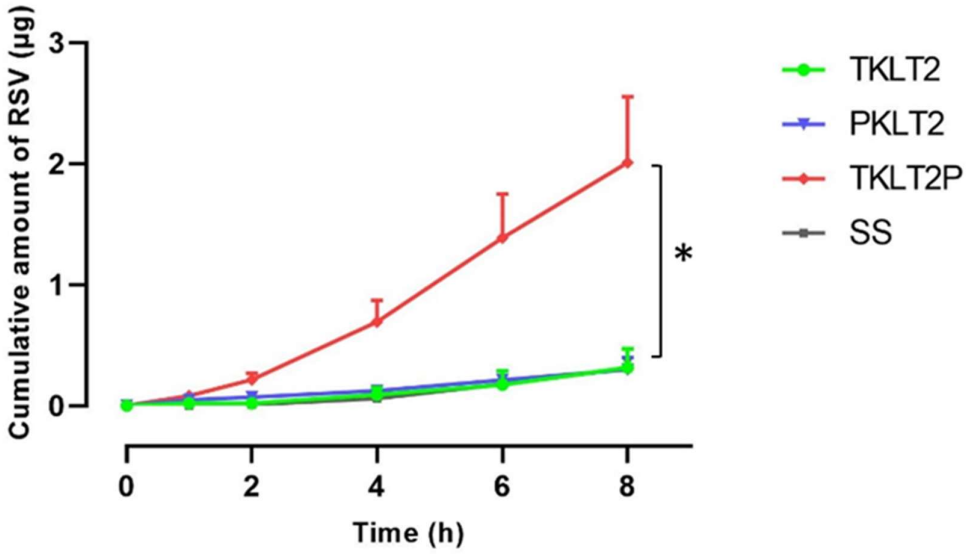

Figure 4.11 Cumulative amount of RSV of TKLT2, PKLT2, and TKLT2P after 8h permeation through the skin ($\bar{x}$ ± SEM; 4 replications; * P < 0.05)

Figure 4.11 shows the permeation profile of RSV of TKLT2, PKLT2, and TKLT2P in 8 hours. Whilst the micellar system (PKLT2) and the lipid-based system (TKLT2) had similar RSV permeation to the RSV saturated solution over 8 hours, the microemulsion system (TKLT2P) showed the highest permeation of RSV through the skin (2.009 ± 0.545 µg) ($P < 0.05$).

The complete experimental data of RSV skin permeation is presented in Table 4.9. TKLT2 and PKLT2 showed low fluxes and long lag time similar to the saturated solution. TKLT2P reduced the lag time as the flux significantly increased. TKLT2P enhanced the RSV skin permeation in five folds, approximately.

Table 4.9 Experimental data of RSV skin permeation in initial nanoformulations ($\bar{x}$ ± SEM; 5-6 replications)

Formula	Cumulative amount (μg)	Flux (μg/cm^2/h)		Lag time (h)	ER
		Steady state flux (J_{ss})	Maximum flux (J_{max})		
TKLT2	0.316 ± 0.154	0.047 ± 0.022	0.088 ± 0.041	2.679 ± 1.046	0.92
PKLT2	0.298 ± 0.102	0.036 ± 0.012	0.074 ± 0.024	1.178 ± 0.175	0.70
TKLT2P	2.009 ± 0.545	0.276 ± 0.078	0.612 ± 0.173	0.612 ± 0.173	5.42
RSV saturated aqueous solution	0.309 ± 0.074	0.051 ± 0.009	0.051 ± 0.009	3.185 ± 0.176	1.00

Notes: ER=enhancement ratio, was calculated based on the ratio of average values of flux of the formulations to RSV saturated aqueous solution

4.3.3.2 Effect of modifying the oil phase and surfactant composition

The next stage of formulation study was to modify the oil phase and surfactant composition to evaluate the effect on the physical, skin penetration and skin permeation characteristic. The RSV loading of all formulas were 2%. The pH of all formulations was 6.

In developing TKTP, the oil phase (Triacetin™) and Kolliphor™ RH 40 as the surfactant reduced to 5% and 20%, respectively. The TKTP was made without Labrasol™. The TKTP formulation was transparent (Figure 4.12) with the refractive index of 1.3769 ± 0.0005, globule size of 13.72 ± 0.40 nm, PDI of 0.106 ± 0.072, and the viscosity of 0.110 ± 0.026 dPas. The solubility of RSV in TKTP was 44.771± 4.159 mg/mL.

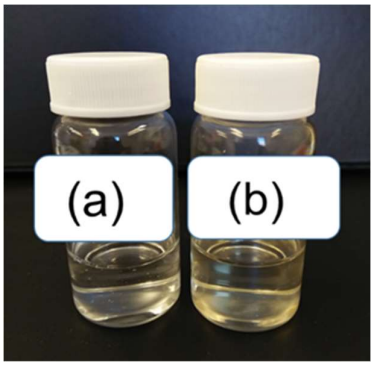

Figure 4.12 Physical appearance of TKTP: (a) blank TKTP; (b) RSV-TKTP

The amount RSV of TKTP distributed on the SC (1.998 ± 0.383 μg/cm^2) and the epidermal-dermal-follicular (E+D+F) level (5.359 ± 0.845 μg/cm^2) were twice as the amount of those of TKLT2P, although the difference in the E+D+F was not statistically significant (Figure 4.13).

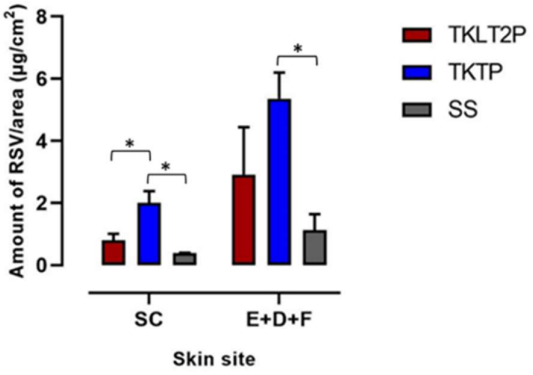

Figure 4.13 Skin distribution of RSV in the SC and in the area of E+D+F of TKLT2P and TKTP ($\bar{x}$ ± SEM; 5-6 replications; * P < 0.05)

The permeation of RSV of TKTP also significantly increased compared to TKLT2P (Figure 4.14) with the cumulative amount of TKTP and TKLT2P were 0.853 ± 0.091 µg and 0.278 ± 0.086 µg, respectively ($P < 0.05$). The steady state flux of TKTP was 0.103 ± 0.006 µg/cm^2/h whereas the flux of TKLT2P was 0.038 ± 0.010 µg/cm^2/h. TKTP permeated three times faster than TKLT2P, although the lag time of both formulations were similar.

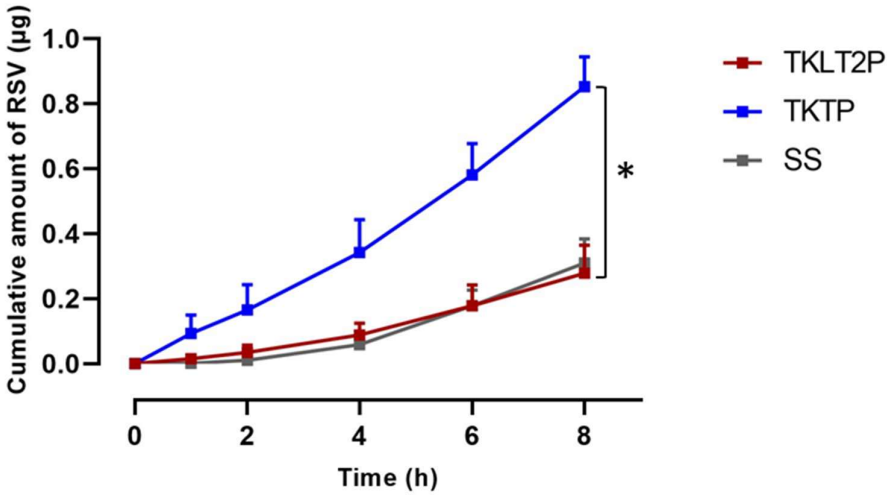

Figure 4.14 Cumulative amount of RSV of TKLT2P and TKTP after 8h permeation through the skin ($\bar{x}$ ± SEM; 5-6 replications; * P < 0.05)

TKTP appeared to be a promising nanoformulation for RSV with good skin penetration and permeation characteristics. To further enhance the penetration and permeation of RSV, the addition of natural terpenes as chemical penetration enhancers was considered.

4.3.3.3 Effect of terpene addition

The addition of eugenol (5%) required an increase in the concentration of Kolliphor® RH 40 as the surfactant, in order to provide RSV nanoformulations with good clarity and surfactant capacity. Kolliphor® RH 40 with 30% concentration was sufficient for the ETKTP to show good transparency although it was highly viscous (1.621 ± 0.119 dPas), 16x times more viscous than TKTP ($P < 0.05$) (Figure 4.15 and table 4.10). Although the high viscosity may assist the spreadability on skin application of the formula, it created a problem in the solubility determination. The centrifuge failed to separate or precipitate the undissolved RSV of the excess RSV from the system (turbid appearance). Moreover, phase separation occurred as the system could not resist the high-speed centrifugation (15,000 rcf). The separated phases and the turbidity in oil-surfactant-cosurfactant phase led to unreliable solubility values.

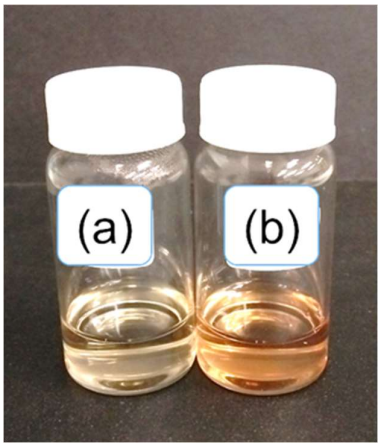

Figure 4.15 Physical appearance of ETKTP: (a) blank ETKTP; (b) RSV-ETKTP

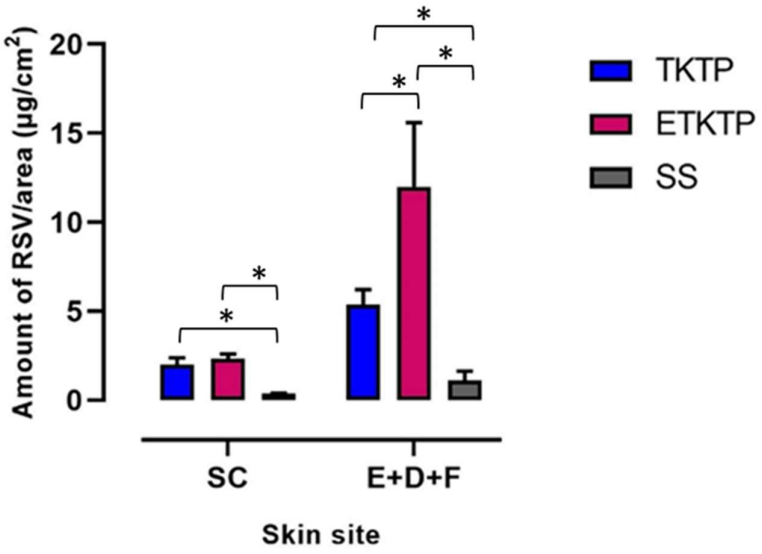

Figure 4.16 Skin distribution of RSV in the SC and in the area of E+D+F of TKTP and ETKTP ($\bar{x}$ ± SEM; 5-6 replications; * P < 0.05)

Figure 4.16 shows the comparison of RSV skin penetration of TKTP and ETKTP at 8 hours incubation. A similar amount of RSV of both nanoformulations (ETKTP and TKTP) was found on the SC, however there was 2.5-fold increase in the amount of RSV in the epidermis-dermis-follicles (12.000 ± 3.598 µg/cm^2) of ETKTP compared to TKTP ($P < 0.05$).

ETKTP also showed higher permeation of RSV ($P < 0.05$) compared to TKTP (Figure 4.17). The cumulative amount and steady state flux of ETKTP was 2.973 ±1.051 µg and 0.358 ± 0.125 µg/cm^2/h compared to 0.853 ± 0.091 µg and 0.103 ± 0.006 µg/cm^2/h for TKTP. The enhancement ratio for ETKTP and TKTP compared to the

RSV saturated solution was 6.98 and 2.01, respectively. Lag time was similar for ETKTP and TKTP, with both approximately half the lag time of RSV saturated aqueous solution.

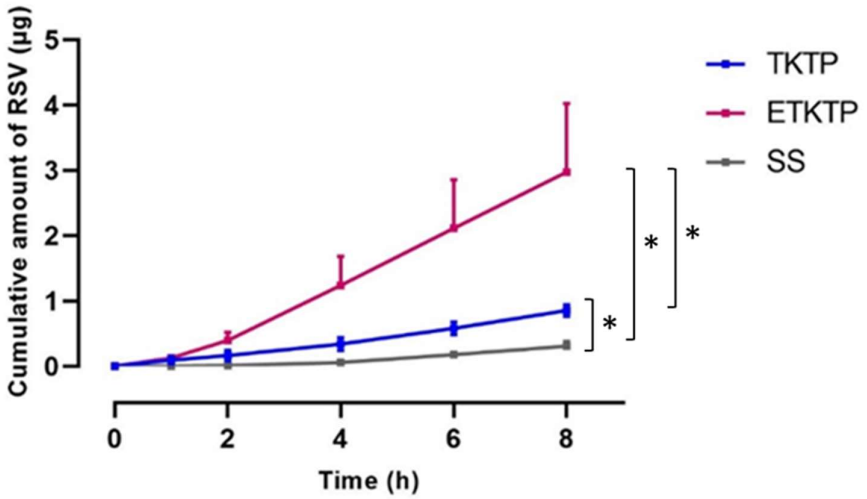

Figure 4.17 Cumulative amount of RSV of TKTP and ETKTP after 8h permeation through the skin ($\bar{x}$ ± SEM; 5-6 replications; * P < 0.05)

To observe whether the promising results of ETKTP system was due to the interaction of eugenol and triacetin, the next formula was developed without applying Triacetin (E5K30TP).

4.3.3.4 Effect of the absence of triacetin

E5K30TP contained only eugenol as the oil phase without the existence of triacetin. Similar to ETKTP, E5K30TP had a light-brown, single phase, transparent appearance (Figure 4.18). However, the E5K30TP had lower viscosity (1.060 ± 0.450 dPas), with slight difference in the refractive index (E5K30TP and ETKTP were 1.3850 ± 0.0033 and 1.4021 ± 0.0002, respectively). The size and PDI of E5K30TP was also slightly lower than ETKTP.

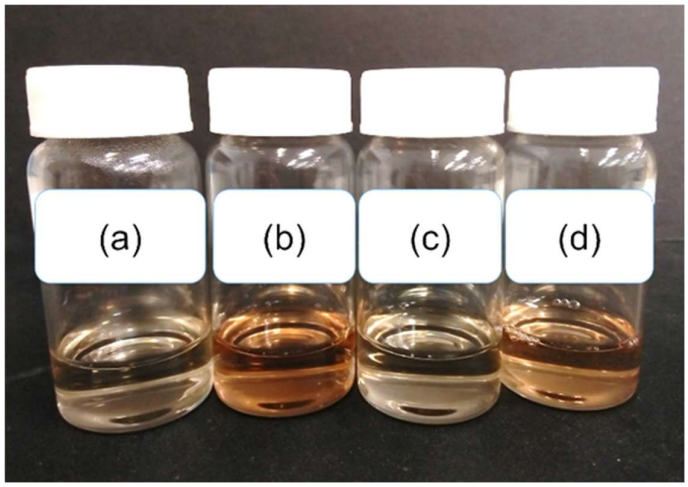

Figure 4.18 Physical appearance of ETKTP and E5K30TP nanoformulations: (a) blank ETKTP; (b) RSV-ETKTP; (c) blank E5K30TP; (d) RSV-E5K30TP

The distribution of RSV in the SC (Figure 4.19) of ETKTP (2.342 ± 0.269 μg/cm^2) and E5K30TP (2.104 ± 0.297 μg/cm^2) were similar, with both significantly higher than RSV saturated solution (0.378 ± 0.025 μg/cm^2). In the E+D+F region, the amount of RSV of E5K30TP penetrated was reduced by 50% to 5.914 ± 1.169 μg/cm^2 ($P < 0.05$). The absence of triacetin resulted in a reduction of the amount of RSV in the skin.

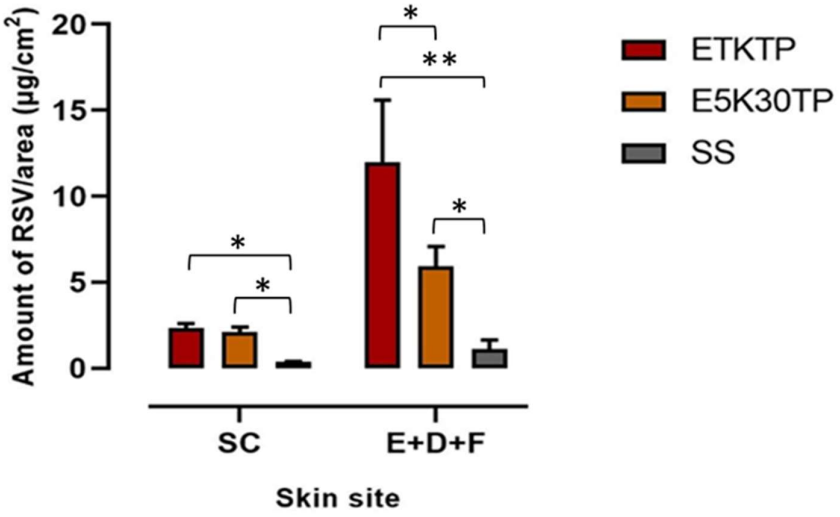

Figure 4.19 Skin distribution of RSV in the SC and in the area of E+D+F of ETKTP and E5K30TP ($\bar{x}$ ± SEM; 5-6 replications; * P < 0.05, ** P < 0.01)

The cumulative amount of RSV permeated over 8 hours (Figure 4.20) was significantly higher for both ETKTP and E5K30TP (2.973 ±1.051 µg and 2.017 ± 0.954 µg, respectively) than from the saturated RSV solution (0.309 ± 0.074 µg) ($P < 0.05$). There was no significant difference of RSV cumulative amount of ETKTP and E5K30TP permeated through the skin over 8 hours (Figure 4.20).

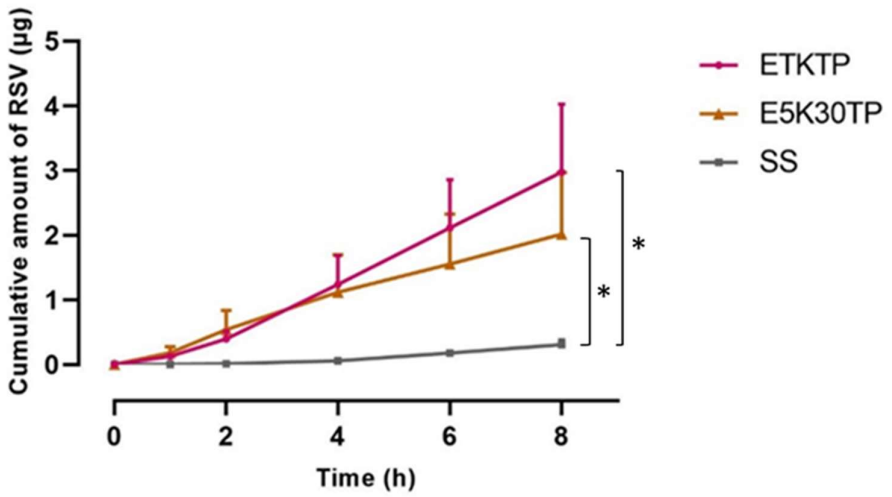

Figure 4.20 Cumulative amount of RSV of ETKTP and E5K30TP permeated through the skin ($\bar{x}$ ± SEM; 5-6 replications; * P < 0.05)

4.3.3.5 Effect of reducing the surfactant (Kolliphor™ RH 40) concentration

The concentration of surfactant in the E5K30TP formulation was reduced from 30% to 20%. The appearance of the blank nanoemulsion was clear (refractive index: 1.3992 ± 0.0040) with the size of 16.54 ± 0.08 nm (PDI of 0.084 ± 0.003), and the viscosity was reduced (0.248 ± 0.022 dPas). However, when RSV was incorporated in the formula at concentration of 2%, the appearance was turbid (Figure 4.21) showing that the solubility of RSV was significantly reduced with the reduction in surfactant. The solubility of RSV in the formula was 6.189 ± 0.082 mg/mL, below the loading concentration. It was visually obvious that the particle size of RSV was not in a nanometer range due to the aggregation and lack of solubilizing capacity of surfactant-cosurfactant in the system.

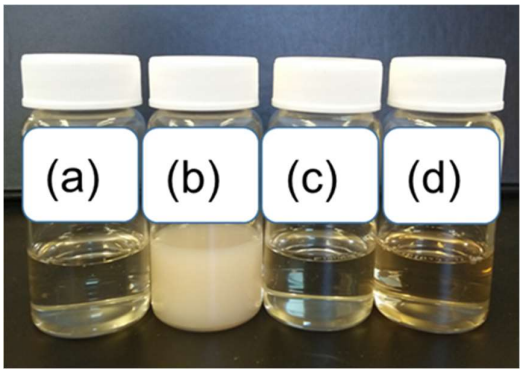

Figure 4.21 Physical appearance of E5K20TP nanoformulations: (a) blank E5K20TP; (b) RSV-E5K20TP; (c) blank E5K30TP; (d) RSV-E5K30TP

4.3.3.6 Effect of reducing the composition of eugenol and surfactant in E5K30TP

As E5K20TP failed to meet the formulation criteria, the concentration of eugenol and surfactant in the formula E5K30TP was reduced to 1 and 20%, respectively. The formula named E1K20TP. The blank nanoformulation appeared to be transparent with refractive index of 1.3747 ± 0.0003 and low viscosity (0.099 ± 0.013 dPas). The solubility of RSV in the system increased five times (34.092 ± 1.133 mg/mL) from the previous formula (6.189 ± 0.082 mg/mL), and resulted in the transparency of the system.

In comparison to E5K30TP (Figure 4.22), the amount of RSV of E1K20TP in the SC was 1.022 ± 0.129 μg/cm^2, which was less than that of E5K30TP (2.104 ± 0.297 μg/cm^2) ($P < 0.05$). Although the RSV of E1K20TP distributed less in the SC, the skin distribution of RSV in the E+D+F of both formula (E1K20TP and E5K30TP) were similar.

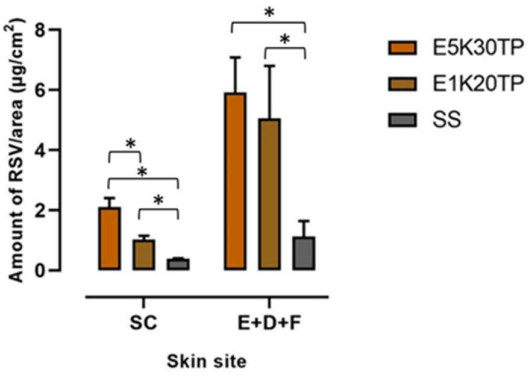

Figure 4.22 Skin distribution of RSV in the SC and in the area of E+D+F of E5K30TP and E1K20TP ($\bar{x}$ ± SEM; 5-6 replications; * P < 0.05)

The permeation profiles of E5K20TP and E1K20TP were similar (Figure 4.23). The cumulative amount of RSV of E1K20TP permeated over 8 hours was 0.918 ± 0.126 µg with steady state flux of 0.142 ± 0.017 µg/cm^2/h. Whilst there was a trend towards lower permeation with lower surfactant in the formulation, there were no significant differences in the cumulative amount, steady state flux, and lag time among E5K30TP, E5K20TP and E1K20TP.

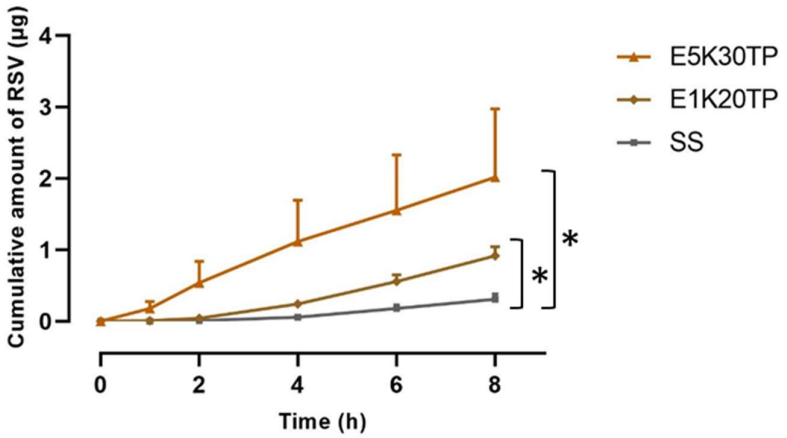

Figure 4.23 Cumulative amount of RSV of E5K30TP and E1K20TP after 8h permeation through the skin ($\bar{x}$ ± SEM; 5-6 replications; * P < 0.05)

4.3.3.7 A comparison of terpene-based RSV nanoemulsions

A comparison of terpene-based RSV nanoemulsions was further investigated to observe the role of natural terpenes as chemical penetration and permeation enhancers in the RSV nanoformulation in this study. Eugenol, D-limonene and Eucalyptol were incorporated in the systems as the oil phase in the concentration of 1 %. The formulations show excellent clarity (Figure 4.24).

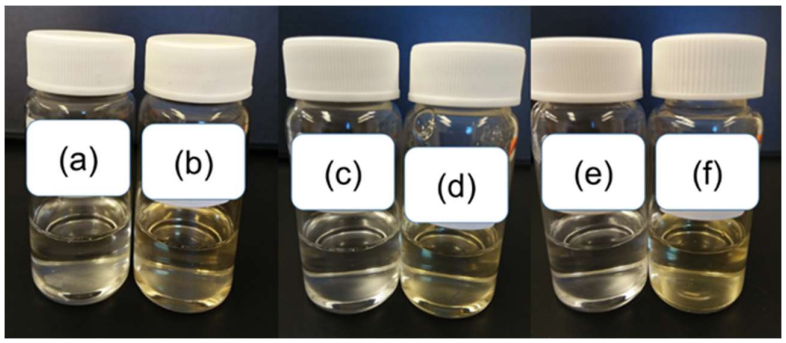

Figure 4.24 Physical appearance of terpene nanoformulations: (a) blank E1K20TP; (b) RSV-E1K20TP; (c) blank LKTP; (d) RSV-LKTP; (e) blank EuKTP; (f) RSV-EuKTP

Three different terpenes in the formulation exhibited similar physical characteristics in terms of appearance, RSV solubility, viscosity, and refractive index (Table 4.10), except that the globule size of LKTP (15.73 ± 0.07 nm) and EuKTP (14.54 ± 0.04 nm) was slightly larger than E1K20TP (13.84 ± 0.01 nm).

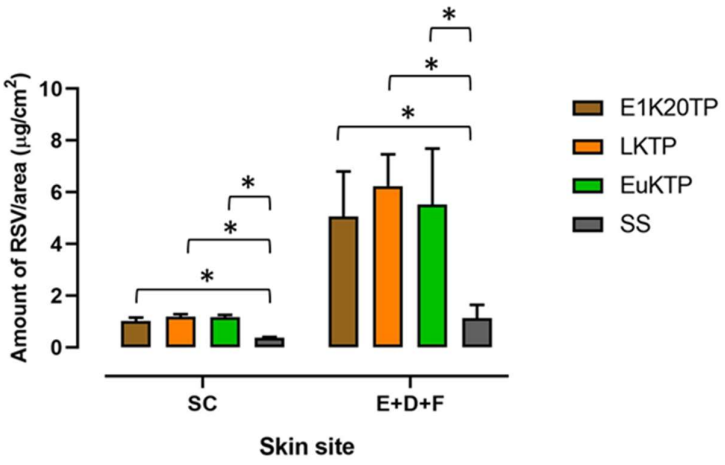

Figure 4.25 Skin distribution of RSV in the SC and in the area of E+D+F of E1K20TP, LKTP, EuKTP ($\bar{x}$ ± SEM; 5-6 replications, * P < 0.05)

Figure 4.25 illustrates the skin uptake of RSV in three different terpene-based formulation. The RSV retained in the skin of those nanoformulations were comparable.

The cumulative amount of RSV permeated of LKTP and EuKTP were similar and both were significantly higher than the RSV in E1K20TP (Figure 4.26) (P < 0.05). Flux and lag time of LKTP and EuKTP were also similar, with 10-13-fold enhancement compared to RSV saturated solution.

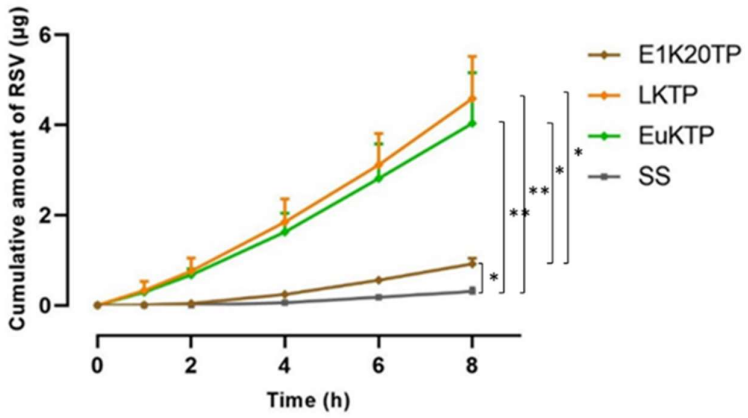

Figure 4.26 Cumulative amount of RSV of E1K20TP, LKTP, and EuKTP after 8h permeation through the skin ($\bar{x}$ ± SEM; 5-6 replications, * P < 0.05, ** P < 0.01)

Table 4.10 Physical characteristics of RSV nanoformulations ($\bar{x}$ ± SD; 4 replications)

Formula	Appearance			Globule Size (nm)*	PDI*	RSV solubility (mg/mL)	Viscosity (dPas)*	Refractive index*
	Clarity	Single phase	Colour					
TKLT2P	translucent	✓	Light brown	14.30 ± 0.05	0.229 ± 0.010	177.16 ± 25.95	0.790 ± 0.070	1.4253 ± 0.0007
TKTP	transparent	✓	Light brown	13.72 ± 0.40	0.106 ± 0.072	44.77 ± 4.16	0.107 ± 0.021	1.3769 ± 0.0005
ETKTP	transparent	✓	Light brown	13.97 ± 0.18	0.055 ± 0.007	n. a	1.627 ± 0.136	1.4021 ± 0.0002
E5K30TP	transparent	✓	Light brown	13.60 ± 0.07	0.046 ± 0.008	n. a	1.280 ± 0.053	1.3850 ± 0.0033
E5K20TP	opaque	X	Light brown	16.54 ± 0.08	0.084 ± 0.003	6.19 ± 0.08	0.250 ± 0.000	1.3992 ± 0.0040
E1K20TP	transparent	✓	Light brown	13.84 ± 0.01	0.071 ± 0.010	34.09 ± 1.13	0.097 ± 0.006	1.3747 ± 0.0003
LKTP	transparent	✓	Light brown	15.73 ± 0.07	0.117 ± 0.003	35.46 ± 1.60	0.083 ± 0.015	1.3732 ± 0.0011
EuKTP	transparent	✓	Light brown	14.54 ± 0.04	0.091 ± 0.044	37.25 ± 3.68	0.093 ± 0.015	1.3918 ± 0.0329

Notes:
n. a: not available
* measurements were carried out on blank nanoformulations

Table 4.11 RSV distribution in the skin ($\bar{x}$ ± SEM; 5-6 replications)

Formula	RSV distribution in the skin		ER
	SC	E+D+F	
TKLT2P	0.805 ± 0.208	2.915 ± 1.523	2.48
TKTP	1.998 ± 0.383	5.359 ± 0.845	4.90
ETKTP	2.342 ± 0.269	12.000 ± 3.598	9.55
E5K30TP	2.104 ± 0.297	5.914 ± 1.169	5.34
E1K20TP	1.022 ± 0.129	5.059 ± 1.744	4.05
LKTP	1.190 ± 0.092	6.234 ± 1.231	4.94
EuKTP	1.172 ± 0.085	5.526 ± 2.160	4.46
RSV saturated solution	0.378 ± 0.025	1.124 ± 0.519	1.00

Notes: SC: stratum corneum; E+D+F: epidermis, dermis, and follicles; ER: enhancement ratio, was calculated based on the ratio of average values of the RSV amount deposited in the skin from the nanoformulations to RSV saturated aqueous solution.

Table 4.12 Experimental data for RSV skin penetration/permeation parameters in nanoemulsions ($\bar{x}$ ± SEM; 5-6 replications)

Formula	Cumulative amount (µg)	Flux (µg/cm^2/h)		Lag time (h)	ER
		Steady state flux (J_{ss})	Maximum flux (J_{max})		
TKLT2P	0.278 ± 0.086	0.038 ± 0.010	0.339 ± 0.091	2.330 ± 0.248	0.75
TKTP	0.853 ± 0.091	0.103 ± 0.006	0.227 ± 0.013	1.711 ± 0.605	2.01
ETKTP	2.973 ±1.051	0.358 ± 0.125	n. a	1.195 ± 0.280	6.98
E5K30TP	2.017 ± 0.954	0.116 ± 0.059	n. a	0.636 ± 0.188	2.27
E1K20TP	0.918 ± 0.126	0.142 ± 0.017	0.258 ± 0.029	2.689 ± 0.224	2.76
LKTP	4.585 ± 0.936	0.647 ± 0.103	1.191 ± 0.209	1.252 ± 0.715	12.61
EuKTP	4.036 ± 1.125	0.510 ± 0.153	0.920 ± 0.277	1.143 ± 0.164	9.95
RSV saturated aqueous solution	0.309 ± 0.074	0.051 ± 0.009	0.051 ± 0.009	3.185 ± 0.176	1.00

ER=enhancement ratio, was calculated based on ratio of J_{ss} of the formula to the saturated solution.

Table 4.13 Mass balance of *in vitro* penetration/permeation study of RSV into and through the skin ($\bar{x}$ ± SEM; 5-6 replications)

Formula	IA (µg)	RSV distribution (µg)					Total of RSV distribution (µg)	RECOVERY (%)
		RA	SC	E+D+F	R	S		
TKTP	20179.55 ± 104.73	18766.40 ± 1623.40	3.70 ± 1.02	7.42 ± 1.78	0.95 ± 0.16	1.41 ± 0.26	18779.88 ± 1625.73	93.14 ± 8.44
ETKTP	19965.18 ± 346.78	17545.95 ± 322.43	3.60 ± 0.41	14.30 ± 4.31	2.97 ± 1.05	3.19 ± 0.49	17570.02 ± 319.98	88.04 ± 1.37
E5K30TP	19331.13 ± 26.40	18120.08 ± 174.14	3.27 ± 0.46	7.07 ± 1.37	2.02 ± 0.95	4.03 ± 1.01	18136.46 ± 174.27	93.82 ± 0.96
E1K20TP	19866.22 ± 56.66	17739.43 ± 199.86	1.57 ± 0.20	6.12 ± 2.18	0.90 ± 0.14	1.03 ± 0.12	17749.05 ± 199.64	89.35 ± 1.03
LKTP	20136.18 ± 406.76	18399.50 ± 277.81	1.89 ± 0.160	7.34 ± 1.77	4.02 ± 0.91	0.87 ± 0.12	18413.62 ± 278.65	91.64 ± 2.70
EuKTP	20513.03 ± 437.89	17485.12 ± 464.87	1.80 ± 0.13	6.60 ± 2.59	4.04 ± 1.13	1.33 ± 0.16	17498.90 ± 462.76	85.42 ± 2.61
RSV-SS	34.13 ± 0.20	29.57 ± 1.33	0.58 ± 0.04	1.42 ± 0.71	0.31 ± 0.01	0.42 ± 0.07	32.30 ± 0.63	94.65 ± 1.86

Notes: IA: initial amount of RSV in the donor compartment; RA: remaining amount of RSV in the donor compartment; SC: amount of RSV in the stratum corneum; E+D+F: amount of RSV in epidermis, dermis and follicles; R: amount of RSV in the receptor compartment; S: amount of RSV on the surface (µg); RSV SS: saturated RSV in PBS pH 6.0

4.3.4 Stability of RSV in the nanoformulations during storage

Table 4.14 RSV stability during a short term of storage (1 month) at 22-25°C

Formula	Physical stability			Chemical stability (%)
	Clarity	Single phase	Tendency of darker appearance	($\bar{x}$ ± SD; 4 replications)
Protected from light				
TKLT2	transparent	✓	+	90.52 ± 5.04
PKLT2	transparent	✓	+	114.03 ± 12.50
TKLT2P	transparent	✓	+	83.88 ± 6.74
TKTP	transparent	✓	+	86.41 ± 6.27
ETKTP	transparent	✓	+	92.74 ± 4.20
E1K20TP	transparent	✓	+	103.93 ± 4.84
LKTP	transparent	✓	+	89.22 ± 3.17
EuKTP	transparent	✓	+	109.98 ±3.72
Not protected from light				
TKLT2	transparent	✓	+	80.92 ± 4.33
PKLT2	transparent	✓	+	114.50 ± 12.73
TKLT2P	transparent	✓	+	82.69 ± 5.02
TKTP	transparent	✓	+	85.28 ± 5.05
ETKTP	transparent	✓	++	88.36 ± 9.27
E1K20TP	transparent	✓	++	100.68 ± 4.47
LKTP	transparent	✓	+	82.31 ± 4.13
EuKTP	transparent	✓	+	105.93 ± 3.82

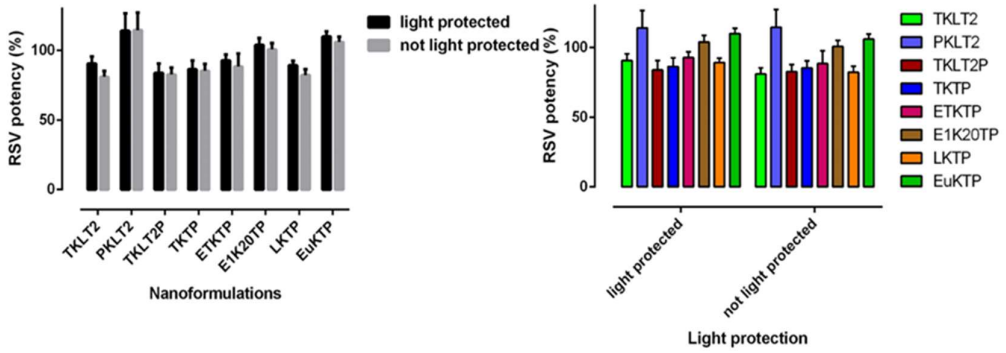

Figure 4.27 RSV potency during 1-month storage at 22-25°C ($\bar{x}$±SD; 4 replications)

The nanoformulations which were kept at 22-25°C for 1 month were stable with the RSV potency of 82-114 % (Figure 4.27 and Table 4.14). This potency remained stable, with or without protection from light. The nanoformulations maintained their physical and chemical stability at 2-5°C for up to approximately 6-month storage with the RSV potency of more than 89% (Table 4.15).

Saturated RSV in PBS pH 6 was relatively stable in one month at 22-25°C when it was protected from light, with a potency of 81.01 ± 1.05 %. The potency significantly reduced when it was kept without light protection (52.43 ± 13.55 %).

Table 4.15 RSV nanoformulations stability during a long term of storage (5-8 months) at 2-5°C and protected from light

Formula	Duration of storage (month)	Physical stability			Chemical stability (%) ($\bar{x}$± SD; 4 replications)
		Clarity	Single phase	Tendency of darker appearance	
TKTP	8	transparent	✓	+	98.73 ± 4.00
ETKTP	5	transparent	✓	++	89.25 ± 1.70
E1K20TP	6	transparent	✓	++	93.39 ± 8.17
LKTP	6	transparent	✓	+	107.02 ± 8.73
EuKTP	6	transparent	✓	+	108.41 ± 4.62

4.4 Discussion

The liquid nanoformulations containing RSV met the target product profile in terms of feasibility and scalability of fabrication, clarity, viscosity and skin penetration-permeation. In addition, a suitable HPLC assay method including skin extraction and quantification of RSV was developed and validated. The HPLC analytical method for RSV provided suitable sensitivity, linearity, precision and was fit for purpose as demonstrated by the mass balance of > 90% achieved in all skin permeation and penetration studies.

Surfactant-containing liquid formulas were of interest in this study as they offer advantages in terms of simplicity of fabrication, excellent solubilizing capacity, and attractive appearance. Quality criteria set for the product, were that these nanoformulations of RSV must be clear (attractive appearance), simple (fabrication), stable (physically and chemically), safe and effective (reasonable amounts of RSV penetrate into the skin). The clarity of the formulations can also be further used as a visual tool that the RSV is solubilised completely in a single phase nanoformulation.

The RSV nanocarrier formulations in this study were modified from nanoemulsifying formulations developed by Pund et al.[62], who developed lipid based nanoemusifying formulations for oral administration of RSV. They suggested that the composition of the formulation created a broad area of clear and spontaneous nanoemulsification in the pseudo-ternary phase diagram. Their nanoemulsifying formulation was thermodynamically stable although it was naturally a micellar system. The formulation seemed promising as a reference for developing a skin-targeted nanoemulsion for RSV.

Initially, three surfactant-containing liquid formulations were investigated: a lipid based nanoformulation (TKLT2), a micellar system (PKLT2), and a microemulsion (TKLT2P), employing low energy method of fabrication. The lipid-based formulation is basically a combination of oil phase and surfactant/cosurfactant. The micellar system is the surfactant-rich aqueous system which confers micelles with their solubilizing property.[65, 66] The microemulsion consists of a mixture of oil phase, aqueous phase, surfactant and cosurfactant. These three formulation types contain the same surfactant and cosurfactant, which also have chemical penetration enhancers abilities.[51, 61, 67-70] Moderate agitation at room temperature was applied to provide homogeneous mixtures. RSV was incorporated after blank nanoformulations formed and the formulations were kept out of light.

Triacetin (glyceryl triacetate) was selected as the oil phase as it gives good clarity, low viscosity and good compatibility in the nanoemulsion system, providing a clear-single phase system. Triacetin is commonly used as a solvent, solubilizer and the oil phase of nanoemulsions[71] and categorised as "Generally Recognised as Safe" by the FDA.[72] Triacetin has also shown a skin penetration enhancement effect.[73] Kolliphor® RH 40 (polyoxyl 40 hydrogenated castor oil) was selected as the surfactant. It is a non-ionic solubilizer and emulsifying agent.[74-76] The hydrophobic part of Kolliphor® RH 40 is developed from a combination of glycerol polyethyleneglycol hydroxystearate and fatty acid glycerol polyglycol esters, while the hydrophilic part is a combination of polyethylene glycols and glycerol ethoxylate.[75] The hydrophilic-lipophilic balance of this surfactant is between 14-16[75] which is appropriate for o/w nanoemulsions. Transcutol® P is a high purity grade of diethylene glycol monoethyl ether (DEGEE), which was selected as the cosurfactant in this study to aid in stabilizing the emulsion system. Transcutol® is an excellent and safe hydroalcoholic solubilizer and skin permeation enhancer without compromising skin integrity.[77-80] The mechanisms underlying the skin penetration/permeation enhancement of the drug include increasing drug thermodynamic driving force, improving drug solubility-partition in the SC, escalating the intercellular lipid fluidisation, and preserving the SC hydration.[80] PBS pH 6 was used as the aqueous phase to maintain the stability of RSV[18] and to support skin compatibility.[81]

All formulations were clear and transparent, except for blank TKLT2P, which was translucent (Figure 4.9). Interestingly, the TKLT2P formulation became transparent after RSV incorporation. This is likely due to the interaction between RSV hydroxyl groups and the nanosystem. The solubility of RSV in three formulations was similar, at around 150 mg/mL (Table 4.7), and much greater than RSV solubility in aqueous solution (0.034 mg/mL). In terms of viscosity, the TKLT2 and TKLT2P possessed similar viscosity, whereas PKLT2 was highly viscous. The high viscosity of PKLT2 may be due to the high level of hydration of water molecules around the hydrophilic region of surfactant.[82]

The capacity of nanoformulations to enhance the penetration and permeation of RSV in the skin was evaluated as the endpoint parameter of the skin targeted formulation development. The penetration of RSV into the skin was conducted in order to assess RSV deposition in SC and in area of epidermis, dermis, and follicles (E+D+F). The permeation of RSV through the skin was also carried out to evaluate the cumulative amount of RSV in the deeper area of dermis. The *in vitro* skin penetration-permeation study was conducted based on Franz's protocol[83] with some modification. Preliminary experiments were conducted to optimize the *in vitro* skin diffusion methods, in terms

of skin preparation, selection of receptor fluid, permeation profile of RSV saturated solution in PBS pH 6 and the stability of RSV in sample fluids.

Due to the lack of availability of human skin, we used the newborn pig skin, as pig skin is well accepted as a good human skin surrogate.[64, 84-92] Veet™ cream was shown to break the hair shafts without compromising the skin and follicles. This was used in preference to razor shaving, as the cream application still maintained an intact SC (see Figure 4.5 and Figure 4.6). Ethanol-based solution (20% ethanol in PBS pH 6) with a total receptor volume removal and replacement protocol was used as the receptor fluid to maintain RSV stability and sink conditions (Cs< 70.11µg/mL) and minimise variability (Figure 4.7). Total receptor volume removal and replacement is beneficial especially for an unstable, lipophilic compound such as RSV, to minimize the aqueous diffusion layer effect within the receptor compartment[93] and to assist the analysis of the stable form of RSV. The stability of RSV in sample fluids was maintained well during the sampling process and analysis.

A saturated solution of RSV in PBS pH 6 was used as the baseline formulation for comparison of developed nanoformulations. The maximum flux was 0.051 ± 0.009 µg/cm^2/h at maximum solubility of RSV of 34.13 ± 0.20 µg/m (Figure 4.8).

TKLT2P showed the highest deposition of RSV in the SC (Figure 4.10 and Table 4.8), which was likely due to the greater solubility and partition of RSV in SC compared to the other two formulations. Although RSV of PKLT2 appeared to be higher in the epidermis-dermis-follicle region, the amount differences were not statistically significant. TKLT2P also showed the highest permeation through the skin compared to TKLT2 and PKLT2 (Figure 4.11). High solubilisation and partitioning capacity are the main features of topical and transdermal ME-NE formulations which can improve the drug loading capacity and dose application thereby enabling higher concentration gradients and eventually improving skin deposition and transdermal flux of the drug.[51, 61, 94-96] Given TKLT2P was promising in terms of RSV penetration into and permeation through the skin, this was selected as the primary formulation, and therefore was further modified and evaluated.

The main focus of the current study was modification to develop nanoemulsions which required less oil, surfactants and cosurfactant but maintained good physical qualities of the nanoformulation and enhanced skin penetration and permeation of RSV. The aim of reducing the oil content was to improve skin sensory properties. Surfactant and cosurfactant reduction results in solubility decrease of the drug, thus increases the thermodynamic activity[97] and reduces the potential for skin irritation. In addition, in

principle there is a range of commercial and environmental advantages to the reduction in the use of materials to increase efficiency in production cost.

The physical characteristics are summarised in Table 4.10. All nanoemulsions showed light brown colour due to original colour of RSV loaded, with the eugenol-incorporated formulations showing higher intensity of brown colour with respect to the colour of eugenol. Most formulations were transparent except E5K20TP. This formulation was opaque due to the lower solubility of RSV in this system. It is likely that the surfactant-cosurfactant composition in this formula has less capacity to solubilize the RSV.

The viscosity of the blank formulations varied, depending on the amount and composition of the excipients. The most viscous formulation was the ETKTP as expected. ETKTP contains eugenol and triacetin at 5% concentration on each. The viscosity reduced in the order of ETKTP > E5K30TP > TKLT2P > E5K20TP > TKTP.

Based on the skin permeation results, the nanoformulations demonstrate that with lower solubility of RSV in the formulation, there is higher penetration and permeation of RSV into and through the skin. This phenomenon is in agreement with Hamishehkar et al[98] who evaluated the effect of pure or binary mixtures of solvents on tadalafil solubility and transdermal delivery in rat skin. They reported that decrease of the solubility of tadalafil resulted in increase of tadalafil transdermal flux. This follows the basic principles of thermodynamics, as a permeant with lower solubility in the vehicle is more thermodynamically active and therefore more likely to partition from the vehicle to the skin.[99]

Terpenes are known to be potent chemical penetration enhancers.[37] The mechanism of terpenes in enhancing penetration and permeation is associated with SC intercellular lipid disruption by creating polar microchannels and an increase in permeant diffusivity.[100-103] Eugenol was selected as the initial terpene selected, based on its medium viscosity which was expected to facilitate the spread ability of the product on the skin and its pleasant aroma. The addition of eugenol (5%) in the nanoformulation significantly increased the amount of RSV in the epidermis-dermis-follicles area and the RSV permeation through the skin compared to TKTP (Figure 4.16 and Figure 4.17). The increase in skin deposition is likely due to the role of the interaction of eugenol with the system to disrupt the SC lipids and increase lipid fluidisation.[104] The RSV skin penetration and permeation reduced with the absence of triacetin, suggesting that eugenol and triacetin synergistically increased the skin penetration and permeation of RSV. Triacetin is also a known penetration enhancer

with the same suggested mechanism of increasing SC lipid fluidisation as terpenes.[105, 106]

The effects of three terpenes-based formulations (Eugenol - E1K20TP, D-limonene - LKTP and Eucalyptol - EuKTP) were further investigated. The physical characteristics and RSV distribution in the skin was similar for the three different terpene-based nanoformulations (Figure 4.25). However, the permeation of RSV through the skin was higher for LKTP and EuKTP than that of E1K20TP (Figure 4.26). This was unlikely associated to differences in thermodynamic activity as the solubility of RSV in those formulations was similar. We suggest that the lipophilicity of terpenes apparently affected the RSV skin permeation. The degree of lipophilicity (Log P) of eugenol, eucalyptol, and D-limonene is 2, 2.5 and 3.4, respectively.[107-109] El Kattan et al[110, 111] when investigating the effect of terpenes on the permeation of hydrocortisone in hairless mouse skin SKH1, also reported a positive correlation between degree of lipophilicity of the terpenes and cumulative amount of hydrocortisone permeating through skin. The higher the lipophilicity of the terpenes, the better the drug partitioned in the skin thus permeated through the skin.[110, 111]

Nanoformulations were stable in both short- and long-term storage condition. In short term conditions, at 22-25°C, nanoformulations remained stable with and without light protection compared to RSV saturated aqueous solution, suggesting that nanoformulations are capable to maintain the stability of RSV. This capability is likely due to the nanosized globules of nanoformulations which encapsulated RSV with high kinetic stability.[112]

In summary, we successfully developed self-assembly, stable, and suitable RSV nanoemulsions to enhance the penetration and permeation of RSV into and through the skin, which met the quality of formulation criteria. These nanoformulations have the potential to facilitate skin delivery of RSV and potentially exert an antioxidant effect in the skin.

4.5 References

1. Amri A, Chaumeil JC, Sfar S, Charrueau C. Administration of resveratrol: What formulation solutions to bioavailability limitations? J Control Release. 2012;158(2):182-193.
2. Athar M, Back JH, Tang X, et al. Resveratrol: A review of pre-clinical studies for human cancer prevention. Toxicol Appl Pharmacol. 2007;224(3):274-283.
3. Aggarwal BB, Bhardwaj A, Aggarwal RS, et al. Role of resveratrol in prevention and therapy of cancer: Preclinical and clinical studies. Anticancer Res. 2004;24(5A):2783-2840.
4. Rudolf JL, Resurreccion AVA, Saalia FK, Phillips RD. Development of a reverse-phase high-performance liquid chromatography method for analyzing trans-resveratrol in peanut kernels. Food Chem. 2005;89(4):623-638.
5. Sales JM, Resurreccion AVA. Resveratrol in peanuts. Crit Rev Food Sci Nutr. 2013;54(6):734-770.
6. Souto AA, Carneiro MC, Seferin M, et al. Determination of trans -resveratrol concentrations in brazilian red wines by HPLC. J Food Compost Anal. 2001;14(4):441-445.
7. Farris P, Krutmann J, Li Y-H, McDaniel D, Krol Y. Resveratrol: A unique antioxidant offering a multi-mechanistic approach for treating aging skin. J Drugs Dermatol. 2013;12(12):1389-1394.
8. Renaud S, de Lorgeril M. Wine, alcohol, platelets, and the French paradox for coronary heart disease. The Lancet. 1992;339(8808):1523-1526.
9. Carluccio MA. Olive oil and red wine antioxidant polyphenols inhibit endothelial activation: antiatherogenic properties of mediterranean diet phytochemicals. Arterioscler Thromb Vasc Biol. 2003;23(4):622-629.
10. Tennen Ruth I, Michishita-Kioi E, Chua Katrin F. Finding a target for resveratrol. Cell. 2012;148(3):387-389.
11. Salehi B, Mishra AP, Nigam M, et al. Resveratrol: A double-edged sword in health benefits. Biomedicines. 2018;6(3):91.
12. Renaud J, Martinoli MG. Resveratrol as a protective molecule for neuroinflammation: A review of mechanisms. Curr Pharm Biotechnol. 2014;15(4):318-329.
13. Rege SD, Geetha T, Griffin GD, Broderick TL, Babu JR. Neuroprotective effects of resveratrol in Alzheimer disease pathology. Front Aging Neurosci. 2014;6(218).
14. Szkudelski T, Szkudelska K. Resveratrol and diabetes: from animal to human studies. Biochimica et Biophysica Acta (BBA) - Molecular Basis of Disease. 2015;1852(6):1145-1154.
15. Agarwal B, Baur JA. Resveratrol and life extension. Ann N Y Acad Sci. 2011;1215(1):138-143.
16. Baxter RA. Anti-aging properties of resveratrol: review and report of a potent new antioxidant skin care formulation. J Cosmet Dermatol. 2008;7(1):2-7.
17. Resveratrol Compound Summary [Internet].[cited 2015 August 13]. Available from: http://pubchem.ncbi.nlm.nih.gov/summary/summary.cgi?cid=445154&loc=ec_rcs.
18. Zupančič S, Lavrič Z, Kristl J. Stability and solubility of trans-resveratrol are strongly influenced by pH and temperature. Eur J Pharm Biopharm. 2015;93:196-204.
19. López-Nicolás JM, García-Carmona F. Aggregation state and pKa values of (E)-resveratrol as determined by fluorescence spectroscopy and UV−Visible absorption. J Agric Food Chem. 2008;56(17):7600-7605.
20. Trela BC, Waterhouse AL. Resveratrol: isomeric molar absorptivities and stability. J Agric Food Chem. 1996;44(5):1253-1257.
21. Figueiras T, Neves-Petersen M, Petersen S. Activation energy of light induced isomerization of resveratrol. Journal of Fluorescence. 2011;21(5):1897-1906.

22. Camont L, Cottart C-H, Rhayem Y, et al. Simple spectrophotometric assessment of the trans-/cis-resveratrol ratio in aqueous solutions. Anal Chim Acta. 2009;634(1):121-128.
23. Flieger J, Tatarczak-Michalewska M, Blicharska E. Characterization of the cis/trans Isomerization of resveratrol by High-Performance Liquid Chromatography. Analytical Letters. 2017;50(2):294-303.
24. Freitas JV, Lopes NP, Gaspar LR. Photostability evaluation of five UV-filters, trans-resveratrol and beta-carotene in sunscreens. Eur J Pharm Sci. 2015;78:79-89.
25. Francioso A, Mastromarino P, Masci A, Erme M, Mosca L. Chemistry, stability and bioavailability of resveratrol. Medicinal Chemistry. 2014;10(3):237-245.
26. Walle T. High Absorption but Very Low Bioavailability of oral resveratrol in humans. Drug Metabolism and Disposition. 2004;32(12):1377-1382.
27. Wenzel E, Somoza V. Metabolism and bioavailability of trans-resveratrol. Mol Nutr Food Res. 2005;49(5):472-481.
28. Vitaglione P, Sforza S, Galaverna G, et al. Bioavailability of trans-resveratrol from red wine in humans. Mol Nutr Food Res. 2005;49(5):495-504.
29. Walle T. Bioavailability of resveratrol. Ann N Y Acad Sci. 2011;1215(1):9-15.
30. Goldberg DM, Yan J, Soleas GJ. Absorption of three wine-related polyphenols in three different matrices by healthy subjects. Clin Biochem. 2003;36(1):79-87.
31. Murakami I, Chaleckis R, Pluskal T, et al. Metabolism of skin-absorbed resveratrol into its glucuronized form in mouse skin. PLoS One. 2014;9(12).
32. Hung C-F, Lin Y-K, Huang Z-R, Fang J-Y. Delivery of resveratrol, a red wine polyphenol, from solutions and hydrogels *via* the skin. Biol Pharm Bull. 2008;31(5):955-962.
33. Barry BW. Lipid-protein-partitioning theory of skin penetration enhancement. J Control Release. 1991;15(3):237-248.
34. Benson HAE, McIldowie M, Prow T. Magnetophoresis: Skin penetration enhancement by a magnetic field. In: Dragicevic N, I. Maibach H, editors. Percutaneous penetration enhancers physical methods in penetration enhancement. Berlin, Heidelberg: Springer Berlin Heidelberg; 2017. p. 195-206.
35. Hadgraft J. Passive enhancement strategies in topical and transdermal drug delivery. Int J Pharm. 1999;184(1):1-6.
36. Moser K, Kriwet K, Naik A, Kalia YN, Guy RH. Passive skin penetration enhancement and its quantification *in vitro*. Eur J Pharm Biopharm. 2001;52(2):103-112.
37. Barry B. Penetration enhancer classification. In: Percutaneous penetration enhancers, Second Edition. CRC Press; 2005. p. 3-15.
38. Barry BW. Mode of action of penetration enhancer in human skin. J Control Release. 1987;6(1):85-97.
39. Williams AC, Barry BW. Penetration enhancers. Advanced Drug Delivery Reviews. 2012;64:128-137.
40. Ansari KA, Vavia PR, Trotta F, Cavalli R. Cyclodextrin-based nanosponges for delivery of resveratrol: *In vitro* characterisation, stability, cytotoxicity and permeation study. AAPS PharmSciTech. 2011;12(1):279-286.
41. Caddeo C, Nacher A, Vassallo A, et al. Effect of quercetin and resveratrol co-incorporated in liposomes against inflammatory/oxidative response associated with skin cancer. Int J Pharm. 2016;513(1):153-163.
42. Cosco D, Paolino D, Maiuolo J, et al. Ultradeformable liposomes as multidrug carrier of resveratrol and 5-fluorouracil for their topical delivery. Int J Pharm. 2015;489(1-2):1-10.
43. Doppalapudi S, Mahira S, Khan W. Development and *in vitro* assessment of psoralen and resveratrol co-loaded ultradeformable liposomes for the treatment of vitiligo. Journal of Photochemistry and Photobiology B: Biology. 2017;174:44-57.
44. Fabbrocini G, Staibano S, De Rosa G, et al. Resveratrol-containing gel for the treatment of acne vulgaris. Am J Clin Dermatol. 2011;12(2):133-141.

45. Friedrich RB, Kann B, Coradini K, et al. Skin penetration behaviour of lipid-core nanocapsules for simultaneous delivery of resveratrol and curcumin. Eur J Pharm Sci. 2015;78:204-213.
46. Hu C, Wang Q, Ma C, Xia Q. Non-aqueous self-double-emulsifying drug delivery system: A new approach to enhance resveratrol solubility for effective transdermal delivery. Colloids and Surfaces A: Physicochemical and Engineering Aspects. 2016;489:360-369.
47. Pando D, Caddeo C, Manconi M, Fadda AM, Pazos C. Nanodesign of olein vesicles for the topical delivery of the antioxidant resveratrol. J Pharm Pharmacol. 2013;65(8):1158-1167.
48. Sinico C, Pireddu R, Pini E, et al. Enhancing topical delivery of resveratrol through a nanosizing approach. Planta Med. 2017;83(5):476-481.
49. Sun R, Zhao G, Ni S, Xia Q. Lipid based nanocarriers with different lipid compositions for topical delivery of resveratrol: comparative analysis of characteristics and performance. Journal of Drug Delivery Science and Technology. 2014;24(6):591-600.
50. Tsai M-J, Lu IJ, Fu Y-S, et al. Nanocarriers enhance the transdermal bioavailability of resveratrol: *In-vitro* and *in-vivo* study. Colloids and Surfaces B: Biointerfaces. 2016;148:650-656.
51. Nastiti CMRR, Ponto T, Abd E, et al. Topical nano and microemulsions for skin delivery. Pharmaceutics. 2017;9(4):37.
52. Abolmaali SS, Tamaddon AM, Farvadi FS, Daneshamuz S, Moghimi H. Pharmaceutical nanoemulsions and their potential topical and transdermal applications. Iranian Journal of Pharmaceutical Sciences. 2011;7(3):139-150.
53. Gupta A, Eral HB, Hatton TA, Doyle PS. Nanoemulsions: formation, properties and applications. Soft Matter. 2016;12(11):2826-2841.
54. Shakeel F, Shafiq S, Haq N, Alanazi FK, Alsarra IA. Nanoemulsions as potential vehicles for transdermal and dermal delivery of hydrophobic compounds: an overview. Expert Opinion on Drug Delivery. 2012;9(8):953-974.
55. Singh M, Jain S. Nanoemulsions for skin targeting: present status and future prospects. Drug Delivery Letters. 2011;1(2):159-170.
56. Acharya DP, Hartley PG. Progress in microemulsion characterization. Current Opinion in Colloid & Interface Science. 2012;17(5):274-280.
57. Fanun M. Microemulsions as delivery systems. Current Opinion in Colloid & Interface Science. 2012;17(5):306-313.
58. Heuschkel S, Goebel A, Neubert RHH. Microemulsions—modern colloidal carrier for dermal and transdermal drug delivery. J Pharm Sci. 2008;97(2):603-631.
59. Danielsson I, Lindman B. The definition of microemulsion. Colloids and Surfaces. 1981;3(4):391-392.
60. Juškaitė V, Ramanauskienė K, Briedis V. Design and formulation of optimized microemulsions for dermal delivery of resveratrol. Evid Based Complement Alternat Med. 2015;2015:10.
61. Kreilgaard M. Influence of microemulsions on cutaneous drug delivery. Advanced Drug Delivery Reviews. 2002;54, Supplement:S77-S98.
62. Pund S, Thakur R, More U, Joshi A. Lipid based nanoemulsifying resveratrol for improved physicochemical characteristics, *in vitro* cytotoxicity and *in vivo* antiangiogenic efficacy. Colloids and Surfaces B: Biointerfaces. 2014;120:110-117.
63. Zhang Q, Grice JE, Li P, et al. Skin solubility determines maximum transepidermal flux for similar size molecules. Pharm Res. 2009;26(8):1974-1985.
64. Songkro S, Purwo Y, Becket G, Rades T. Investigation of newborn pig skin as an in vitro animal model for transdermal drug delivery. S.T.P. Pharma Sciences. 2003;13(2):133-139.
65. Lawrence MJ. Surfactant systems: their use in drug delivery. Chem Soc Rev. 1994;23(6):417-424.

66. Lawrence MJ. Surfactant systems: Microemulsions and vesicles as vehicles for drug delivery. Eur J Drug Metab Pharmacokinet. 1994;19(3):257-269.
67. Azeem A, Khan ZI, Aqil M, et al. Microemulsions as a surrogate carrier for dermal drug delivery. Drug Dev Ind Pharm. 2009;35(5):525-547.
68. Vadlamudi HC, Narendran H, Nagaswaram T, et al. Microemulsions based transdermal drug delivery systems. Current Drug Discovery Technologies. 2014;11(3):169-180.
69. Date AA, Patravale VB. Microemulsions: Applications in transdermal and dermal delivery. Critical ReviewsTM in Therapeutic Drug Carrier Systems. 2007;24(6):547-596.
70. Kogan A, Garti N. Microemulsions as transdermal drug delivery vehicles. Adv Colloid Interface Sci. 2006;123-126:369-385.
71. Sobhani H, Tarighi P, Ostad SN, et al. Formulation development and toxicity assessment of triacetin mediated nanoemulsions as novel delivery systems for rapamycin. Iranian journal of pharmaceutical research : IJPR. 2015;14(Suppl):3-21.
72. Flume M, Cosmetic Ingredients Review Expert Panel. Final report on the safety assessment of triacetin. Int J Toxicol. 2003;22(Suppl 2:1-10).
73. Quan D, Deshpanday NA, Venkateshwaran S, Ebert CD, inventors; Allergan Sales LLC, assignee. Triacetin as a penetration enhancer for transdermal delivery of a basic drug US 1997.
74. Berthelsen R, Holm R, Jacobsen J, et al. Kolliphor surfactants affect solubilisation and bioavailability of fenofibrate. Studies of *in vitro* digestion and absorption in rats. Mol Pharm. 2015;12(4):1062-1071.
75. Technical Information. Kolliphor RH 40. BASF, USA:2019.
76. Tran T, Rades T, Müllertz A. Formulation of self-nanoemulsifying drug delivery systems containing monoacyl phosphatidylcholine and Kolliphor® RH40 using experimental design. Asian Journal of Pharmaceutical Sciences. 2018;13(6):536-545.
77. Csizmazia E, Erős G, Berkesi O, et al. Penetration enhancer effect of sucrose laurate and Transcutol on ibuprofen. Journal of Drug Delivery Science and Technology. 2011;21(5):411-415.
78. Harrison JE, Watkinson AC, Green DM, Hadgraft J, Brain K. The relative effect of Azone® and Transcutol® on permeant diffusivity and solubility in human stratum Corneum. Pharm Res. 1996;13(4):542-546.
79. Javadzadeh Y, Adibkia K, Hamishekar H. Transcutol® (Diethylene Glycol Monoethyl Ether): A potential penetration enhancer. In: Dragicevic N, Maibach HI, editors. Percutaneous penetration enhancers chemical methods in penetration enhancement: modification of the stratum corneum. Berlin, Heidelberg: Springer Berlin Heidelberg; 2015. p. 195-205.
80. Osborne DW, Musakhanian J. Skin penetration and permeation properties of Transcutol®—Neat or diluted mixtures. AAPS PharmSciTech. 2018;19(8):3512-3533.
81. Lambers H, Piessens S, Bloem A, Pronk H, Finkel P. Natural skin surface pH is on average below 5, which is beneficial for its resident flora. Int J Cosmet Sci. 2006;28(5):359-370.
82. Desai TR, Dixit SG. Interaction and viscous properties of aqueous solutions of mixed cationic and nonionic surfactants. J Colloid Interface Sci. 1996;177(2):471-477.
83. Franz TJ. Percutaneous absorption. On the relevance of *in vitro* data. J Invest Dermatol. 1975;64(3):190-195.
84. Barbero AM, Frasch HF. Pig and guinea pig skin as surrogates for human *in vitro* penetration studies: A quantitative review. Toxicol In Vitro. 2009;23(1):1-13.
85. Chessa M, Caddeo C, Valenti D, et al. Effect of penetration enhancer containing vesicles on the percutaneous delivery of quercetin through new born pig skin. Pharmaceutics. 2011;3(3):497.
86. Cilurzo F, Minghetti P, Sinico C. Newborn pig skin as model membrane in in vitro drug permeation studies: A technical note. AAPS PharmSciTech. 2007;8(4):97-100.

87. Dick IP, Scott RC. Pig ear skin as an in vitro model for human skin permeability. J Pharm Pharmacol. 1992;44(8):640-645.
88. Gerstel D, Jacques-Jamin C, Schepky A, et al. Comparison of protocols for measuring cosmetic ingredient distribution in human and pig skin. Toxicol *In Vitro*. 2016;34:153-160.
89. Lademann J, Richter H, Meinke M, Sterry W, Patzelt A. Which skin model is the most appropriate for the investigation of topically applied substances into the hair follicles? Skin Pharmacol Physiol. 2010;23(1):47-52.
90. Nastiti CMRR, Mohammed Y, Telaprolu KC, et al. Evaluation of quantum dot skin penetration in porcine skin: Effect of age and anatomical site of topical application. Skin Pharmacol Physiol. 2019.
91. Schmook FP, Meingassner JG, Billich A. Comparison of human skin or epidermis models with human and animal skin in in-vitro percutaneous absorption. Int J Pharm. 2001;215(1–2):51-56.
92. Simon GA, Maibach HI. The pig as an experimental animal model of percutaneous permeation in man: Qualitative and quantitative observations – An overview. Skin Pharmacol Physiol. 2000;13(5):229-234.
93. Yousef S, Liu X, Mostafa A, et al. Estimating maximal *in vitro* skin permeation flux from studies using non-sink receptor phase conditions. Pharm Res. 2016;33(9):2180-2194.
94. Salim N, Ahmad N, Musa SH, et al. Nanoemulsion as a topical delivery system of antipsoriatic drugs. RSC Advances. 2016;6(8):6234-6250.
95. Roberts MS, Mohammed Y, Pastore MN, et al. Topical and cutaneous delivery using nanosystems. J Control Release. 2017;247:86-105.
96. Kreilgaard M, Pedersen EJ, Jaroszewski JW. NMR characterisation and transdermal drug delivery potential of microemulsion systems. J Control Release. 2000;69(3):421-433.
97. Pawar KR, Babu RJ. Lipid materials for topical and transdermal delivery of nanoemulsions. 2014;31(5):429-458.
98. Hamishehkar H, Khoshbakht M, Jouyban A, Ghanbarzadeh S. The relationship between solubility and transdermal absorption of tadalafil. Advanced pharmaceutical bulletin. 2015;5(3):411-417.
99. Otto A, Du Plessis J, Wiechers JW. Formulation effects of topical emulsions on transdermal and dermal delivery. Int J Cosmet Sci. 2009;31(1):1-19.
100. Herman A, Herman AP. Essential oils and their constituents as skin penetration enhancer for transdermal drug delivery: A review. J Pharm Pharmacol. 2015;67(4):473-485.
101. Williams AC, Barry BW. The enhancement index concept applied to terpene penetration enhancers for human skin and model lipophilic (oestradiol) and hydrophilic (5-fluorouracil) drugs. Int J Pharm. 1991;74(2):157-168.
102. Williams AC, Barry BW. Terpenes and the Lipid–Protein–Partitioning theory of skin penetration enhancement. Pharm Res. 1991;8(1):17-24.
103. Cornwell P, Barry B. The routes of penetration of ions and 5-fluorouracil across human skin and the mechanisms of action of terpene skin penetration enhancers. Int J Pharm. 1993;94(1-3):189-194.
104. El Khayat NW, Donia AA, Mady OY, El Maghraby GM. Optimisation of eugenol microemulsion for transdermal delivery of indomethacin. Journal of Drug Delivery Science and Technology. 2018;48:311-318.
105. Shakeel F, Baboota S, Ahuja A, Ali J, Shafiq S. Celecoxib nanoemulsion: Skin permeation mechanism and bioavailability assessment. J Drug Target. 2008;16(10):733-740.
106. Shakeel F, Baboota S, Ahuja A, Ali J, Shafiq S. Skin permeation mechanism and bioavailability enhancement of celecoxib from transdermally applied nanoemulsion. Journal of Nanobiotechnology. 2008;6(1):8.

107. PubChem Database. Eugenol, CID=3314, [Internet]. [cited June 9, 2019]. Available from: https://pubchem.ncbi.nlm.nih.gov/compound/Eugenol
108. PubChem Database. Eucalyptol, CID=2758, [Internet]. [cited June 9, 2019]. Available from: https://pubchem.ncbi.nlm.nih.gov/compound/Eucalyptol
109. PubChem Database. D-limonene, CID=440917, [Internet]. [cited June 9, 2019]. Available from: https://pubchem.ncbi.nlm.nih.gov/compound/D-Limonene
110. El-Kattan AF, Asbill CS, Kim N, Michniak BB. The effects of terpene enhancers on the percutaneous permeation of drugs with different lipophilicities. Int J Pharm. 2001;215(1):229-240.
111. El-Kattan AF, Asbill CS, Michniak BB. The effect of terpene enhancer lipophilicity on the percutaneous permeation of hydrocortisone formulated in HPMC gel systems. Int J Pharm. 2000;198(2):179-189.
112. Wang X, Wang Y-W, Huang Q. Enhancing stability and oral bioavailability of polyphenols using nanoemulsions. In: Huang Q, Given P, Qian M, editors. Micro/nanoencapsulation of active food ingredients. ACS Symposium Series. 1007. American Chemical Society; 2009. p. 198-212.

Chapter 5. Enhancing Skin Penetration and Permeation of Resveratrol Using A Combination of Chemical and Physical Enhancement Techniques

5.1 Background

A number of approaches can be applied to enhance the skin penetration of resveratrol (RSV). In Chapter 4 we demonstrated the enhanced skin delivery of RSV with nanocarrier formulations, particularly with the inclusion of terpene chemical enhancers. Terpene based nanoformulations showed considerable results as targeted skin delivery. However, for some other formulations, a combination of chemical and physical enhancement techniques was considered to be substantial to enhance RSV skin penetration into and permeation across the skin.

Physical permeation enhancement techniques involve the administration of energy to the stratum corneum surface to drive molecules into the skin (iontophoresis, sonophoresis, magnetophoresis) or the minimally invasive disruption of the stratum corneum (ablation methods, powder and liquid jet propulsion systems, microneedle arrays).[1-4] Among those techniques, our focus is on the effect of magnetophoresis and microneedle array application to explore their effect on RSV skin delivery in combination with nanocarrier and terpene penetration enhancers.

Magnetophoresis is defined as the mobility of diamagnetic or paramagnetic particles as a result of a magnetic field induction.[5] This term is also applied to physical enhancement in skin delivery involving a magnetic field application.[6] Benson et al.[5] categorised the magnetic enhancement techniques in 4 types: static magnetic fields, pulsed electromagnetic fields, magnetic film array, and field in motion. Over a series of literature reports, Murty's group consistently demonstrated the enhanced permeation of several compounds through the skin using static magnets of different strengths.[7-9] Benson's group utilised optical coherence tomography (OCT) to monitor skin hydration *in vivo* coupled with *in vitro* human skin permeation data to investigate the effect of a magnetic array on the skin permeation of urea.[5, 10] They demonstrated a 4-fold enhancement in urea permeation through the skin and a 2-fold increase in skin thickness due to hydration with the magnetic array. The advantage of the magnetic array technology is that it is light, flexible and inexpensive and can therefore be easilty adapted as a patch for skin application.[5]

Microneedles (MN) are designed to physically disrupt the SC by applying an array of micron-size needles (25-2000 µm length) to create micro-channels through the SC.[11-13] This approach aimed to significantly enhance the transdermal permeation without creating bleeding or painful sensations as the needles do not penetrate deeply enough to interact with the cutaneous blood vessels and nerves.[14] MN are designed in five main types: solid, hollow, coated, dissolving, and swelling MN.[15] Coated MN are basically solid MN which are coated by the drug formulation and used as a carrier to deliver the water-soluble formulation in the skin, while the term of solid MN refers to the MN used for piercing the skin to create microchannels. Hollow MN facilitate a liquid drug formulation to be passed through the hollow conduits of the MN into the skin. Dissolving MN are polymer-based MN in which the drug is dissolved or dispersed and is then released into the skin when the polymer dissolved following insertion and uptake of interstitial fluid. Swelling MN release are also composed of polymer that takes up interstitial fluid but does not dissolve, thus contained drug release is based on a diffusion mechanism following the swelling of the polymer.[15,16] Figure 1.3 (chapter 1) summarised the mechanistic concepts of microneedle application. The focus of our work is solid MN, utilising the so called “poke and patch” method.[17] Solid MN have been proved to enhance the permeation of 5-aminolevulinic acid[18] and meso-tetra porphine tetra tosylate, a photosensitiser.[19] Mohammed et al.[20] in delivering cosmeceutically-relevant peptides to human skin *in vitro*, reported that the fluorescence signals of melanostatin, rigin and pal-KTTS were improved 2-22 folds by solid MN application.

We aimed to investigate the skin delivery of RSV with an energy based and a minimally invasive physical penetration enhancement technique. Magnet array application and MN pre-treatment were investigated individually and in combination to evaluate their capacity in enhancing RSV penetration into and permeation across the skin. The effect of combination of chemical and physical enhancement was further evaluated to get a better understanding of the role of enhancement techniques for RSV skin delivery.

5.1.1 Research questions

Research questions addressed in this study:

1. Does the application of magnet array enhance the permeation of RSV from a saturated aqueous solution?
2. Does MN pre-treatment enhance the permeation of RSV from a saturated aqueous solution?

3. Does a combination of MN pre-treatment and magnet array application provide a synergistic enhancement of the skin permeation of RSV from a saturated aqueous solution?
4. Does the application of magnet array enhance the skin permeation of RSV from nanoformulations?
5. Does MN pre-treatment enhance the permeation of RSV from nanoformulations?
6. Does a combination of MN pre-treatment and magnet array application provide a synergistic enhancement of the skin permeation of RSV from a nanoformulation?

5.2 Experimental section

5.2.1 Materials

RSV was purchased from PCCA (99% purity, Australia). Orthophosphoric acid and acetonitrile were purchased from Thermo Fisher Scientific (Australia), sodium hydroxide (Merck, Australia), sodium chloride (Lab-Scan, Thailand). TKTP and ETKTP formula was in house production (see Chapter 4 Table 4.3), ultrapure water (Milli-Q, Merck, Australia)

5.2.2 *In vitro* penetration/permeation study

5.2.2.1 Skin preparation

Newborn pig skin (NBPS) was obtained from the same source and was treated with the same protocol described in the section 4.2.5.1.

5.2.2.2 Experimental design

The permeation and penetration of RSV on the skin treated with magnet and MN were initially evaluated individually. The combination of both treatments (magnet and MN) was further investigated. Vertical Franz-type diffusion cell experimental was set up to investigate the *in vitro* penetration/permeation of RSV into and through the newborn pig skin. Skin preparation was conducted under protocol described in the section 4.2.5.1.

Franz cell study set up

In general, the set-up of experiment, sampling protocol, and skin distribution study followed the procedure as described in the section 4.2.5.2 and table 4.4. RSV aqueous saturated solutions, TKTP, ETKTP were applied as donors.

Magnet array application

Flat circular static magnetic film arrays (diameter: 0.6 cm) of unpowered flexible array matrix ETP 012 (OBJ Ltd, WA, Australia) were used with the peak magnetic field strength of 40mT and total magnetic gradient of 2T/m^2 (due to the arrangement and alternating poles distribution across the surface). An applicator was used to apply the magnet array in the donor compartment, at a distance of 2-4mm above the skin surface and in good contact with the donor.

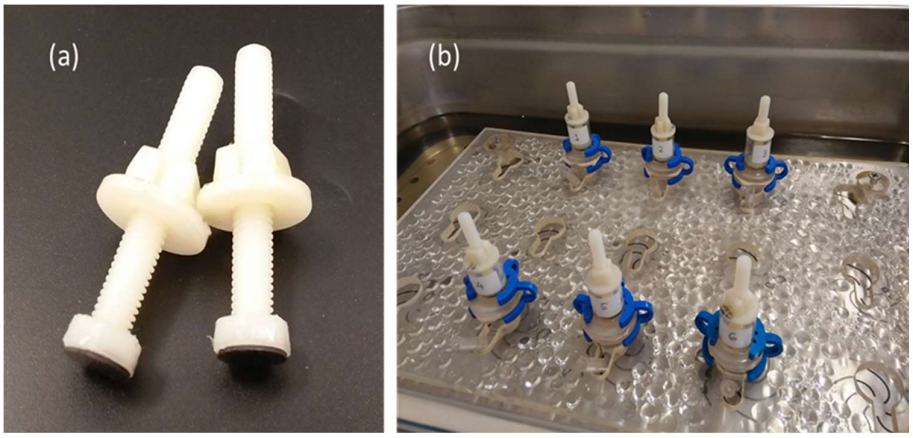

Figure 5.1 Franz cell set up with magnet application: (a) magnet applicator attached with a magnet array at the bottom, (b) set of Franz cells in the water bath

MN skin pre-treatment

A 3M™ Microchannel Skin System (3M, Singapore) was applied as pre-treatment to create microchannels through the SC. This consists of a sterile, single use rectangular array of pyramidal-shape needles (13 x 27 needles) with needle length of 700 µm, attached on an oval patch in a tip-to-tip space of the needles of 500µm[21, 22] (Figure 5.2). The 3M™ Microchannel Skin System was applied using the applicator in the centre of the skin with an applied pressure of 800-900g for 30 seconds. The MN treated skin was then placed in the Franz cell SC upwards. One gram of the saturated RSV solution or RSV nanoformulation was applied to the SC surface of the skin in the donor compartment.

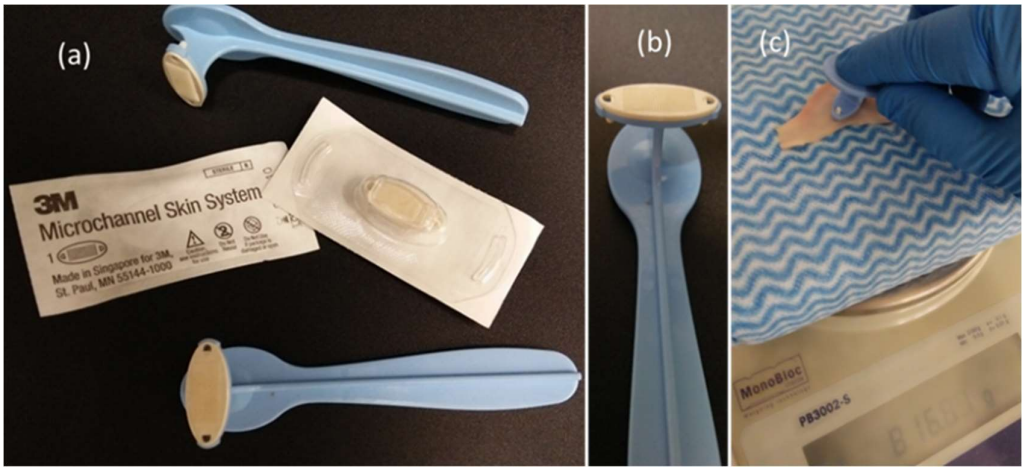

Figure 5.2 MN equipment and pre-treatment

Combination of magnet and MN application

The skin was pretreated with MN as described above (Figure 5.2. (c)), then placed in the Franz diffusion cell. The topical formulation was applied, and the magnet placed in contact with the formulation, as previously described above (Figure 5.1.(b)).

Chemical Analysis

Quantification of RSV was achieved using a validated HPLC method described in section 4.2.2 and table 4.1.

Data and statistical analysis

All data were presented as mean ± SEM. Raw data were calculated and analysed based on the formula provided in the section 4.2.6. Statistical analysis was performed following the method described in section 4.2.7.

5.3 Results

The primary measures in all experiments were the penetration of RSV through the skin into the receptor compartment and the distribution of RSV in skin tissues due to permeation from each formulation in the absence or presence of physical penetration enhancement.

5.3.1 Effects of physical enhancement on the permeation of RSV from a saturated aqueous solution

5.3.1.1 Effect of magnet application on the permeation of RSV

Figure 5.3 shows the permeation profile of RSV in saturated aqueous solutions applied with or without magnet application for 8 hours. The cumulative amount of RSV permeated through the skin treated with magnet was approximately two times higher

than passive diffusion permeation (0.690 ± 0.209 µg and 0.309 ± 0.074 µg, respectively: $P < 0.05$). Although the lag time and permeability coefficient were similar, the rate of RSV permeated through the skin treated with magnet was also two times faster than the passive diffusion ($P < 0.05$). The flux of RSV with magnet application and passive diffusion were 0.097 ± 0.026 µg/cm^2/h and 0.051 ± 0.009, respectively; $P < 0.05$).

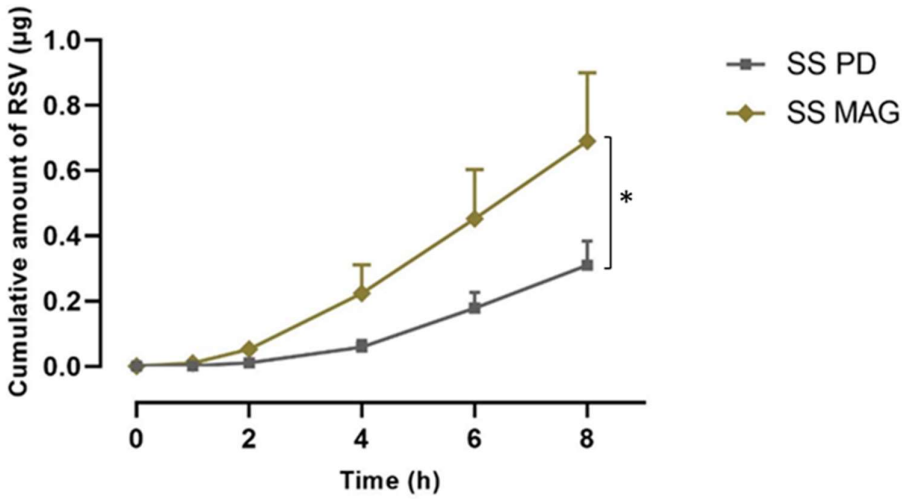

Figure 5.3 Cumulative amount of RSV administered in a saturated aqueous solution in passive diffusion (SS PD) and magnet application (SS MAG) in 8h permeation ($\bar{x}$ ± SEM; 5-6 replications; * P < 0.05)

The RSV distribution in the skin tissues is presented in the Figure 5.4.

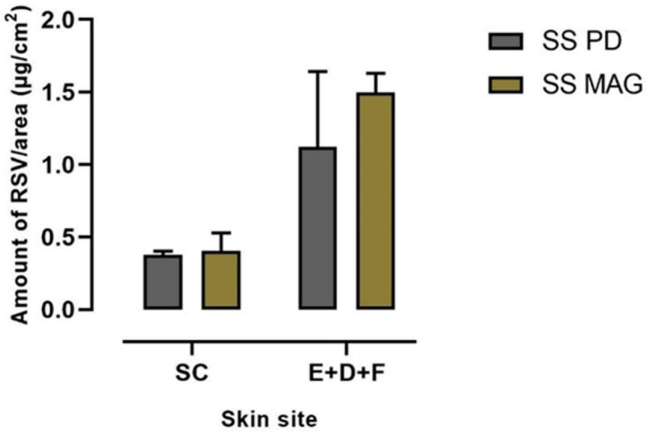

Figure 5.4 Skin distribution of RSV in the stratum corneum (SC) and epidermis, dermis and follicles (E+D+F) after 8h following application of RSV saturated aqueous solution with magnet application (SS MAG) or untreated skin (SS PD) ($\bar{x}$ ± SEM; 5-6 replications)

The amount of RSV retained in the SC (Figure 5.4) was similar for passive diffusion and magnet application (0.378 ± 0.025 μg/cm^2 and 0.403 ± 0.126 μg/cm^2 respectively). In the combined areas of the epidermis, dermis and follicles the amount of RSV was approximately 30% higher with magnetic application (1.124 ± 0.519 μg/cm^2 and 1.497 ± 0.134 μg/cm^2 respectively) but this was not a statistically significant increase in RSV deposition.

5.3.1.2 Effect of MN application on the penetration/permeation of RSV

Figure 5.5 presents the profile of RSV permeation from a saturated aqueous solution in passive diffusion or following MN pre-treatment. MN pre-treatment significantly increased the RSV flux across the skin by 4.57 times compared with passive application (0.051 ± 0.009 μg/cm^2/h and 0.234 ± 0.074 μg/cm^2/h respectively; P < 0.01). The cumulative amount of RSV permeated the skin was approximately 6.5 times with MN than without (P < 0.05).

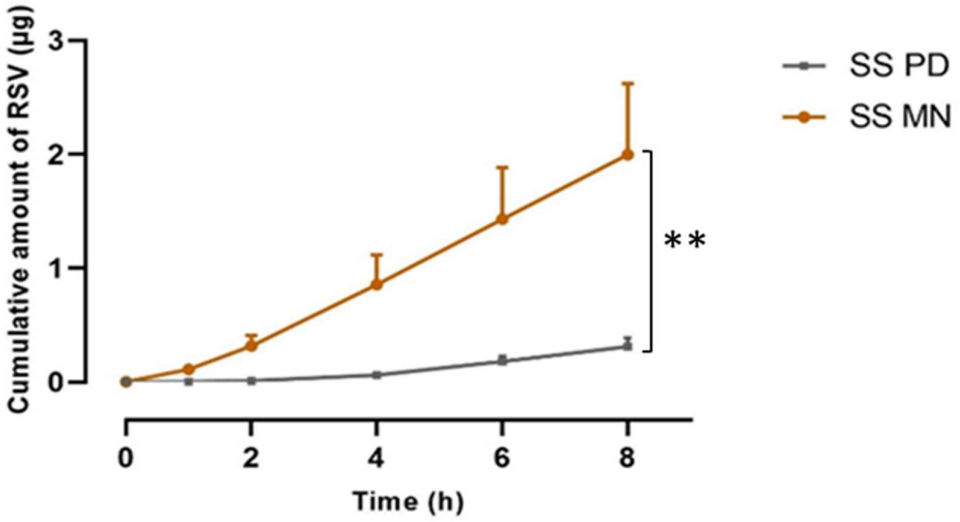

Figure 5.5 Cumulative amount of RSV of administered in a saturated aqueous solution to microneedle pre-treatment (SS PD) or untreated skin (SS MN) in 8h permeation through the skin ($\bar{x}$ ± SEM; 5-6 replications; ** P < 0.01)

The amount of RSV in the SC (Figure 5.6) of microneedle-treated skin was significantly higher than that in passive diffusion (1.064 ± 0.115 μg and 0.378 ± 0.025 μg, respectively; P < 0.05). The amount of RSV in the other skin areas (E+D+F) was approximately four times greater following microneedle pre-treatment (1.124 ± 0.519 μg and 4.006 ± 0.378 μg respectively; P < 0.01).

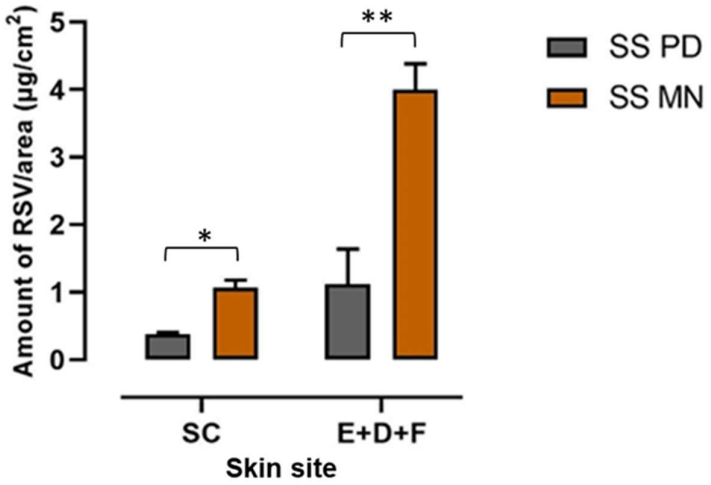

Figure 5.6 Skin distribution of RSV in the SC and E+D+F at 8h following application of RSV saturated aqueous solution to microneedle pretreated (SS MN) or untreated skin (SS PD) ($\bar{x}$ ± SEM; 5-6 replications; * P < 0.05, ** P < 0.01)

5.3.1.3 Effect of combination of MN pre-treatment and magnet application on the permeation of RSV

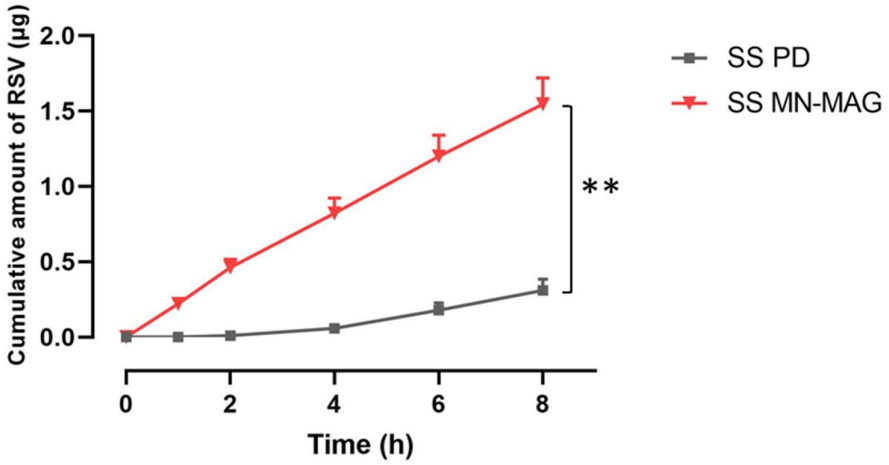

Figure 5.7 Cumulative amount of RSV of administered in a saturated aqueous solution by a combination of microneedle pre-treatment and magnet application (SS MN-MAG) or passive application (SS PD) in 8h permeation through the skin ($\bar{x}$ ± SEM; 5-6 replications; ** P < 0.01)

Similar to the previous result in microneedle application, the combination of physical enhancement techniques also significantly increased skin permeation of RSV (P < 0.01). The cumulative amount of RSV permeated the skin, when applied for 8 h as a saturated aqueous solution of RSV with a combination of microneedle pre-treatment and magnet, was 1.546 ± 0.173 µg. The combination of treatments provided a small

increase of RSV flux and a decrease of lag time compared to MN application alone, but there was no statistically significant improvement in skin delivery with the combined treatments.

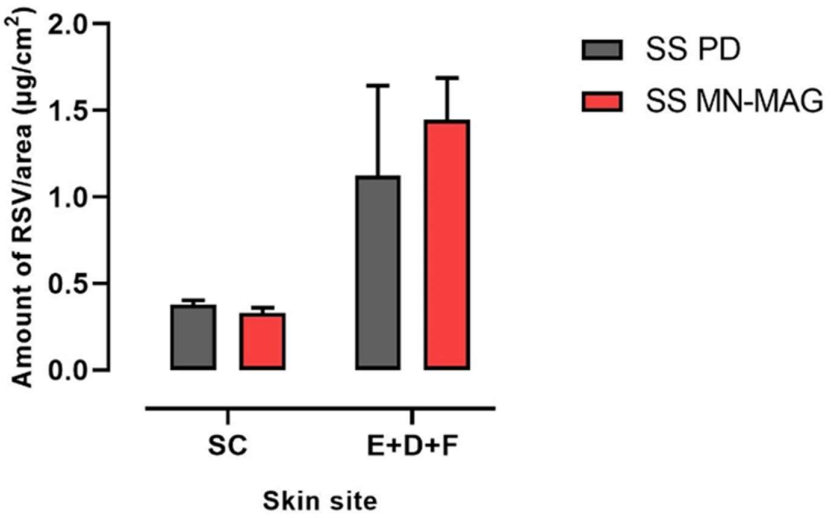

Figure 5.8 Skin distribution of RSV in the SC and E+D+F of RSV administered in a saturated aqueous solution by a combination of microneedle pre-treatment and magnet application (SS MN-MAG) or passive application (SS PD) after 8h permeation through the skin ($\bar{x}$ ± SEM; 5-6 replications)

Figure 5.8 shows the RSV retained in the skin after 8h application with magnet on MN pretreated skin. Whilst there was an approximately 30% increase in the mean amount of RSV in the E+D+F area with the combination treatment, this was not statistically significant. It is also interesting to note that the amount of RSV in the E+D+F area was significantly less when applied to microneedle pretreated skin with magnets in place than without the magnets (Table 5.1).

5.3.2 Effect of magnet application, microneedle pre-treatment, and combination of MN pre-treatment and magnet application on the skin permeation of RSV applied as nanoformulations

5.3.2.1 Effect of magnet application, microneedle pre-treatment, and combination of MN pre-treatment and magnet application on the skin permeation of RSV applied as TKTP nanoemulsion

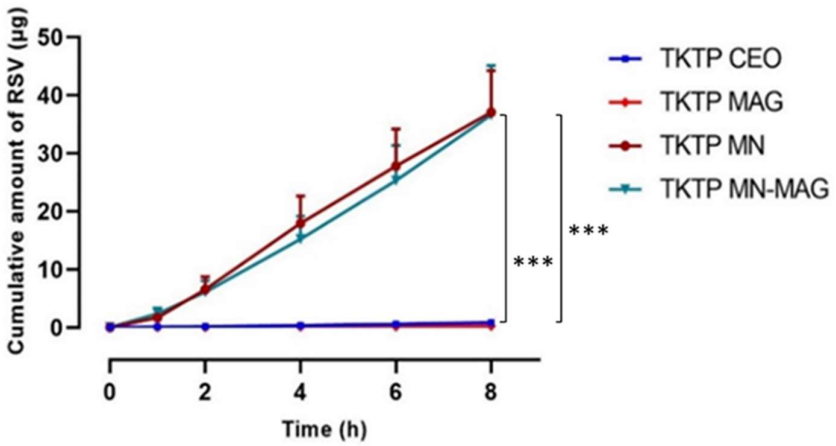

Figure 5.9 Cumulative amount of RSV of following application of TKTP nanoemulsion with magnet application (TKTP MAG), microneedle pre-treatment (TKTP MN), combination of magnet application and microneedle pre-treatment (TKTP MN-MAG), and no physical skin treatment-chemical enhancement only (TKTP CEO) in 8h permeation through the skin ($\bar{x}$ ± SEM; 5-6 replications; *** P < 0.001)

Figure 5.9 displays the permeation profile of RSV applied in the TKTP nanoformulation with magnet application alone, MN pre-treatment alone, the two techniques combined and compared to no physical enhancement (designated passive enhancement). The magnet application did not increase RSV permeation from the nanoemulsion. In contrast, there was 78.37 times increase in RSV flux when the nanoemulsion was applied to microneedle pretreated skin. The permeation profile for the combination of magnet application and MN pre-treatment was similar to the MN treatment alone (Figure 5.9). The RSV flux of the microneedle application and the combination treatments were 4.019 ± 0.666 µg/cm^2/h and 4.452 ± 0.929 µg/cm^2/h, respectively.

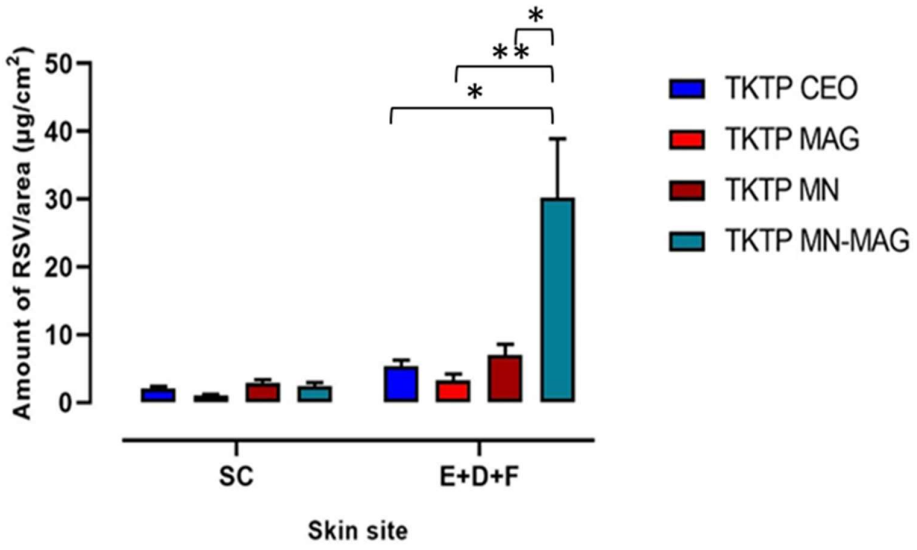

Figure 5.10 The skin distribution of RSV in the SC and E+D+F after 8h following application of TKTP MAG, TKTP MN, TKTP MN MAG, and TKTP CEO ($\bar{x}$ ± SEM; 5-6 replications; * P < 0.05, ** P < 0.01)

There was no significant difference in the amount of RSV in the SC at 8h after application in the TKTP nanoemulsion with or without physical enhancement techniques (Figure 5.10). In contrast, the combination of MN pre-treatment and magnetic application of RSV in the TKTP nanoemulsion (TKTP MN-MAG) resulted in almost six times the amount of RSV in the E+D+F tissues, an amount that was significantly greater than any other treatment ($P < 0.05$). The amount of RSV retained in E+D+F the TKTP MN-MAG and the TKTP without physical skin treatment were 30.214 ± 8.711 µg/cm^2 and 5.359 ± 0.845 µg/cm^2, respectively.

5.3.2.2 Effect of magnet application, microneedle pre-treatment, and combination of MN pre-treatment and magnet application on the skin permeation of RSV applied as ETKTP nanoemulsion

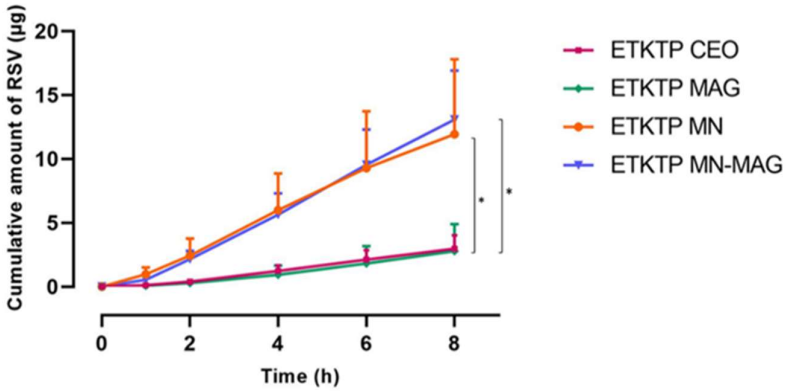

Figure 5.11 Cumulative amount of RSV of following application of ETKTP nanoemulsion with magnet application (ETKTP MAG), microneedle pre-treatment (ETKTP MN), combination of magnet application and microneedle pre-treatment (ETKTP MN-MAG), and no physical skin treatment-chemical enhancement only (ETKTP CEO) in 8h permeation through the skin ($\bar{x}$ ± SEM; 5-6 replications; * P < 0.05)

Figure 5.11 presents the permeation profile of RSV applied as EKTP nanoemulsion to untreated skin and skin with microneedle pre-treatment alone, magnet application, and a combination of microneedle and magnet application. As with the TKTP nanoemulsion, the permeation profile shows that the microneedle pre-treatment enhanced permeation both alone and in combination with the magnet, but the magnet alone did not increase RSV permeation.

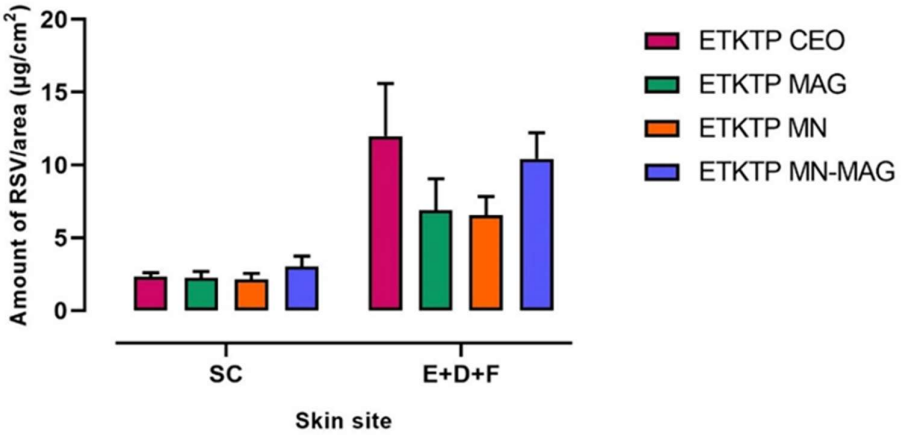

Figure 5.12 The skin distribution of RSV in the SC and E+D+F after 8h following application of ETKTP MAG, ETKTP MN, ETKTP MN MAG, and ETKTP CEO ($\bar{x}$ ± SEM; 5-6 replications)

Figure 5.12 shows the skin uptake of RSV applied as ETKTP nanoemulsion with and without the physical permeation enhancement techniques. The combination of treatments (magnet-microneedle) retained slightly higher amount of RSV in SC compared to the others. However, the amount of RSV retained in the E+D+F was relatively comparable in the untreated skin and all treatments.

5.3.3 Summary of results

Table 5.1 summarises the *in vitro* penetration/permeation data for RSV applied to piglet skin in a range of formulations with and without physical enhancement techniques.

Table 5.2 presents the mass balance data for all experiments conducted. The recovery was between 85-112%.

Table 5.1 Experimental data of *in vitro* penetration/permeation study of RSV with physical permeation enhancements ($\bar{x}$ ± SEM; 5-6 replications)

Formula	RSV distribution in the skin (μg/cm^2)		Cumulative amount (μg)	Steady state flux (J_{ss}; μg/cm^2/h)	Lag time (h)	ER
	SC	E+D+F				
RSV saturated solution						
Passive diffusion	0.378 ± 0.025	1.124 ± 0.519	0.309 ± 0.074	0.051 ± 0.009	3.185 ± 0.176	1.00
Magnet	0.403 ± 0.126	1.497 ± 0.134	0.690 ± 0.209	0.097 ± 0.026	2.565 ± 0.498	1.88
MN	1.064 ± 0.115	4.006 ± 0.378	1.995 ± 0.625	0.234 ± 0.074	1.096 ± 0.307	4.57
MN-Magnet	0.331 ± 0.028	1.445 ± 0.242	1.546 ± 0.173	0.151 ± 0.016	1.172 ± 0.149	2.94
TKTP						
Chemical enhancer only	1.998 ± 0.383	5.359 ± 0.845	0.853 ± 0.091	0.103 ± 0.006	1.234 ± 0.886	2.01
Magnet	1.010 ± 0.224	3.204 ± 0.979	0.264 ± 0.087	0.036 ± 0.013	1.516 ± 0.558	0.70
MN	2.828 ± 0.522	6.998 ± 1.586	37.075 ± 7.150	4.019 ± 0.666	0.933 ± 0.472	78.37
MN-Magnet	2.436 ± 0.512	30.214 ± 8.711	36.583 ± 8.554	4.452 ± 0.929	1.291 ± 0.133	86.82

Table 5.1. ***Continued***

Formula	RSV distribution in the skin (μg/cm^2)		Cumulative amount (μg)	Steady state flux (J_{ss}; μg/cm^2/h)	Lag time (h)	ER
	SC	E+D+F				
			ETKTP			
Chemical enhancer only	2.342 ± 0.269	12.000 ± 3.598	2.973 ±1.051	0.358 ± 0.125	1.195 ± 0.280	1
Magnet	2.258 ± 0.436	6.900 ± 2.167	2.789 ± 2.105	0.344 ± 0.286	2.584 ± 0.355	0.96
MN	2.152 ± 0.407	6.543 ± 1.305	11.944 ± 5.868	1.308 ± 0.616	0.426 ± 0.213	3.65
MN-Magnet	3.028 ± 0.731	10.428 ± 1.787	13.091 ± 3.835	1.556 ± 0.472	0.921 ± 0.072	4.35

Notes: ER: enhancement ratio. Enhancement ratio was considered based on the ratio of average values of steady state flux of each treatment to passive diffusion or chemical enhancer only, at the same formula

Table 5.2 Mass balance of *in vitro* skin penetration/permeation study ($\bar{x}$ ± SEM; 5-6 replications)

Physical permeation enhancement	IA (µg)	RSV distribution (µg)					Total of RSV distribution (µg)	RECOVERY (%)
		RA	SC	E+D+F	R	S/S+W		
RSV SOLUTION								
Magnet	36.31 ± 0.18	9.60 ± 1.61	0.62 ± 0.19	1.79 ± 0.17	0.69 ± 0.21	20.23 ± 3.37	30.98 ± 5.50	85.25 ± 5.07
MN	32.94 ± 0.16	21.50 ± 0.71	1.55 ± 0.17	4.80 ± 0.37	2.68 ± 0.85	0.18 ± 0.03	30.65 ± 0.36	93.03 ± 1.03
MN-Magnet	35.55 ± 0.12	28.89 ± 7.82	0.48 ± 0.03	1.47 ± 0.13	1.56 ± 0.21	7.68 ± 0.98	40.08 ± 8.72	112.48 ± 24.15
TKTP								
Magnet	20486.86 ± 35.31	18128.11 ± 317.17	1.55 ± 0.35	3.84 ± 1.17	0.25 ± 0.09	148.30 ± 30.95	18282.05 ± 307.17	89.23 ± 1.44
MN	20200.15 ± 77.34	19474.48 ± 661.84	4.35 ± 0.80	8.25 ± 1.85	38.73 ± 7.16	2.21 ± 0.32	19526.37 ± 659.99	96.63 ± 3.06
MN-Magnet	18549.28 ± 64.27	17240.13 ± 287.44	3.75 ± 0.79	36.58 ± 11.09	36.58 ± 8.55	378.33 ± 45.93	17695.37 ± 283.08	95.39 ± 1.38

Table 5.2 ***continued***

Physical permeation enhancement	IA (µg)	RSV distribution (µg)					Total of RSV distribution (µg)	RECOVERY (%)
		RA	SC	E+D+F	R	S/S+W		
				ETKTP				
Magnet	20260.93 ± 41.54	18599.37 ± 403.05	3.47 ± 0.64	8.33 ± 2.60	2.79 ± 2.10	683.43 ± 35.64	19297.39 ± 406.17	95.25 ± 2.11
MN	20062.61 ± 76.39	18954.09 ± 127.81	3.31 ± 0.63	7.90 ± 1.64	12.73 ± 5.87	2.97 ± 0.80	18981.01 ± 133.81	94.62 ± 0.94
MN-Magnet	20476.16 ± 32.21	19381.90 ± 374.19	4.66 ± 1.12	12.53 ± 2.18	13.09 ± 3.84	926.87 ± 245.37	20339.05 ± 557.89	97.07 ± 3.32

Notes : IA = initial amount of RSV in the donor compartment (µg); RA = remaining amount of RSV in the donor compartment (µg); SC = amount of RSV in the stratum corneum (µg); E+D+F = amount of RSV in epidermis, dermis and follicles (µg) ; R= amount of RSV in the receptor compartment; S/S+W = amount of RSV on the surface or on surface and in washing liquid (µg)

5.4 Discussion

The development and evaluation of RSV nanoformulations was described in chapter 4 of this thesis. The nanoformulations including terpene-based nanoformulations for skin delivery of RSV performed well as chemical penetration/permeation enhancers. This current study demonstrated the potential of physical techniques (magnetophoresis and microneedle application) in enhancing the penetration /permeation of RSV administered in a saturated aqueous solution. This is also the first study investigating effects of a combination of chemical (TKTP and ETKTP) and physical enhancement techniques (magnetophoresis and MN array) in RSV skin delivery. Our hypothesis was that the most effective combination would be pre-treatment with MN to open channels through the SC, followed by administration of the terpene based nanoformulations that could present higher RSV concentration and improve permeation within the skin tissue. Addition of the magnetic push was aimed at improving diffusion and flow of the formulation within the MN induced channels. We investigated each of these enhancement technologies alone and in combination.

First, we investigated the effect of the physical enhancement techniques on a saturated aqueous solution of RSV, in our case using PBS to control the pH to maintain RSV stability. The magnet array application doubled the permeation of RSV (cumulative amount and flux) when the RSV saturated aqueous solution was applied as the donor (Figure 5.3 and Table 5.1). Magnetohydrokinesis, a phenomenon of material transport by water movement across the skin in the presence of a magnetic field[8], is likely to be the mechanism underpinning the permeation. Water is categorised as a diamagnetic solvent which naturally moves away from a magnet. Any substances dissolved in water are likely transported across the skin in the presence of the magnetic field. Hence, in a saturated aqueous solution, the dissolved RSV (in the PBS pH 6) was likely transported across the SC by flow of the aqueous solvent.

Significant permeation enhancement of RSV administered in a saturated aqueous solution was observed in MN pretreated skin (Figure 5.5 and Table 5.1). We applied a solid MN device called 3M™ Microchannel Skin System (3M, Singapore) as pre-treatment in order to create microchannels through the SC, through which the RSV could cross the SC. The system was sterile, single use rectangular array of pyramidal-shape needles (13 x 27 needles) with needle length of 700 µm, attached on an oval patch in a tip-to-tip space of the needles of 500µm.[21, 22] The system has been reported to be safe and well tolerated.[23, 24] Li et al.[22] reported that the depth of penetration of

3M™ Microchannel Skin system was in correlation with the force of application. The force of 10 N provided the depth of penetration of approximately 100 μm in human skin. From this information, considering that newborn pig skin structure is relatively similar to human skin, we can predict that the depth of penetration of the MN in this study was around 80-100μm. MN pre-treatment in this study increased the cumulative amount of RSV permeated and flux approximately 4.57-fold and 2-fold, respectively, compared to passive diffusion. The lag time was also halved. Substantially enhanced skin delivery has been shown following the application of solid MN in a wide range of small and macromolecules due to providing direct transfer channels across the SC barrier.[13, 15] For example, copper peptide, a skin regeneration and wound healing agent, was delivered across 3M Microchannel Skin System-treated human skin at 134 ± 12 and 705 ± 84 nmoles for its peptide and copper, respectively, without inducing skin irritation.[22]

The combination of MN pre-treatment and magnet array application also significantly enhanced RSV permeation compared to passive diffusion of the saturated aqueous solution (Figure 5.7 Table 5.1). The similar results of RSV skin permeation with MN treatment alone and in combination with magnet application suggested that the magnet array application did not further contribute to the enhanced permeation of RSV compared to the MN alone. This suggests that when RSV was applied to the skin as an aqueous solution, the provision of MN derived channels provided optimal skin delivery and no increased flow within the channels was achieved for this formulation by application of magnetic energy.

We also investigated the effect of the physical enhancement techniques with the optimal terpene-based nanoemulsions developed in Chapter 4. As expected, the amounts of RSV delivered to and through the skin were substantially higher than from the aqueous solution (data in agreement with Chapter 4). When the nanoemulsions were applied with the magnet array, there was no statistically significant enhancement of permeation of RSV (Figure 5.9, Figure 5.11, and Table 5.1). The phenomenon could be explained by understanding the nature of the formulations. The nanoemulsion composition of TKTP and ETKTP solubilized more RSV compared to PBS pH 6. In chapter 4 we have demonstrated that nanoformulations significantly increased the solubility of RSV. For example, the RSV solubility in TKTP was 44.771 ± 4.159 mg/mL compared to only 34.13 ± 0.20 μg/mL in PBS pH 6 solution. High solubilisation of RSV in nanoformulation increased the efficiency (loading capacity and dose application) of RSV in the droplets to penetrate across the SC.[25, 26] Theochari et al.[27], when formulating the lipophilic antitumor PLX4720 in a

microemulsion containing triacetin, Tween 80, and water, confirmed that this lipophilic compound was located mainly in triacetin, based on electron paramagnetic resonance (EPR) studies. Hung et al.[28] also argued that RSV is likely to be non-ionic in oil. Hence, in our nanoformulations, we expect that the RSV is in non-ionic form and less exists in the aqueous phase. This reduces the opportunity for enhanced RSV transport via magnetohydrokinesis.

In contrast, MN pre-treatment and the combination of MN pre-treatment and magnet array application significantly increased the permeation of RSV in both nanoemulsions ($P < 0.05$) (Figure 5.9, Figure 5.11, and Table 5.1). Considering first TKTP, there were large increase in the flux of RSV administered in TKTP in MN-treated skin (78.37-fold) and in the comibination of MN pre-treatment and magnet array application (86.82-fold) compared to the nanoemulsion alone. The low viscosity of the TKTP (0.110 ± 0.026 dPas) enabled the nanoformulation to effectively pass through the microchannels created by MN pre-treatment. The lubricating effect of triacetin may also facilitate the flow of nanoemulsion and hence the rate of RSV permeation through the microchannels. Having bypassed the SC, the presence of triacetin, Kolliphor® RH 40 and Transcutol® were able to facilitate diffusion within the skin tissues by enhancing the partitioning of RSV in the skin. Transcutol®, in particular, increases water absorption from the skin to maximize the drug thermodynamic activity due to drug solubility alteration.[29-31]

MN pre-treatment alone and in combination with magnet application also enhanced the RSV flux when applied in ETKTP although skin delivery was 4-5 times less than when TKTP was applied with the physical enhancer combination (ETKTP) ($P < 0.05$). The ETKTP nanoemulsion has a higher viscosity than TKTP (1.621 ± 0.119 dPas), which may impede the flow of nanoemulsion through the SC microchannels. The steady state flux and cumulative amount of RSV was higher with the combination compared to MN alone, but this was not a statistically significant increase (Figure 5.11, and Table 5.1).

Interestingly, the deposition of RSV in the epidermis, dermis and follicles was significantly higher for TKTP nanoemulsion formulations when applied with the combination of MN pre-treatment and magnet array application ($P <0.05$) (Figure 5.10 and Table 5.1), suggesting that significant lateral diffusion might occur due to the synergistic effects of the combination of microneedle pre-treatment, magnet array and nanoemulsion constituents. This significant increase in skin distribution of RSV was not seen for any of the enhancement treatments alone. The result was in agreement

with a study reported by Prow et al.[32], when they investigated the effect of a combination of magnet application (ETP012) and MN pre-treatment on Melanostatin skin penetration. They suggested that magnet application enhanced the average delivery signal of melanostatin 1.48 times of that in MN treated skin. They further suggested that only the SC, epidermis and the uppermost dermis were affected by ETP012 application. However, the combination of MN pre-treatment and magnet application had less effect on the skin distribution of RSV applied in ETKTP as the nanoemulsion itself has already facilitated the optimum penetration.

Magnet array application is one of a number of promising non-invasive physical permeation enhancement tenhiques.[5, 7, 33] Magnet-derived increase of skin flux of a number of compounds has been reported, including benzoic acid, salbutamol sulphate, torbutaline sulphate, lidocaine hydrochloride, naltrexone hydrochloride, urea, and amino levulinic acid.[6-10, 34-36] The main mechanism of skin penetration enhancement are suggested as magnetohydrokinesis and magnetorepulsion, and are appropriate for these mainly polar compounds that have been applied in an aqueous/hydrophilic environment or in an electrolyte solution.

However, the effect of magnetic application with compounds that are not diamagnetic or are applied in more complex formulations are less well documented. It is known that magnetic enhanced cosmetics are currently marketed by Procter & Gamble, with both cream and polymer-based face mask formulations commercially available. In addition, Krishnan et al.[35] showed enhanced skin permeation of 20nm gold nanoparticles when applied to human skin with an electromagnet. They concluded that this could only occur if the magnet was capable of disrupting the SC barrier, similar to the effect of fluidisation of the lipid bilayers caused by chemical penetration enhancers, including terpenes.[37-40]

The development of a wide range of MN fabrications has been well documented and their ability to form microchannels in the SC is being exploited in many different ways.[17, 41-44] Indeed a number of phase III trials of MN delivered vaccines[45, 46] and insulin[47] are well underway. Whilst there is no doubt that they can provide significant enhancement of skin delivery of a range of compounds, there can be a high variation in delivery, particularly for “poke and patch” type systems if the channels fill or partially fill with fluid and start to close thereby affecting flow of applied topical formulation within the channels.[48, 49] Incomplete insertion of MN may also cause inefficiency of dose delivery. For example, less than 2% of the topically applied coumarin 6-loaded PLGA nanoparticles was delivered in Sprague Dawley rat skin because of shallow

insertion depth of the a 3M™ Microchannel Skin System in the skin.[50] In addition, a compound applied into the microchannels still needs to flow from the site of deposition through the skin tissues. Wei et al.[51] showed that the degree of diffusion varied with molecular weight and skin layer, following the deposition of dextrans into the skin via a nanopatch MN delivery system.

Various combinations of enhancement approaches have been investigated.[1] For example, iontophoresis in combination with MN was reported to enhance insulin delivery up to three fold in newborn pig skin compared to iontophoresis alone.[52] An optimised combination of MN and sonophoresis increased permeation of bovine serum albumin across porcine ear skin at approximately 10 times that of passive diffusion[53]. The flux of lidocaine hydrochloride in magnetophoretically-treated rat skin was up to 6.44-fold greater when applied with gel containing menthol as the chemical penetration enhancer, compared to the gel without penetration enhancer and magnetophoretic patch application. Prow et al.[32] indicated enhancement capacity of a static magnet array ETP012 on melanostatin and sodium fluorescence in human skin, although the effects were localised in the skin. In our investigations of these combinations, we have shown that there is scope for combining technologies that disrupt the SC barrier, with those that increase diffusion and flow, and enhance active solubility.

We demonstrated for the first time the capacity of combination magnet application and MN pre-treatment with nanoformulations to increase RSV skin penetration into the skin, thus this strategy is promising for skin-targeted delivery of RSV.

5.5 References

1. Dragicevic N, Maibach H. Combined use of nanocarriers and physical methods for percutaneous penetration enhancement. Advanced Drug Delivery Reviews. 2018;127:58-84.
2. Dragicevic N, Maibach HI, editors. Percutaneous penetration enhancers physical methods in penetration enhancement: Springer-Verlag Berlin Heidelberg; 2017. XVII, 508 p. doi:10.1007/978-3-662-53273-7.
3. Benson HAE. Transdermal drug delivery: Penetration enhancement techniques. Current Drug Delivery. 2005;2(1):23-33.
4. Benson HAE, Namjoshi S. Proteins and peptides: Strategies for delivery to and across the skin. J Pharm Sci. 2008;97(9):3591-3610.
5. Benson HAE, McIldowie M, Prow T. Magnetophoresis: Skin penetration enhancement by a magnetic field. In: Dragicevic N, I. Maibach H, editors. Percutaneous penetration enhancers physical methods in penetration enhancement. Berlin, Heidelberg: Springer Berlin Heidelberg; 2017. p. 195-206.
6. Murthy SN, Hiremath SRR. Effect of magnetic field on the permeation of salbutamol sulphate. Indian Drugs. 1999;36:663-664.
7. Murthy SN. Magnetophoresis: an approach to enhance transdermal drug diffusion. Pharmazie. 1999;54(5):377-379.
8. Murthy SN, Sammeta SM, Bowers C. Magnetophoresis for enhancing transdermal drug delivery: Mechanistic studies and patch design. J Control Release. 2010;148(2):197-203.
9. Sammeta SM, Repka MA, Narasimha Murthy S. Magnetophoresis in combination with chemical enhancers for transdermal drug delivery. Drug Dev Ind Pharm. 2011;37(9):1076-1082.
10. Benson HA, Krishnan G, Edwards J, Liew YM, Wallace VP. Enhanced skin permeation and hydration by magnetic field array: preliminary *in-vitro* and *in-vivo* assessment. J Pharm Pharmacol. 2010;62(6):696-701.
11. McAlister E, Garland MJ, Singh TRR, Donnelly RF. Microporation using Microneedle arrays. In: Dragicevic N, I. Maibach H, editors. Percutaneous penetration enhancers physical methods in penetration enhancement. Berlin, Heidelberg: Springer Berlin Heidelberg; 2017. p. 273-303.
12. McCrudden MTC, McAlister E, Courtenay AJ, et al. Microneedle applications in improving skin appearance. Exp Dermatol. 2015;24(8):561-566.
13. Tuan-Mahmood T-M, McCrudden MTC, Torrisi BM, et al. Microneedles for intradermal and transdermal drug delivery. Eur J Pharm Sci. 2013;50(5):623-637.
14. Prausnitz MR. Microneedles for transdermal drug delivery. Advanced Drug Delivery Reviews. 2004;56(5):581-587.
15. Quinn HL, Kearney M-C, Courtenay AJ, McCrudden MTC, Donnelly RF. The role of microneedles for drug and vaccine delivery. Expert Opinion on Drug Delivery. 2014;11(11):1769-1780.
16. Kim Y-C, Park J-H, Prausnitz MR. Microneedles for drug and vaccine delivery. Advanced Drug Delivery Reviews. 2012;64(14):1547-1568.
17. Arora A, Prausnitz MR, Mitragotri S. Micro-scale devices for transdermal drug delivery. Int J Pharm. 2008;364(2):227-236.
18. Donnelly RF, Morrow DIJ, McCarron PA, et al. Microneedle-mediated intradermal delivery of 5-aminolevulinic acid: Potential for enhanced topical photodynamic therapy. J Control Release. 2008;129(3):154-162.
19. Donnelly RF, Morrow DIJ, McCarron PA, et al. Microneedle arrays permit enhanced intradermal delivery of a preformed photosensitiser. Photochem Photobiol. 2009;85(1):195-204.
20. Mohammed YH, Yamada M, Lin LL, et al. Microneedle enhanced delivery of cosmeceutically relevant peptides in human skin. PLoS One. 2014;9(7):e101956.

21. Duan D, Moeckly C, Gysbers J, et al. Enhanced delivery of topically-applied formulations following skin pre-treatment with a hand-applied, plastic microneedle array. Current Drug Delivery. 2011;8(5):557-565.
22. Li H, Low YSJ, Chong HP, et al. Microneedle-mediated delivery of copper peptide through skin. Pharm Res. 2015;32(8):2678-2689.
23. Hoesly FJ, Borovicka J, Gordon J, et al. Safety of a novel microneedle device applied to facial skin: A subject- and rater-blinded, sham-controlled, randomized trial. Arch Dermatol. 2012;148(6):711-717.
24. Hoesly FJ, Gordon J, Borovicka J, Alam M. A novel microneedle device is safe and well-tolerated when applied to facial skin in adults of all skin phototypes. J Am Acad Dermatol. 2012;66(4, Supplement 1):AB208.
25. Salim N, Ahmad N, Musa SH, et al. Nanoemulsion as a topical delivery system of antipsoriatic drugs. RSC Advances. 2016;6(8):6234-6250.
26. Roberts MS, Mohammed Y, Pastore MN, et al. Topical and cutaneous delivery using nanosystems. J Control Release. 2017;247:86-105.
27. Theochari I, Goulielmaki M, Danino D, et al. Drug nanocarriers for cancer chemotherapy based on microemulsions: The case of Vemurafenib analog PLX4720. Colloids and Surfaces B: Biointerfaces. 2017;154:350-356.
28. Hung C-F, Lin Y-K, Huang Z-R, Fang J-Y. Delivery of resveratrol, a red wine polyphenol, from solutions and hydrogels *via* the Skin. Biol Pharm Bull. 2008;31(5):955-962.
29. Ganem-Quintanar A, Lafforgue C, Falson-Rieg F, Buri P. Evaluation of the transepidermal permeation of diethylene glycol monoethyl ether and skin water loss. Int J Pharm. 1997;147(2):165-171.
30. Osborne DW, Musakhanian J. Skin penetration and permeation properties of Transcutol®—Neat or diluted mixtures. AAPS PharmSciTech. 2018;19(8):3512-3533.
31. Barry BW. Novel mechanisms and devices to enable successful transdermal drug delivery. Eur J Pharm Sci. 2001;14(2):101-114.
32. Prow TW, Mohammed YH, Ansaldo AB, Benson HAE. Topical microneedle drug delivery enhanced with magnetophoresis. In: Advances in dermatological sciences. The Royal Society of Chemistry; 2014. p. 169-177.
33. Wong TW. Electrical, magnetic, photomechanical and cavitational waves to overcome skin barrier for transdermal drug delivery. J Control Release. 2014;193:257-269.
34. Murthy SN, Hiremath SRR. Physical and chemical permeation enhancers in transdermal delivery of terbutaline sulphate. AAPS PharmSciTech. 2001;2(1):1-5.
35. Krishnan G, Edwards J, Chen Y, Benson HA. Enhanced skin permeation of naltrexone by pulsed electromagnetic fields in human skin *in vitro*. J Pharm Sci. 2010;99(6):2724-31.
36. Namjoshi S, Caccetta R, Edwards J, Benson HA. Liquid chromatography assay for 5-aminolevulinic acid: application to *in vitro* assessment of skin penetration *via* Dermaportation. J Chromatogr B Analyt Technol Biomed Life Sci. 2007;852(1-2):49-55.
37. Chen J, Jiang Q-D, Chai Y-P, et al. Natural terpenes as penetration enhancers for transdermal drug delivery. Molecules. 2016;21(12):1709.
38. El-Kattan AF, Asbill CS, Kim N, Michniak BB. The effects of terpene enhancers on the percutaneous permeation of drugs with different lipophilicities. Int J Pharm. 2001;215(1):229-240.
39. Williams AC, Barry BW. Terpenes and the Lipid–Protein–Partitioning theory of skin penetration enhancement. Pharm Res. 1991;8(1):17-24.
40. Zhao K, Singh J. Mechanisms of percutaneous absorption of tamoxifen by terpenes: eugenol, d-limonene and menthone. J Control Release. 1998;55(2):253-260.
41. Bariya SH, Gohel MC, Mehta TA, Sharma OP. Microneedles: an emerging transdermal drug delivery system. J Pharm Pharmacol. 2012;64(1):11-29.

42. Cheung K, Das DB. Microneedles for drug delivery: trends and progress. Drug Delivery. 2016;23(7):2338-2354.
43. Donnelly RF, Singh TRR, Garland MJ, et al. Hydrogel-forming microneedle arrays for enhanced transdermal drug delivery. Advanced Functional Materials. 2012;22(23):4879-4890.
44. Dharadhar S, Majumdar A, Dhoble S, Patravale V. Microneedles for transdermal drug delivery: a systematic review. Drug Dev Ind Pharm. 2019;45(2):188-201.
45. Arnou R, Eavis P, De Juanes Pardo J-R, et al. Immunogenicity, large scale safety and lot consistency of an intradermal influenza vaccine in adults aged 18–60 years: Randomized, controlled, phase III trial. Human Vaccines. 2010;6(4):346-354.
46. Arnou R, Icardi G, De Decker M, et al. Intradermal influenza vaccine for older adults: A randomized controlled multicenter phase III study. Vaccine. 2009;27(52):7304-7312.
47. Norman JJ, Brown MR, Raviele NA, Prausnitz MR, Felner EI. Faster pharmacokinetics and increased patient acceptance of intradermal insulin delivery using a single hollow microneedle in children and adolescents with type 1 diabetes. Pediatr Diabetes. 2013;14(6):459-465.
48. Gupta J, Gill HS, Andrews SN, Prausnitz MR. Kinetics of skin resealing after insertion of microneedles in human subjects. J Control Release. 2011;154(2):148-155.
49. Kalluri H, Banga AK. Formation and closure of microchannels in skin following microporation. Pharm Res. 2011;28(1):82-94.
50. Su L-C, Chen M-C. Efficient delivery of nanoparticles to deep skin layers using dissolvable microneedles with an extended-length design. Journal of Materials Chemistry B. 2017;5(18):3355-3363.
51. Wei JCJ, Haridass IN, Crichton ML, et al. Space- and time-resolved investigation on diffusion kinetics of human skin following macromolecule delivery by microneedle arrays. Sci Rep. 2018;8(1):17759.
52. Garland MJ, Caffarel–Salvador E, Migalska K, Woolfson AD, Donnelly RF. Dissolving polymeric microneedle arrays for electrically assisted transdermal drug delivery. J Control Release. 2012;159(1):52-59.
53. Han T, Das DB. Permeability enhancement for transdermal delivery of large molecule using low-frequency sonophoresis combined with microneedles. J Pharm Sci. 2013;102(10):3614-3622.

Chapter 6. General Discussion, Future Directions and Conclusions

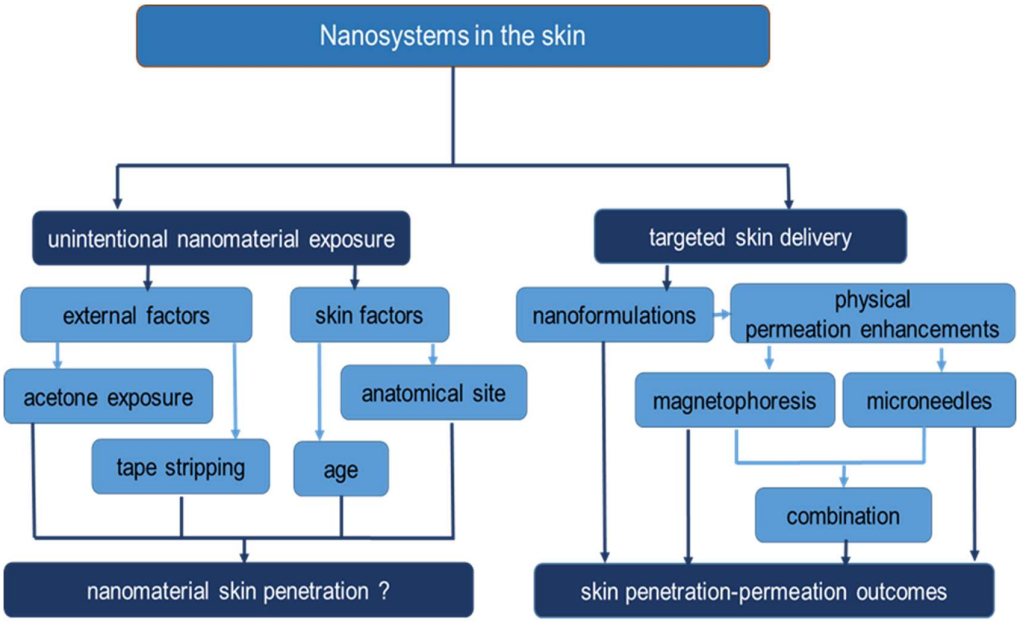

Figure 6.1 A summary of the current research project

6.1 General discussion and future directions

Whilst the general consensus is that nanoparticle exposure does not lead to penetration in healthy, intact skin, questions remain about damaged skin. Solvent exposure and tape stripping may compromise the skin barrier thus facilitating nanoparticle penetration. In Chapter 2, the effect of acetone pre-treatment and tape stripping on the porcine skin permeability was investigated with two objectives: (1) to observe the change of porcine skin morphology as a result of acetone and tape stripping pre-treatment, and (2) to assess nanomaterial distribution within skin layers. Multiphoton tomography (MPT) equipped with fluorescence lifetime imaging (FLIM) was used to observe the skin condition in the deeper layers of the epidermis as it offers excellent resolution.[1, 2] Saline-hydrated skin morphology allowed baseline imaging of the structure differences of keratinocytes in every layer of the viable epidermis. Acetone application resulted in skin shrinkage and flakiness. Significant barrier disruption and the loss of some keratinocytes in SG and SS was seen following exposure to 100% acetone, but not 10% acetone. Thirty times tape stripping removed the SC completely. Hydrophilic CdSe quantum dots (QDs) applied in acetone solution or following tape stripping pre-treatment were primarily located in the skin furrows.

Some QDs were observed in the upper SG following tape-stripping but none were detected in the deeper epidermal layers. Although acetone application altered the skin barrier, it did not facilitate penetration of the solid nanomaterial into the skin. Our finding confirms the study of zinc oxide skin penetration on tape stripped human skin.[3] This localization may due to the role of tight junctions in supporting the skin barrier.[4-6]

The effect of age and anatomical site on the penetration of QDs in porcine skin was presented in Chapter 3.[7] The ears and abdomen of adult pig skin, weanling pig skin and newborn pig skin were evaluated, thus providing a range in follicle density and diameter. Skin condition and QDs presence in the epidermal layers was observed by MPT and quantified by ICP-MS following QDs application with 2 minute-finger rubbing, a protocol shown to be important to Lademann group's "ratchet effect"[8] of nanoparticle deposition into follicles. Applied QDs were located in the furrows and follicles with no penetration in the keratinocytes, in agreement with other nanomaterial skin penetration studies.[9, 10] Follicular deposition of cadmium varied in different age of pigs, with higher levels in ears on adult and weanling pigs than newborns. This variation was likely due to the follicle density and follicle diameter differences related to the age of the pigs. In addition, regional differences of follicle size and density also influenced the amount of QDs deposited except for newborn pig skin. This study again supports the body of literature that topical exposure to solid nanomaterial does not result in skin penetration, which is reassuring regarding the safety concerns of nanomaterial exposure. *In vivo* visualisation study involving human volunteers is essential to conduct in the future, in order to investigate the actual duration of the nanomaterial existence in the follicles and the possibility of nanomaterials to penetrate into the skin via follicles.

Nanoformulations for skin delivery of the lipophilic natural substance resveratrol (RSV) were developed and evaluated in Chapter 4. RSV has potential as a topical antiaging or sun exposure recovery product, based on its antioxidant and anti-inflammatory properties.[11, 12] Three different types of nanoformulations (emulsion-type, lipid-based and micellar systems) were initially developed and characterised in terms of physical appearance, RSV solubility, viscosity, refractive index, and stability. RSV skin penetration/permeation following topical administration was determined across porcine skin mounted Franz-type diffusion cells. RSV was quantified in the SC, the area of epidermis-dermis-follicles, and the cumulative amount in the receptor compartment after 8 hours. Development of nanoemulsions with less oil, surfactant and cosurfactant was further focused in order to obtain better quality of RSV nanoformulations which showed reasonable amount of RSV penetrate

into and permeate through the skin. The effects of terpenes were also investigated. All nanoformulations were successfully formulated, showing excellent clarity and quantifiable amounts of RSV in and through the skin. Thermodynamic activity of the system likely affects the degree of RSV skin permeation for the non-terpene formulations. Higher RSV solubility in the nanoformulations correlated with higher thermodynamic stability but lower skin permeation of RSV permeated. RSV permeation was higher for nanoemulsions containing terpenes, and increased with increasing lipophilicity of the terpenes. Nanoformulations containing eugenol and triacetin showed maximum deposition in the skin (2.342 ± 0.269 μg/cm^2) with 9.55-fold enhancement compared to the control. The highest cumulative amount of RSV permeation was from the formulations containing D-limonene (4.585 ± 0.936 μg) and eucalyptol (4.036 ± 1.125 μg), with 12.61-fold and 9.95-fold permeation enhancement respectively, compared to the control.

Chapter 5 took this a step further, adding physical penetration enhancement in the form of microneedles and or magnetophoresis. The solid microneedle array was employed as a skin pre-treatment with pressure of 800-1000g for 30 seconds and was subsequently removed. A magnet array was applied in contact with the donor formulation above the skin for the duration of the experiment. The magnetic array doubled the permeation of RSV in the saturated aqueous solution, but did not enhance the permeation from the nanoformulations. It is likely that the main enhancement mechanism of magnetohydrokinesis was effective for the aqueous solution but less effective in the other solvent vehicles. Microneedles significantly enhanced RSV permeation in saturated aqueous solution and both nanoformulations. It has been suggested that applying magnetophoresis to microneedle-porated skin may enhance flow of the applied topical vehicle within the pores. When this combination was used with the nanoformulations there was significantly enhanced delivery of RSV into the skin, but permeation through to the receptor compartment was not enhanced. We suggest that the physical enhancement combination contributed more to the lateral diffusion in the skin. Formulation and *in vitro* studies in this research project have led to important information to develop and evaluate nanoformulations for targeted skin delivery of RSV. Human i*n vivo* efficacy studies of the RSV nanoformulations as the antiaging and safety assessment of nanoformulations involving human volunteers should be carried out in the next stage, in order to fully dedicate the formulations for human application. However, due to time and resource constraints, human *in vivo* studies could not be conducted in this project. The nanoemulsions can also be further challenged to target the delivery of

other natural products and protein-peptides in the skin. The MPT visualisation of the effect of nanoformulations on the depth of penetration could also be of significant benefit to investigate.

6.2 Conclusions

This thesis has highlighted that there is minimum potential for toxicity of undesirable nanomaterial (solid nanoparticles) exposure to the skin as the nanomaterials accumulate on the skin surface and follicles, unless the skin barriers are perturbed. Novel nanoemulsions were also successfully developed for skin-targeted delivery of natural potent antioxidant resveratrol. Nanoformulations in combination with magnet application and MN skin pre-treatment is a promising strategy for improving skin-targeted delivery of RSV.

6.3 References

1. König K, Ehlers A, Stracke F, Riemann I. *In vivo* drug screening in human skin using femtosecond laser multiphoton tomography. Skin Pharmacol Physiol. 2006;19(2):78-88.
2. Roberts MS, Roberts MJ, Robertson TA, et al. *In vitro* and *in vivo* imaging of xenobiotic transport in human skin and in the rat liver. Journal of Biophotonics. 2008;1(6):478-493.
3. Leite-Silva VR, Sanchez WY, Studier H, et al. Human skin penetration and local effects of topical nano zinc oxide after occlusion and barrier impairment. Eur J Pharm Biopharm. 2016;104:140-147.
4. Bäsler K, Bergmann S, Heisig M, et al. The role of tight junctions in skin barrier function and dermal absorption. J Control Release. 2016;242:105-118.
5. Kirschner N, Houdek P, Fromm M, Moll I, Brandner JM. Tight junctions form a barrier in human epidermis. Eur J Cell Biol. 2010;89(11):839-842.
6. Yoshida K, Yokouchi M, Nagao K, et al. Functional tight junction barrier localizes in the second layer of the stratum granulosum of human epidermis. J Dermatol Sci. 2013;71(2):89-99.
7. Nastiti CMRR, Mohammed Y, Telaprolu KC, et al. Evaluation of quantum dot skin penetration in porcine skin: Effect of age and anatomical site of topical application. Skin Pharmacol Physiol. 2019.
8. Radtke M, Patzelt A, Knorr F, Lademann J, Netz RR. Ratchet effect for nanoparticle transport in hair follicles. Eur J Pharm Biopharm. 2017;116:125-130.
9. Baroli B, Ennas MG, Loffredo F, et al. Penetration of metallic nanoparticles in human full-thickness skin. J Invest Dermatol. 2007;127(7):1701-1712.
10. Gratieri T, Schaefer UF, Jing L, et al. Penetration of quantum dot particles through human skin. J Biomed Nanotechnol. 2010;6(5):586-95.
11. Baxter RA. Anti-aging properties of resveratrol: review and report of a potent new antioxidant skin care formulation. J Cosmet Dermatol. 2008;7(1):2-7.
12. Ratz-Łyko A, Arct J. Resveratrol as an active ingredient for cosmetic and dermatological applications: a review. J Cosmet Laser Ther. 2019;21(2):84-90.

APPENDIX

To Whom It May Concern

I, Christofori Maria Ratna Rini Nastiti, as the first author, contributed the following to **Chapter 3: Evaluation of Quantum Dots (QDs) Skin Penetration in Porcine Skin: Effect of Age and Anatomical Site of Topical Application**

- Conception and design
- Acquisition of data & method
- Data conditioning & manipulation
- Analysis & statistical method
- Interpretation & discussion
- Final approval
- Manuscript preparation and submission

_____

I as a co-author, endorse that this level of contribution by the candidate indicated above is appropriate.

Dr. Yousuf Mohammed _____

Krishna C. Telaprolu _____

Dr. Xiaowen Liang _____

Dr. Jeffrey E.Grice _____

Prof. Michael S. Roberts _____

A/P Dr. Heather A.E. Benson _____

Paper **"Evaluation of Quantum Dot Skin Penetration in Porcine Skin: Effect of Age and Anatomical Site of Topical Application"** Journal of Skin Pharmacology and Physiology (2019) pages 1- 10. doi:10.1159/000499435

Christofori M.R.R. Nastiti[1,2], Yousuf Mohammed[3], Krishna C. Telaprolu[3], Xiaowen Liang[3], Jeffrey E. Grice[3], Michael S. Roberts [3,4,5] , Heather A.E. Benson[1]

[1]School of Pharmacy and Biomedical Sciences, Curtin Health Innovation Research Institute, Curtin University, Bentley, (Western Australia), Australia

[2]Faculty of Pharmacy, Sanata Dharma University, Yogyakarta, Indonesia

[3]Therapeutics Research Centre, Faculty of Medicine, University of Queensland Diamantina Institute, Woolloongabba, (Queensland), Australia

[4]School of Pharmacy and Medical Sciences, University of South Australia, Adelaide, (South Australia), Australia

[5]Therapeutics Research Centre, Basil Hetzel Institute for Translational Medical Research, Queen Elizabeth Hospital, Adelaide, (South Australia), Australia

	conception and design	**acquisition of data & method**	**data conditioning & manipulation**	**analysis &statistical method**	**interpretation & discussion**	**final approval**
Dr. Yousuf Mohammed	✓	✓	✓	✓	✓	✓
I acknowledge that these represent my contribution to the above research output.						
Krishna C.Telaprolu		✓				✓
I acknowledge that these represent my contribution to the above research output.						
Dr. Xiaowen Liang		✓	✓			✓
I acknowledge that these represent my contribution to the above research output.						
Dr. Jeffrey E. Grice		✓	✓	✓	✓	✓
I acknowledge that these represent my contribution to the above research output.						
Prof. Michael S. Roberts	✓	✓	✓	✓	✓	✓
I acknowledge that these represent my contribution to the above research output.						
A/P Dr. Heather A.E. Benson	✓	✓	✓	✓	✓	✓
I acknowledge that these represent my contribution to the above research output.						

ELSEVIER LICENSE
TERMS AND CONDITIONS

Jul 13, 2019

This Agreement between Christofori Nastiti ("You") and Elsevier ("Elsevier") consists of your license details and the terms and conditions provided by Elsevier and Copyright Clearance Center.

License Number	4626421364045
License date	Jul 12, 2019
Licensed Content Publisher	Elsevier
Licensed Content Publication	Journal of Controlled Release
Licensed Content Title	Topical and cutaneous delivery using nanosystems
Licensed Content Author	MS Roberts,Y Mohammed,MN Pastore,S Namjoshi,S Yousef,A Alinaghi,IN Haridass,E Abd,VR Leite-Silva,HAE Benson,JE Grice
Licensed Content Date	Feb 10, 2017
Licensed Content Volume	247
Licensed Content Issue	n/a
Licensed Content Pages	20
Start Page	86
End Page	105
Type of Use	reuse in a thesis/dissertation
Intended publisher of new work	other
Portion	figures/tables/illustrations
Number of figures/tables/illustrations	3
Format	both print and electronic
Are you the author of this Elsevier article?	No
Will you be translating?	No
Original figure numbers	Fig.1, Fig.2, Fig.3
Title of your thesis/dissertation	Nanosystem in the skin: from undesired nanomaterial exposure to novel nanoformulations
Expected completion date	Aug 2019
Estimated size (number of pages)	150
Requestor Location	Christofori Nastiti Curtin University Bld 306.102 Kent Street Bentley, Western Australia 6102 Australia Attn: Christofori Nastiti
Publisher Tax ID	GB 494 6272 12
Total	0.00 AUD
Terms and Conditions	

ELSEVIER LICENSE
TERMS AND CONDITIONS

Jul 13, 2019

This Agreement between Christofori Nastiti ("You") and Elsevier ("Elsevier") consists of your license details and the terms and conditions provided by Elsevier and Copyright Clearance Center.

License Number	4626421458169
License date	Jul 12, 2019
Licensed Content Publisher	Elsevier
Licensed Content Publication	Current Opinion in Colloid & Interface Science
Licensed Content Title	Penetration of drugs through skin, a complex rate-controlling membrane
Licensed Content Author	Marie-Alexandrine Bolzinger,Stéphanie Briançon,Jocelyne Pelletier,Yves Chevalier
Licensed Content Date	Jun 1, 2012
Licensed Content Volume	17
Licensed Content Issue	3
Licensed Content Pages	10
Start Page	156
End Page	165
Type of Use	reuse in a thesis/dissertation
Intended publisher of new work	other
Portion	figures/tables/illustrations
Number of figures/tables/illustrations	1
Format	both print and electronic
Are you the author of this Elsevier article?	No
Will you be translating?	No
Original figure numbers	Fig 2
Title of your thesis/dissertation	Nanosystem in the skin: from undesired nanomaterial exposure to novel nanoformulations
Expected completion date	Aug 2019
Estimated size (number of pages)	150
Requestor Location	Christofori Nastiti Curtin University Bld 306.102 Kent Street Bentley, Western Australia 6102 Australia Attn: Christofori Nastiti
Publisher Tax ID	GB 494 6272 12
Total	0.00 USD

Copyright Clearance Center

Confirmation Number: 11830603
Order Date: 07/10/2019

Customer Information

Customer: Christofori Nastiti
Account Number: 3001418107
Organization: Christofori Nastiti
Email: c.nastiti@postgrad.curtin.edu.au
Phone: +61 (8)92661357
Payment Method: Invoice

This is not an invoice

Order Details

Current drug delivery

Billing Status: **N/A**

Order detail ID: 71941732
ISSN: 1567-2018
Publication Type: Journal
Volume:
Issue:
Start page:
Publisher: BENTHAM SCIENCE PUBLISHERS, LTD

Permission Status: Granted
Permission type: Republish or display content
Type of use: Thesis/Dissertation
Order License Id: 4625310931344

Requestor type	Not-for-profit entity
Format	Print, Electronic
Portion	chart/graph/table/figure
Number of charts/graphs/tables/figures	1
The requesting person/organization	Christofori MRR Nastiti
Title or numeric reference of the portion(s)	Fig. (2)
Title of the article or chapter the portion is from	Physical Enhancement of Transdermal Drug Application: Is Delivery Technology Keeping up with Pharmaceutical Development?
Editor of portion(s)	N/A
Author of portion(s)	S.E Cross and M.S. Roberts
Volume of serial or monograph	1
Page range of portion	81-92
Publication date of portion	2004
Rights for	Main Product, any product related to main product, and other compilations/derivative products
Duration of use	Life of current edition
Creation of copies for the disabled	no
With minor editing privileges	no
For distribution to	Worldwide
In the following language(s)	Original language of publication
With incidental promotional use	no

Lifetime unit quantity of new product	Up to 999
Title	Nanosystem in the skin: from undesired nanomaterial exposure to novel nanoformulations
Institution name	n/a
Expected presentation date	Aug 2019

Note: This item was invoiced separately through our **RightsLink service.** More info **$ 0.00**

Total order items: 1 **Order Total: $0.00**

About Us | Privacy Policy | Terms & Conditions | Pay an Invoice

ELSEVIER LICENSE
TERMS AND CONDITIONS

Jul 13, 2019

This Agreement between Christofori Nastiti ("You") and Elsevier ("Elsevier") consists of your license details and the terms and conditions provided by Elsevier and Copyright Clearance Center.

License Number	4626430244703
License date	Jul 12, 2019
Licensed Content Publisher	Elsevier
Licensed Content Publication	International Journal of Pharmaceutics
Licensed Content Title	Micro-scale devices for transdermal drug delivery
Licensed Content Author	Anubhav Arora,Mark R. Prausnitz,Samir Mitragotri
Licensed Content Date	Dec 8, 2008
Licensed Content Volume	364
Licensed Content Issue	2
Licensed Content Pages	10
Start Page	227
End Page	236
Type of Use	reuse in a thesis/dissertation
Intended publisher of new work	other
Portion	figures/tables/illustrations
Number of figures/tables/illustrations	2
Format	both print and electronic
Are you the author of this Elsevier article?	No
Will you be translating?	No
Original figure numbers	Figure 3, Figure 4
Title of your thesis/dissertation	Nanosystem in the skin: from undesired nanomaterial exposure to novel nanoformulations
Expected completion date	Aug 2019
Estimated size (number of pages)	150
Requestor Location	Christofori Nastiti Curtin University Bld 306.102 Kent Street Bentley, Western Australia 6102 Australia Attn: Christofori Nastiti
Publisher Tax ID	GB 494 6272 12
Total	0.00 USD
Terms and Conditions	

To Whom It May Concern

I, Christofori Maria Ratna Rini Nastiti, as one of the first authors, contributed the following to a review article: **Topical Nano and Microemulsions for Skin Delivery**

- Conception and design
- Literature search and review
- Data conditioning
- Manuscript preparation
- Final approval

_____

I as a first/co-author, endorse that this level of contribution by the candidate indicated above is appropriate.

Thellie Ponto _____

Dr. Eman Abd _____

Dr. Jeffrey E.Grice _____

A/P Dr. Heather A .E. Benson _____

Prof. Michael S. Roberts _____

Review article: **Topical Nano and Microemulsions for Skin Delivery**

Pharmaceutics 2017, 9(4), 37; pages 1-25
https://doi.org/10.3390/pharmaceutics9040037

Christofori M.R.R. Nastiti[1,2 *], Thellie Ponto[1 *], Eman Abd[3], , Jeffrey E. Grice[3], Heather A.E. Benson[1], Michael S. Roberts [3,4,5]

[1]School of Pharmacy and Biomedical Sciences, Curtin Health Innovation Research Institute, Curtin University, Bentley, (Western Australia), Australia
[2]Faculty of Pharmacy, Sanata Dharma University, Yogyakarta, Indonesia
[3]Therapeutics Research Centre, Faculty of Medicine, University of Queensland Diamantina Institute, Woolloongabba, (Queensland), Australia
[4]School of Pharmacy and Medical Sciences, University of South Australia, Adelaide, (South Australia), Australia
[5]Therapeutics Research Centre, Basil Hetzel Institute for Translational Medical Research, Queen Elizabeth Hospital, Adelaide, (South Australia), Australia
*These authors contributed equally to this work.

	Conception and design	**Literature search and review**	**Data conditioning**	**Manuscript preparation**	**Final approval**
Thellie Ponto	✓	✓	✓	✓	✓
I acknowledge that these represent my contribution to the above research output.					
Dr. Eman Abd		✓	✓		✓
I acknowledge that these represent my contribution to the above research output.					
Dr. Jeffrey E Grice		✓	✓	✓	✓
I acknowledge that these represent my contribution to the above research output.					
A/P Dr. Heather A.E. Benson	✓	✓	✓	✓	✓
I acknowledge that these represent my contribution to the above research output.					
Prof. Michael S. Roberts	✓	✓	✓	✓	✓
I acknowledge that these represent my contribution to the above research output.					

pharmaceutics

MDPI

Review

Topical Nano and Microemulsions for Skin Delivery

Christofori M. R. R. Nastiti [1,2,†], Thellie Ponto [1,†], Eman Abd [3], Jeffrey E. Grice [3], Heather A. E. Benson [1] and Michael S. Roberts [3,4,*]

1 School of Pharmacy, Curtin Health Innovation Research Institute, Curtin University, G.P.O. Box U1987, Perth, WA 6845, Australia; c.nastiti@postgrad.curtin.edu.au (C.M.R.R.N.); thellie.ponto@postgrad.curtin.edu.au (T.P.); H.Benson@curtin.edu.au (H.A.E.B.)

2 Faculty of Pharmacy, Sanata Dharma University, Yogyakarta 55282, Indonesia

3 Therapeutics Research Centre, The University of Queensland Diamentina Institute, Faculty of Medicine, Translational Research Institute, Woolloongabba, QLD 4102, Australia; e.abd@uq.edu.au (E.A.); jeff.grice@uq.edu.au (J.E.G.)

4 School of Pharmacy and Medical Sciences, University of South Australia, Adelaide, SA 5000, Australia

* Correspondence: m.roberts@uq.edu.au; Tel.: +61-7-34438031; Fax: +61-7-34437779

† These authors contributed equally to this work.

Received: 11 August 2017; Accepted: 13 September 2017; Published: 21 September 2017

Abstract: Nanosystems such as microemulsions (ME) and nanoemulsions (NE) offer considerable opportunities for targeted drug delivery to and via the skin. ME and NE are stable colloidal systems composed of oil and water, stabilised by a mixture of surfactants and cosurfactants, that have received particular interest as topical skin delivery systems. There is considerable scope to manipulate the formulation components and characteristics to achieve optimal bioavailability and minimal skin irritancy. This includes the incorporation of established chemical penetration enhancers to fluidize the stratum corneum lipid bilayers, thus reducing the primary skin barrier and increasing permeation. This review discusses nanosystems with utility in skin delivery and focuses on the composition and characterization of ME and NE for topical and transdermal delivery. The mechanism of skin delivery across the stratum corneum and via hair follicles is reviewed with particular focus on the influence of formulation.

Keywords: microemulsion; nanoemulsion; transdermal; skin penetration; penetration enhancer; nanosystem